ELECTROCHEMILUMINESCENCE: FROM BIOMOLECULES TO WHOLE CELLS

Author

KERILENG MILDRED MOLAPO, MSc

A thesis submitted at Dublin City University for the degree of

Doctor of Philosophy

School of Chemical Sciences:

Supervisors:

Prof. Tia E. Keyes

Prof. Robert J. Forster and

Prof Emmanuel I. Iwuoha (UWC)

March 2016

DECLARATION

I hereby certify that this material, which I now submit for assessment on the programme of study leading to the award of doctor of philosophy is entirely my own work, that I have exercised reasonable care to ensure that the work is original, and does not to the best of my knowledge breach any law of copyright, and has not been taken from the work of others save and to the extent that such work has been cited and acknowledged within the text of my work.

Signed: _____ ID No.: _____ Date:_____

DEDICATION

To my Mother: Mpho Ruth Phitlho

ACKNOWLEDGEMENTS

This thesis appears in its current form due to the support and guidance of several people, thus it is a pleasant moment for me to express my heartfelt gratitude to all the people who helped me accomplish this work.

Firstly and above all, I would like to thank the My God, true source of light in my life, for blessing me with the grace to work, patience and method which carried me throughout the course of my research work.

I would like to offer my profoundest gratitude to my supervisors Prof. Tia Keyes, Prof. Robert Forster and Professor Emmanuel Iwuoha for their valuable encouragement, inspiration, continued insightful discussions, advice the have always given me in all aspects related to my research project. Mere words are not sufficient to express my heartfelt thanks for your enthusiastic support, guidance advice and for always critically reviewing aspects of this study.

I would also like to extend my thanks to Dr Anitha Venkatanarayanan for her friendly assistance and great efforts as my Post Doc.

My heartfelt thanks goes to Aisling Byrne, your help with the cell work is truly appreciated. You were willing to help me anyday which I asked for help, with no complains or excuse, for this I am truly grateful. I would like to extend by

sincere gratitude to Christopher Burke for his help with the DPPZ work, and always treating everything I ask for with a sense of urgency.

Thank you to the technical staff from the umbrella office in the National Centre for Sensor Research. Especially Maurice Burke, for always being willing to help me with any technical issues I encountered with the Raman Instruments, fixing anything which I need. He did this a smile and attended to anything as a matter of urgency and for this I am grateful. Thank you to Barry O'Connel for helping me with any problems I encountered with the electrochemiluminecence instrument, and advice with the electrochemistry cell constructions.

I would to extend my thanks to Una Prendergast, for training me on using the AFM and helping me out with Raman whenever needed, you did this with true patience.

My Sincere thanks is extended to the School of Chemical Sciences technical staff for their great help, especially those I dealt with personally Veronica, John, and Vinny thanks for the training you gave me in the different instruments I needed. To Ambrose thanks so much for being so helpful in the School of Chemical Sciences stores, and also for the funny jokes you always cracked.

Special thanks goes to Josephine Ozoani from the NCSR stores, always providing me any lab consumables very efficiently and always doing her job

with a smile. Also thanks for your words of encouragement and upliftment which you always gave me.

My thanks are extended to all my research colleagues in Dublin City University, for your help, the discussions we shared and for providing such a friendly wonderful environment to work with in in the lab.

On a personal note, I would like to say I am eternally grate for my family, I must offer the Molapo family a giant thanks, these are people who have brought me thus far in life and always encouraged me to hold on, thanks for everything you have ever done for me. Special thanks goes to the Motlhabi, Gaoboihi and Modibane families, for your prayers and support.

A special warm thank you goes to my loving parents Mpho and Kagiso for instilling the love of learning within me, from a very young age. To a remarkable woman my Mom Mpho, the simple phrase “thank you” is not enough but I am extremely thankful, I am here today because of your unconditional love that raised me, sound advice, constant encouragement and endless patience. I certainly wouldn’t be where I am in life without your love. To Hope Chweu, thanks for the times you have cheered me up with your jokes, your calls and for always being patient for me to come back home for holidays

Special thanks goes to the man I love, Desmond Kwena Modibane. Thank you my love, for always supporting and encouraging me to finish with my

studies. I am thankful for the times you laughed and smiled, cheered and encouraged me on through the hard times and celebrated each accomplishment.

To my good friend Gcineka Mbambisa , this woman is remarkable, she is always willing to give a listening ear and dropping everything of hers to help me when I am in need. I would like to thank her from the bottom of my heart. Thanks to my African Society friends, Sammy D., Mohammed, Tifa, Nabil “Big Fry” and David, thank you for the good times we shared together.

Thanks to my friends from home, Takalani, Nthabiseng, Norma, Kelebogile and Lindiwe, Friendship is not about long calls, or seeing each other everyday, but it is about being able to pick up from where you left, even after not seeing each other for a long time. Thanks for being very good friends, and for bearing with me even for the times I used to be very boring to you, due to having academic commitments.

I want to lastly acknowledge the financial assistance for the PhD studies from SensorLab and South African Synthetic Oil Limited (SASOL).

TABLE OF CONTENTS

LIST OF SYMBOLS

C	: Coulomb
De	: Diffusion coefficient
E_S	: Energy required to populate singlet excited state
E_T	: Energy required to populate triplet excited state
E_{final}	: Final potential
$E_{initial}$	: Initial potential
$E^{o\prime}$	: Formal electrode potential
E^{o}_{donor}	: Formal potential reduction
$E^{o}_{acceptor}$	: Formal potential oxidation
E_p	: Peak potential
$E_{p,a}$	: Anodic peak potential
$E_{p,c}$	: Cathodic peak potential
ΔE_p	: Separation peak potential
F	: Faraday constant
I	: Current
I_o	: Scaling factor
$I_{p,c}$	: Cathodic reaction
$I_{p,a}$	: Current for the anodic reaction
I_p	: Peak current
$I(t)$	: Impulse response function
k	: Overall relaxation rate

n : Number of electrons transferred

Q : Charge

R : Sample resistance

$\mathbf{S_0}$: Ground singlet state

$\mathbf{S_1}$: Excited singlet state

T : Triplet state

v : Scan rate

V : Applied voltage

Γ^* : Surface concentration

σ : Specific conductivity

$\mathbf{\Phi_F}$: Fluorescence quantum yield

τ : Lifetime

λ : Wavelength

ΔG : Gibbs energy

LIST OF ABBREVIATIONS

ADP : Adenosine diphosphate

ATP : Adenosine monophosphate

AMA : Antimycin A

ATP : Adenosine triphosphate

BODIPY : Boron dipyromethene

BPO : Benzoyl peroxide

bpy : 2,2'-bipyridyl

bpz : 2,2′- bipyrazine

CCD : Charge coupled device

CL : Chemiluminescence

CPs : Conducting polymers

CRP : C-reactive protein

CV : Cyclic voltammetry

$DPACl_2$: 9,10-Dichloroanthracene

DCM : Dichloromethane

DMF : Dimethyl formamide

DMSO : Dimethylsulfoxide

DMEM : Dulbecco’s modified Eagle’s medium

DPA : 9,10-Diphenylanthracene

DPBS : Dulbecco’s phosphate buffer solution

dp-bpy : 4,4'-diphenyl-2,2'-bipyridine

dp-phen : 4,7–diphenyl-1,10- phenantroline

ECL : Electrochemiluminescence

EDC : 1-ethyl-3-[3-dimethylaminopropyl] carbodiimide hydrochloride

EIS : Electrochemical impedance spectroscopy

EL : Electroluminescence

EtOH : Ethanol

FCCP : Carbonyl-cyanide-4-(trifluoromethoxy) phenylhydrazone

FWHM : Full width at half maximum

HOMO : Highest occupied molecular orbital

H-NMR : Proton nuclear magnetic resonance

HPLC : High performance liquid chromatography

IUPAC : International Union of Pure and Applied Chemistry

LUMO : Lowest unoccupied molecular orbital

MeCN : Acetonitrile

MLCT : Metal to ligand charge transfer

MUA : 11-mercapto-1-undercanoic acid

NADH : Nicotinamide adenine dinucleotide

NHS : N-hydroxysuccinimide

NIR : Near infrared

PANI : Polyaniline

PADPA : *p*-aminodiphenylamine

PAHs : Polyaromatic hydrocarbons

PANSA : Poly(8-anilino-1-naphthalene sulfonic acid)

PBS : Phosphate buffer solution

PEG : poly (ethylene glycol) bis (3-aminopropyl)

phen : 1,10-phenanthroline

PMT : Photo multiplier tube

PPy : Polypyrrole

PTh : Polythiophene

RUB : Rubrene

SAM : Self-assembled monolayers

SCE : Saturated calomel electrode

TBATFB : Tetrabutylammonium tetrafluoroborate

TCSPC : Time-correlated single photon counting

Terpy : 2,2′,2″- terpyridine

THF : Tetrahydrofuran

TMPD : Tetramethyl-*p*-phenylenediamine

TPrA : Tripropylamine

TPTZ : 2,4,6-tripyridyl-2-triazine

UV : Ultraviolet

Vis : Visible

LIST OF SCHEMES

LIST OF FIGURES

LIST OF TABLES

RESEARCH OUTPUTS

Published papers

1) Molapo, K.M., Venkatanarayanan, A., Dolan, C.M., Prendergast, U., Baker, P.G.,Iwuoha, E.I., Keyes, T.E., Forster, R.J., High Efficiency Electrochemiluminescence from Polyaniline: Ruthenium Metal complex film, *Electrochemical Communications*., **2014**, 48, 95-98.

2) Venkatanarayanan, A., Martin, A., Molapo, K.M., Iwuoha, E.I, Keyes, T.E., Forster, R.J., Tuning the electrochemiluminescence potential from immobilized BODIPY by co-reactant selection, *Electrochemical Communications*., **2013**, 31, 116-119.

3) Molapo, K.M., Byrne, A., Martin, A., Iwuoha, E.I., Forster, R.J., Keyes, T.E., Electrochemiluminescence method assessment of metabolic status of live HeLa cells. *Article in preparation.*

4) Molapo, K.M., Burke, C., Forster, R.J., Iwuoha, E.I., Keyes, T.E., DNA binding induced ECL generation at monolayers of a molecular light switch. *Article in preparation.*

Poster presentations

1) **Electrochem 2012, Dubin: Ireland (4-6** Sept 2012**)**

Molapo, K.M., Venkatanarayanan , A., Dolan, C.M., Prendergast, U., Baker, P.G.,Iwuoha, E.I., Keyes, T.E., Forster, R.J. Modulation of the luminescence and electronics of derivatised polyanilines with a novel ruthenium (II) phenanthroline luminophore.

2) **Plastic Electronics , Dresden : Germany** (4-9 Oct 2012**)**

Molapo, K.M., Venkatanarayanan , A., Dolan, C.M., Prendergast, U., Baker, P.G.,Iwuoha, E.I., Keyes, T.E., Forster, R.J. Modulation of the luminescence and electronics of derivatised polyanilines with a novel ruthenium (II) phenanthroline luminophore.

ELECTROCHEMILUMINESCENCE: FROM BIOMOLECULES TO WHOLE CELLS

Kerileng Mildred Molapo

ABSTRACT

The aim of this thesis is to apply interfacial electrochemiluminescence (ECL) of novel ruthenium probes to the determination of important biomolecules and the assessment of cell viability. There are six chapters in this study with Chapters 1 providing an overview of the relevant literature. Chapter 2 presents the photophysics, electrochemical and electrochemiluminescent properties of a novel 1,3,5,7-tetramethyl-8-[(2-fluorophenyl)-6-methoxy-1,5-naphthyridine-3-carboxy]-4,4'-difluoroboradiazaindacene (BODIPY-COOH) dye are reported. It was observed that the ECL turn-on potential of BODIPY-COOH could be controlled by changing the identity of the coreactant (benzoyl peroxide (BPO) or hydrogen peroxide). Also thin films of the BODIPY-COOH dye prepared on platinum electrodes exhibited strong luminescence in water, thereby making them potentially useful for ECL application in biological media. Chapter 3 reports a rapid and effective method of confining a ruthenium ECL luminophore on an electrode surface by the electrodeposition of polyaniline (PANI) film in the presence of ruthenium 2,2'-bipyridyl(2,2'-bipyridyl)-2(4-carboxyphenyl)imidazo[4,5][1,10]phenanthroline ($[Ru(bpy)_2PIC]^{2+}$) to form a composite $Ru(bpy)_2PIC]^{2+}$-PANI film that exhibited the highest ECL efficiency value (1.00%) reported for any surface confined ruthenium complex. This behaviour is attributed to the efficient luminophore regeneration rate of the

$Ru(bpy)_2PIC]^{2+}$-PANI film which indicates the film's usefulness in the development of highly sensitive ECL based sensors for biochemical species such as DNA and amino acids. In Chapter 4 the generation of molecular light switch by the binding of DNA to a novel *bis*-(4-(4-carboxyphenyl) -2,2'-bipyridine) dipyridophenazine ruthenium (II) dichloride $[Ru(dppz)(bpyArCOOH)_2]^{2+}$ dye monolayer is presented. Evidence for the binding of DNA to $[Ru(dppz)(bpyArCOOH)_2]^{2+}$ was obtained through Raman, ECL and electrochemistry studies. The generation of ECL from living cancer cells (used as cofactor) and ruthenium 2,2'-bipyridyl-2, 2'-quarterpyridyl ($[Ru(bpy)_2Qbpy]^{2+}$) dye is explained in Chapter 5 to be due to the adenosine 5' triphosphate (ATP) released from the cancer cells, and it opens up a whole new possibility of interrogating cell health and using cell ECL as cell viability marker. Chapter 6 draws the most important insights of the thesis together and discusses useful next steps for future direction.

CHAPTER ONE:

LITERATURE REVIEW

1.1. INTRODUCTION

1.1.1. OVERVIEW

Electrochemiluminescence also known as electrogenerated chemiluminescence (ECL) is described as chemiluminescence (CL) produced directly or indirectly as a result of electrochemical reactions.[1,2] In general, ECL involves the electrochemical production of reactive intermediates from stable precursors at the surface of an electrode and the intermediates then react under a variety of conditions to form excited states that emit light.[3,4] Although a number of optical analytical methods exist for the detection of chemical and biological analytes of interest, ECL offers a number of important analytical advantages including high sensitivity and selectivity. Futhermore, the method is compatibile with solution phase and thin film formats,[5,6] there is no background optical signal. It is highly selective as excited states are generated in situ at the electrodes by combining analytical advantages of chemiluminescent analysis with ease of reaction control by applying electrode potential,[7,8] allowing greater control over initiation, rate and course of the reaction. Moreover, it is typically a non-destructive technique since reagents can be regenerated at the electrodes, to partake in the reaction with analyte again. ECL based detection methods are of vital importance in a number of commercial analytical applications including pharmaceuticals,

chromatography, trace analysis environmental assays such as food and water testing, biodefence, biosensors, and clinical diagnostics.[2,3]. Enhanced selectivity of ECL analysis is reached by variation of electrode potential thus controlling species that are oxidized/reduced at the electrode and take part in ECL reaction,[3] and advancements in development of materials such as interfacial thin films, organic molecules such conducting polymers, organic and inorganic nanoparticles coated on electrodes and the production of novel luminophores.[9] The aim of this thesis is to explore a number of novel materials and methods for the application of interfacial electrochemiluminescence to the detection of biological materials.

1.2. PRINCIPLES AND FUNDAMENTALS OF ELECTROCHEMILUMINESCENCE

1.2.1. ECL GENERATION PATHWAYS

Classical ECL takes place when an electron transfer reaction between electrochemically generated species, such as radical ions, results in the formation of an excited species that then relaxes by emitting light, this approach is typically known as the annihilation pathway. In recent years, an important advance in ECL was the discovery of reaction schemes for generating ECL via the use of coreactants.[10] A coreactant is a species which upon oxidation or reduction produces an intermediate that can react with an ECL luminophore to produce an emissive excited states.[11] The commonality between annihilation and coreactant pathways is that in both cases two

species are generated electrochemically and those two species undergo electron transfer reactions that produce an emissive state. The two pathways can further be classified into more specific mechanisms known as the singlet (S-route) and triplet (T-route) pathway.[12]

1.2.2. ANNIHILATION PATHWAY

In an annihilation reaction, oxidized and reduced forms of the luminophore are generated at the electrode through an electrochemical reaction which involves direct pulsing of the electrode potential. Subsequently, an interaction between the oxidized and reduced form of the luminophore takes place, resulting in the formation of both a ground state and electronically excited state.[12,13] The electronically excited species relaxes to ground state and this process is accompanied by light emission. A classic example that demonstrates ECL generation via annihilation is Rubrene (RUB) as demonstrated in Equation 1.1 to1.4. Rubrene (5,6,11,12-tetraphenyltetracene) is a polycyclic aromatic hydrocarbon that undergoes electrochemiluminescence. Upon applying a double step potential, anion ($RUB^{\bullet -}$) and cation ($RUB^{\bullet +}$) radicals are generated, which then recombined to produce a ground state and an electronically excited state.[3,14]

$RUB + e^- \rightarrow RUB^{\bullet -}$ (reduction at electrode) $E° = + 0.95$ V vs SCE **[1.1]**

$RUB \rightarrow RUB^{\bullet +} + e^-$ (oxidation at electrode) $E° = - 1.37$ V vs SCE **[1.2]**

$RUB^{\bullet +} + RUB^{\bullet -} \rightarrow RUB^{*} + RUB$ (excited-state formation) **[1.3]**

$RUB^{*\bullet} \rightarrow RUB + hu$ (light emission) **[1.4]**

In this example, RUB in Equation 1.1 is an electron acceptor which is reduced and in Equation 1.2, RUB is an electron donor which is oxidized at the electrode surface. The formal potentials for the ground state reduction and oxidation process are termed E°_{Donor} and $E^{\circ}_{Acceptor}$, respectively. The difference between the two is used to calculate the corresponding free energy for the annihilation reaction (ΔG) as indicated in Equation 1.5. It should be noted that the electron donor and acceptor may be the same molecule as in this example or a different molecule.[12]

$$\Delta G = nF(E^{\circ}_{Donor} - E^{\circ}_{Acceptor}) \quad \textbf{[1.5]}$$

For RUB, it was reported that E°_{Donor} is +0.95 V and $E^{\circ}_{Acceptor}$ is -1.37 V, and ΔG is evaluated as 2.32 eV.[3] The energy required to populate the singlet excited state, E_s, of RUB is estimated from the wavelength of maximum emission of 540 nm upon photoexcitation at 77 K, to be 2.30 eV, according to Equation 1.6 below,

$$E_s(eV) = \frac{1239.81}{\lambda(nm)} \quad \textbf{[1.6]}$$

When the free energy of annihilation (2.32 eV) is compared to the E_s (2.30 eV), it is evident that ΔG exceeds the required energy to populate singlet excited, thus the reaction is energy sufficient and the excited state is accessible, making ECL possible.[3] Energy sufficient systems such as RUB are categorized under the S-route, since light emission is directly produced from excited singlet state to ground state. In contrast the other T-route is

energy deficient because it involves the triplet-triplet annihilation mechanism.[1,3] A classic example of a T-route annihilation system, is illustrated in Equations 1.7-1.11 which show is the ECL cross reaction of radical anion 9,10-diphenylanthracene (DPA) and the cation radical of N,N,N*,N*-tetramethyl-p-phenylenediamine (TMPD).[15]

$DPA + e \rightarrow DPA^{\bullet -}$ (reduction at electrode, E= -1.89 V vs SCE) **[1.7]**

$TMPD - e \rightarrow TMPD^{\bullet +}$ (oxidation at electrode, E= +0.24 V vs SCE) **[1.8]**

$DPA^{\bullet -} + TMPD^{\bullet +} \rightarrow {}^{3}DPA^{*} + TMPD$ **[1.9]**

${}^{3}DPA^{*} + {}^{3}DPA^{*} \rightarrow {}^{1}DPA^{*} + DPA$ (triplet triplet annihilation) **[1.10]**

${}^{1}DPA^{*} \rightarrow DPA + h\upsilon$ **[1.11]**

The reaction in Equation 1.10 is termed a triplet triplet annihilation reaction because the energy for the population of the first excited singlet comes from Equation 1.8 and 1.9 where the energy from the two electron transfer is combined to provide sufficient energy. The overall example demonstrates an energy deficient system (T-route) which lacks sufficient energy to form singlet excited state directly as demonstrated in Scheme 1.1 below.

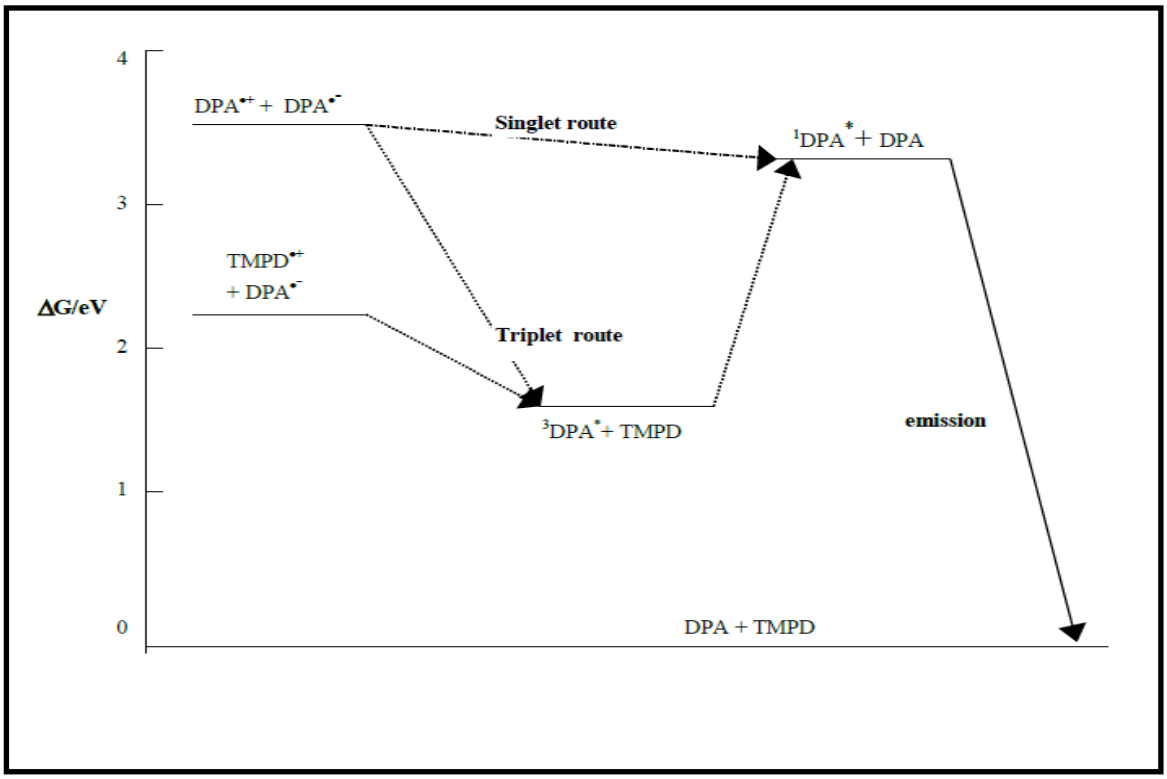

Scheme 1.1: Energy level diagram for DPA and TMPD system showing both the singlet route and the triplet route. Adapted from Knight, A., Trends Anal. Chem., **1999**, 18, 47-62.

In order to obtain an intense annihilation ECL signal from an electrochemiluminescent reagent the following characteristics are the basic prerequisites the luminophore should satisfy. Firstly, stable radical ions of the precursor molecules should be formed via oxidation or reduction and this should take place in a potential range that is attainable within the solvent of choice.[7] Secondly, the product from the electron transfer reaction should possess sufficient energy to produce the excited state. Finally, the precursors participating in the homogeneous electron transfer leading to the light emitting

excited state should be generated at electrodes through heterogeneous electron transfer reactions.[7]

To generate ECL by the annihilation pathway, only the electrochemiluminescent species, a solvent and a supporting electrolyte is required for the reaction to take place. However, the disadvantage about annihilation systems is that they require the use of rigorously purified and deoxygenated non aqueous solvents. This is because the available potential range in aqueous solvents is too narrow to generate the required energetic precursors, thus these reactions are conducted in organic solvents such as acetonitrile and N-N- dimethylformamide. Consequently, application of annihilation pathway is often of limited applicability in studies which investigate biological samples and analytes, as these are typically studied in aqueous medium. Thus the difficulty of performing annihilation ECL in aqueous media has popularized the use of the coreactant pathway.

1.2.3. COREACTANT PATHWAY

A key advantage of the coreactant approach is that it facilitates ECL generation in aqueous solution, opening up opportunities to conduct a wide range of assays for molecules of diagnostic or biological relevance. ECL can also be achieved by applying a single step potential or uni directional potential scanning at the electrode, in a solution containing a coreactant species such as oxalate ($C_2O_4^{2-}$) and a luminophore. Upon applying an oxidative or reductive potential at the working electrode, the coreactant chemically

decomposes to form strong reducing or oxidizing intermediates, which then react with the either oxidized or reduced luminophore to produce the light emitting excited species.[11] Several experimental studies in this work used different coreatants such TPA {where TPA = Tri-n-propylamine = $CH_3CH_2CH_2)_3N$}, Hydrogen peroxide (H_2O_2) and oxalate and the following section will focus on how these coreactants work.

1.2.3.1. Tripropylamine

The ECL system of ruthenium tris-bipyridyl, $[Ru(bpy)_3]^{2+}$/ TPA is a common example of ECL generation through the coreactant pathway demonstrated in Scheme 1.2 below. To date the, $[Ru(bpy)_2]^{3+}$ / TPA system has proven to exhibit the most optimal ECL properties in commercial applications.[11] The interest in using Ru /TPA systems stems from the system allowing efficient ECL generation in aqueous media, and also at the physiological pH 7.4. Coupled to the fact that Ru exhibits high quantum yields and is able to undergo one electron transfer processes at easily attainable potentials.

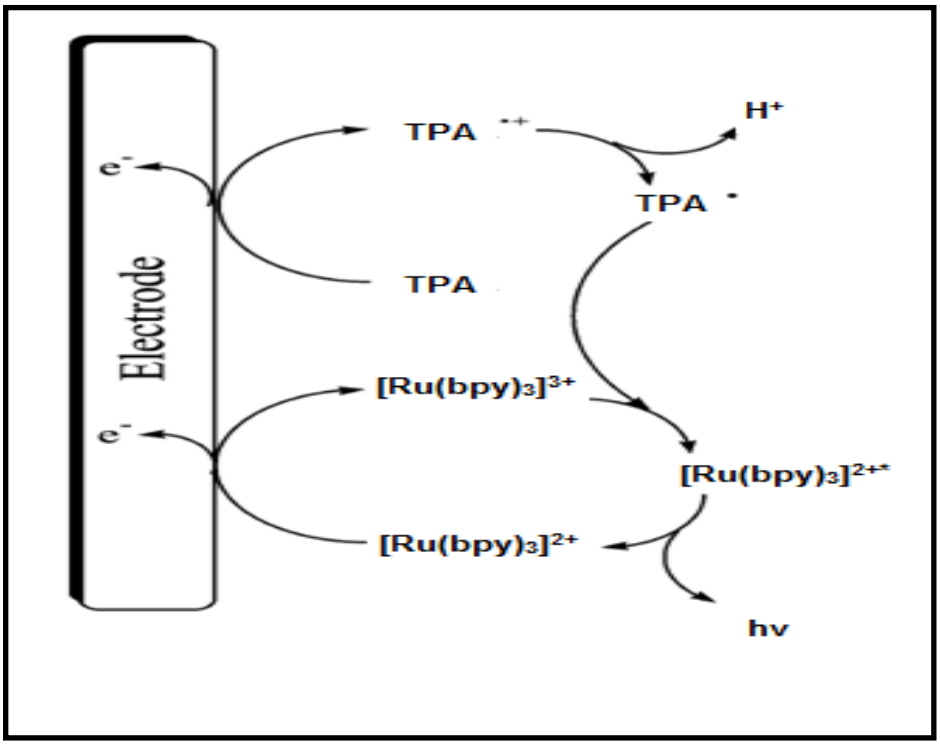

Scheme 1.2: Proposed mechanism for $[Ru(bpy)_3]^{2+}$/ TPA ECL system. Reprinted from; Electrochemiluminescence (ECL), Richter, M. M., Chem. Rev, **2004**, 104, 3003-3036.

When a sufficiently positive potential is applied to the electrode, $[Ru(bpy)_3]^{2+}$ and TPA are both oxidized at the surface of the electrode to form $[Ru(bpy)_3]^{3+}$and $[TPA^{\bullet}]^{+}$. Upon oxidation of $[Ru(bpy)_3]^{2+}$ and TPA at the electrode, the short-lived $[TPA^{\bullet}]^{+}$ undergoes deprotonation from its α carbon and forms a strong reducing intermediate TPA which is a highly reactive radical. The radical $TPA^{\bullet}$ proceeds to reduce $[Ru(bpy)_3]^{3+}$ to produce the excited state $[Ru(bpy)_3]^{2+}$*, which decays to the ground state $[Ru(bpy)_3]^{2+}$ by emitting light at approximately 620 nm.[16,17] In the $[Ru(bpy)_3]^{2+}$/ TPA ECL system, both the luminophore and coreactant are oxidized at the surface of the electrode in a single potential step, the coreactant produces a strong

reducing agent upon oxidation. Hence, the coreactant is classified as an oxidative or oxidative–reductive system.[18]

1.2.3.2. Oxalate system

The first account of using a coreactant in ECL was reported by Bard's group in 1977.[19] They studied the electrochemical oxidation of an oxalate ion ($C_2O_4^2$) in acetonitrile in the presence of fluorescent thianthrene and naphthalene compounds. The $C_2O_4^{2-}$ and the fluorescent compound were simultaneously oxidized on a platinum electrode. Electrochemical oxidation of $C_2O_4^{2-}$ yields a highly reducing intermediate $CO_2^{\bullet-}$ at a formal potential of 1.9 V vs NHE. An example is outlined below in Equations 1.12-1.18 where an aqueous solution of $[Ru(bpy)_3]^{2+}$ gives ECL in the presence of $C_2O_4^{2-}$ upon oxidation.[20]

$$[Ru(bpy)_3]^{2+} + e \rightarrow [Ru(bpy)_3]^{3+} \quad \textbf{[1.12]}$$

$$[Ru(bpy)_3]^{3+} + C_2O_4^{2-} \rightarrow [Ru(bpy)_3]^{2+} + C_2O_4^{\bullet-} \quad \textbf{[1.13]}$$

$$C_2O_4^{\bullet-} \rightarrow CO_2^{\bullet-} + CO_2 \quad \textbf{[1.14]}$$

$$[Ru(bpy)_3]^{3+} + CO_2^{\bullet-} \rightarrow [Ru(bpy)_3]^{2+*} + CO_2 \quad \textbf{[1.15]}$$

$$[Ru(bpy)_3]^{2+} + CO_2^{\bullet-} \rightarrow [Ru(bpy)_3]^{+} + CO_2 \quad \textbf{[1.16]}$$

$$[Ru(bpy)_3]^{3+} + Ru(bpy)_3]^{+} \rightarrow [Ru(bpy)_3]^{2+*} + [Ru(bpy)_3]^{2+} \quad \textbf{[1.17]}$$

$$[Ru(bpy)_3^{2+*} \rightarrow [Ru(bpy)_3]^{2+} + hu \quad \textbf{[1.18]}$$

$[Ru(bpy)_3]^{2+}$ is initially oxidized to $[Ru(bpy)_3]^{3+}$, subsequently $[Ru(bpy)_3]^{3+}$ oxidizes $C_2O_4^{2-}$ to form a radical anion $C_2O_4^{\bullet-}$. The radical ion decomposes into carbon dioxide and $CO_2^{\bullet-}$ which is a highly reducing radical anion. The radical anion $CO_2^{\bullet-}$ either reduces $[Ru(bpy)_3]^{3+}$to $[Ru(bpy)_3]^{2+*}$ or alternatively it may reduce $[Ru(bpy)_3]^{2+}$ to $Ru(bpy)_3^{+}$, which then reacts with $[Ru(bpy)_3]^{3+}$ to form the excited state $[Ru(bpy)_3]^{2+*}$. The excited state $[Ru(bpy)_3]^{2+*}$ relaxes to the ground state $[Ru(bpy)_3]^{2+}$ by emitting light .Oxalate falls under the same category of oxidative-reductive coreactant like TPA, due to its ability to form a strong reducing agent upon electrochemical oxidation.[11]

1.2.3.3 Hydrogen peroxide (H_2O_2)

Zou and Ju.[21] were the first to demonstrate ECL, employing hydrogen peroxide as a coreactant where CdSe- quantum dots were the ECL luminophore. In a separate study, Bard *et al.*[22] also demonstrated that H_2O_2 can be used as coreactant to generate ECL from $[Ru(bpy)_3]^{2+}$ via reduction-oxidation in aqueous solution.

$$H_2O_2 + e^- \longrightarrow {}^{\bullet}OH + OH^- \qquad \textbf{[1.19]}$$

$$[Ru(bpy)_3]^{2+} + e^- \longrightarrow [Ru(bpy)_3]^{+} \qquad \textbf{[1.20]}$$

$$[Ru(bpy)_3]^{+} + {}^{\bullet}OH \longrightarrow [Ru(bpy)_3]^{2+*} + OH^- \qquad \textbf{[1.21]}$$

$$[Ru(bpy)_3]^{2+*} \longrightarrow [Ru(bpy)_3]^{2+} + h\nu \qquad \textbf{[1.22]}$$

The reduction of H_2O_2 and $[Ru(bpy)_3]^{2+}$ yields the hydroxyl radical ${}^{\bullet}OH$, and $[Ru(bpy)_3]^{+}$, respectively. The hydroxyl radical is a strong oxidizing agent,

readily capable of oxidizing $[Ru(bpy)_3]^+$ to the electronically excited and light emitting $[Ru(bpy)_3]^{2+*}$. In a situation where the coreactant is reduced at the electrode to yield a strong oxidizing agent, then the coreactant is classified as a reductive-oxidative coreactant.

It should be noted that a coreactant should satisfy certain required criteria for it to be used for ECL generation and the criteria are as follows: the coreactant should be soluble in the reaction mixture and the intermediate species produced from its electrochemical and chemical decomposition reactions should be adequately stable within the lifetime of the experiment. The coreactant should not give any ECL background in the potential window of interest.[11] Furthermore, the coreactant and its intermediates should not be capable of quenching the ECL luminophore, but should possess adequate reducing or oxidizing energy to react with the oxidized-reduced luminophore to form the light emitting excited state species. Lastly, the reaction between the intermediates produced by the coreactant and the redox luminophore should take place rapidly.[7] Hence, ECL luminophores are discussed in the following sections.

1.3. ECL LUMINOPHORES

ECL luminophores can be conveniently categorized into transition metal based inorganic and organic systems, and these will be discussed in the following sections.

1.3.1. INORGANIC LUMINOPHORE SYSTEMS

During the development of ECL many inorganic complexes have been investigated these include complexes and/or clusters containing metals such as Ag, Al, Au, Cd, Cr, Cu, Eu, Hg, Ir, Mo, W,Os, Pd, Pt, Re, Ru, Si, and Tb.[7] Comprehensive surveys of ECL active inorganic luminophores have been reviewed previously.[3,7] Due to the breadth of this field for complexes that are used as ECL luminophores, the following section will focus on Ruthenium complexes as inorganic luminophores. Ru is chosen because it is directly relevant to the current study, because three different ruthenium polypyridyl complexes are employed as luminophores in the ECL studies in Chapter 3,4,5.

1.3.1.1. Ruthenium

Among the many ECL inorganic systems that have been studied, most investigations have been centred around $[Ru(bpy)_3]^{2+}$ and its derivatives (Figure 1.1). The first report of metal chelates being employed in ECL was in 1972, were annihilation of oxidized $[Ru(bpy)_3]^{2+}$ reduced $[Ru(bpy)_3]^{+}$ species to generate excited state $[Ru(bpy)_3]^{2+*}$ in aprotic media.[23]

Since then, $[Ru(bpy)_3]^{2+}$ has become the most widely used luminophore in the literature. Ruthenium polypyridyl complexes continue to play important role in ECL based assay systems. Their dominance stems from the rather unique

properties which include, chemical stability in different solvents and strong phosphorescence as well as the versatility of the polypridine ligands. It also exhibits favourable reversible electrochemical redox reactions easily attainable potentials.[24] Since the discovery of ECL of $[Ru(bpy)_3]^{2+}$, researchers have devoted significant efforts to designing novel high bright luminophores using different ligands which can be attached to ruthenium to form other ruthenium chelates Figure 1.1, illustrates some of the commonly used ligands used. Their main objective being to design complexes with high ECL efficiencies ϕ_{ECL} ,which do not only have excellent electrochemical and photophysical properties, but also possess biomolecule binding capabilities.

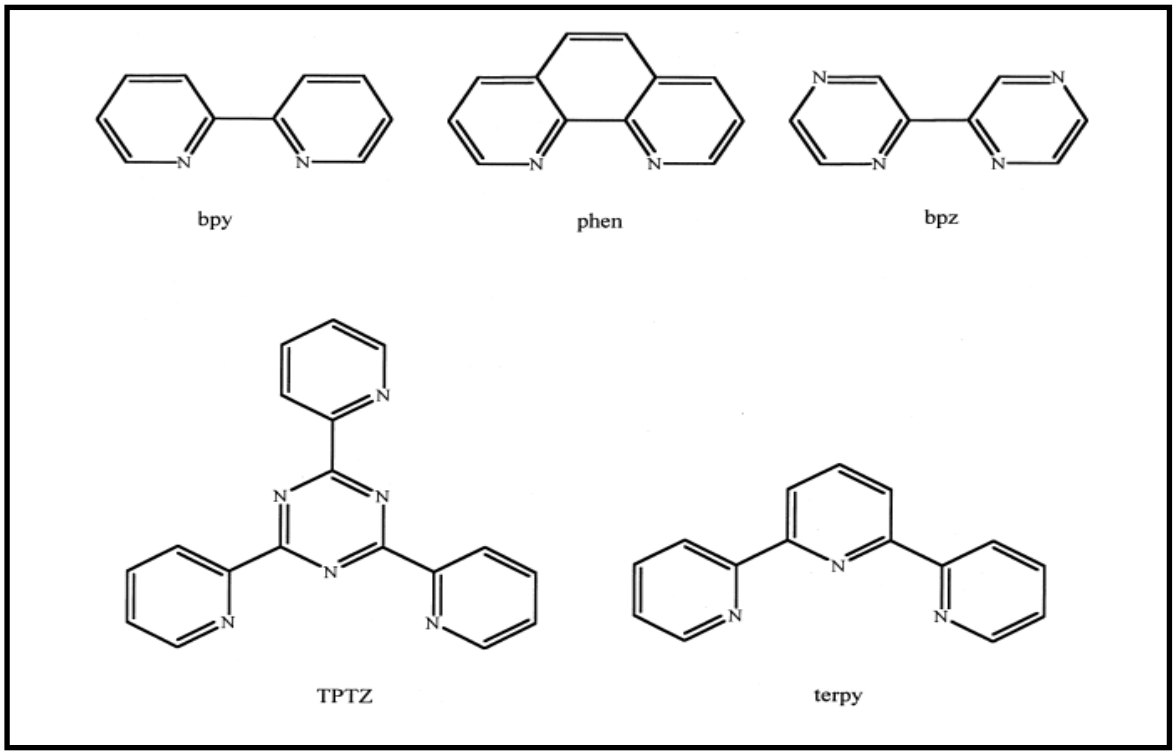

Figure 1.1: Structures of ligands most commonly used; 2,2′-bipyridine (bpy), 1,10 – phenanthroline (phen), 2,2′- bipyrazine (bpz), 2,4,6 – tripyridyl-2-triazine (TPTZ), 2,2′,2″- terpyridine (terpy). Reprinted from; *Electrogenerated Chemiluminescence,*ed. Bard, A. J., **2004**, New York: Marcel Dekker.

The first ruthenium polypyridyl complex which is investigated in this work in Chapter 3, is $[Ru(bpy)_2PIC]^{2+}$, were bpy is 2,2'-bipyridyl and PIC is (2,2'-bipyridyl)-2(4-carboxylphenyl) imidazo [4,5][1,10] phenanthroline which was originally developed by Pellegrin and co workers.[25] The $[Ru(bpy)_2PIC]^{2+}$ complex contains a carboxyl group which can be coupled to amine bounds of biomolecules and its quantum yield has been reported to be 30% higher than that of Ruthenium (II) tris bipyridine.[26,27,28]

The ECL properties of $[Ru(bpy)_2PIC]^{2+}$ have been previously reported by Venkatanarayanan *et al.*[29] In their study they covalently coupled the carboxyl terminal of $[Ru(bpy)_2PIC]^{2+}$ to the amine groups of the silica spheres to produce significant ECL. The current study aims to improve the ECL efficiency of $[Ru(bpy)_2PIC]^{2+}$, by incorporating in a conducting polymer backbone polyaniline through to form a composite film PANI-Ru .

The second ruthenium polypyridyl complex which is investigated in this work in Chapter 4 is novel *bis*-(4-(4-carboxyphenyl)-2,2'-bipyridine) dipyridophenazine ruthenium(II) dichloride $[Ru(dppz)(bpyArCOOH)_2]^{2+}$ complex. Ru complexes containing the dipyridophenazine (dppz) ligand have have been widely reported.[30,31]

These complexes have unique photophysical properties, that is they are non-emissive in aqueous solution, however when the phenanzine nitrogens of the dppz ligands are shielded , from water they become emissive,[32]. For example upon DNA binding the compounds become highly emissive, thus they are called molecular light switch complexes. Studies reported about Ru

complexes containing the dipyridophenazine (dppz) ligand fall mainly into two areas of interest, the binding of these complexes with DNA and their photophysical behaviour.[33,34]

ECL of dppz containing Ru complexes and its DNA binding properties have been reported previously reported in solution Xu and co- workers.[35] In their study they showed that ECL of $[Ru(bpy)_2dppz]^{2+}$ is negligible in aqueous solution in the presence of oxalate as a coreactant and it increases ~ 1000 times when $[Ru(bpy)_2dppz]^{2+}$ intercalates into a nucleic structure. The current study aims to investigate the electrochemiluminescence behaviour of $[Ru(dppz)(bpyArCOOH)_2]^{2+}$ bound to the surface of an electrode and its DNA binding properties.

1.3.2. ORGANIC LUMINOPHORE SYSTEMS

Organic luminophores such as Polyaromatic hydrocarbons (PAHs) have good characteristics such as high fluorescence quantum yield and they are able to form stable radical cations and anions.[36] Most noticeable examples in literature are 5,6,11,12-tetraphenylteracene, rubrene (RUB) and 9,10-diphenylanthracene (DPA) owing to their high fluorescence quantum yields.[36] These PAHs were among the initial organic systems to be explored for ECL generation and they have been extensively studied. However, many studies on other PAHs have since followed, these include; N,N,N*,N*-tetramethyl-*p*-phenylenediamine (TMPD), luminol, acridium esters, polymers and siloles.[36] However, the development of the organic ECL systems requires a thorough

understanding of the variables that contribute to light emission. These system can be categorized into two groups, those which are single systems where the annihilating radical ions are generated from the same precursor, and mixed systems which involve radical ions being generated from different precursors.[37]

1.3.2.1. Single systems for organic ECL

Polyaromatic hydrocarbons exhibit many of the features required to achieve ECL from single system. Typically, they can undergo electron transfer process as to yield stable radical anion and cations, and they have excited states that are accessible with the energy arising through radical ion annihilation reactions. DPA is regarded as a model compound for ECL from organic single systems. Given that DPA is reversibly oxidized ($E°$ = 1.37 V vs SCE) and reduced (E° = -1.79 V vs SCE) to give rise to stable radical ions DPA^+ and DPA^-, hence the free energy released during the annihilation of DPA is of the order of -3.16 eV. This energy exceeds the amount of energy required to directly populate the single excited state (Es = 3.06 eV) and the triplet excited state is also accessible (E_T = 1.8 eV), thus ECL is possible.[38] ECL emission from this compound is very bright with ϕ_F that can unity. It should be noted that DPA is known as the most efficient material for single system ECL in solution studies, yielding extremely bright ECL emission with an ECL efficiency that can approach 25%. Many PAHs have characteristics that make them suitable to be used in ECL of single systems, however, their observed ECL efficiencies are often lower than those of DPA and RUB.

1.3.2.2. Mixed systems for organic ECL

In mixed systems the redox species that are generated via oxidation and reduction are generated from two different precursor molecules. One of the generated species does not form the excited state and it is known as the non-emissive partner. While the other species forms the excited states and it is deemed the emissive partner. Non emissive partners display high excited states which result in a positive ΔG and slow electron transfer to excited states or they may form excited states, however, they exhibit very low quantum efficiency and they remain undetected.[7] A common example of non-emissive partner is TMPD, which undergoes an irreversible oxidation process to form a stable radical cation ($E°$ = 0.24 V vs SCE). The energy required to directly populate the singlet emitting state is 3.52 eV and 2.83 eV, for the triplet state. Thus it is not possible to populate these states when TMPD is employed as a single system, however, by introducing DPA in the reaction, and creating a mixed system of TMPD and DPA, ECL becomes thermodynamically feasible. The radical cation is generated by TMPD while DPA produces the radical anion and the excited state is formed via triplet-triplet annihilation pathway making it possible to generate ECL via the energy insufficient pathway.[7]

1.4. BODIPY DYES

1.4.1. INTRODUCTION

There is an on-going need for the introduction of novel ECL reagents and Boron dipyrromethene (BODIPY) are upcoming novel organic luminophores which have currently gained interest among researches in the field of ECL. Chapter three focuses on the ECL properties of novel BODIPY –COOH dye, although researchers have published ECL investigations of other BODIPY dyes in solution, the aim of this work is to investigate the solid state ECL of the dye BODIPY –COOH, which may lead to potential applications.

Boron dipyrromethene (BODIPY) dyes represent an important class of molecule characterized by strong absorption and emission profiles in the visible region, high photostability and small Stokes shift and good exhibit electrochemical and spectroscopic properties.[39,40] Moreover, the intensity and energy of BODIPY emission can be tuned through the addition of properly placed electron donor and/or acceptor substituents on the BODIPY core BODIPY are upcoming novel organc luminophores which have currently gained interest among researches in the field of ECL.

1.4.2. THE CORE STRUCTURE OF BODIPY COMPOUNDS

The molecular structure of all BODIPY dyes have the 4,4-difluoro-4-bora-3a,4a-diaza-s-indacene core structure as indicated in Figure 1.2 According to the IUPAC numbering system for the BODIPY core structure, the carbons

directly adjacent to the nitrogens on the pyrroles are known as the α positions.[41,42] While the position of the central carbon which is directly opposite to the BF_2 moiety is referred to as the *meso* position and all other carbons are known as the β–positions.[43,44]

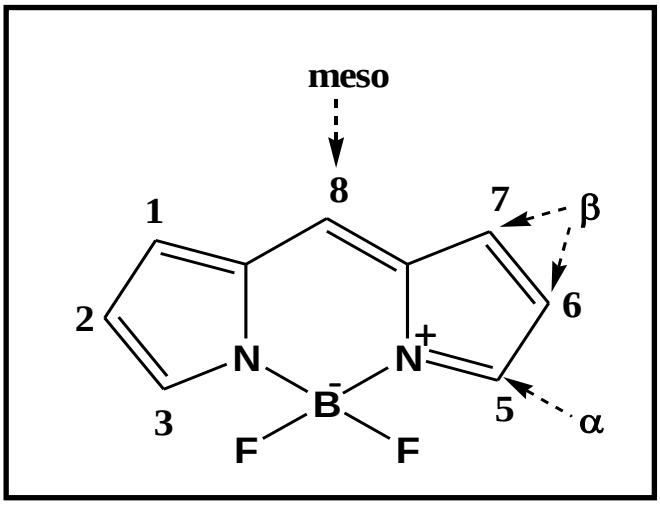

Figure 1.2: Numbering of positions of BODIPY compounds. Reprinted from Nepomnyashchii, *et al.*, J. Am. Chem. Soc. **2011**, 133, 19498–19504.

1.4.3. PROPERTIES OF BODIPY DYES

1.4.3.1. Electrochemical properties

The redox characteristics of BODIPY derivatives are directly dependent on the level of substitutions on the *meso*, α, β positions on the BODIPY core structure in Figure 1.2. As more substituents are added to the core, the redox processes stabilize leading to well resolved cyclic voltammograms.[45] Nepomnyashcii *et al*.[41] demonstrated that when the BODIPY core is completely substituted, stable radical ions are produced and a reversible Nernstian one-electron oxidation and reduction behaviour are observed. For

the reduction of BODIPY, which lacks substitution on the *meso* position, a more reactive radical anion is produced. Moreover, lack of substitutions on positions 2,3,5,6 leads to irreversible redox behaviour due to a decrease in the stability of the radical cation produced on oxidation. The irreversible redox behaviour can also be caused by chemical side reactions; a typical example is oxidative polymerization. It has also been demonstrated that the redox potentials of BODIPY dyes are tunable, depending on whether an electron donating or withdrawing group is substituted at β2 or β6 position.[45]

1.4.3.2. Photophysical and optical spectroscopic properties

BODIPY dyes have remarkable photophysical and optical properties, synthesis allows one to alter and modify the photophysical characteristics of BODIPY derivatives by simply changing substituents on the core structure.[46,47] The photophysical properties are influenced by the nature, number, as well as the position of the attached substituent. The dyes are typically soluble in most organic solvents and they usually do not self-aggregate in most solutions such as phosphate buffer solution and aqueous solution of acetonitrile.[39] Other properties include; high fluorescence quantum yields, typically above 0.60 and high molar absorption coefficients {(4.0 – 8.0) $x10^4$ M^{-1} cm^{-1}}. BODIPY dyes are highly coloured,[48] with fluorescence emission profiles which are in the visible region, with narrow bandwidths and high fluorescence quantum yield, 0.67, which BODIPY-COOH is ten times higher than $[Ru(bpy)_3]^{2+}$ (quantum yield of emission, 0.062).[23,49]

Zheng *et al.*[50] demonstrates how the photophysics properties of BODIPY dyes can be tuned by altering or introducing different substituents on the BODIPY core. In their study they synthesized two BODIPY dyes, called PY1 and PY2 which are presented in Figure 1.3. The fluorescence quantum yield of PY1 dye which is the meso phenyl compound PY1 is much less than of its more substituted analogue PY2 owing to its aromatic structure. Interestingly the absorption and emission of PY2 are hypsochromically shifted compared to PY1. The observed differences in the photophysics properties are attributed to the β substituents on PY1 which are the two methyl groups, these prevent free rotation of the phenyl group, which reduces loss of energy from the excited states via non irradiative molecular relaxation. Furthermore, the methyl groups on PY1 can also lead to an increase in the dihedral angle between the BODIPY core and the phenyl group which results in a hypsochromic shifted absorbance or emission spectra.[41]

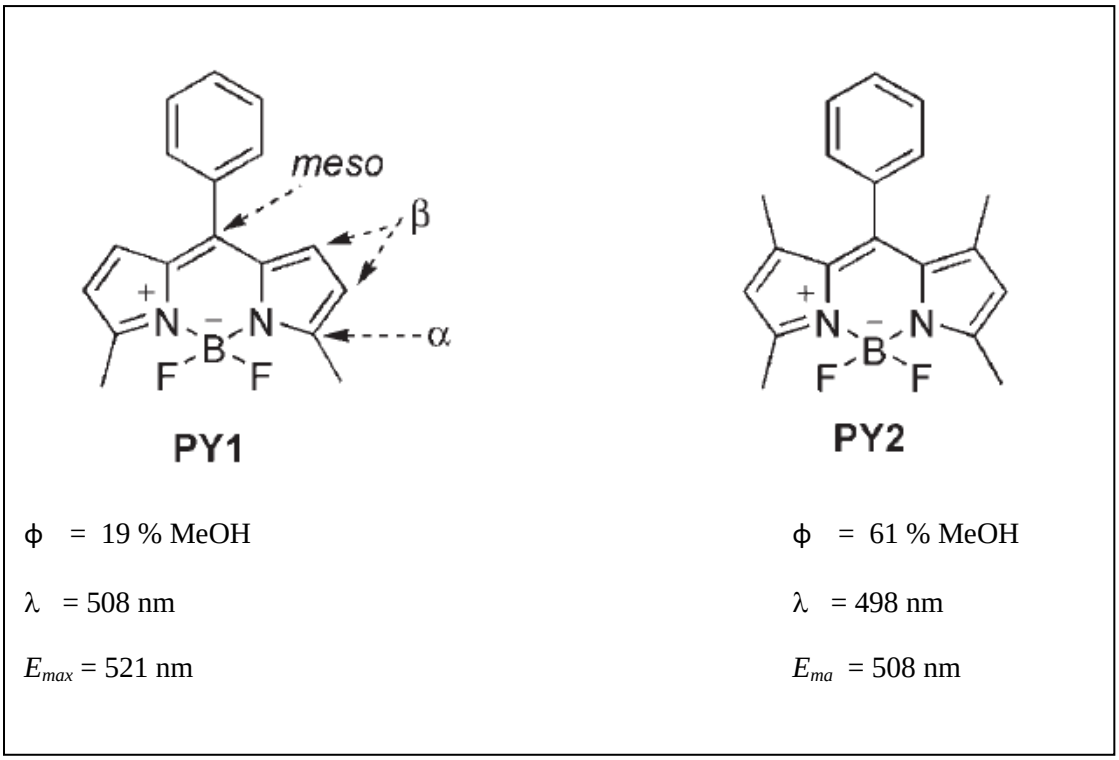

Figure 1.3: Chemical structures and Photophysical properties of PY1 and PY2. Reprinted from Zheng, Q., Xu, G., Prasad, P.N., *Chem. Euro. J*, **2008**,14, 5812-5819.

1. 4.3.3. Applications OF BODIPY dyes

The excellent photophysical and optoelectronic properties of BODIPY dyes make them among the most versatile fluorophores.[51] Highlights of their application include, laser dyes,[52] fluorescent switches, fluorescent labels for biomolecules and cellular imaging.[53] They are also used as light harvesters and photosensitizers which are used as cell killing dyes in photodynamic therapy.[54] Other areas of application in which BODIPY dyes have gained recognition are in; chromogenic probes and chemical sensors, solar cell technology,[55] thin film photovoltaics, fluorescent polymeric materials,

electroluminescent films in light emitting diodes and in electrochemiluminescence.[23,56]

1.5. ECL APPLICATIONS

ECL has been widely employed, in a wide range of analytical applications such as clinical diagnostics, immunoassays, biosensors, capillary electrophoresis, in trace analysis, liquid chromatography. Furthermore, ECL has also been used to determine different biochemical and chemical analytes in food and water, as well as also having applications in chemical warfare defence and pharmaceutical studies.[36]

1.5.1. CLINICAL DIAGNOSTICS

One of the most important applications of ECL is its use in commercial diagnostic assay market.[57] Due to a large number of analytes that have been studied and published reviews,[58] only a few examples are highlighted here. Usually the intensity of ECL emission is proportional to the concentration of the emitter or the coreactant, thus ECL can be used to analyze both the emitter and the coreactant. Most clinical assays use a format in which the label concentration is measured in the presence of excess coreactant TPA. Currently a variety of assays have been developed for a wide variety of applications including those for; thyroid diseases,[59] tumor and cardiac markers,[60] bone metabolism,[61] adrenal disorders,[62] analytes relevant to infectious diseases[63] and fertility and hormone tests.[64,65] Health conditions

such as renal failure, intestinal diseases, vitamin deficiencies and hyperoxaluria, are normally accompanied by high concentrations of oxalate in urine and blood. Formation of kidney stones which may lead to renal tissue damage has also been linked to precipitation of calcium oxalate in kidneys.[66] Bard and co-workers[39] developed a selective and precise method of determining oxalate in synthetic urine, in experiments that showed that $[Ru(bpy)_3]^{2+}$can generate ECL emission in the presence of oxalate as coreactant. The ECL intensity was linearly related to the concentration of oxalate over the range of 10^{-6} to 10^{-4} M, and this range incorporates oxalate concentration levels found in normal blood and urine.[67]

1.5.2. IMMUNOASSAYS

Many efforts have been taken to improve the sensitivity and extend applications of ECL immunoassays.[1,3] Since, biological targets are not ECL active hence, ECL tags are required to label biomolecules. In labelling biomolecules with ECL generating species, analytes can be determined at sub-picomolar levels. Most commercial assays are based on the $[Ru(bpy)_3]^{2+}$/ Tripropylamine (TPA) system , in which reactive groups are attached to the bipyridyl ligands to form active labels for proteins and nucleic acids, while TPA is present as coreactant in 100 mM excess concentration.[11] The $[Ru(bpy)_3]^{2+}$ derivative is covalently bound one of the partner species involved in the affinity binding reaction and luminescence depends on the concentration of the ECL emitter present. Hence, the ECL from the emitters is correlated to the concentration of analyte. For example a very sensitive sandwich-type immunoassay for the quantification of C-reactive protein (CRP) in human

plasma serum and a key maker of myrocardial infarction and inflammations has been developed.[9] The experiments illustrated with Figure 1.4, involved linking a biotinylated anti-CRP onto a gold electrode which has been pre-modified with a mixed thiol self-assembled monolayer of 3-mercaptopropanoic acid and 16 mercaptohexadecanoic acid which is covalently linked it to avidin, in the presence of 3-(3-dimethylaminopropyl) carboiimide hydrochloride (EDC) and *N*-hydroxysuccinimide (NHS). Subsequently, $[Ru(bpy)_3]^{2+}$ label was used to tag the anti-CRP and this modified electrode was immersed in a solution containing TPA. ECL generated by this label, its intensity was found to be proportional to the concentration of CRP analyte of interest over a dynamic range (1-24 μg/mol CRP). This dynamic range is biologically relevant as it covers most of the human plasmas and serums (0.2 – 15 g/mol CRP).[68]

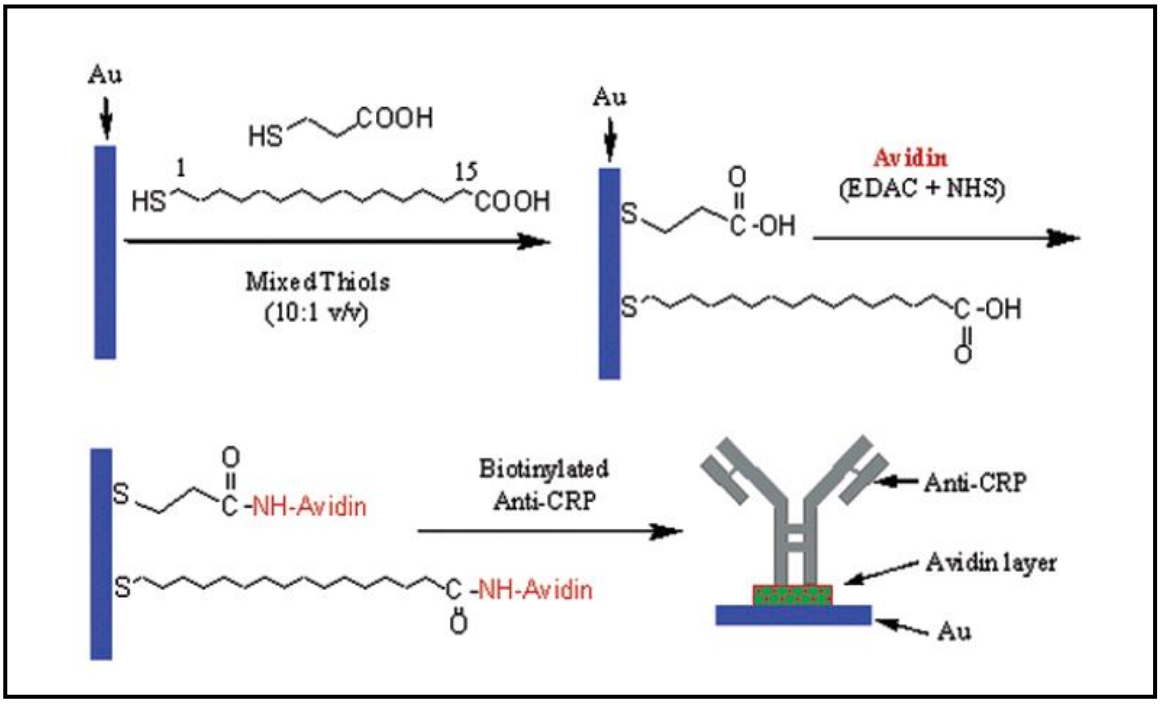

Figure 1.4: The attachment of anti CRP on the surface of Au (111) mixed SAMs / avidin layer. Reprinted from Miao, W., Bard, A. J., *Anal.Chem,* **2003**, 75, 5825-5834.

1.5.3. DNA DETECTION AND QUANTIFICATION

DNA detection and quantification are of great importance in a wide range of areas including; clinical diagnostics, pathogen detection, forensic chemistry, environmental investigations, and mutated gene diagnosis associated with human diseases.[69] Accordingly, efforts are aimed at the study of $[Ru(bpy)_3]^{2+}$ or its derivative are used as ECL label and TPA has been employed as a coreactant.[11,14] Many efforts have been undertaken to improve sensitivity of the DNA assays and these include several strategies, such as immobilization of multiple ECL labels on polystyrene microspheres, carbon nanotubes or gold or nano-particles.[70,71] Direct ECL detection of DNA using ultra thin films (~10 nm) of an ECL generating metallopolymer $[Ru(bpy)_2(PVP)_{10}]^{2+}$ where

PVP is poly (vinylpyridine) and guanine bases as coreactants has been demonstrated.[72] The ultra-thin films of the polymer were formed on the electrode through layer by layer assembly with DNA, the method was based on the idea that when guanine base were present in the oligonucleotide significant ECL can be generated.[73] The study has also been successfully extended to detection of oxidative and chemical DNA damage, whereby the metal centre was changed from ruthenium to osmium.[74] In a separate study, another approach has been employed to detect DNA using ECL, in which a biosensor was constructed by assembling a thiolated hairpin DNA on gold electrodes as the recognition element and a ruthenium complex as the luminophore. In the absence of the target single strand DNA the ECL probe immobilized on the electrode exhibited a strong ECL signal. Figure 1.5 illustrates that upon the introduction of target single strand DNA, the ECL probe on the electrode was converted into a double helix due to hybridization resulting in the tag moving far from the electrode surface. This resulted in a significant decrease of the ECL signal, which is associated with an increase of target DNA. A detection limit of 90 pM complementary single strand DNA limit was achieved.[75]

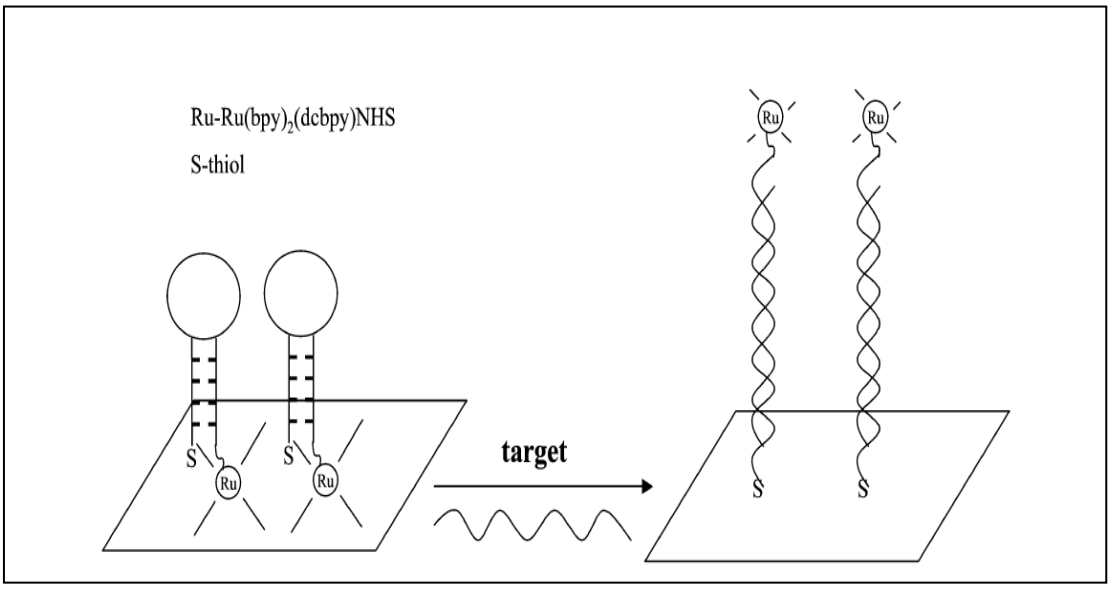

Figure 1.5: Schematic diagram of the hairpin- DNA probe detection for DNA hybridization. Reprinted from Zhang, J., Qi, H., Li, Y., Yang, J., Gao, Q., Zhang, C., *Anal. Chem.,* **2008**, 80, 2888-2894.

1.5.4. APTAMER BASED SENSORS

Electrochemiluminescent aptasensors have been developed for the detection of small molecules such as cocaine.[76] Aptamers are oligonucleic acid or peptide molecules that can selectively bind a specific target molecule. Recently, an ECL aptamer sensor based on a bipolar electrodes (BPEs) for detection of adenosine extracted from leukemia cells has been reported.[77] In this approach, the cathodic pole of the BP electrode was modified with a ferrocene labelled adenosine aptamer, which hybridized with its complementary DNA single strand. The presence of ATP was reflected by the decrease of the ECL Signal from BPE anodic pole caused by the target induced removal of the ferrocene.

1.6. CURRENT ECL LIMITATIONS AND THEIR SOLUTIONS

ECL has many distinct advantages over conventional chemiluminescence as discussed previously, however like many analytical techniques, it also has its own limitations. In electrogenerated chemiluminescence, there are two key origins of interferences with ECL. These include by-products of the CL reaction as well as species that are electrochemically active that may interfere with reaction at the electrode. Thus, some ECL methods include using chromatography or HPLC separation prior to ECL measurements.[1]

Despite the wide ECL analytical applications that have presented in the previous section, it is evident that only certain luminophores have widespread applicability. Annihilation ECL with organic luminophores has also limited applicability, this is because in general reactions involved take place in organic solvents, and if there is any water or oxygen in the solvents this can lead to quenching, thus the solvents need to be rigorously degassed prior to any measurements.[1] Furthermore, researchers have partially solved the problem of compatibility with aqueous solvents by synthesizing water soluble derivatives of organic luminophores.[1]

1.7. INTERFACIFIAL MODIFICATION OF ELECTRODES

1.7.1. OVERVIEW

The aforementioned applications have demonstrated that ECL is a powerful analytical technique, however, the solution based approach of generating ECL has numerous limitations. High reagent consumption rate is one key disadvantage because the luminescent reagent needs to be continuously supplied to the reaction zone. Furthermore, diffusion of the luminophore out of the detection zone, results in the loss of signal. One method of overcoming these disadvantages is by employing the luminophore in an immobilized format.[5] Ruthenium (II) tris (bipyridine) is one of the most extensively studied ECL luminophore and this is because of previously mentioned advantages it offers. As a result, researchers have devoted significant efforts towards developing methods of immobilizing luminophores such as $[Ru(bpy)_3]^{2+}$, as a means of overcoming the mentioned disadvantages. Moreover, the ability to modify electrode surface with ECL reagents increases the scope of potential ECL applications within biomedical sensor and device design.

Several strategies have been developed to immobilize luminophores on electrode surfaces, one of the approaches is by non covalent attachment to the electrode, for example Langmuir-Blodgett films or electrostatic self-assembled monolayers.[73] Considerable attention has been paid to incorporation of $[Ru(bpy)_3]^{2+}$ into a cationic ion exchange polymer such as Nafion.[67] Bartetoncello *et al.*[62] reported ECL detection from $[Ru(bpy)_3]^{2+}$ that

has been incorporated in Nafion Langmuir-Schaefer (LS) films (Nafion-$[Ru(bpy)_3]^{2+}$) using a novel one step procedure that allowed the $[Ru(bpy)_3]^{2+}$ to be directly incorporated within the Langmuir monolayer formation. These electrodes were tested for the electrocatalytic reduction of tripropylamine. Significant catalysis was observed due to the rapid turnover of $[Ru(bpy)_3]^{2+/3+}$ between the electrode surface and outer boundary of the film.[62] High concentration of luminophore can be immobilized on the electrode using the above mentioned strategies, however, non-covalent attachment can lead to the surface material leaching from the electrode.[62] This makes it challenging to unambiguously confirm whether emission that is measured arises from the bound material or of leached surface material into the surrounding electrolyte.[54,72]

To overcome this challenge, the luminophore can be covalently attached to the surface of the electrode and examples of luminophore being covalently bonded encapsulated in the sol gels have been previously reported.[78] Sykora and Meyer[79] reported ECL of $[PS\text{-}\ CH_2CH_2NHCO\text{-}(Ru^{II})_{18}]^{36+}$ immobilized in a silica sol gel matrix in the presence oxalate. ECL has also observed from $[Ru(bpy)_3]^{2+}$ encapsulated in sol gel glasses using TPA as coreactant. Several factors should be taken into consideration when developing interfacial film based ECL. For example sufficient concentration of the luminophore should be attached to the electrode surface, as the ECL intensity is directly proportional to the luminophore concentration. Bartetoncello *et al.*[62] reported the concentration of Nafion-$[Ru(bpy)_3]^{2+}$ composites in immobilised and

solution phases to be 0.13 and 0.33 mol.dm^{-3}, lower concentration was due to the compactness of the LS films. The composite films should be able to sustain electron transfer between the electrode and the luminophore. Finally, the interaction between the luminophore and the immobilization medium should be strong enough to avoid leaching of the luminophore, to ensure good stability and reproducibility. In the current work a method of confining an ECL luminophore $[Ru(bpy)_2PIC]^{2+}$ to the electrode is investigated by incorporating it within a conducting polymer polyaniline film . The resulting films show well defined redox processes associated with the $Ru^{2+/3+}$ couple and reveal significant electronic interactions between the PANI and ruthenium complex.

1.7.2. MODIFICATION WITH SELF-ASSEMBLED MONOLAYERS (SAM)

BODIPY-COOH ECL reagent (Chapter 2) is immobilized to a platinum electrode via cysteamine or L-cysteine self assembled monolayers (SAM). SAMs are organized assemblies formed by adsorption of molecular constituents from gas or solid phase onto substrate.[80] The substrate is the platform upon which the modifying layer is assembled, generally substrates are chosen for good mechanical and chemical stability, strong bond with monolayer and often pre-treated before modification. The pre-treatment can involve processes such as polishing the electrode, or chemical procedure which prepares the surface for subsequent modification steps.

The molecules that form SAM comprise of a head group, which has a specific affinity to the substrate, such as SH of an alkane thiol and stabilizing lateral interactions are important[81,73]. Head groups bind to different substrates such as specific metals, metal oxides and semiconductors.[80,79] A comprehensive list of examples of head groups and examples of the substrates they can bind to is reported in a review elsewhere.[74,75] The most investigated class of SAMs are those derived from alkane thiols on gold,[81] mercury,[82] silver,[83] copper, palladium,[84] and platinum,[85]. Thiols and related molecules have several attractive characteristics and the monolayers can be easily formed on the above mentioned substrates by exposing them to the thiol dissolved solutions.[86,87] For gold the thiol- metal bond is very stable with a bond strength of 100 kJ mol^{-1} as a consequence of this strength the functionalized surfaces are stable when in contact with a wide range of solvents, potentials and temperature.

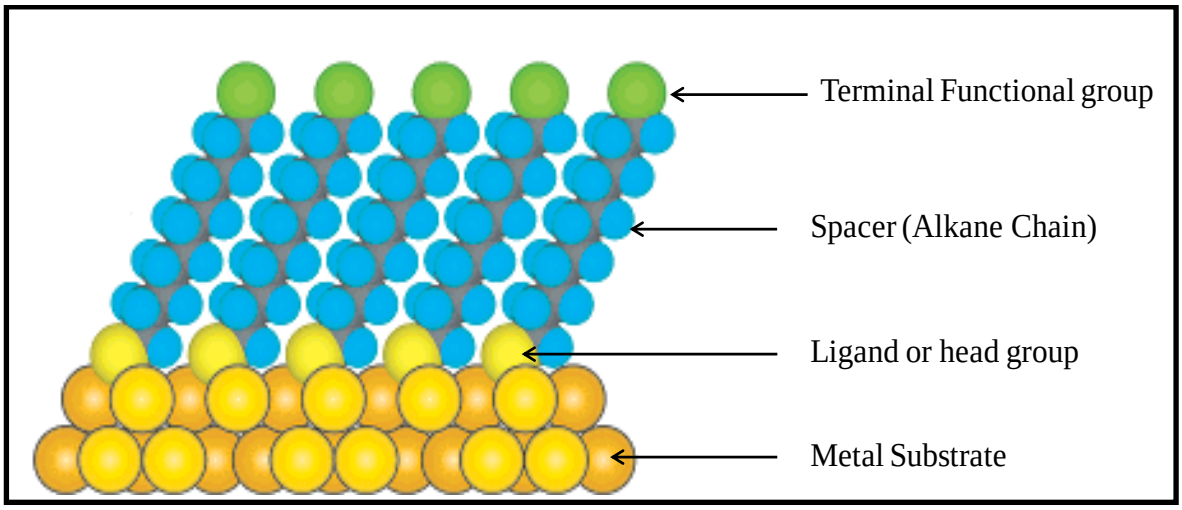

Figure 1.6: Schematic representation of an ideal single crystalline SAM on a gold surface with a (111) texture. Reprinted from; Love *et al*., Self-assembled monolayers of thiolates on metals as form of nanotechnology*, Chem. Rev.* **2005**, 1103-1169.

Figure 1.6 above represents a typical SAM and its components, which all serve a specific purpose. The ligand or head group serve to stabilize the atoms on the surface and modifies the electronic states. The alkane chains make up an organic interface which acts as physical barrier and provides well defined thickness. Lastly, the terminal groups, determine the surface properties and present functional groups for coupling of electrode and complex. In the case of attaching an ECL luminophore to the SAM,[88] the type of terminal functional group on the SAM will improve photophysical and electrochemical properties of the electrode.[89,90]

1.7.3. OVERVIEW OF PROCESSES AT A MODIFIED ELECTRODE

Heterogeneous electron transfer across the electrode/ monolayer interface is an important principal process in a case where a monolayer is contact with a supporting electrolyte. To fully understand properties of thin films on electrodes, mass transfer and reaction kinetics must be considered. Figure 1.7 illustrates the electrochemical and mass transport events that can occur at an electrode polymer modified electrode, wherein a primary reactant A, in the external solution is converted to a product B. This can occur by mass transport of A moving through the film to the underlying electrode or by the cross reacting with a catalyst Q, contained in the film and renewed electrochemically.[91] For an ideal responding redox properties of the material immobilized at the surface of an electrode, several assumptions are made and these are as follows. Firstly, it is assumed that since the redox couple is

not in solution, but adsorbed on the electrode surface its contribution to Faradiac current is negligible since its concentration is sufficiently low. Furthermore, all adsorption sites on the surface are equivalent and the oxidized and reduced forms occupy equal areas on the surface. Other assumptions are that the free energy of adsorption at maximum surface coverage is equal to the surface activity, and independent of the applied potential. Finally, it is also assumed that the Faradaic and capacitive currents can be separated.[91]

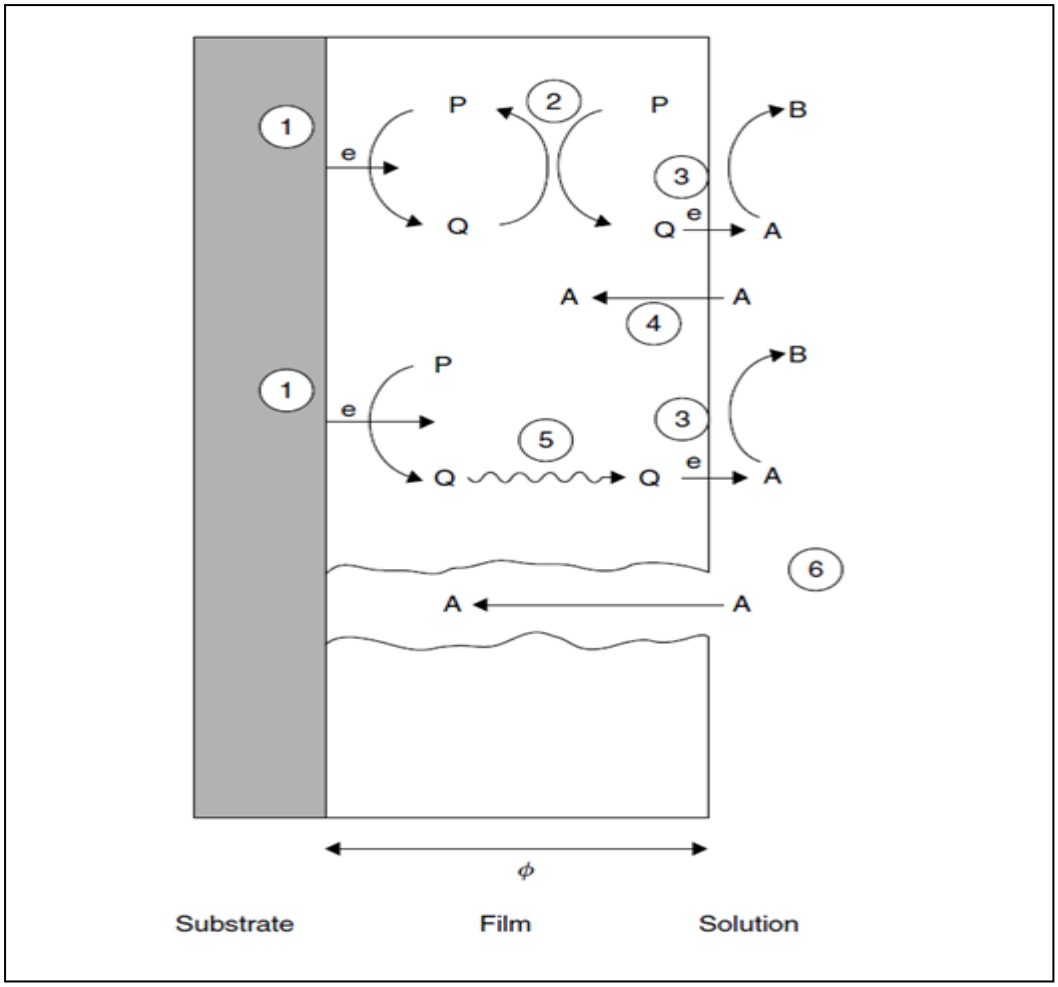

Figure 1.7: Schematic illustration of the processes that can occur at a modified electrode, where P represents a reducible substance in a film on the electrode surface and A is a species in solution. Processes shown are; (1) Heterogeneous electron transfer to P to produce the reduced form Q, (2) Electron transfer from Q to another P in the film (electron diffusion or electron hopping in the film), (3) Electron transfer from Q to A at the film/solution interface; (4) Penetration of A into the film (where it can also react with Q or at the substrate / film interface); (5) movement (mass transfer) of Q within the film; (6) movement of A through a pinhole or channel in the film to the substrate where it can be reduced in the film to the substrate where it can be reduced. Reprinted from Bard, A.J., Faulkner, L.R., *Electrochemical methods: Fundamentals and Applications*, 2nd ed, **2001**, John Wiley and Sons Inc: New York.

1.8. EXPERIMENTAL TECHNIQUES

For ECL experiments to be carried out, the fundamental redox behaviour of the compounds of interest must be understood. Therefore as a prelude to ECL, preliminary electrochemical studies such as; cyclic voltammetry or voltammetry at an RDE, DC- polarography are carried out.[92,93] In this study cyclic voltammetry was the technique of choice used to investigate the electrochemistry and understand the redox properties of the compound of interest. In addition, spectroscopic techniques were used for characterization of the material deposited on the electrode.

1.8.1. CYCLIC VOLTAMMOGRAM (POTENTIAL SWEEP)

Cyclic voltammetry is a widely used electrochemical technique, which gives both qualitative and quantitative information about the electrochemical reactions. It is frequently used for qualitative analysis, as it offers a rapid means of determining the redox potentials of the electro active species, to detect reaction intermediates and to evaluate follow up reactions of products formed at the electrodes.[94] Furthermore, CV provides quantitative information about the thermodynamics and kinetics of electron transfer across the electrode/ film interface. The most common configuration for running a CV experiment involves the use of three electrodes, which are all connected to a commercially available potentiostat. These include the working electrode such as gold or platinum, a reference electrode for example Ag/AgCl (saturated

KCl) or SCE and a counter (auxiliary) electrode normally a platinum wire is used. The potential applied at the working electrode is scanned with respect to a reference electrode with time at a controlled scan rate in a solution of compound(s) of interest in a solvent and supporting electrolyte which is required to achieve the required conductivity. The applied potential is initially swept in one direction from the $E_{initial}$ towards the E_{final}, subsequently the sweep direction is reversed to the initial potential. This constitutes one complete cycle in cyclic voltammetry and a CV may use one full cycle, a partial cycle or several cycles.[95] For the duration of the potential sweep the potentiostat measures the resulting current that results from the applied potential. A typical result output obtained from this experiment is a plot of current *versus* applied voltage (*I* vs *E*).

1.8.2.1. CV of solution phase species

In a solution containing the oxidized form of redox couple, O, of the electroactive analyte, the potential is initially swept linearly from a potential at which no faradic reaction takes place to a negative potential direction. When the potential reaches the redox potential of the species, an increase in cathodic current density is observed. Figure 1.8 illustrates the expected response of a CV for a species in solution which is fully reversible, displaying important parameters which are normally monitored.

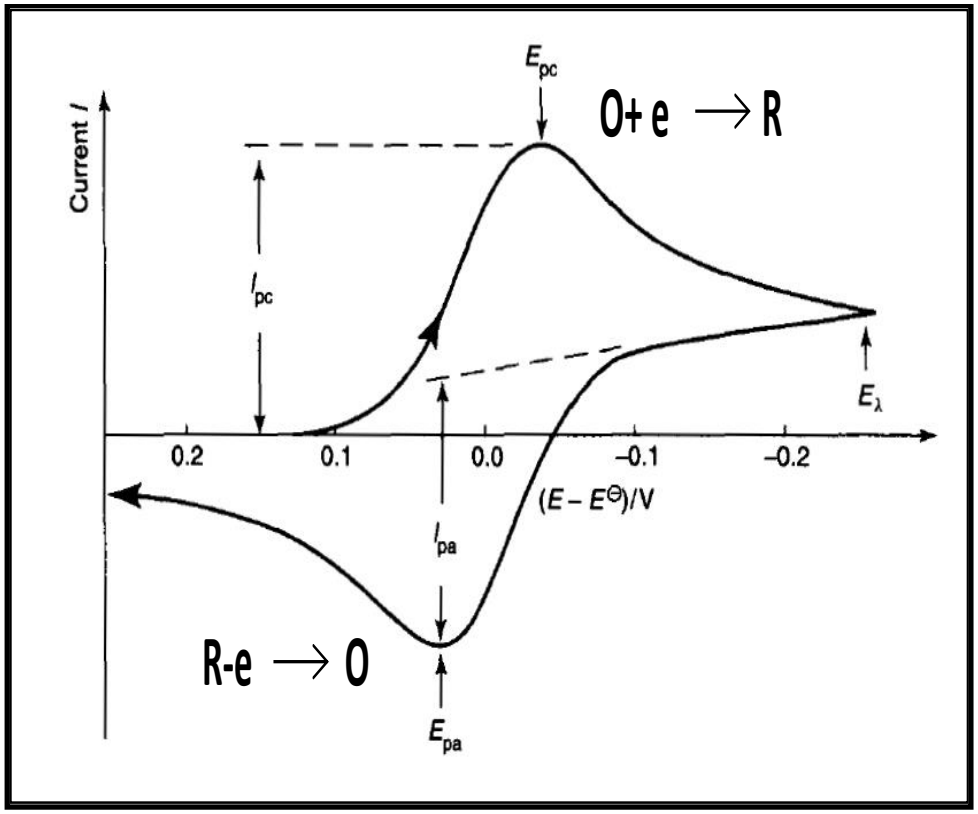

Figure 1.8: Cyclic voltammogram for redox reaction at a solid electrode. The initial solution contained only the oxidized form of the redox couple. The upper (cathodic) peak represents the reaction, while the lower (anodic) peak represents the electrode reaction. Reprinted from; Monk, P., *Fundamentals of Electro-Analytical Chemistry*, **2001**, Manchester: John Wiley and Sons.

The parameters which are normally monitored in a CV, include anodic and cathodic peak current (I_{pa} and I_{pc}), peak potentials (E_{pa} and E_{pc}), At the formal potential, 50:50 ratio of oxidized to reduced species exists in solution. At the cathodic peak potential, the current starts to decay as the diffusion layer extends further away from the surface and as the potential becomes sufficiently negative, reduction can no longer occur resulting in the Faradic current reaching zero. At this point, oxidation of the reduced species begins, resulting in an increase in the anodic peak current and a depletion of the

oxidized species. The independent variables are the potential window over which the scan is conducted, and the voltage scan rate. The latter can be varied typically between 0.005 to 0.900 V s^{-1} and by varying the scan rate insights about the redox system can be gained. Under reversible conditions, the scan rate can be related to the peak current according to the Randles-Sevçik Equation [1.23].

$$i_P = (2.69x10^5)n^{3/2}AD_{CT}{}^{1/2}Cv^{1/2} \quad \textbf{[1.23]}$$

where *n* is the number of electrons transferred, *A* is the area of the electrode (cm^{-2}), *D* is the diffusion coefficient (cm^2 s^{-1}) and *C* is the concentration of the redox species (mol/cm^{-3}). In a reversible system, it was reported that the peak potentials are not related to the change in scan rate. However, they can be influenced by ohmic (*IR*) drop effects. Ohmic drop results from currents flowing through a solution generating a potential that decreases the applied potential by an amount *IR*, whereby *I* is the total current flow in the solution and *R* is the solution resistance.[96] The effects of the ohmic drop can be minimized by using high concentrations of the supporting electrolyte which are highly conducting and also by working with low currents. When ohmic effects and slow electron transfer rates are not present, under semi diffusion conditions for a reversible electrode reaction at 25 °C, the peak to peak splitting, $\Delta E_{p,}$ and the formal potential, $E°$, are calculated according Equation 1.24 and 1.25.

$$\Delta E_p = \frac{57}{n} \text{ mV} \quad \textbf{[1.24]}$$

$$E° = (E_{pa} + E_{pc}) / 2 \quad \textbf{[1.25]}$$

1.8.2.2. CV of surface adsorbed species

Cyclic voltammograms obtained from materials which are in solution and those which are adsorbed on the surface of the electrode exhibit distinct voltammetric responses. This is because when the material is surface-confined the redox active material is adsorbed on the electrode and thus, it does not have to diffuse to/or from the electrode surface. Under ideal conditions the resulting CV of the surface-adsorbed species are Gaussian in shape, symmetrical and the peak to peak separation is zero compared to a free diffusing species.[97] These characteristics can be ascribed to the existence of fixed amount of species on the electrode surface, which is not influenced by mass transfer. Figure 1.9 displays a cyclic voltammogram of a theoretical response for a slow scan of an electrochemically reversible couple that is confined to the surface of the electrode.

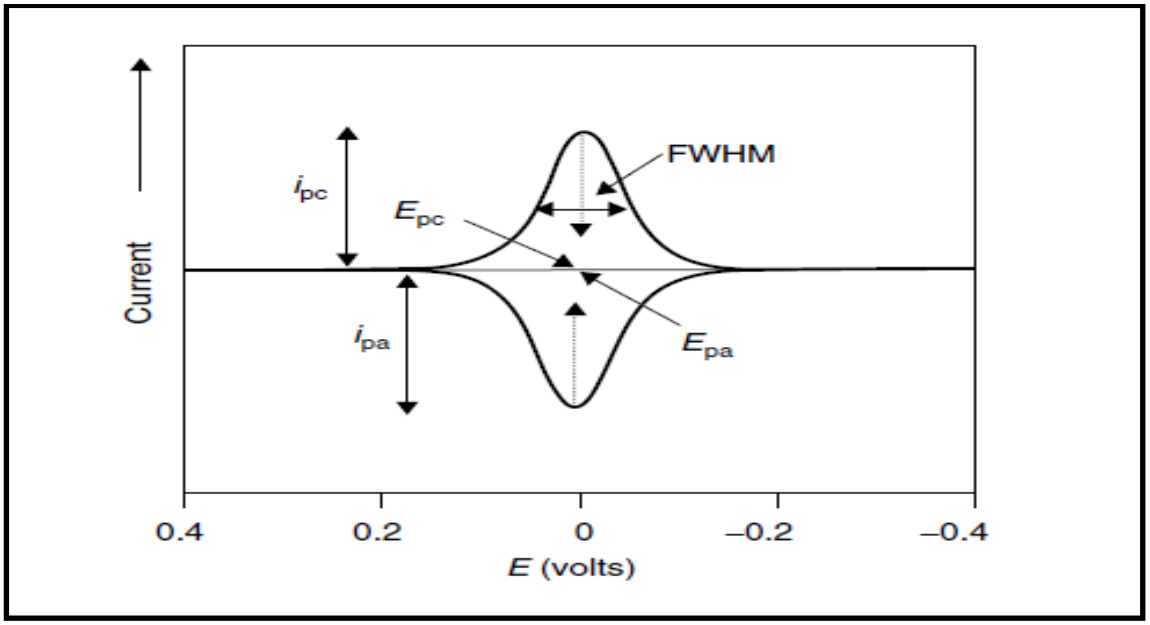

Figure 1.9: Current-potential curves obtained from cyclic voltammetry measurements for the reduction and oxidation of an adsorbed interfacial supramolecular assembly under finite diffusion conditions. Reprinted from Forster, R. J., Keyes T. E., Vos, J. G. *Interfacial Supramolecular Assemblies*, **2003**, England , John Wiley & Sons, Ltd.

The characteristic features of an ideal cyclic voltammogram of a surface confined species are presented as according to Equations 1.26-1.27.

$$E_{pc} = E_{pa} \qquad \textbf{[1.26]}$$

$$\frac{I_{pc}}{I_{pa}} = 1 \qquad \textbf{[1.27]}$$

$$I_p = \frac{n^2 F^2}{4RT} \text{ v A } \Gamma \qquad \textbf{[1.28]}$$

Equation 1.38 shows that peak current can be related to the surface coverage, Γ, Whereby, F is the Faraday constant (C mol^{-1}), R is the gas constant (J K^{-1} mol^{-1}) and T is the absolute temperature (K) for estimation of surface coverage in solution. In the case of a surface adsorbed species, the peak current varies linearly with scan rate in contrast to a freely diffusing species in solution, which varies with the root of scan rate according to the Randles-Sevçik Equation [1.33]. The surface coverage (mol cm^2), can be determined by measuring the Faradaic charge, Q, passed under the current potential curve, during oxidation and reduction of the adsorbed layer according the following equation;

$$\Gamma = \frac{Q}{nFA} \qquad \textbf{[1.39]}$$

where n is the number of electrons transferred, F is the Faraday constant, A is the real or microscopic area of the electrode (cm^{-2}). Assuming that there are no lateral interactions between the surface adsorbed species, under Nernstian conditions, no peak to peak splitting is expected and full width at maximum (FWHM) of the anodic and cathodic peak, can be determined as given in Equation 1.40.

$$\text{FWHM} = \frac{90.6}{n}\ \text{mV} \qquad \textbf{[1.40]}$$

It should be noted that voltammetric response may deviate from the ideal voltammetry due to several reasons. A non-zero peak splitting may indicate intermolecular interactions between redox centers, ion paring or where switching the redox composition causes structural change in the orientation of

the adsorbates.[1,2] Moreover, large values of FWHM may be caused by a distribution of the formal potentials, thus a non-uniform or disorganized adsorbed layer may result in peak broadening as the local potential or the microenvironment of each individual adsorbed redox molecule may differ.[21]

1.8.3. SPECTROSCOPY

1.8.3.1. Luminescence spectroscopy

Luminescence is the emission of light from molecules that have been promoted to an excited state, by for example light absorption and were used in this work for electronic and absorptions of the material on the electrode.

The principle behind this method is explained by the Jablonski diagram shown in Figure 1.10. The diagram illustrates photophysical processes for an excited singlet ground, the first excited electronic states are depicted by S_0, and S_1. At each of these electronic states, fluorophores can exist in vibrational energy levels numbered v = 0,1,2,3, and 4. Following absorbance of light, molecules are excited from the lowest vibrational energy level v = 0, of the ground electronic state, S_0 and populate one of the higher vibrational levels of higher electronic states, *i.e.* S_1 or S_2. Fluorescence occurs when the excited molecule undergoes collisional deactivation and as a result relaxes from the v = 0 state of S_1 to the different vibrational levels of the S_0, resulting in the emission spectrum.[14,98]

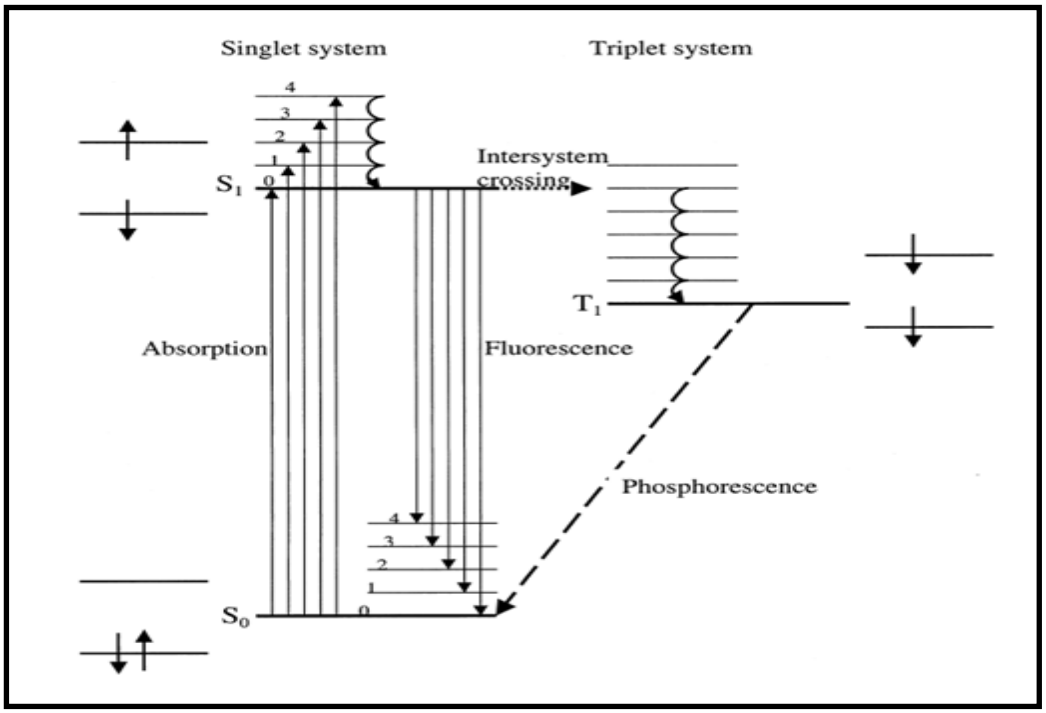

Figure 1.10: Jablonski diagram: Representation of energy levels and molecular orbital during the absorption and emission of radiation. Reprinted from; *Electrogenerated Chemiluminescence,* ed. Bard, A. J., **2004**, New York: Marcel Dekker.

Figure 1.10 also shows that some molecules which are in condensed phases can rapidly relax from a higher vibrational level, e.g. v = 0 to the lowest vibration level of S_1 and this process is known as internal conversation and it generally occurs within 10^{-12} seconds. Molecules in the excited singlet state can also undergo a spin conversion to the first triplet state, T_1 and the processing of converting from S_1 to T_1 is known as intersystem crossing. Emission from T_1 to S_0 is a radiative process termed phosphorescence, however this transition is forbidden, thus, the rate constant of this process is several orders of magnitude lower than that of fluorescence.

1.8.3.2. Raman spectroscopy

Raman is a vibrational spectroscopic technique which involves the measuring of wavelength and the intensity of in elastically scattered light from molecules. In a typical experiment a monochromatic incident laser beam is focused onto a sample using a microscope and the radiation scattered from the sample is monitored. The scattered light is directed back along the same optical path and focused through a pin hole to a charge coupled detector. The incident light from a substrate can be scattered in two possible ways which are; Rayleigh or and Raman scattering.[99] In the event that most of the light is scattered without change in photon frequency, *.i.e.* the wavelength of light is preserved the process is known as Raleigh scattering and this is an elastic process. In Raman scattering, a small fraction of the exciting wavelength interacts with the polarized field of a vibrating molecule, this causes the photons to scatter in with either additional energy (anti – Stokes lines) or less energy (Stokes lines).[100]

Raman spectroscopy (RS) in this study was used to investigate interfacial films on the electrodes. RS it can provide insights about film structural, but because the potential of the Raman scatter is weak it is often challenging to sensitively detect monolayers.[72] Thus to achieve greater sensitivity for detection of monolayers or films Resonance Raman spectroscopy (RRS). RRS can be applied in a case where the frequency of the laser overlaps within the electronic transition of the sample this leads to enhancement because there is greater interaction between the light and the molecules in the sample. For example in Chapter 4 RRS was used to investigate the

binding of DNA to $[Ru(dppz)(bpyArCOOH)_2]^{2+}$ monolayer. RRS has low detection limits, and the Raman bands are enhanced 10^2 to 10^6 times greater than the normal bands.

1.8.4. MICROSCOPY

Confocal fluorescence microscopy is an imaging technique that uses point illumination and a spatial pinhole to eliminate out of focus light in samples that are thicker than the focal plane, hence, this microscopy was used to provide surface morphology of the species coated on the electrode.[97,101] In a confocal system light from the excitation source is passed through a pinhole before it reaches a condenser lens, using an objective lens the light is focused into a cone shaped beam, this allows for maximum intensity of light to strike a specific spot with in the sample.[97] However, fluorescence from around, *i.e.* above and below the focal point is still observed, thus using a dichroic mirror this fluorescence is focused onto a second pinhole aperture, such that only light from the focal point reaches the detector. This eliminates the fluorescent light from outside the sample volume, yielding very high sensitivity and a sub-micron spatial resolution.

1.9. CONCLUSION

Chapter 1 presented a review of literature related to practise and application. The chapter introduced basic concepts of ECL, it also highlighted the pathways and mechanisms involved in generating ECL. The literature presented here focuses on the types of luminophores used and different coreactants, such as BPO, H_2O_2, TPA which are all used in the ECL studies of Chapter 2 and 3. $[Ru(bpy)_3]^{2+}$ has been the luminophore of choice in most ECL studies, indicated by its use in most of the applications highlighted in the applications presented here, however. There is ongoing need for introduction of new novel ECL luminophores, and BODIPY dyes are one of these new dyes which are studied in Chapter 2 to reveal their RCL properties and potential applications. It has been indicated that solid state ECL exhibits several advantages over solution phase, and since Chapter 3 deals with immobilization of ruthenium complex in polymer, the literature reviewed here discussed, strategies of immobilizing ECL reagent using a conduction polymer or self-assembled monolayers. Chapter 4 and 5 deal with application of ECL for detection of biological molecules (e.g DNA and cells), the literature that has been surveyed, it is evident that ECL is powerful tool with many applications in a variety of areas such as DNA detection and quantification, clinical diagnostic assays being the most important commercial application to date.

1.10. REFERENCES

[1] Knight, A., *Trends Anal. Chem.,* **1999***,* 18, 47-62.

[2] Liu, Z., Qi, W., Xu, G., *Chem. Soc. Rev.*, **2015**, 44, 3117-3142.

[3] Richter, M. M., *Chem. Rev.,* **2004***,*104, 3003-3036.

[4] Sentic, M., Arbault, S., Bouffier, L., Manojlovic, D., Alexander Kuhn, A., Sojic N., *Chem. Sci.*, **2015**, 6, 4433-4437.

[5] Forster , R. J., Hogan , C. F., *Anal. Chem.,* **2000***,*72, 5576-5582.

[6] Han, X., Huang, C., Chen, X., Lu Y., Yang, W., *Chem. Commun.*, **2015**, 51, 14720-14723.

[7] Knight, W. G.,Greenway, G. M., *Analyst*, **1999**, 119, 879-890.

[8] Khoshfetrat, S. M., Ranjbari, M., Shayan, M., Mehrgardi, M. A., Kiani, A., *Anal. Chem.*, 2015, 87, 8123-8131.

[9] Bertoncello, P., Forster, R.J, *Biosens. Bioelectron.*, **2009**, 24,191–3200.

[10] Lai, R. Y., Bard, A. J., *J. Phys. Chem. B*, **2003**, 107, 5036-5042.

[11] Miao, W., Choi, J.,*Coreactants. In Electrogenerated Chemiluminescence,* ed. Bard, A. J., **2004**, New York: Marcel Dekker.

[12] Forster, R. J., Bertoncello, P., Keyes, T. E., *Annu. Rev. Anal.l Chem.,* **2009**, 2, 18.1-18.27.

[13] Swanick, K. N., Dodd, D. W., Price, J. T., Brazeau, A. L., Jones, N. D., Hudson, R. H., Ding, Z., *Phys. Chem. Chem. Phys.,* **2011**, 13, 17405-17412.

[14] Bard, A. J., *Introduction in Electrogenerated Chemiluminescence,*ed. Bard. A. J., **2004**, New York: Marcel Dekker.

[15] Pyati, R., Richter, M. M., *Annu. Rep. Prog. Chem. Sect. C: Phys.Chem.,* **2007**, 103,12–78.

[16] Wei, H., Wang, E**.**, *Lumines.*, **2011**, 26 , 77–85.

[17] Luo, X., Li, Y., Zheng, J., Qi, H., Liang Z., Ning X., *Chem. Commun.*, **2015**, 51, 9487-9490.

[18] Leland, J. K., Powell, M. J., *J. Electrochem. Soc.*, **1990**, 318, 3127-3131.

[19] Chang, M. M., Saji, T., Bard, A. J., *J. Amer. Chem. Soc.,* **1977**, 99, 5399-5403.

[20] Rubinstein, I., Bard, A., *J. Amer. Chem. Soc.,* 1**981**, 103, 512-516.

[21] Zou, G., Ju, H., *Anal. Chem.,* **2004**, 76, 6871-6876.

[22] Choi, J., Bard, A. J., *Anal. Chim. Acta*., **2005**, 541, 143-150.

[23] Tokel, N. E., Hemingway, R. E., Bard, A. J., *J. Amer. Chem. Soc.,* **1973**, 95, 6582-6589.

[24] Lee, W. Y., *Mikrochim. Acta.*, **1997**, 127, 19-39.

[25] Pellegrin, Y., Keyes, T.E., Forster, R.J., *Inorg. Chim. Acta*., **2009**, 362, 1715-1722.

[26] Pinter, J.S., Brown, K.L., Deyoung, P.A., Peaslee, G.F., *Talanta.*, **2007,** 71, 1219-1225.

[27] Angenendt, P., *Drug Discovery Today.*, **2005**, 10, 503-511.

[28] Wolf, M., Juncker, D., Michel, B., Hunziker, P., Delamarche, E., *Biosen. Bioelectron.*, **2004**, 19, 1193-1202

[29] Venkatanarayanan, A., Crowley, K., Lestini, E., Keyes,T. E., Rusling, J.F Forster, R. J*., Biosen. Bioelectron.*,, **2012**,31, 233- 230

[30] Johnston, D. H., Glasgow, K. C., Thorp, H. H. *J. Amer. Chem. So*c., **1995**, 8901-8938.

[31] Weltch, T.W., Corbett, A. H., Thorp, H. H., *J. Phys. Chem.*, **1995,**99, 11757-11763.

[32] Ontko, A. C., Armistead, P. M., Kircus, S. R., Thorp, H. H.**,** *Inorg. Chem*., **1999,** 38, 1842-1846.

[33] Barton, J. K., Goldberg, J. M., Kumar, C. V.,Turro, N. J., *J. Amer. Chem. Soc*., **1986,**108, 2028-2090.

[34] Kumar, C. V., Barton, J. K., Turro, N. J., *J. Am. Chem. Soc.*, **1985**, 105, 5518- 5523.

[35] Hu, L., Bian, Z., Li, H., Han, S., Yuan, Y., Gao, L., Xu, G., *Anal. Chem,* **2009***,* 81, 9807-9811.

[36] Hu, L., Xu, G., *Chem. Soc. Rev.*, **2010**, 39, 3275-3304.

[37] Forry, S. P., Wightman, R.. M., *Organic ECL Systems in Electrogenerated Chemiluminescence.* ed. Bard., A. J., **2004**, New York: Marcel Dekker.

[38] Collinson, M. M., Wightman, R. M., Pastore, P., *J. Phys. Chem.,* **1994**, 98, 11942-11947.

[39] Nepomnyashchii, A. B., Bard, A. J., *Acc. Chem. Res.*, **2011**, 45, 1844-1853.

[40] Adarsh, N., Krishnan, M. S., Ramaiah, D., *Anal. Chem.*, **2014**, *86*, 9335-9342.

[41] Nepomnyashchii, A. B., Broring, M., Ahrens, J., Bard, A. J., *J. Amer. Chem. Soc.,* **2011,** 133, 19498-19504.

[42] Schmitt, A., Hinkeldey,B., Wild., M.**2009**, *J. Fluoresc.*, 19, 755-758.

[43] Loudet, A., Burgess,K.,*Chem. Rev.*, **2007**,107, 4891-4932.

[44] Hesari, M., Swanick, K. N., Lu, J. S., Whyte, R., Wang, S., Ding, Z., *J. Amer. Chem. Soc.,* **2015**, 137, 11266-11269.

[45] Benniston, A.C., Copley, G., *Phys. Chem. Chem. Phys.,* **2009***,* 11, 4124-4131.

[46] Qin, W., Baruah, M., Van der Auweraer,M., De Schryver, F.C., Boens,N., *J. Phys. Chem. A.,* **2005**, 109, 7371-7384.

[47] Hesari, M., Barbon, S. M., Staroverov, Zhifeng Ding, Z., Gilroy, J. B., *Chem. Commun.*, **2015**, 51, 3766-3769.

[48] Maar, R. R., Barbon, S. M., Sharma, N., Groom, H., Luyt, L. G., Gilroy, J. B., *Chem. Eur. J.*, **2015**, 21, 15589-15599.

[49] Qin, W., Rohand, T., Baruah, M., Stefan, A., Van der Auweraer, M., *Chem. Phys. Let.*, **2006**, 420, 562-568.

[50] Zheng, Q., Xu, G., Prasad, P.N., *Chem. Eur. J.*, **2008**, 14, 5812-5819.

[51] Martin, A.,Long, C., Forster, R.J., Keyes,T.E**.**, *Chem. Commun.*, **2012**, 48, 5617-5619.

[52] Costela, A., Morenoa, I., Sierrab,M., Guerrib, F., Lirasc, M*., J. Photochem. Photobiol. A.*, **2008**, 198, 192-199.

[53] Didiera, P., Ulrich ,G., Mélya,Y., Ziessel,R., *Org. Biomol. Chem.,* **2009**, 7, 3639-3664.

[54] Atilgan, S., Ekmekci, Z., Dogan,L., Gucb, D., Akkaya,E.U., *Chem. Commun.*, **2006**, 42, 4398–4400.

[55] Kolemen, S., Cakmak, Y.,Erten-Ela, S., Altay, Y., Brende, J., Thelakkat, M., Akkaya, E. U., *Org. Let.,* **2010**, 12, 3812-3815.

[56] Zhu, X., Huang, H., Liu, R., Jin, X., Li, Y., Wang, D., Wang, Q., Zhu, H., *J. Mater. Chem. C*., **2015**, 3, 3774-3782.

[57] Deaver, D. R, *Nature.*, **1995**, 377, 758-760.

[58] Richter,M. M., *Chem. Rev., **2004**,*104, 3003-3036.

[59] Sanchez- Carbayo, M., Mauri, M., Alfayate, A., Miralles, C., Soria. F., *Clin. Biochem.*, **1999**, 32, 395-403.

[60] Miao, W., *Chem. Rev.,* **2008**, 108, 2506-2553.

[61] Seck, T., Diel, H., Bismar, Ziegler, R., Pfeilschifter, *J. Bone.*, **2002**, 30, 217-222.

[62] Verschraegen, I., Anckaert, E., Schiettecatte, J., Mees, M., Garrido, A., Hermsen, D., Lentjes, E. G., W. M., Liebert, A., Roth, H., Stamminger, G., Smitz, *J. Clin. Chim. Acta.,* **2007***,* 380, 75-80.

[63] Weber, B., Bayer, A., Kirch, A., Schluter, V., Schlieper, D., Melchior, D., *J. Clin. Microbiol.,* **1999**, 37, 2639- 2647.

[64] Gassler, N., Peuschel, T., Pankau, R., *Clin. Lab.*, **2000**, 46, 553-560.

[65] Debad, J. D., Glezer, E. M., Leland, J. K., Sigal, G. B., Wohlstadter, J., *Clinical and Biological applications of ECL in Electrogenerated Chemiluminescence.* ed. Bard, A. J., **2004**, New York: Marcel Dekker.

[66] Rubinstein, I., Martin, C. R., Bard, A. J., *Anal. Chem.*, **1983,** 55, 1580-1582.

[67] Bertoncello, P., Dennany, L., Forster, R. J., Unwin, P. R., *Anal. Chem.*, **2007**, 79, 7549-7554.

[68] Miao, W., Bard, A. J., *Analytical Chemistry,* **2003**, 75, 5825-5834.

[69] Sun, H., Ma, Sk8., Li, Y., Qi, H., Ning, X., Zheng, J., *Biosen. Bioelectron.*, **2015**, DOI: 10.1016/j.bios.2015.11.068.

[70] Sykora, M., Meyer, T., *J. Chem. Mater.*, **1999**, 11, 1186-1189.

[71] Valenti, G., Zangheri, M., Sansaloni, S. E., Mirasoli, M., Penicaud, A., Aldo Roda, A., Paolucci, F., *Chem. Eur. J.*, **2015**, 21, 12640-12645.

[72] Collinson, M. M., Novak, B., Martin, S. A., Taussig, J. S., *Anal. Chem.*, **2000**, 72, 2914-2920.

[73] Dennany, L., Forster, R. J., Rusling, J. S., *J. Amer. Chem. Soc.*, **2004**, 125, 5213-5218.

[74] Ulrich, G.,Ziesse,R.L., Harriman,A., *Angew. Chem. Int. Ed. Engl*., **2008**, 47, 1184–1201.

[75] Zhang, J., Qi, H., Li, Y., Yang, J., Gao, Q., Zhang, C., *Anal. Chem.,* **2008**, 80, 2888-2894.

[76] Li, Y., Qi, H., Peng, Y., Yang , J., Zhang., *Electrochem. Commun.,* **2007**, 9, 2571-2575.

[77] Li, Z., Chang, S.,Williams,R.S., *Langmuir.,* **2003**, 19, 6744-6749.

[78] Collinson, M. M., Novak, B., Martin, S. A., Taussig, J. S., *Anal. Chem.*, **2000**, 72, 2914-2920.

[79] Sykora, M., Meyer, T., *J. Chem. Mater.*, **1999**, 11, 1186-1189.

[80] Love, J. C., Estroff, L. A., Kriebe, J. K., Nuzzo, R. G., Whitesides, G. M., *Chem. Rev.*, **20005**, 105, 1103-1169.

[81] Spain, E., Brennan, E., McArdle, H., Keyes, T. E., Forster, R. J., *Anal. Chem.*, **2012**, 84, 6471-6476.

[82] Adaligil, E. , Shon, Y., Slowinski, K., *Langmuir.,***2010**, 26, 1570–1573.

[83] Fenter, P., Eisenberger, P., Li, J., Camillone, N., Bernasek, S., Scoles, G., Ramanarayanan, T. A ., Liang, K.. S**.**, *Langmuir.,***1991**,7, 2013–2016.

[84] Carvalho, A., Geissler, M., Schmid, H., Michel, B., Delamarche, E., *Langmuir.,* **2002**, 2406-2412.

[85]McKinley, A. W., Lincoln, P.,Tuite, E. M., *Coord. Chem. Rev.*, **2001**, 255, 2676-2692.

[86] Emilsson, G., Schoch, R. L., Feuz, L., Höök, F., Lim, R. Y. H., Dahlin, A. B., *ACS Appl. Mater. Inter.,* **2015**, *7*, 7505-7515.

[87] Sun, L., Zhao, H., *Langmuir.,* **2015**, *31*, 1867-1873.

[88] Kedracki, D., Chekini, M., Maroni, P., Schlaad, H., Nardin, C., *Biomacromol.,* **2014**, *15*, 3375-3382.

[89] Takasu, K., Kushiro, K., Hayashi, K., Iwasaki, Y., Inoue, S., Tamechika, E., Takai, M., *Sens. Actuator B* **2015**, *216*, 428-433.

[90] Steenackers, M., Küller, A., Stoycheva, S., Grunze, M., Jordan, R., *Langmuir.,* **2009**, *25*, 2225-2231.

[91] Bard, A.J., Faulkner, L.R., *Electrochemical methods : Fundamentals and Applications*, 2nd ed, **2001**, John Wiley and Sons Inc: New York

[92] Ludvik, J., *J. Solid State Electrochem.*, **2011**, 15, 2065-2081.

[93] Abbou, J.; Anne, A.; Demaille, C, *J. Amer. Chem. Soc.* **2004**, *126*, 10095-10108.

[94] Skoog, D. A., West, D. M., Holler, F. J**.** *Fundamentals of Analytical Chemistry.* 8th ed . **2004**, Fort Worth: Saunders College Publishing.

[95] Monk, P.*Fundamentals of Electro-Analytical Chemistry,* **2001**, Manchester: John Wiley & Sons Ltd.

[96] Brennan, J.L., Keyes,T. E., Forster, R.J., *Langmuir.*, **2006**, 22, 10754-10761.

[97] Forster, R. J., Keyes T. E., Vos, J. G. *Interfacial Supramolecular Assemblies*, **2003**, England , John Wiley & Sons, Ltd.

[98] Safin, D. A., Mitoraj, M. P., Robeyns,K., Filinchuk, Y., Vande Velde, C. M. L., *Dalton Trans.*, **2015**, 44, 16824-16832.

[99] Tu, Q., Chang, C., *Nanomed: Nanatechn. Biol. Med.,* **2012**, 8, 545-588.

[100] Das, R. S., Agrawal, Y. K., *Vib. Spectrosc.*, **2011**, 57, 163-176.

[101] Widin, J. M., Kim, M., Schmitt, A. K., Han, E., Gopalan, P., Mahanthappa, M. K., *Macromol.,* **2013**, *46*, 4472-4480.

CHAPTER TWO:

INVESTIGATION OF THE ELECTROCHEMILUMINESCENCE OF A NOVEL CARBOXY FUNCTIONALIZED BODIPY DYE

2.1. INTRODUCTION

To date $[Ru(bpy)_3]^{2+}$ has been the luminophore of choice in most ECL studies. The focus on this luminophore is not surprising given its excellent properties. One of the reasons why $[Ru(bpy)_3]^{2+}$ has received much attention is its low-lying metal-to-ligand charge transfer (MLCT) excited states.[1]

Due to the fact that MLCT excitation does not affect the metal-ligand bonding or initiate competing unimolecular photoreations,[2] intense luminescence can be obtained with $[Ru(bpy)_3]^{2+}$ under ambient condition. In addition, the synthesis of $[Ru(bpy)_3]^{2+}$ is not complicated; and it has high photostability and luminescence quantum efficiency, long-lived triplet excited state and exhibits rich electrochemistry.[3] Although these properties of $[Ru(bpy)_3]^{2+}$ make it a useful luminophore for sensitive and selective analytical methods[2] there is an ongoing need for the introduction of novel ECL reagents. These should be highly efficient reagents that have emission properties that can enable simultaneous determination of several analytes in a single sample.[4] BODIPY dyes are known to have strong absorption and emission properties in the visible region and high photostability.[5,6,7]

They have high extinction coefficients (which are known to greatly influence their electrochemiluminescence response), and they also have sharp absorbance. [8] However, their Stokes shift is particularly small, making it challenging to resolve the emission and excitation, and re-absorbance of the emitted photon can occur. The photophysical properties of BODIPY dyes can be fine-tuned by altering the nature, as well as the position of the attached substituents on the parent difluoroboron dyprromethane core.[9]

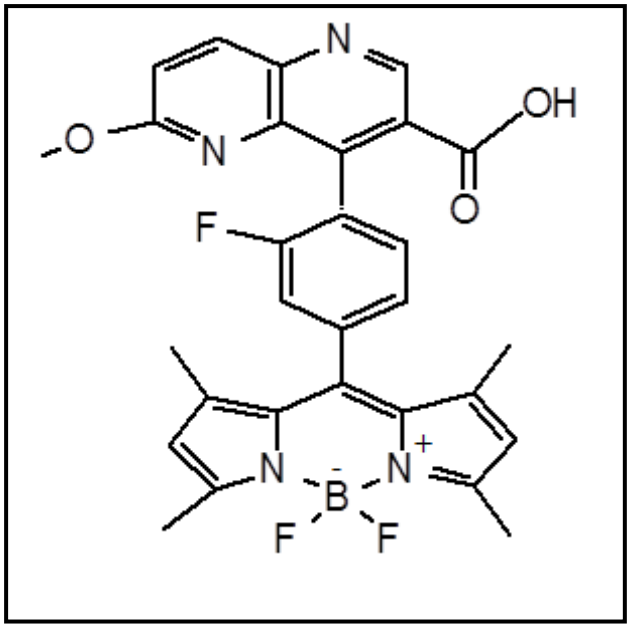

Figure 2.1: Molecular structure of 1,3,5,7-tetramethyl-8-[(2-fluorophenyl)-6-methoxy-1,5-naphthyridine-3-carboxy]-4,4'-difluoroboradiazaindacene complex.

In this chapter, the photophysics and electrochemistry of a novel BODIPY 1,3,5,7-tetramethyl-8-[(2-fluorophenyl)-6-methoxy-1,5-naphthyridine-3 carboxy]-4,4'-difluoroboradiazaindacene, (BODIPY-COOH) synthesized by Dr Martin in the group (Figure 2.1) were investigated to estimate the thermodynamic parameters of the dye which would indicate their value as ECL reagents. This BODIPY derivate contains a carboxyl terminal which can be easily conjugated to biomolecule e.g. coupling with proteins through simple peptide conjugation, hence making it an attractive fluorophore dye for application in biological assays.[10]

The main objective of this chapter is to probe the ECL behaviour of BODIPY-COOH in solution and as thin films. The aims include investigating the photophysics and electrochemical properties of the dye in different solvents, probing the ECL behaviour using benzoyl peroxide and hydrogen peroxide as co-reactants, and investigating the ECL in an ionic liquid and on interdigitated electrodes.

2.2. EXPERIMENTAL

2.2.1. MATERIALS AND REAGENTS

All the dyes used in this thesis were synthesized by other colleagues within the group. The 1,3,5,7-tetramethyl-8-[(2-fluorophenyl)-6-methoxy-1,5-naphthyridine-3-carboxy]-4,4'-difluoroboradiazaindacene (BODIPY-COOH) dye used in this was synthesized by Dr Aaron Martin according to a method previously described elsewhere.[11]

All other chemicals and solvents were purchased from Sigma-Aldrich. Spectroscopic measurements were carried out with solvents which were of HPLC grade. The chemicals were used as received from Sigma-Aldrich, with the exception of tetrabutylammonium tetrafluoroborate, TBATFB (98% Analar grade), used as the supporting electrolyte for some of the electrochemical studies reported in this chapter. TBATFB was placed in the oven at 36 °C to remove any residual water content prior to use. All aqueous solutions were prepared with deionised water which was purified by passing it though a Milli-Q plus 18.5 milliΩ cm^{-1} Millipore purifying system.

The Milli-Q water was deoxygenated by bubbling nitrogen gas for 30 min, prior to any measurement. All experiments were carried out at room temperature.

2.2.2. ELECTROCHEMISTRY

Electrochemical measurements were carried out using a CH Instruments Model 760B Potentiostat. Cyclic voltammetry was conducted using a single-compartment three-electrode cell consisting of a platinum or gold disk (2 mm diameter) working electrode, silver wire (0.5 mm diameter) reference electrode and a platinum wire (1.0 mm diameter) counter electrode. All potentials are quoted with respect to versus a silver wire in this chapter.

2.2.3. ELECTRODE CLEANING AND FABRICATION

The platinum and gold working electrodes were cleaned by successive polishing using 1, 0.3 and 0.05 μm alumina micro polish and polishing pads purchased from Buehler, IL, USA, followed by rinsing with deionized water and sonication in ethanol and water to remove all traces of alumina polish. After sonication, the electrodes were rinsed with ethanol and deionized water and dried under a nitrogen stream. Then an electrochemical cleaning step involving 20 voltammetric cycles was performed with the Pt electrodes (from -0.25 to 1.2 V) and the Au electrodes (from -0.25 to 1.5 V) in 0.5 M H_2SO_4.

2.2.4. ELECTROCHEMILUMINESCENCE

2.2.4.1. ECL with macroelectrodes

The ECL measurements were performed with an Oriel 70680 Photomultiplier Tube (PMT) biased at -850 V using a high-voltage power supply (Oriel model 70705 PMT power supply) and an amplifier/recorder (Oriel, model 70701). During the experiments, the cell was placed inside a specially constructed holder, which positioned the working electrode in a reproducible manner directly opposite the face of a fibre optic bundle, the other end of which was coupled to the PMT. The entire electrode assembly was contained inside a light-tight box to avoid ambient light interference, and the experiments were conducted in a dark room.

2.2.4.2. ECL with interdigitated electrodes

The platinum interdigitated electrodes (IDA) consist of sixty five 10 µm-width pairs with a spacing of 5 µm and length of 2 mm which were purchased from EC-Lab Ltd (United Kingdom). To generate ECL, the potential of the two working electrodes were independently controlled using two separate potentiostats. The generator (cathode) was scanned from 0 to -2 V and reversed using the CH instrument model 600, while the collector electrode (anode) was kept at a constant potential of -0.95 V unless stated otherwise, using the CH instrument Model 7.[4]

2.2.5. SPECTROSCOPIC METHODS

2.2.5.1. Absorption spectroscopy

UV/Vis spectra were recorded on a Jasco V-670 UV/Vis/NIR spectrophotometer and the measurement were conducted at room 15°C temperature in a Hellma quartz cuvette of 1 cm optical path length. The solution phase measurements were carried out by dissolving BODIPY-COOH in DMF, DMSO, MeCN or DCM. The UV/Vis data were background–corrected using a blank. The solvents used as blanks were DMF, DMSO, MeCN or DCM.

2.2.5.2. Fluorescence spectroscopy

Fluorescence emission and excitation experiments were performed with a Varian Cary Eclipse Fluorescence spectrophotometer with an excitation slit width of 5 nm and an emission slit width of 5 nm. All experiments were conducted at room temperature in 1 cm path length quartz cuvette and the background was corrected for blank fluorescence before each measurement. Experiments were performed with DMSO, DCM and MeCN.

2.2.5.3. Luminescent lifetimes

The lifetimes were recorded using a FluoTime 100 Time-Correlated Single Photon Counting (TCSPC) instrument. The 450 nm laser was provided from a Picoquant 'PDL 800-B' pulsed diode laser, 10000 counts were collected for

each life time measurement. An average of two measurements was taken for each sample, and analysis was performed using Nanoharp software. The calculation of the luminescent lifetimes was performed with a PicoQuant-FluoFtit software by fitting an exponential decay function to each decay plot. The data was fitted to the mono-exponential decay function of the baseline decay curve using a tail fit that ensures a χ^2 value of between 1 and 1.2.

2.2.5.4. Luminescene Spectroscopy

The luminescence spectra of BODIPY thin films on platinum electrodes were also collected with Horiba Jobin-Yvon Labram HR 2000 confocal Raman microscope. The photoluminescence emission spectra were measured using an argon ion laser (Coherent) to excite the sample at 488 nm. A 100x microscope objective was used to focus the laser (488 nm) beam on samples. The x-axis was calibrated versus the Rayleigh line (0 nm) and the phonon mode from silicon wafer (520 cm^{-1}). Typical acquisitions were 5 s in length and performed three times to acquire a spectrum, and the spectral data were analysed using LabSpec software.

2.2.6. THIN FILM FABRICATION

2.2.6.1. Deposition of BODIPY-COOH films on a platinum substrate using cysteamine layer

BODIPY-COOH thin films were formed on freshly polished and electrochemically cleaned 2 mm diameter Pt electrodes, by firstly immersing the electrodes in a freshly prepared 1 mM ethanolic solution of cysteamine hydrochloride for either 1 h or 16 h at room temperature. The electrodes were then removed and washed with ethanol and deionised water to remove any non-specifically adsorbed cysteamine. N-hydroxysuccinimide (NHS) (10 mg) and 1-ethyl-3-[3-dimethylaminopropyl] carbodiimide hydrochloride (EDC) (5 mg) were added to 200 µL of 5 mM of BODIPY-COOH in DMF and the solution was stirred for 15 min. Subsequently, the cysteamine modified electrodes were immersed in this solution for 3 h in the dark. The modified electrodes were washed thoroughly with ethanol to remove any loosely bound BODIPY-COOH and used immediately.

2.2.6.2. Deposition of BODIPY-COOH films on a platinum substrate using L-cysteine poly (ethylene glycol)bis(3-aminopropyl) [PEG] layer

Platinum electrodes were immersed in a 1 mM ethanolic solution of L-cysteine for an hour, followed by rinsing the electrode with ethanol and water to remove any loosely bound cysteine. Approximately, 1 mM PEG was prepared in 1 mL DMF, and to this solution NHS (10 mg) and EDC (5 mg) were added and the L- cysteine modified electrodes were immersed in this solution for 2-3

h. The L-cysteine-poly(ethylene glycol)bis(3-aminopropyl) [PEG] layer modified electrodes were rinsed with ethanol and water, respectively. N-hydroxysuccinimide (NHS) (10 mg) and 1-ethyl-3-[3-dimethylaminopropyl] carbodiimide hydrochloride (EDC) (5 mg) were added to 200 µL of 5 mM of BODIPY-COOH in DMF and the solution was stirred for 15 min. Subsequently, the PEG layer-modified electrodes were immersed in this solution for 3 h in the dark. The modified electrodes were washed thoroughly with ethanol to remove any loosely bound BODIPY-COOH and used immediately.

2.3. RESULTS AND DISCUSSION

2.3.1. PHOTOPHYSICAL PROPERTIES OF BODIPY-COOH DYE

The optical properties of BODIPY dyes depend strongly on the location and nature of the substituents in the BODIPY core.[12] Consequently, small structural changes can affect the fluorescence wavelength.[13] In the current study, the naphthyridine unit which has a carboxyl terminal group and fluorophenyl are the substituents which were introduced to the BODIPY core in order to achieve absorption and emission in the near infra-red (NIR) region. The basic photophysics of BODIPY-COOH were assessed by a combination of UV-Vis absorption and fluorescence spectroscopy.

2.3.1.1. UV-Vis absorption behaviour

The naphthyridine substituent has donor nitrogens which can induce solvent-dependence in the absorbance and emission properties if they are involved in the lowest energy transitions. This issue was addressed by recording electronic spectra properties of BODIPY-COOH, solvent dependent optical studies were investigated in different solvents; i.e. DMF, DMSO, DCM and MeCN. These solvents were chosen as BODIPY-COOH was soluble in all of them and they were possible solvents in which the subsequent electrochemistry and electrochemiluminescence studies could be performed. Furthermore, an additional hydrogen binding solvent, EtOH was used. It is expected that if the naphthyridine unit induces any solvent effect, it will be clearly observed in the absorbance and emission behaviour in EtOH. Figure 2.2 below presents the absorption spectra of BODIPY-COOH dye in all solvents, showing intense and narrow absorption bands typical of BODIPY dye.[14] The absorption behaviour displayed characteristics of a simple BODIPY monomer with two absorption maxima at 333 and 500 ± 2 nm.

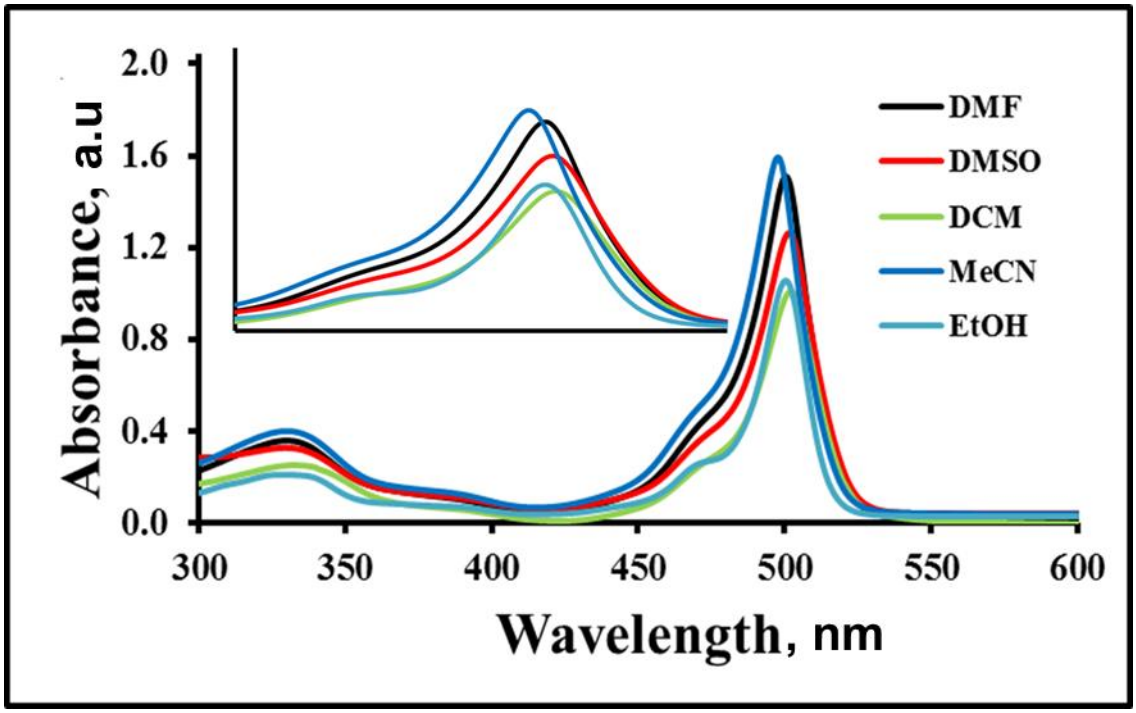

Figure 2.2: UV-Vis absorbance spectra of 5 µM BODIPY-COOH in different solvents. The inset only displays the absorption from 450 to 600 nm.

This absorption spectrum resembles that of a BODIPY dye, 4,4- Difluoro-8-(4-tolyl)-3,5- dimethoxy-4-bora-3a,4adiaza-s-indacene previously reported by Qin *et al.*[15]. A strong absorption band around 500 nm which had a shoulder on the high energy site centred around 480 nm and a weak absorption band at 350 nm.[16] In the present study, the strong absorption band with a narrow spectral bandwidth and an absorption maxima approximately at 500 nm is due to the lowest energy spin-allowed S_0-S_1 (π-π*) transitions of the BODIPY units. The shoulder at 480 nm is attributed to 0 to 1 vibrational transitions, while the weak absorption band with low intensity centred approximately at 333 nm, is attributed to higher energy S_0 to S_2 (π-π*) transitions of the BODIPY moiety. In the absorption spectra, the peak shape are hardly affected by solvent polarity, except that the strong absorption peak in MeCN centred at

approximately 498 nm is slightly blue shifted by 2 nm compared to DMSO and DCM. Hence, the dye appears to have a slightly red shifted absorbance centred at 500 nm in DMSO, DCM and EtOH as compared to MeCN. The red shift may be attributed to either the destabilization of the highest occupied molecular orbital (HOMO) or the stabilization of the lowest unoccupied molecular orbital (LUMO) of the BODIPY-COOH dye. The results imply that 1-5 napthyridine-3-carboxy substituent does not participate in the lowest energy transitions which result in the observed peaks, and all the observed absorbance is localized at the BODIPY core.

2.3.1.2. Luminescence properties

The emission and excitation spectra of BODIPY-COOH in DMSO, DCM and MeCN are presented in Figure 2.3 below. In DMSO, the spectra show that when the dye is excited into either its S_1 or S_2 state, a narrow emission band is observed at 515 nm. The band is red shifted compared to the 502 nm absorption band, therefore, yielding a Stokes shift of 13 nm in DMSO. The emission wavelength of BODIPY-COOH hardly changes in EtOH, as it is observed at 513 nm and it is characterized by an intense emission band with a notably small Stokes shift.[14] The emission appears to be a mirror image of the absorption spectrum. This was probably due to the vibrational spacing in the ground state that is often similar to the first excited single state.

A strong correlation between excitation and corresponding absorption intensities exists for the dye in all solvents as shown in Figure 2.3 below. However, the emission is red shifted compared to the corresponding

absorbance with a Stokes shift of 12 nm in MeCN as well as in DCM. While in EtOH, it is 13 nm as presented Table 3.1 below. The Stokes shift in MeCN, DCM, DMSO and EtOH proves to be solvent independent, indicating that there is no appreciable change between the dipole moments of the ground state and the excited states[17] as the solvent is varied.

The luminescence lifetime and fluorescence quantum yield of emission (Φ_F) of BODIPY-COOH were evaluated in MeCN and DMSO. The lifetime observed was not affected by a change in the solvent as it exhibited a lifetime of 5.90 ± 0.20 and 5.06 ± 0.20 ns in DMSO and MeCN, respectively. However, the quantum yield appeared to be solvent dependent, as it was determined to be 0.88 ± 0.02 and 0.60 ± 0.04 in MeCN and DMSO, respectively. The quantum yield of BODIPY-COOH is lower in DMSO (0.60 ± 0.04) which is more polar than MeCN. This behaviour is similar to what was observed by Qin *et al.*[18] in studies which showed that the Φ_F of 4,4-difluro-3.5-dimethyl-8(aryl)-4-bora-3a,4a-diaza-s-indacene BODIPY derivatives is lower in solvents with higher polarity due to the increase in the rate of non-radiative deactivation. The Φ_F in MeCN (0.88 ± 0.02) is consistent with values previously reported for structurally related BODIPY dyes.[19

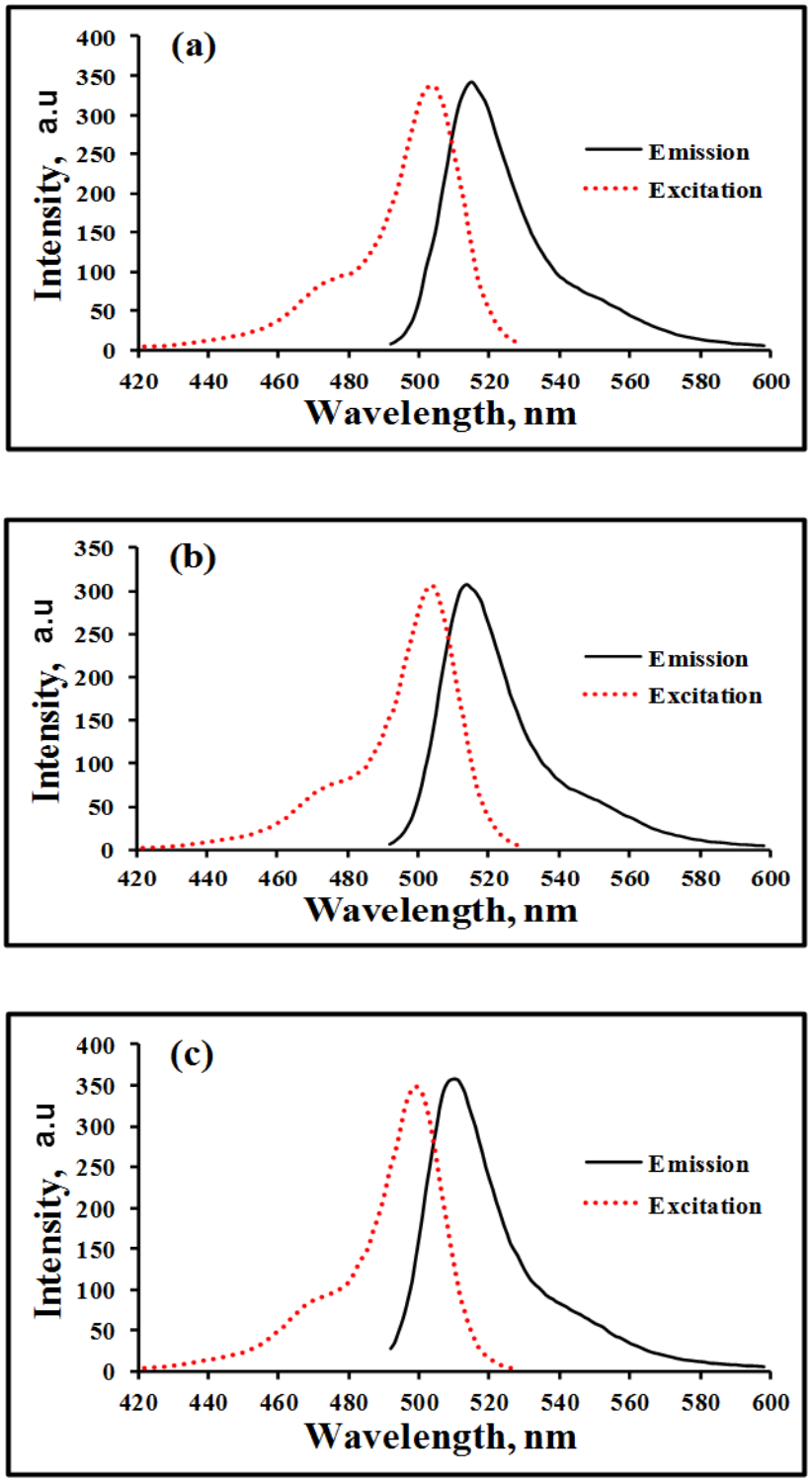

Figure 2.3: Emission (red) and excitation (black) spectra of 5 µM BODIPY-COOH in (a) DMSO, (b) DCM and (c) MeCN. The emission and excitation spectra were collected with a slit width of 5 nm.

The 1,3,5,7-tetramethyl BODIPY parent compound has been reported to exhibit an emission observed at 506 nm in MeCN.[19] The introduction of 8-[(2-fluorophenyl)-6-methoxy-1,5-naphthyridine-3-carboxy] substituent at the *meso* position in the BODIPY-COOH, in the present study, introduced a modest red shift in emission, as the emission in MeCN was observed at 510 nm

Table 2.1: Photophysical properties of BODIPY-COOH derivative in various solvent.

Solvent	λ max			Stoke's shift (nm)	τ_F(ns)	ϕ_F	E_s (eV)
	λ_{ab} (nm)	λ_{em} (nm)	λ_{ex} (nm)				
MeCN	498±2	510±2	500	12±2	5.90 ± 0.20	0.88 ± 0.02	2.43
DMSO	502±2	515±2	503	13±2	5.06 ± 0.20	0.60 ± 0.04	2.41
DCM	502±3	514±3	504	12±3			
EtOH	500±3	513±3	504	13±3			
BODIPY core MeCN Ref[9]	500	506	491	6			

In summary, on the basis of the emission wavelengths obtained from fluorescence λ_{max}, the average energy needed to generate the first singlet state (E_s) for BODIPY-COOH was obtained as 2.43 and 2.41 eV in MeCN and DMSO, respectively, using Equation 2.1.[20]

$$E_s \text{ (in eV)} = \frac{1239.81}{\lambda_{max}(nm)} \qquad \textbf{[2.1]}$$

For ECL to take place, the free energy of annihilation, ΔG_{ann}, has to exceed the energy required to populate the first singlet state and it has to be generated from electrochemical annihilation reaction of the radical ions.[17] Hence, electrochemical characterization of BODIPY-COOH was carried in order to understand the redox behaviour of this dye and estimate the driving force available for the annihilation reaction between an electrochemically generated oxidised and reduced states.

2.3.2. ELECTROCHEMICAL PROPERTIES OF BODIPY-COOH DYE

2.3.2.1. Cyclic voltammetry

Cyclic voltammetry (CV) of the BODIPY-COOH can provide information about the redox behaviour of this dye and thus insights into the thermodynamics of ECL. The CV response was measured in MeCN and DMSO. Figure 2.4 displays a CV of a solution BODIPY-COOH in MeCN and 0.1 M TBATFB as a supporting electrolyte at 2 mm radius platinum electrode, using a scan rate of 0.1 V s^{-1}. In MeCN, the voltammetry displays a reduction peak at E_{pc} = -0.891 V and a small peak at -1.4 V and one anodic wave for the oxidation process at E_{pa} = -0.961 V. Previously reported investigations on a structurally related BODIPY; 2,6-Diethyl-1,3,5,7-tetramethyl-8-[(2-fluorophenyl)-6-methoxy-1.5-naphthyridine-3-carboxy] 4,4′difluoro boradiazaindacene, had a reduction peak at -0.28 V and two oxidation peaks at 1.38 V and 1.61 V in MeCN.[21] The BODIPY core which is the dye without substitution in positions 2, 6 and 8, has been reported to have irreversible oxidation and reduction peaks at 1.17 and -1.15 V respectively, in MeCN.[21]

The voltammograms illustrated in Figure 2.5 show the CVs of the dye in DMSO in the presence of 0.1 M TBATFB supporting electrolyte on a platinum electrode and at a scan rate of 0.1 V s^{-1}. The reduction peak is observed at E_{pc} = -0.956 V and oxidation peak is observed at E_{pa} = -0.817 V. Though the MeCN and DMSO studies were performed at different potential windows larger peak currents were obtained for acetonitrile than for DMSO for the same amount of BODIPY-COOH. The potentials where the redox processes occurred are only slightly different for both solvents, though BODIPY-COOH seemed to exhibit well defined quasi-reversible electrochemistry in DMSO than in MeCN.

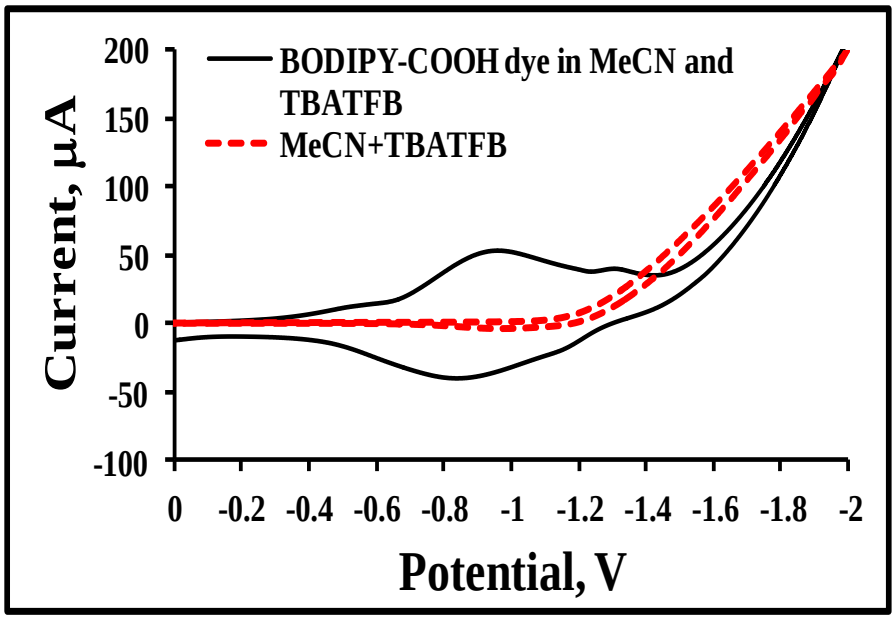

Figure 2.4: Solution phase voltammetry of 5 mM BODIPY-COOH dissolved in MeCN (solid line) containing 0.1 M TBATFB as the supporting electrolyte and blank MeCN TBATFB (dashed line), using a 2 mm diameter platinum electrode at a scan rate of 0.1 V s^{-1}.

From the emission maximum wavelengths of BODIPY-COOH, it was previously established that the energy required to populate the first singlet state for BODIPY-COOH is 2.41 eV. The energy requirements must be fulfilled by the electrochemical annihilation reaction between the electrochemically generated oxidized and reduced species of BODIPY-COOH if annihilation ECL is to be observed. Hence, the free energy of annihilation ΔG_{ann} of this reaction must exceed the energy required to generate the first singlet state (E_s) in order generate the singlet emitting state.

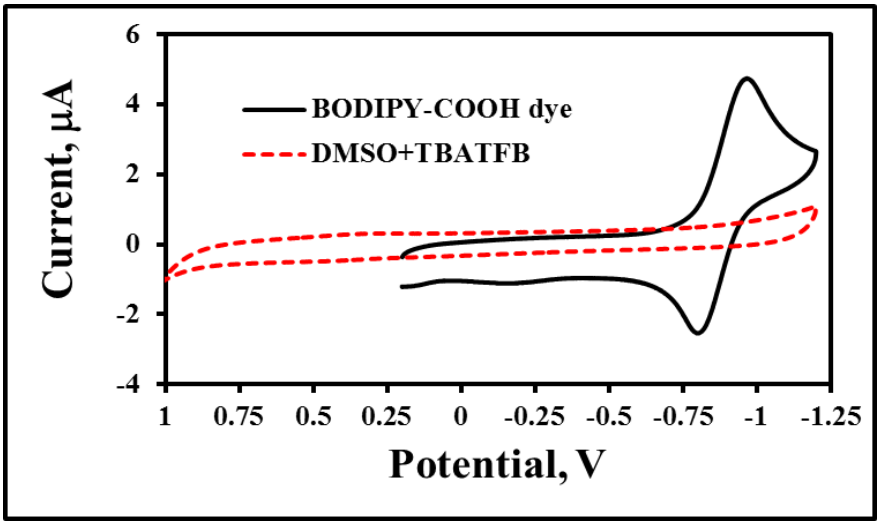

Figure 2.5: Solution phase voltammetry of 5 mM BODIPY-COOH dissolved in DMSO (solid line) containing 0.1 M TBATFB as the supporting electrolyte and blank in DMSO and TBATFB (dashed line), using a 2 mm diameter platinum electrode at a scan rate of 0.1 V s^{-1}.

The ΔG_{ann} is obtained from the half-wave potential difference between the first reduction and first oxidation wave in the cyclic voltammogram of BODIPY.[22] These redox waves are observed at E_{red} = -0.891 V and E_{ox} = -0.961 V in MeCN and in DMSO at E_{red} = - 0.956 V and E_{ox} = - 0.817 V for BODIPY-

COOH, yielding Δ*G* of 0.07 and 0.13 eV in MeCN and DMSO, respectively. This free energy of annihilation is significantly less than the minimum required energy for direct population of the singlet excited state of BODIPY-COOH estimated as 2.43 and 2.41 eV from the emission spectra obtained in MeCN and DMSO, respectively. Moreover, this system also proves to be energy deficient to produce the excited state via the triplet-triplet annihilation pathway, since, the triplet energy has been reported to be approximately 1.63 eV for similar BODIPY derivatives.[23] The results presented above suggest that BODIPY-COOH system is energy insufficient to achieve ECL via the annihilation pathway hence ECL would need to be generated using a co-reactant.

2.3.2.2. Scan rate dependent voltammetry

Figures 2.6 and 2.7 below depict CVs of solution BODIPY-COOH in DMSO and TBATFB as a supporting electrolyte at a platinum electrode. The measurements were conducted from the highest measured scan 0.9 V s^{-1} to the lowest scan rate 0.01 V s^{-1}. Figure 2.6 presents low scan rates (0.01 to 0.09 V s^{-1}) while Figure 2.7 shows the high scan rates of 0.1 to 0.9 V s^{-1} at 273 K, and the insert shows peak current dependence on the root of scan rates. The voltammetric response at the slowest scan rate 0.01 V s^{-1} displays a single reduction peak at E_{pc} = -0.916 V. This potential is less negative than those reported for the parent fluorophore reported by Bard and co-workers[19] where the unsubstituted BODIPY displayed oxidation and reduction peaks at 1.17 and -1.15 V respectively. The peak at -0.916 V shifts to more negative potentials as the scan rate is progressively increased from 0.01 to 0.9 V s^{-1}

and one oxidation peak is observed at E_{pa} = -0.835 V as shown in Figure 3.6 below.

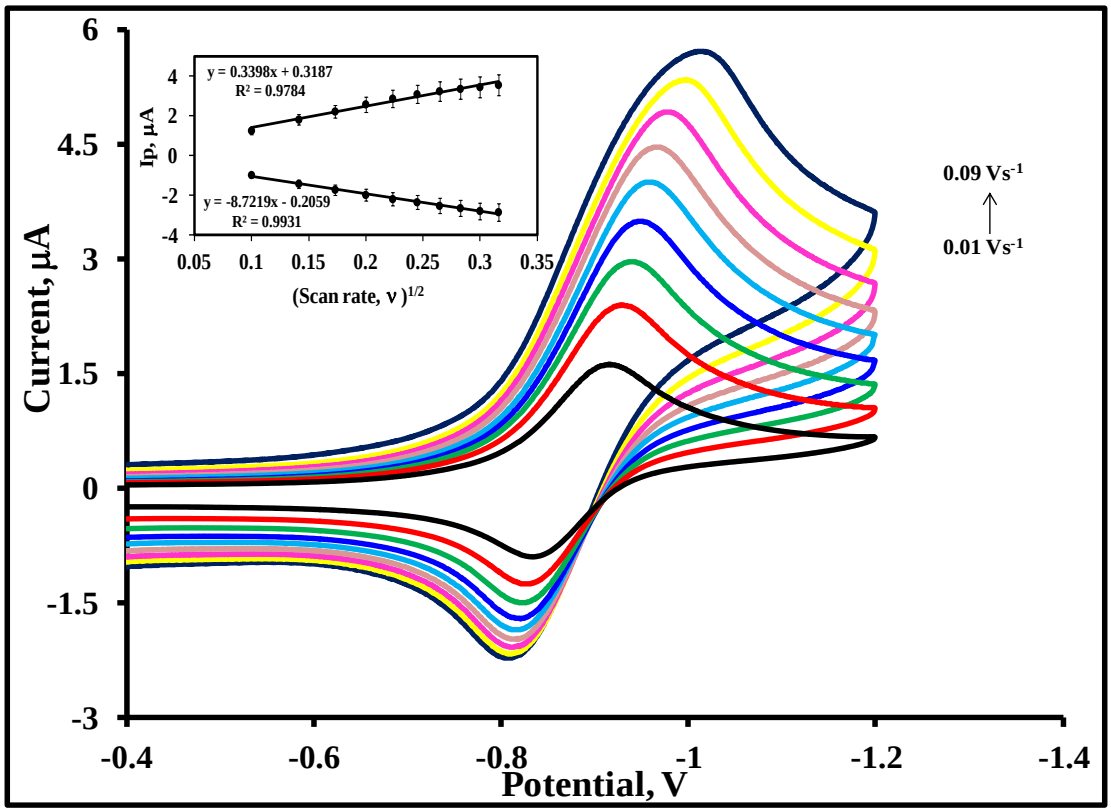

Figure 2.6: Scan rate dependence of the voltammetric responses of 5 mM BODIPY-COOH in DMSO and 0.1 M TBATFB as supporting electrolyte at a 2 mm platinum electrode. CVs are plotted incrementally at 0.01 V s^{-1} intervals, for lower scan rates of 0.01 V s^{-1} (innermost) to 0.09 V s^{-1} (outermost). The inset shows peak current dependence of the square root of scan rate.

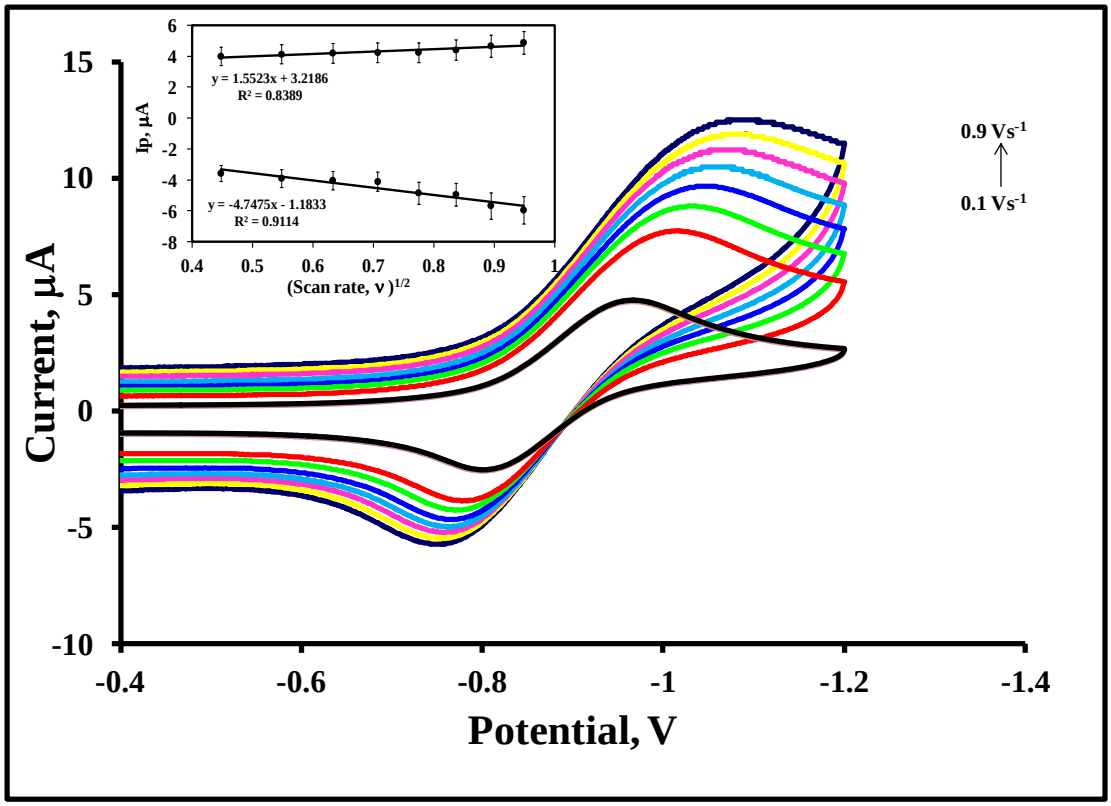

Figure 2.7: Scan rate dependence of the voltammetric response of 5 mM BODIPY-COOH in DMSO and 0.1 M TBATFB as a supporting electrolyte on a 2 mm platinum electrode, at higher scan rates of 0.1, 0.3, 0.4, 0.5, 0.6, 0.7 and 0.9 V s^{-1} (from innermost CV and going outwards). The inset shows peak current dependence of the square root of scan rate.

The peak currents obtained from the voltammograms in Figure 2.6 and 2.7 vary linearly with the square root of scan rate. Also the reduction peak potentials shift to more negative potential values with increasing scan rate, this can also be observed from Table 2.2. This shift in peak potential can be attributed to Ohmic (*IR*) drop and slow heterogeneous electron transfer.Table 2.2 below summarises the electrochemical data acquired from the CVs in Figures 2.6 and 2.7. The results show that the peak current ratio at all scan rates were approximately unity. The observed peak separation between the reduction peak and the first oxidation peak is larger than 0.059 V at all scan

rates, and ΔE_p increased with increasing scan rate. A reversible one electron transfer wave is expected to have a peak separation of 0.059 V to satisfy a Nernstian behaviour.[24] However, in the present case ΔE_p has values from 0.081 to 0.257 V for scan rates of 0.1 to 0.9 V s^{-1}, which suggests that the electron transfer process is quasi-reversible and Equation 1.33 was used to determine the diffusion coefficient:[25]

$$i_P = (2.99 \times 10^5) n(\alpha n_a)^{1/2} A D^{1/2} C v^{1/2} \quad \textbf{[1.33]}$$

n is the number of electrons transferred, α is the transfer coefficient, n_a is the number of electrons involved in the charge transfer step, A is the electrode area in cm^2, D is the diffusion coefficient in cm^2 s^{-1}, C is the bulk molar concentration of the electroactive species in mole cm^{-1} and ν is scan rate is V s^{-1}. The diffusion coefficient was determined to be 4.04 ± 0.02 x $10^{-6}cm^2$ s^{-1} indicating that the diffusion is averagely fast. Diffusion coefficient values in the order of 10^{-6} cm^2 s^{-1} have been reported for structurally related BOPDIPYs.[8]

Table 2.2: Electrochemical data of BODIPY-COOH acquired from cyclic voltammograms ran at different scan rates of 0.01 to 0.9 V s^{-1} presented in Figure 2.6 and 2.7 above.

ν V s^{-1}	E_{pc} V	E_{pa} V	ΔE_p ($E_{pc} - E_{pa}$) V	I_{pa}/I_{pc}
0.01	-0.916	-0.835	0.081	0.803
0.02	-0.93	-0.827	0.103	0.800
0.03	-0.939	-0.822	0.117	0.787
0.04	-0.947	-0.822	0.125	0.778
0.05	-0.957	-0.82	0.137	0.773
0.06	-0.966	-0.815	0.151	0.874
0.07	-0.977	-0.814	0.163	0.790
0.08	-0.995	-0.811	0.184	0.850
0.09	-0.996	-0.808	0.188	0.920
0.1	-0.965	-0.801	0.164	0.800
0.2	-0.996	-0.786	0.21	0.900
0.3	-1.013	-0.778	0.235	0.943
0.4	-1.004	-0.771	0.233	0.958
0.5	-1.011	0.771	1.782	0.968
0.6	-1.02	0.762	1.782	1.138
0.7	-1.023	-0.77	0.253	1.121
0.8	-1.033	-0.776	0.257	1.214
0.9	-1.033	-0.776	0.257	1.228

2.3.3. ELECTROCHEMILUMINESCENCE OF BODIPY-COOH DYE

ECL can be produced by two dominant pathways, namely the annihilation and co-reactant pathways. In each case, two species are generated electrochemically which further undergo an electron-transfer reaction to produce an emissive species.[22] No ECL was observed for a structurally related BODIPY when the potential at the working electrode was stepped between +1.8 V and -0.4 V where oxidized and reduced forms were produced within the diffusion layer.[22] This can be attributed to the fact that there is insufficient energy to create the singlet state directly using the annihilation approach. In the current study, the ΔG_{ann} has been shown to be less than the energy required to populate the first single excited state, hence annihilation ECL is thermodynamically uphill. Thus, ECL would need to be generated in the presence of a co-reactant. Taking advantage of the negative reduction potential of BODIPY-COOH and stability of the formed radical anion, a known co-reactant benzoyl peroxide (BPO) was employed to generate ECL.[17] BPO is known as a co-reactant that allows light generation without electrochemical oxidation of the dye.[26] A second co-reactant used to investigate ECL of BODIPY was hydrogen peroxide and both co-reactants operate via the reductive–oxidative mode.

2.3.3.1. Electrochemiluminescence using BPO as Co-reactant

BPO is known to be irreversibly reduced in organic solvent due to a fast follow-up reaction that generates the strongly oxidizing BPO radical.[21]

Chandross and Sonntag[27] demonstrated that in aprotic solvents BPO reduction is irreversible with a reduction potential that is less than -1.0 V vs SCE.[28] Control CV experiments carried out in DMSO and 0.1 M TBATFB in the presence of 3 mM BPO, with no BODIPY present in the solution, on a platinum electrode scanning at 0.1 V s^{-1}, showed that BPO is reversibly reduced at E_{pc} = -0.98V. To generate ECL in the current system, a potential was applied to a platinum electrode which was immersed in a solution of 5 mM BODIPY-COOH in MeCN or DMSO and TBATFB in the presence of BPO or H_2O_2. The applied potential was swept linearly starting from 0 to -2 V, which is the potential window in which the radical anions are expected to be formed while simultaneously measuring the current and the intensity of the emitted light. Figure 2.8 displays the CV measured simultaneously with the ECL profile obtained as the potential was applied to a Pt electrode immersed in MeCN solution of 5 mM BODIPY–COOH in the presence of 3 mM BPO. Firstly, BODIPY-COOH is reduced to its radical anion BODIPY-COOH$^{\bullet-}$ at -0.89 V and as the scanning proceeds BPO is reduced at -0.98 V to produce BPO$^{\bullet-}$. Subsequently, the BODIPY-COOH$^{\bullet-}$ reacts with the reduced BPO$^{\bullet-}$, as soon as the latter is generated, to produce the excited state ^{1}BODIPY-COOH* at -1.3 V.

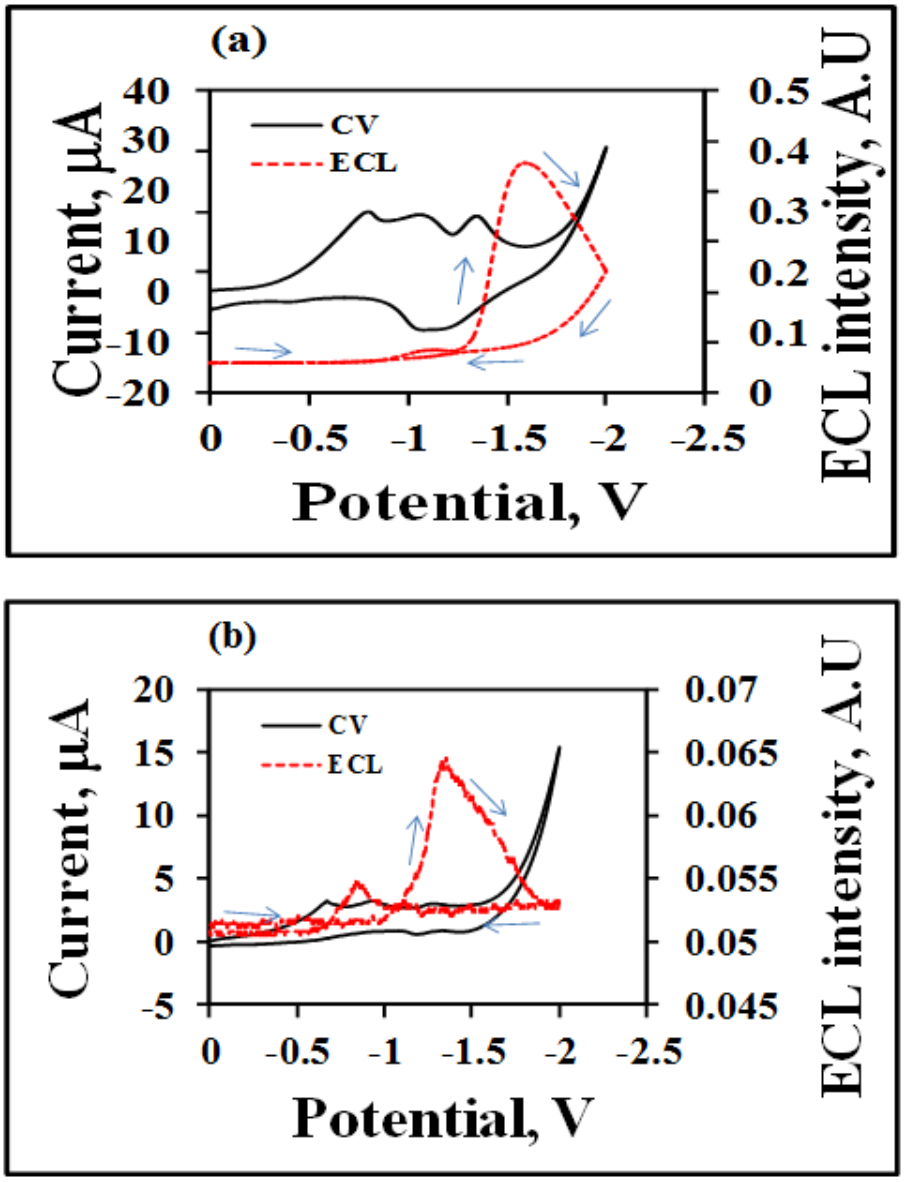

Figure 2.8: Cyclic voltammograms and ECL intensities for MeCN solution of 5 mM BODIPY-COOH dye and 3 mM BPO obtained with a 2 mm platinum electrode at scan rates of 0.1 V s^{-1} (a) and 0.01 V s^{-1} (b). The arrows show the direction of the scan.

The benzoate radical anion, reacts with the BODIPY radical anion to form the excited state ^{1}BODIPY-COOH*. Upon formation of the singlet excited state, ECL onset is observed at -1.32 V, the light generation peaks at -1.61 V and then decreases due to slow diffusional mass transport as depicted in Figure 2.8 (a). It should be noted that on the reverse scan from -2 to 0 V, a relatively weak ECL peak is observed at -0.83 V. This weak ECL peak is clearly observed at slowest scan rates such as 0.01 V s^{-1}, as depicted in Figure 2.8 (b) above.

Figure 2.9(a) below shows the ECL profile of BODIPY-COOH in DMSO at a relatively high scan rate of 0.1 V s^{-1}. BODIPY is reduced at -0.95 V in DMSO compared to -0.89 V in MeCN and BPO is reduced at -0.98 V. When the scan rate is 0.1 V s^{-1}, the ECL onset potential is observed at -0.99 V and light generation peaks at -1.20 V. While at a slowest measured scan rate of 0.01 V s^{-1} in DMSO, ECL is turned on at -1.02 V and peaks at -1.35 V as presented in Figure 2.9(b).

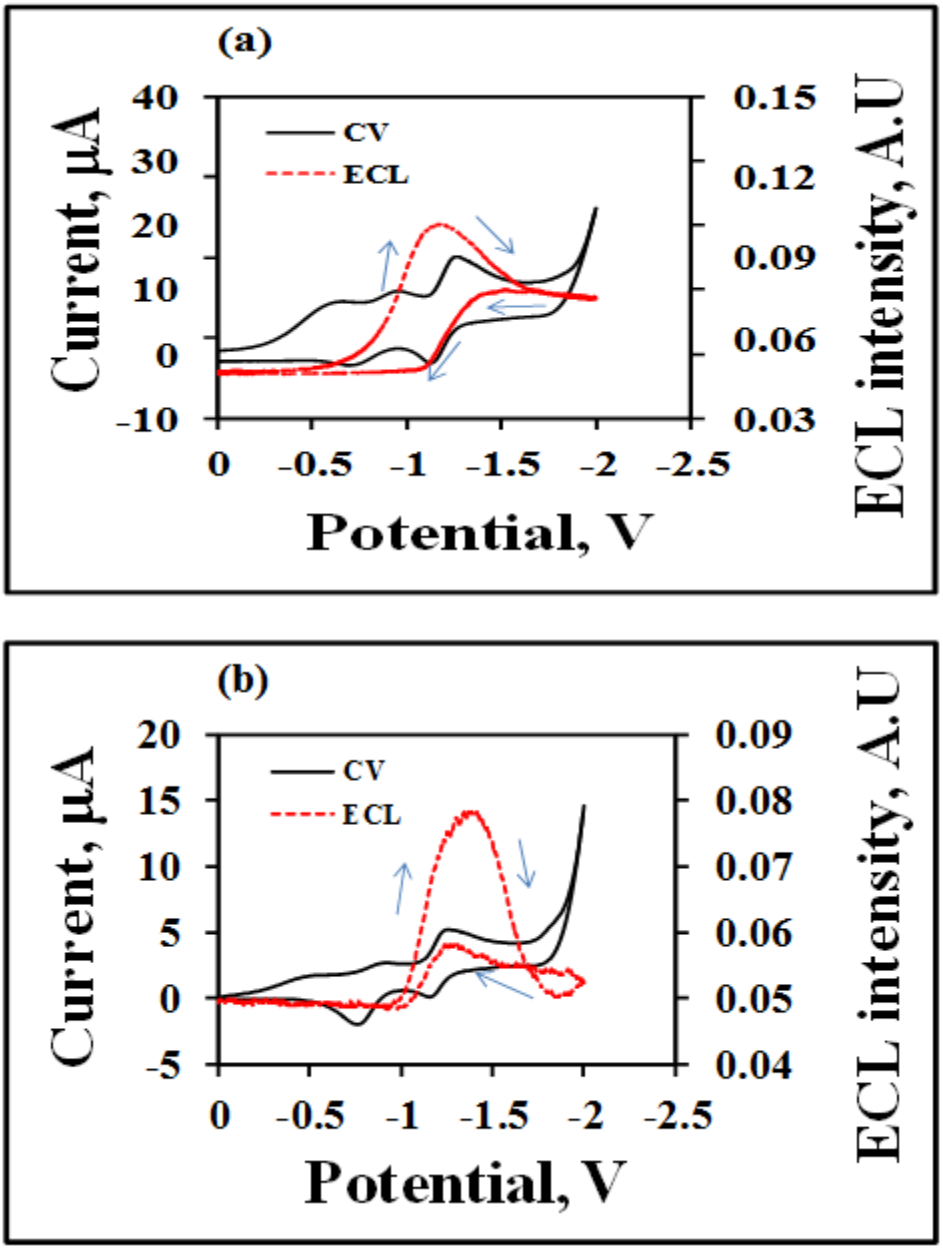

Figure 2.9: Cyclic voltammograms and ECL spectra of DMSO solution of 5 mM BODIPY-COOH dye and 3 mM BPO obtained with a 2 mm platinum at scan rates of 0.1 V s^{-1} (a) and 0.01 V s^{-1} (b). The arrows show the direction of the scan.

There are several processes that influence the ECL intensity as illustrated in Scheme 2.1 below. The first process is the diffusion of BPO to the electrode. The second process is the heterogeneous electron transfer of BODIPY at the electrode. The third process is the cross reaction between the electrochemically generated $BPO^{\bullet -}$ and $BODIPY^{\bullet -}$ to produce the excited state ^{1}BODIPY*. The fourth process is the decomposition of the ^{1}BODIPY* excited state to produce light.

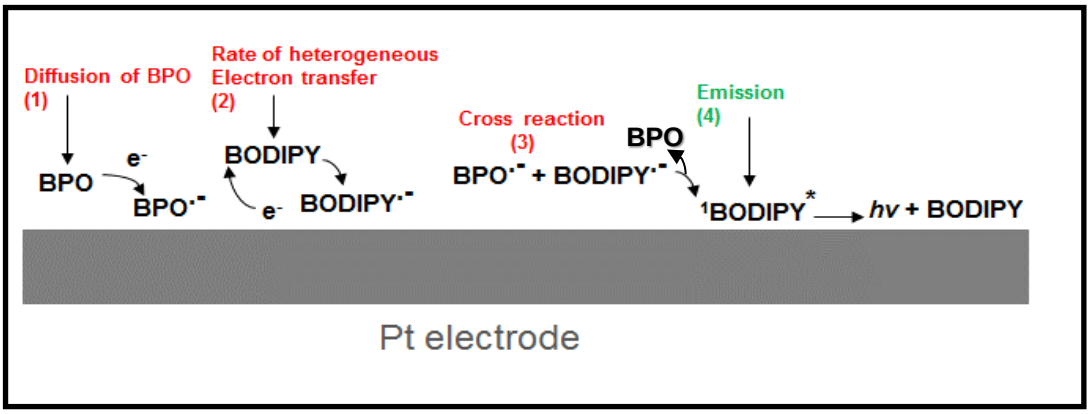

Scheme 2.1: Illustration of the processes that influence ECL intensity response.

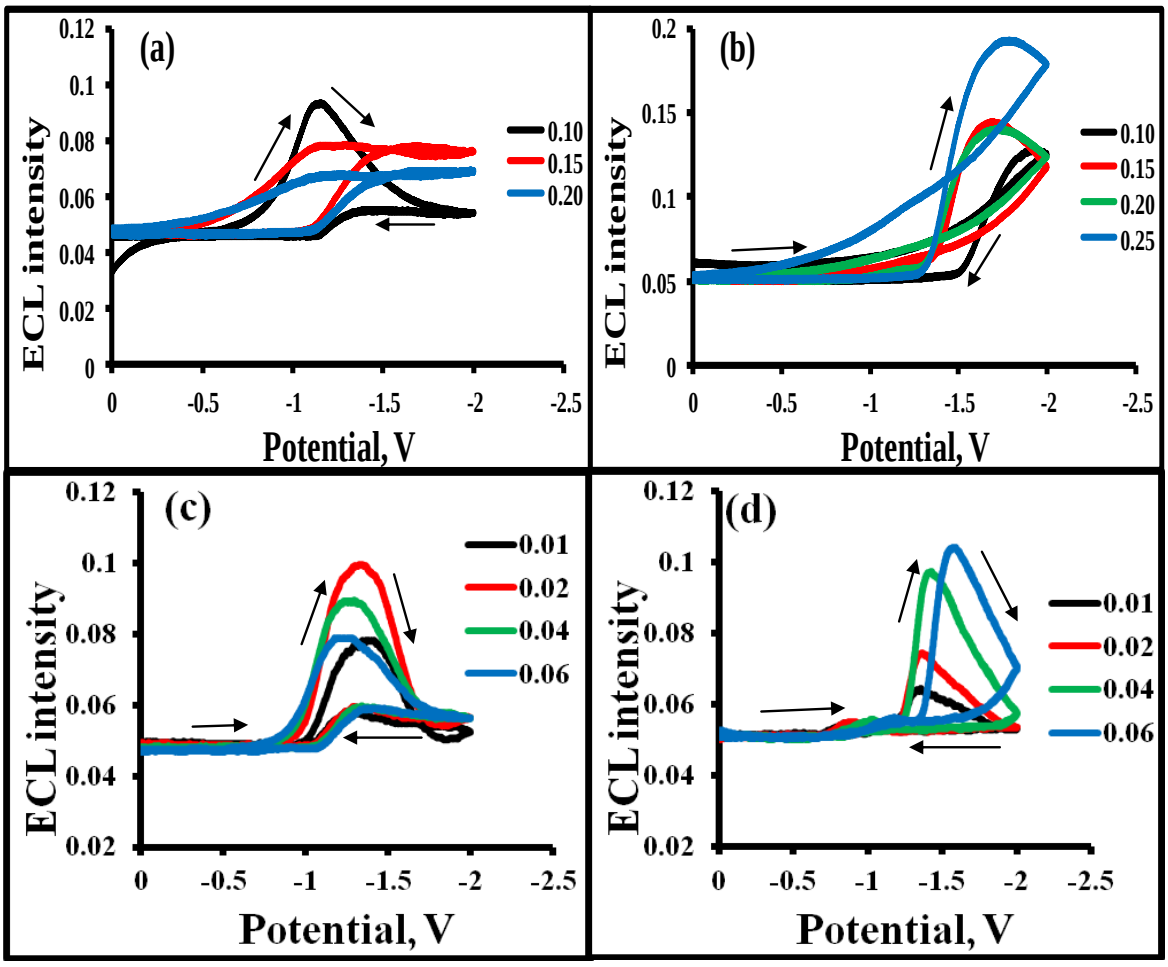

Figure 2.10: ECL generated from a 5 mM BODIPY-COOH solution containing 3 mM BPO in (a) DMSO and (b) MeCN at high scan rate (0.1 - 0.25 V s^{-1}); and (c) DMSO and (d) MeCN at low scan rate (0.01 - 0.06 V s^{-1}). The supporting electrolyte is 0.1 M TBATFB and the working electrode is a 2 mm platinum disk electrode. The initial potential was 0 V and the potential was initially scanned in the negative potential direction and reversed back to the positive direction. The arrows indicate the direction of the scan.

ECL scan rate dependence studies were carried out in MeCN and DMSO at a range of scan rates from lowest 0.01 V s^{-1} to the highest 0.20 V s^{-1}. The ECL profiles are presented in Figure 2.10 (a-d) with their corresponding CVs in

Figure 2.11(a-b). The results of the ECL scan rate dependent studies show that scanning at slow scan rates does not increase the ECL intensity. At the high scan rates, the ECL intensities are not significantly different from the one observed at the low scan rates. The results imply that the rate of heterogeneous electron transfer is least likely to contribute to ECL intensity response because if it did contribute, high ECL intensities should have been observed at the slowest scan rate. This is because at the slow sweep rates all the available BODIPY would be reduced at a diffusion controlled rate to form the $BODIPY^{\cdot -}$, and if a higher concentration of the BODIPY radical anion is produced, the process 3 in Scheme 2.1, will produce more of $^{1}BODIPY^{*}$ excited state which produces light. Whereas when scanning at the fast scan rate only a fraction of the BODIPY would get reduced to form $BODIPY^{\bullet -}$.

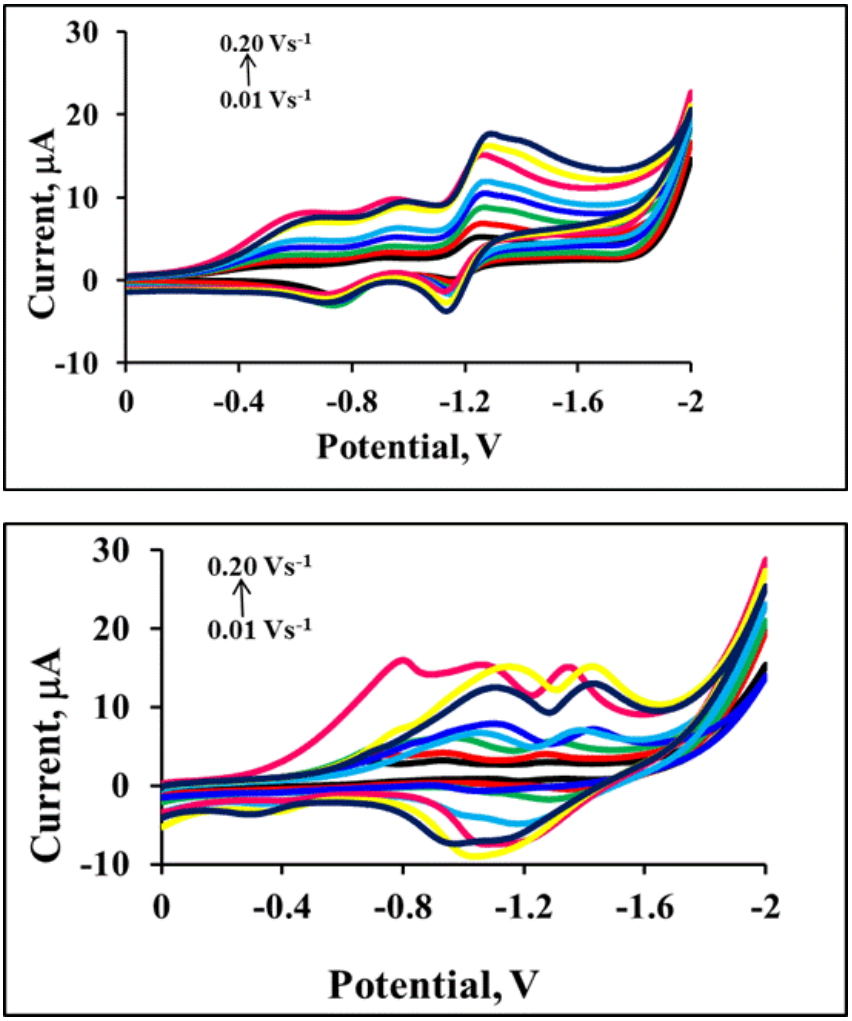

Figure 2.11: Cyclic voltammograms measured simultaneously with ECL of a 5 mM solution BODIPY-COOH in the presence of 3 mM BPO in (a) DMSO and (b) MeCN at scan rates of 0.01 - 0.2 V s^{-1} using a 3 mm platinum working electrode. The supporting electrolyte is 0.1 M TBATFB.

From the ECL scan rate dependence studies in both DMSO and MeCN, the results showed that light generation is only achieved when both BODIPY-COOH and BPO are reduced at the Pt electrode to form radical anions. However, in MeCN the reduction of BPO and BODIPY-COOH does not immediately invoke ECL generation. Light generation is only observed at potentials more negative than -1.3 V, although both BODIPY and BPO are

reduced before -1.00V. This can be accounted for by the reaction of BPO reduction, which yields products which are capable of reacting with BODIPY-COOH, generating reactive radical species of BPO. These in turn react with BODIPY-COOH radical anion, generating the excited state at potentials above - 1.3 V.

After the solution phase ECL studies, a film was noticed on the surface of the electrode and the electrode transferred into blank solution of MeCN and 0.1 M TBATFB, and the CV is presented in Figure 2.12. Two peaks are observed, the first one is observed at - 0.336 V and it suspected to be a reduction potential of a decomposition product of BPO. The second peak is observed at -0.87 V and it attributed to the reduction potential of a BODIPY film formed on the surface of the electrode after ECL is different behaviour from what has been for a structurally related BODIPY.[21] Bard and co-workers attributed the film formation to the lack of electron donating substitutions in positions 2 and 6 of the BODIPY core.[19] They explained that in the absence of substitutions 2 and 6 the radical cations that are generated are unstable by-products which can polymerize and lead to film formation. They products of oxidative polymerization have not yet been identified but another study suggested that these by products could be analogous of polypyrrole.[29]

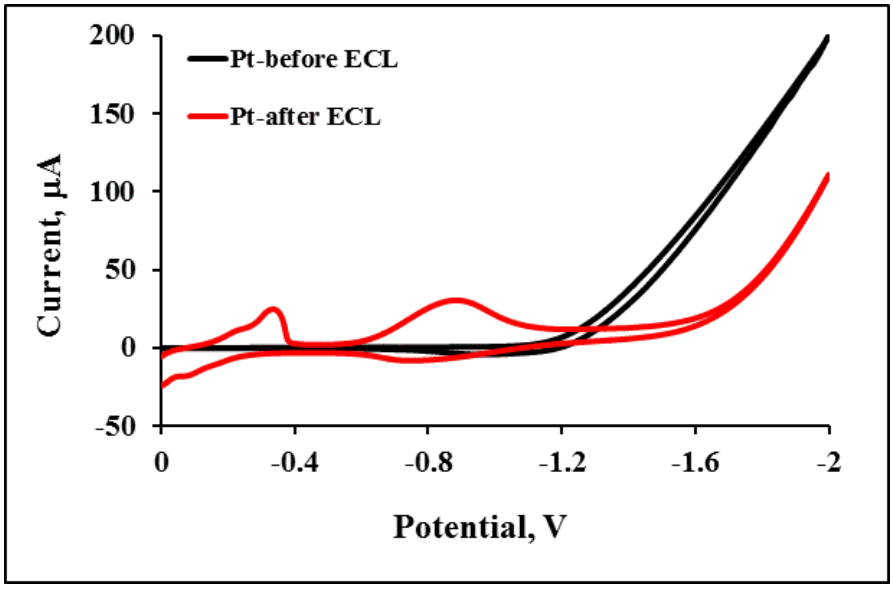

Figure 2.12: Cyclic voltammograms of Pt electrode before and after ECL in a blank MeCN and 0.1 M TBATBF, at 0.1 V s^{-1}.

The ECL mechanism of BODIPY and BPO[30] reaction is outlined below.

$$BODIPY + e \rightarrow BODIPY^{\bullet -} \quad \textbf{[2.2]}$$

$$BPO + e \rightarrow BPO^{\bullet -} \quad \textbf{[2.3]}$$

$$BODIPY^{\bullet -} + BPO^{\bullet -} \rightarrow {}^{1}BODIPY^{*} + BPO \quad \textbf{[2.4]}$$

$${}^{1}BODIPY^{*} \rightarrow BODIPY + h\nu \quad \textbf{[2.5]}$$

Alternatively benzoate radical anion ($BPO^{\bullet -}$) formed in equation 2.3 can dissociate into a benzoate ion ($C_6H_5CO_2^-$) and a benzoyloxy radical ($C_6H_5CO_2^{\bullet}$). The latter then proceeds to react with $BODIPY^{\bullet -}$ to produce the exicited stated BODIPY.

In this study it has been demonstrated that when using BPO as a co-reactant luminescence is observed only when negative potentials greater than -0.5 V

are applied (see Figs 2.8 to 2.10). Hence, it was worth investigating ECL with a co-reactant which is reduced at less negative potentials than the reduction potential of BODIPY-COOH, so as to evaluate whether ECL can be fine-tuned to less negative potentials. It has been previously reported that hydrogen peroxide is irreversibly reduced from –0.4 to -1.4 V in phosphate buffer,[31] hence, H_2O_2 was used as the second co-reactant.

2.3.3.2. Electrochemiluminescence using H_2O_2 as co-reactant

Like in the case of BPO, ECL in the presence of H_2O_2 was measured by linearly applying potential towards a negative potential, from an initial of 0.0 V to a final potential -2.00 V and reversing it back to the initial potential of 0.00 V.

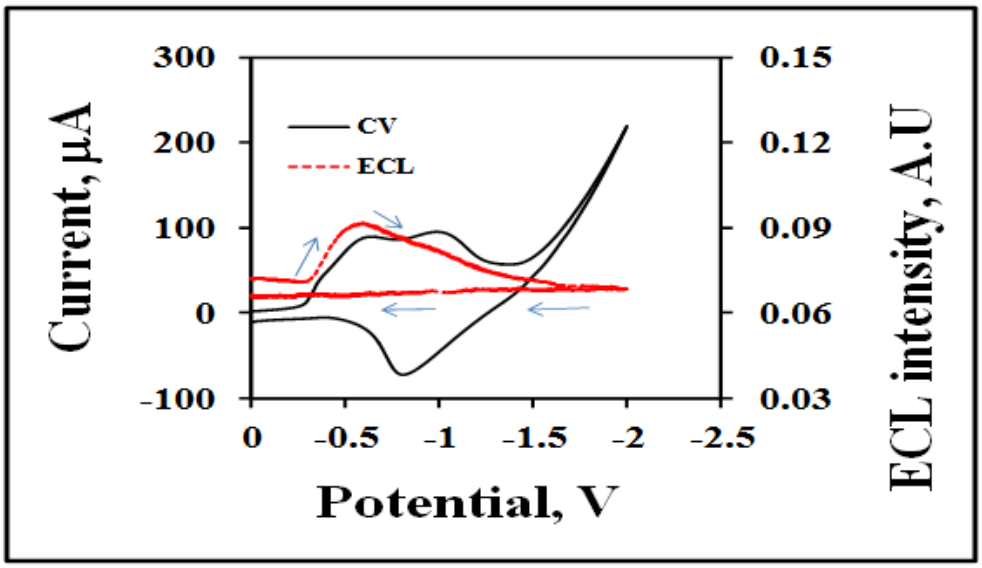

Figure 2.13: Cyclic voltammogram and ECL of MeCN solution of 5 mM BODIPY-COOH dye in the presence of 3 mM H_2O_2 obtained with a 2 mm Pt electrode at a scan rate of 0.1 V s^{-1}. 0.1 M TBATFB was used as the supporting electrolyte.

Control experiments were conducted using a clean platinum electrode, with no BODIPY present in the solution, where the solution only contained 3mM hydrogen peroxide in 0.1 M TBATFB in MeCN at 0.1 V s^{-1} and no ECL was observed. However, the CV measured simultaneously revealed two reduction peaks of hydrogen peroxide, the first one was observed at -0.43 V and the second one is at -1.00 V. The first reduction potential of hydrogen peroxide occurred at a potential which is less negative than the reduction potential of BODIPY-COOH. When 5 mM BODIPY-COOH was added to the solution of 3 mM H_2O_2 in MeCN and TBATFB at platinum electrode, ECL was initiated at an onset of -0.40 V as observed in Figure 2.13.

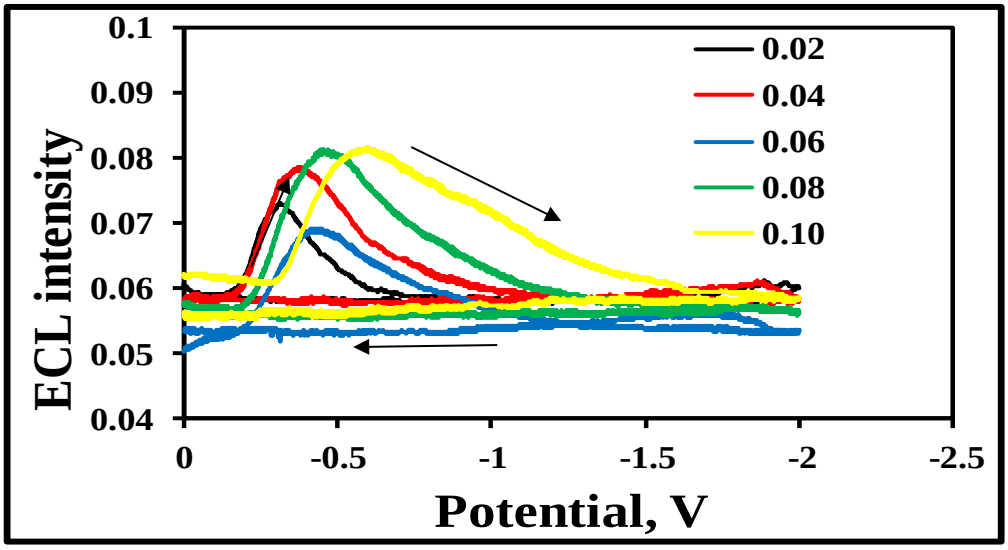

Figure 2.14: ECL responses for a 5 mM BODIPY-COOH solution and 3 mM BPO in MeCN obtained with a 2 mm platinum working electrode at scan rates of 0.02 - 0.1 V s^{-1}. The supporting electrolyte is 0.1 M TBATFB. The initial potential was 0.00 V and the potential was initially scanned in the negative potential direction.

Electrochemiluminescence of BODIPY-COOH in MeCN using H_2O_2 as a coreactant was investigated at different scan rates, *i.e.* 0.02 - 0.1 V s^{-1}. The ECL profiles are presented in Figure 2.14 and reveal that the ECL intensity increases with increasing scan rate. At all scan rates, ECL was generated at less negative potentials in the presence of 3 mM H_2O_2 coreactant in MeCN compared to what was observed in the case of benzoyl peroxide. The CVs obtained simultaneously with ECL shown in Figure 2.15 display a reduction peak at - 0.40 V, and it is at this potential where ECL is initiated, and it corresponds to the reduction potential of H_2O_2.[32]

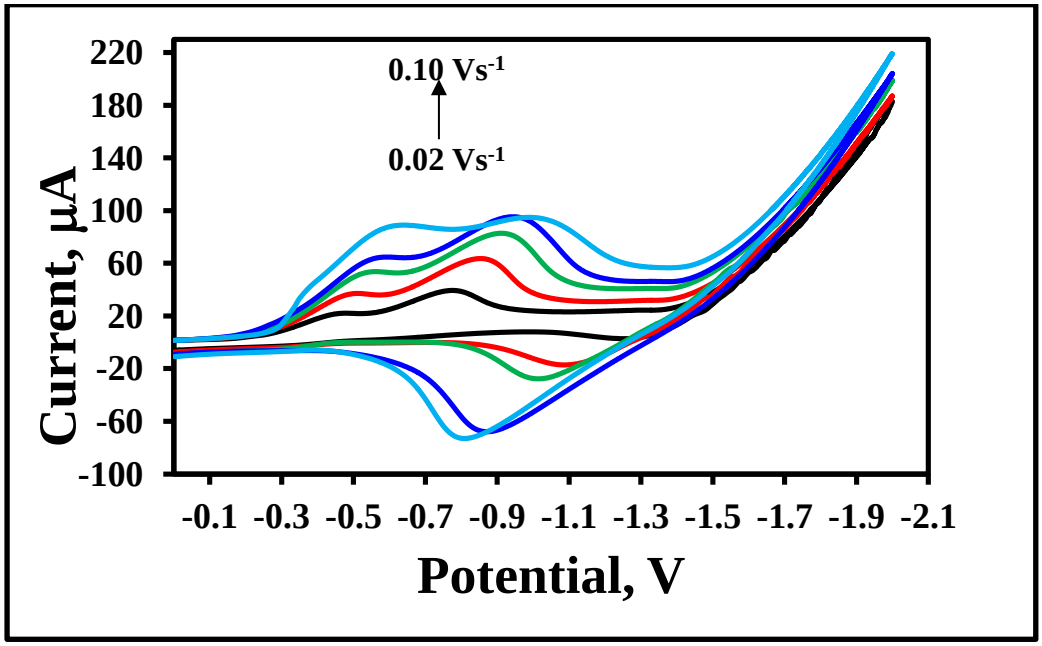

Figure 2.15: Cyclic voltammetry measured during ECL of 5 mM BODIPY-in the presence of 3 mM H_2O_2 coreactant in DMSO and 0.1 M TBATFB as the supporting electrolyte. The working electrode is 3 mm platinum and the scan rate is 0.1 V s^{-1}.

The result of light being turned on 50 mV before the reduction potential of BODIPY is unexpected, because $BODIPY^{\cdot -}$ has to be present in solution for the excited state to be produced from the cross reaction between $BODIPY^{\cdot -}$ and $^{\bullet}OH$. There are two possible factors that can be looked at to rationalize this observation of light being turned on before the reduction potential of BODIPY. The first factor is the environmental sensitivity of the shift of the reduction potential of BODIPY. The reduction of BODIPY has been measured in DMSO or MeCN and TBATFB as the supporting electrolyte and the experimental has shown that BODIPY is reduced at -0.89 and -0.96 V in MeCN and DMSO, respectively.

These results imply that the reduction potential of BODIPY is not significantly sensitive to the local environment. Although, the composition of the solution in which ECL is conducted is different from the above two mentioned solutions, because it contains hydrogen peroxide coreactant, it is unlikely that presence of H_2O_2 will induce a shift of the reduction potential of BODIPY towards -0.4 V. Another factor that can be looked at is the energy involved, the ΔG of this is reaction is 0.5 eV, thus the reaction seems thermodynamically uphill. It is not yet clear what causes the onset of ECL to be tuned to less negative potentials, however, control experiments that were conducted in the absence of BODIPY, where the reaction solution only contained hydrogen peroxide, MeCN and TBATFB, showed that no ECL occurred in the absence of BODIPY. ECL studies of a previously reported structurally related BODIPY in the presence of H_2O_2 reported similar observations where the ECL onset was -0.4 V, while

the reduction potential of BODIPY was observed - 0.67 V in MeCN.[24] Equations 2.6 -2.9 give a mechanism of ECL generation in of this dye in the presence of H_2O_2.

$$H_2O_2 + e \rightarrow OH^- + {}^{\bullet}OH \quad \textbf{[2.6]}$$

$$BODIPY + e \rightarrow BODIPY^{\bullet -} \quad \textbf{[2.7]}$$

$$BODIPY^{\bullet -} + {}^{\bullet}OH \rightarrow BODIPY^{*} + OH^- \quad \textbf{[2.8]}$$

$$BODIPY^{*} \rightarrow BODIPY + h\nu \quad \textbf{[2.9]}$$

Comparing the ECL profiles previously obtained when BPO was used as a coreactant to those obtained by employing H_2O_2 as a coreactant in MeCN, it clear that ECL intensity of those obtained with hydrogen peroxide are significantly less. Although the intensity of ECL generated with H_2O_2 is approximately ~50% of that when BPO is used, employing hydrogen peroxide as a coreactant generates ECL at less negative potentials. The reason for the weak ECL intensity in H_2O_2 can be attributed to the extremely short lifetime of the ${}^{\bullet}OH$ radical. It has been reported that in the first 5 μs of the reaction, only 1% of the initial ${}^{\bullet}OH$ generated remains in the reaction. The rest of the 99% of the initial amount of ${}^{\bullet}OH$ is consumed by reactions with H_2O_2 and other radical ${}^{\bullet}OH$, dissolved CO_2 and O_2 at the electrode in order of microseconds.[33] The results in this study demonstrate the ECL intensity and the onset potential of where the light generation is initiated of BODIPY-COOH largely depends on the coreactant employed.

2.3.4. FORMATION OF BODIPY-COOH THIN FILMS VIA CYSTEAMINE COUPLING

The previous section demonstrated that BODIPY-COOH in solution exhibits ECL with two different coreactants; *i.e.* benzoyl peroxide and hydrogen peroxide. The onset potential at which the light is turned on is greatly influenced by the coreactant that is used. However, the solution based approach ECL has its own limitations such as loss of signal due to the diffusion of the ECL reagent out of the detection zone and having to continuously supply the ECL luminescent reagent to the reaction zone.[34] These limitations restrict the practical applications of ECL.

The ability to immobilize the luminescent reagent on the surface of the electrode circumvents the disadvantages experienced in solution based ECL,[35] and also increases the scope of potential ECL applications.[36] BODIPY-COOH offers the advantage of having the ability to be covalently bound to the electrode via a cysteamine layer. From the aforementioned Scheme 2.1, process 2 which the rates of heterogeneous electron transfer to BODIPY to form its reduced $BODIPY^{\cdot -}$ will be influenced by the distance from the electrode to the luminophore. Scheme 2.2 below presents the coupling of BODIPY-COOH to the amine functionality of cysteamine. The thin films were produced by immersing a clean platinum electrode in a solution of 1 mM cysteamine in ethanol for 16 h. Subsequently, BODIPY-COOH was coupled to

the amine functionality of cysteamine via EDC (1-Ethyl-3-[3-dimethylaminopropyl] carbodiimide hydrochloride) coupling in DMF.

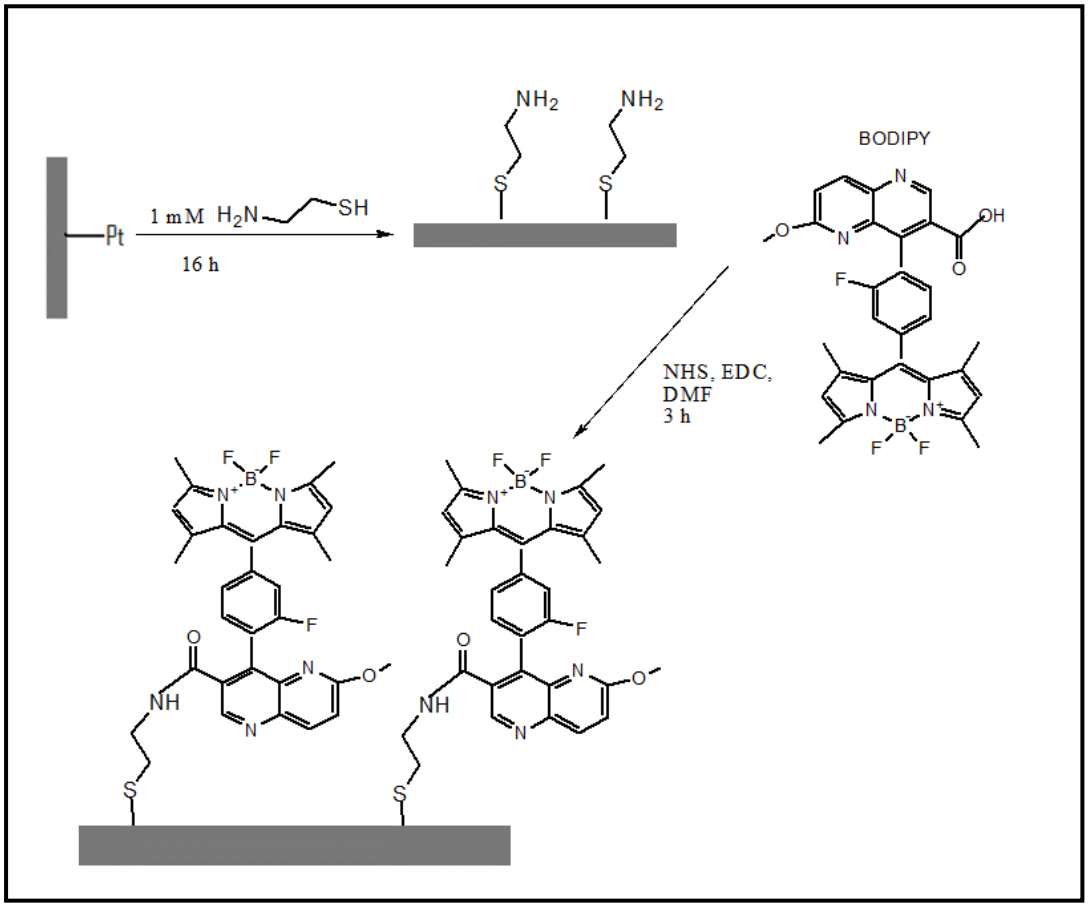

Scheme 2.2: Formation of BODIPY–COOH thin film via EDC coupling on a 2 mm platinum electrode using 1 mM cysteamine dissolved in ethanol.

2.3.4.1. Electrochemical properties of BODIPY-cysteamine SAM

2.3.4.1.1. Cyclic voltammetry

Modifying an electrode with a cysteamine layer introduces a barrier to electron transfer between the electrode and the redox species in solution. Before coupling BODIPY to the cysteamine linker, it was necessary to evaluate whether the cysteamine layer formed successfully on the platinum electrode. Cyclic voltammetry of the same platinum electrode was measured in a ferrocene methanol solution before and after forming the cysteamine layer. Ferrocene was used as a redox probe molecule due to its chemical stability and its ideal reversible electrochemistry in solution. Figure 2.16 (a) shows the reversible electrochemical behaviour of ferrocene methanol dissolved in phosphate buffer solution (PBS), at a bare Pt electrode.

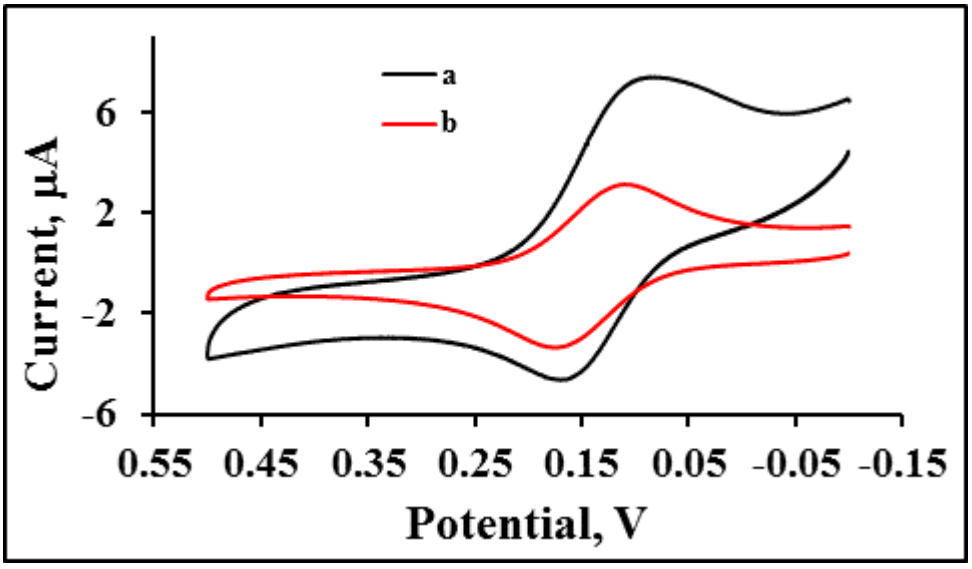

Figure 2.16: Effect of formation of a cysteamine layer on the cyclic voltammetry of ferrocene methanol on a bare platinum electrode (a) and on the same platinum electrode after the electrode has been modified with the

cysteamine layer (b). The voltammetry was assessed in phosphate buffer solution electrolyte, the scan rate was 0.1 V s^{-1}.

The bare platinum electrode in Figure 2.16 appears asymmetrical in shape and displays a reduction peak at 0.11 V, while oxidation is observed at E_{pa} = 0.18 V. The peak to peak splitting is 0.07 ΔE_p and it remains unchanged upon formation of the cysteamine layer as shown in Figure 2.16 (b). When the electrode was modified with cysteamine a significant decrease in the oxidation and reduction current was observed. This could indicate that the cysteamine layer has successfully formed on the electrode surface.

It was also necessary to evaluate the blocking of the electrode in the solvent which will be used for subsequent ECL studies. Figure 2.17 illustrates the voltammetry of ferrocene methanol. However in this case, it was dissolved in DMSO and TBATFB as the supporting electrolyte. The behaviour of the ferrocene was different from what was observed in PBS, *i.e.,* the oxidation shifted to more positive values. The bare electrode in ferrocene methanol in DMSO displays a cathodic reduction peak at 0.2 V, while oxidation is observed at E_{pa} = 0.4 V, suggesting that the redox species has access to the electrode surface as observed in Figure 2.17 (a). When the electrode was modified with cysteamine, the ferrocene had reduced access to the electrode surface resulting in a decrease in current (see Figure 2.17 (b)). The peak to peak separation of ferrocene in DMSO is 0.2 V and it appears to be large when compared to the behaviour observed in phosphate buffer. The results

indicate that the reaction in DMSO involves a slow rate of electron transfer which results in large peak separations.

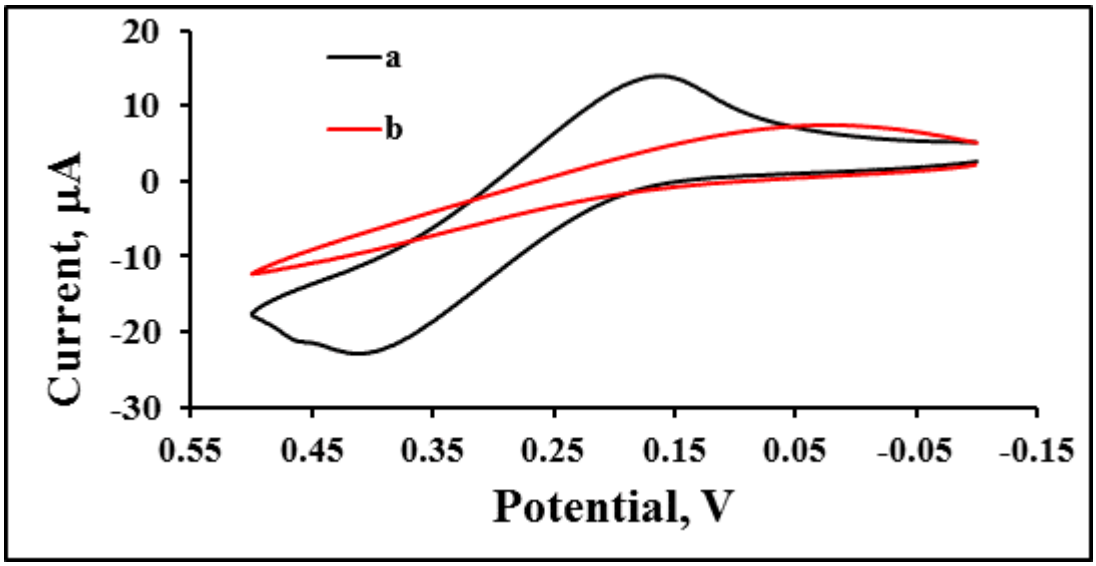

Figure 2.17: Effect of cysteamine thin film formation on the cyclic voltammetry of ferrocene methanol on a bare platinum electrode (a) on the same platinum electrode after modification of the electrode with a cysteamine layer (b). The voltammetry was assessed in DMSO and 0.1 M TBATFB as a supporting electrolyte at a scan rate was 0.1 V s^{-1}.

When cysteamine layer was formed on the electrode the BODIPY dye was coupled to the layer to form a thin film of the dye, as demonstrated Scheme 2.2 above. The electrochemical, luminescence and electrochemiluminescence properties of the BODIPY-COOH thin films were subsequently interrogated and the results are presented below.

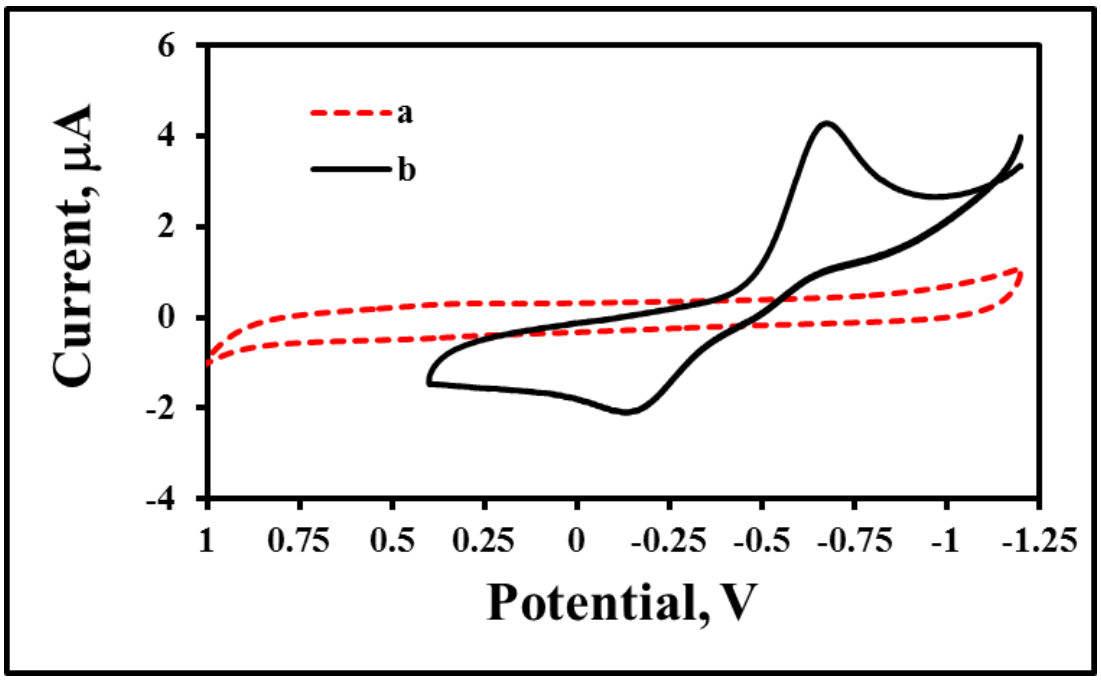

Figure 2.18: Cyclic voltammograms of bare a platinum electrode (a) and BODIPY-COOH thin film (b), in DMSO with 0.1 M TBATFB as supporting electrolyte. The working electrode is 2 mm platinum disc electrode, and the scan rate is 0.1 V s^{-l}.

Figure 2.18 illustrates the CV for the BODIPY film in DMSO at 0.1 V s^{-1} over the potential window 0.4 to -1.2 V shows that a single cathodic wave observed at E_{pc} = -0.677 V ascribed to the reduction of BODIPY and one anodic oxidation wave were observed at -0.163 V. The reduction peak shifts approximately -0.10 V to more negative potentials and the anodic oxidation peak also shifts with approximately -0.10 V to more positive values, as the scan rate increases (Figure 2.19). The peak to peak separation (ΔE_p) between the cathodic and anodic waves and full width at half maximum (FWHM) for BODIPY-COOH film in DMSO at 0.1 V s^{-1} were determined to be

0.514 and the 0.424 V, respectively. When a species is adsorbed to the surface of the electrode, ideally the ΔE_p and FWHM are expected to be 0 mV and 90 n/ mV, respectively, indicating that no interactions are taking place between the adsorbates, where n is the number of electrons transferred.[37] However, for BODIPY-COOH thin films in DMSO across all measured scan rates, ΔE_p is larger than what is expected for an ideal scenario, suggesting there are some destabilizing lateral interactions that exist between the adsorbates of the thin films.[38] The observation of large peak to peak splitting across at all scan rates is not due slow ion mass transport limitations; suggesting that, it is not kinetically controlled. This is because as the scan rate is varied (see Figs 2.19 and 2.20 below), there is relatively small change in the peak potentials. Another factor that can explain the origin of the large peak to splitting is the reoxidation of the ion pair from the TBATFB electrolyte, which causes the cations to move in out of the system. The surface coverage (Γ) of the thin film was estimated by integration of charge (Q) passed under the slowest measured sweep scan rate of 0.01 V s^{-1} according to Equation 1.39, and it was and it was 4.14 x 10^{-9} mol cm^{-2}.

$$\Gamma = \frac{Q}{nFA} \qquad \textbf{[1.39]}$$

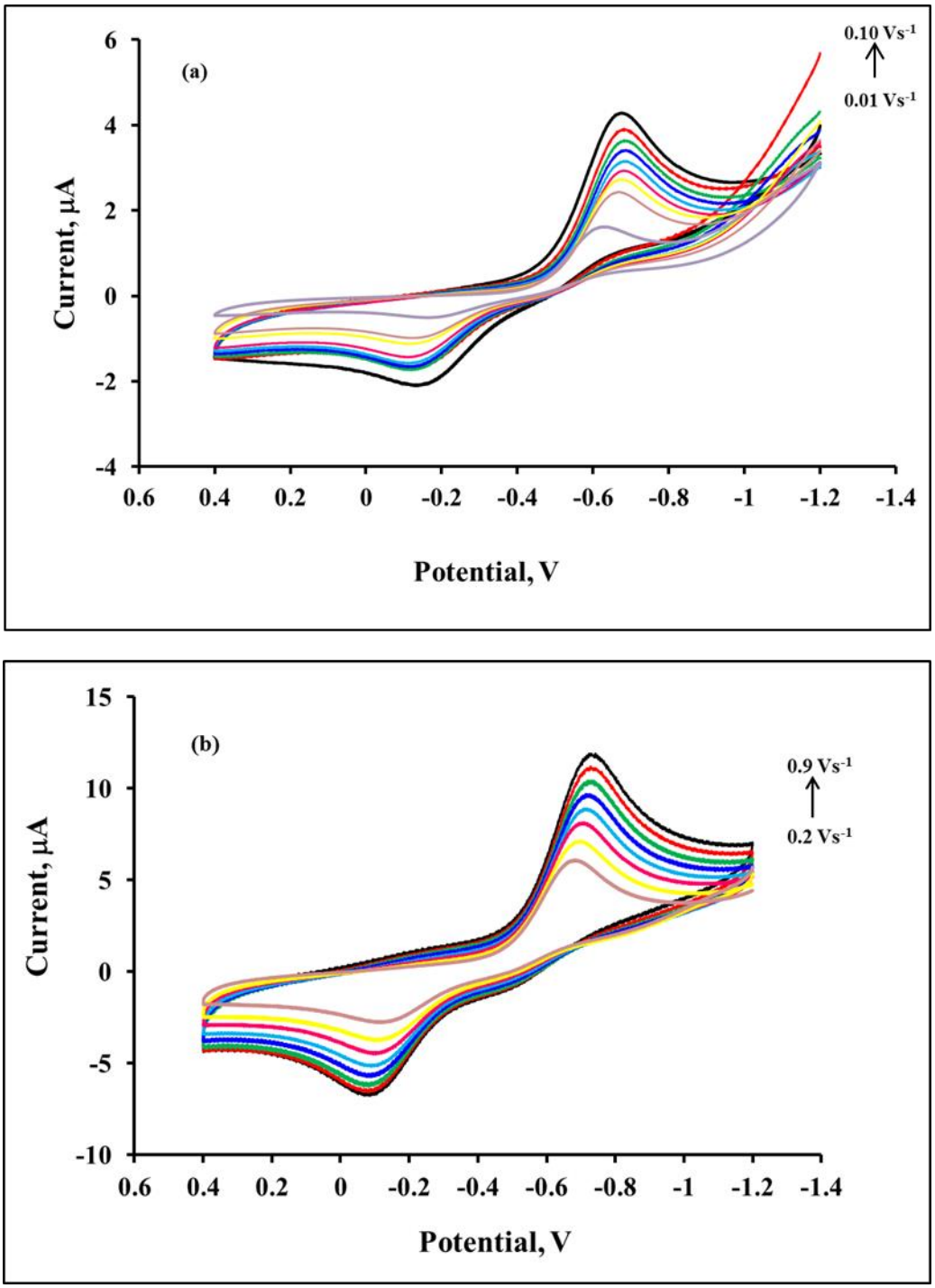

Figure 2.19: Scan rate dependence of the voltammetric responses of BODIPY-COOH thin film, on a 2 mm platinum electrode at (a) the low scan rates (0.01 - 0.1 V s^{-1}) and (b) high scan rates (0.2 - 0.9 V s^{-1}). The CV was

performed in DMSO containing 0.1 M TBATFB supporting electrolyte. The surface coverage is 4.1 x 10^{-9} mol cm^{-2}.

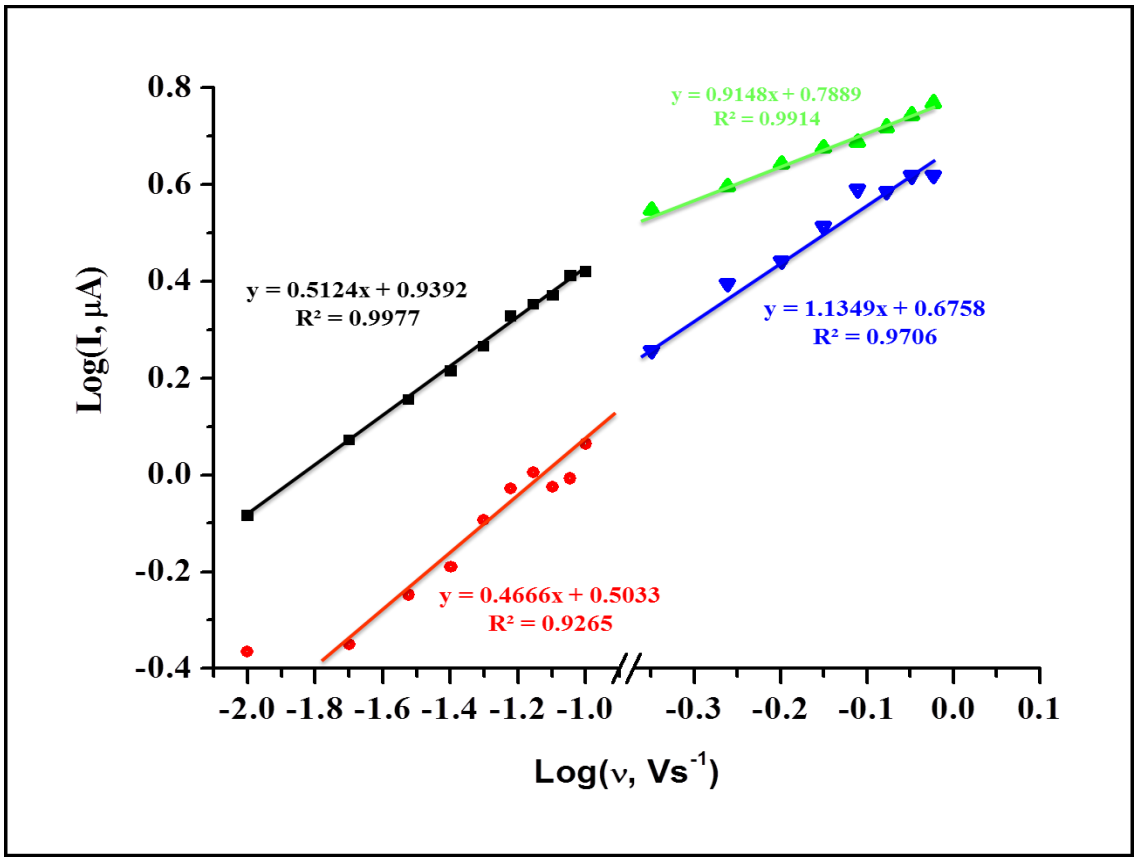

Figure 2.20: The log-log plot of the absolute value of the peak current vs scan rate for the BODIPY thin film for low scan rates (0.01 to 0.1 V s^{-1}) and high scan rates (0.2 to 0.9 Vs^{-1}) in DMSO containing 0.1 M TBATFB supporting electrolyte. The cathodic currents for lower scan rates are denoted in black and the cathodic currents for high scan rates are denoted in green. The anodic currents for low scan rates are denoted in red and the high scan rates in blue.

Figure 2.20 shows the plot of the logarithm of the absolute value of the reductive peak current, I_p, against the logarithm of the scan rate, ν. The result shows a linear relationship with a slope of 0.466 which is close to the expected value of 0.5 for low scan rates (0.01 to .0.1 V s^{-1}) and semi-finite

diffusion control; and a slope of 1.13 for high scan rates (0.2 to 0.9 V s^{-1}) which is close to the expected value of 1 for electrode systems under finite diffusion control. These results indicate that at lower scan rate, the peak current is directly proportional to the square root of the scan rate, and at higher scan rate, the peak current is directly proportional to the scan rate.

The voltammetric behaviour of the BODIPY-COOH thin films was also evaluated in MeCN and the results are presented in Figure 2.21 below. In MeCN at 0.1 V s^{-1}, an irreversible reduction peak is observed at -0.818 V, which is more negative compared to E_{pc} = -0.677 V in DMSO at the same scan rate. The shift to more negative reductive behaviour suggests that it is more difficult to drive reduction of the BODIPY thin film in MeCN compared to in DMSO. Moreover, two oxidation peaks are observed in MeCN, one broad peak at E_{pa} = -0.010 V and a second peak at more positive potentials at E_{pa} = 0.690 V. The reduction potential of BODIPY in MeCN (-0.891 V) is almost the same as that of BODIPY thin film (-0.818 V) which suggest that in MeCN the BODIPY adsorbs on the electrode surface.

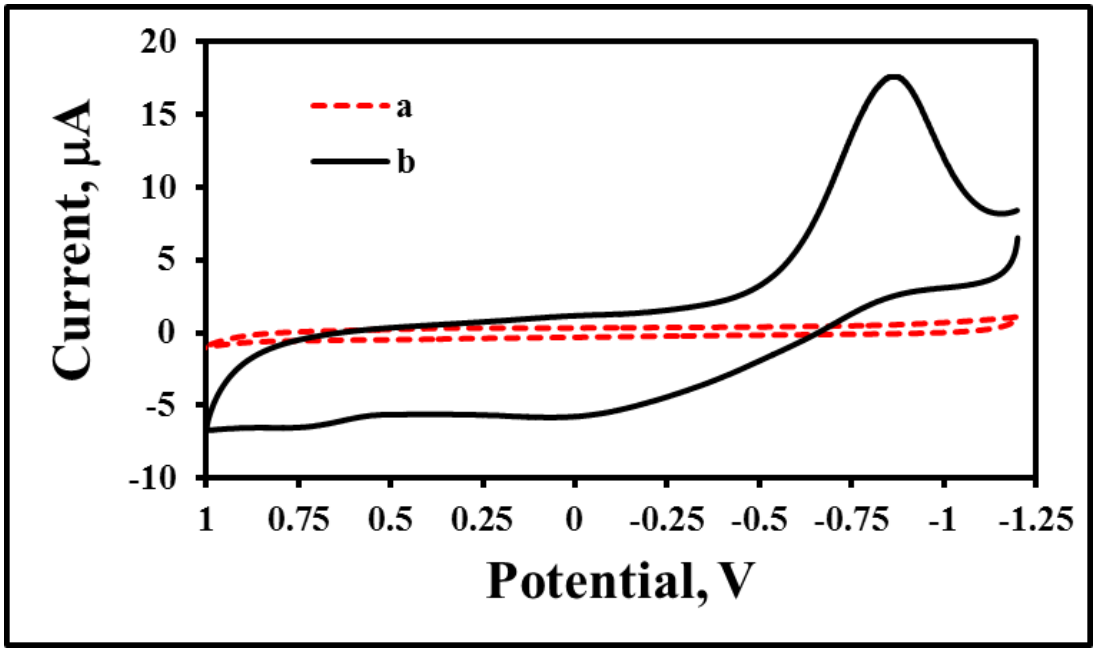

Figure 2.21: Cyclic voltammogram of bare a platinum electrode (a) and BODIPY-COOH thin film (b), in MeCN with 0.1 M TBATFB as supporting electrolyte. The working electrode is 2 mm platinum disc electrode, and the scan rate is 0.1 V s^{-1}.

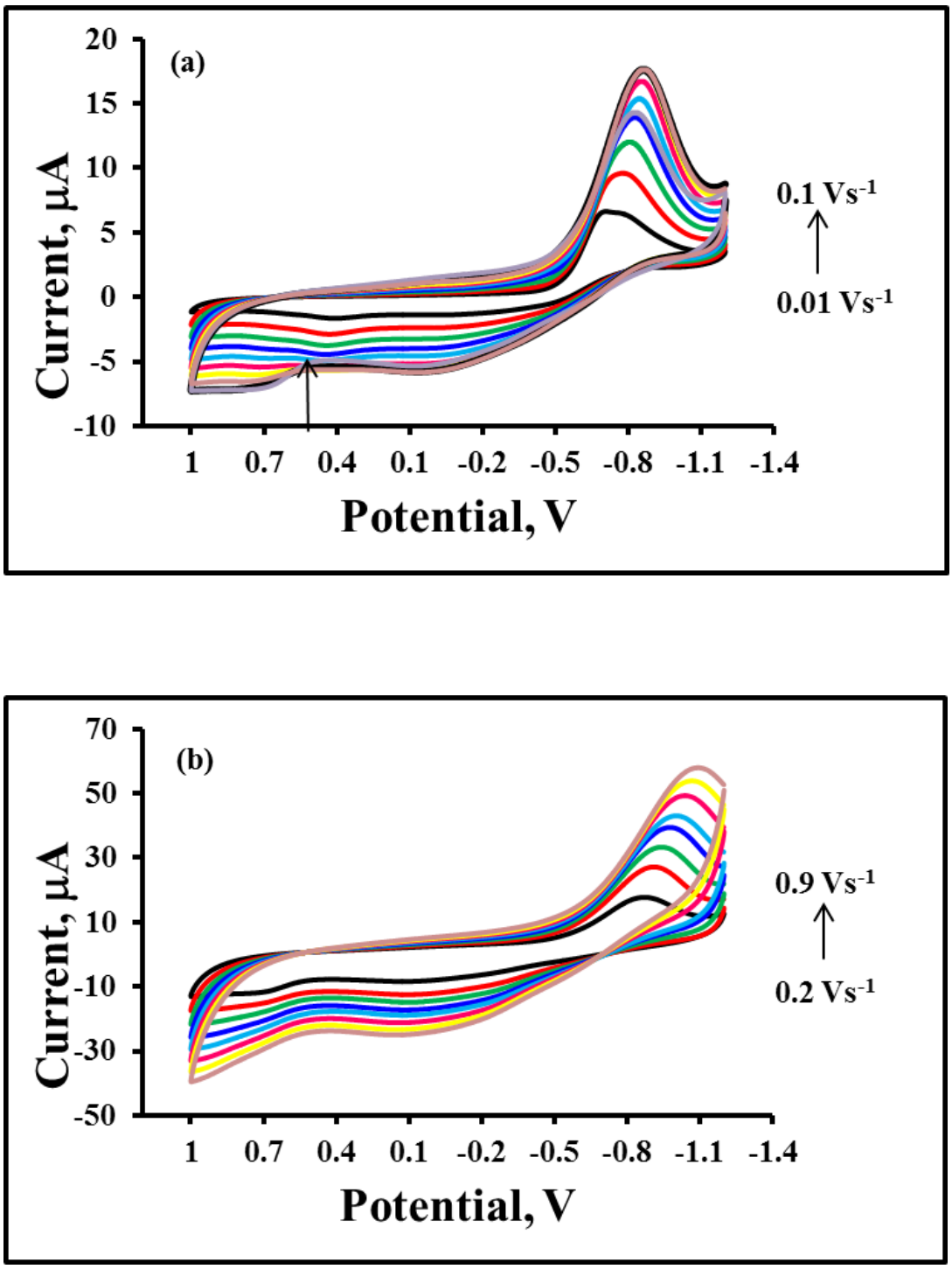

Figure 2.22: Scan rate dependence of the voltammetric responses of BODIPY-COOH thin films on a 2 mm platinum electrode at (a) the low scan rates (0.01 - 0.1 V s^{-1}) and (b) high scan rates (0.2 - 0.9 V s^{-1}). The CV was performed in MeCN containing 0.1 M TBATFB supporting electrolyte and the surface coverage is 1.5 x 10^{9} mol cm^{-2}.

Figures 2.22 above shows the scan rate dependent voltammetry of the BODIPY-COOH films in MeCN. The cathodic reduction peak shifts to more negative values, as the scan rate is increased from 0.01 to 0.9 V s^{-1}. The second oxidation peak observed shifts to more positive oxidation potentials as the scan rate was increased from 0.01 to 0.10 V s^{-1}. It should be noted that, at shorter experimental time, *i.e.* at scan rates beyond 0.20 V s^{-1}, the second oxidation peak is not observed and this is demonstrated in Figure 2.22(b). The surface coverage of the thin film was estimated to be 4.14 ± 0.2 x 10^{-9} and 1.51± 0.1 x 10^{-9} mol cm^{-2} in DMSO and MeCN, respectively It has been previously reported in studies of a structurally related BODIPY that the surface coverage is likely to be controlled by area controlled by the head group of BODIPY rather than the cysteamine linker.[19] The surface coverage variation with solvent may be related to the polarity of the solvent which determines to what extent BODIPY is solvated before it diffuses to the electrode surface.

From the surface coverage, the average area of occupation per adsorbed molecule is estimated to be 4 and 11 $Å^2$ in DMSO and MeCN, respectively. Crystallography data previously reported in study of an un-substituted 4,4-difluoro-4-bora-3a,-4a-diaza-BODIPY core, suggested that the area occupied per molecule is approximately 100 $Å^2$ for perpendicularly orientated molecule, or 180 $Å^2$ for parallel orientation.[17] That means more than one monolayer is

deposited if average area of occupation per adsorbed molecule is less than 100 $Å^2$.

2.3.4.1.2. Photoluminescence properties of BODIPY-COOH thin films

When one compares the ECL of the BODIPY derivative in solution versus when it is within a self-assembled monolayer or thin film, the molecule is in a very different environment in each case and this can have a very significant impact on the photophysics of the luminophore. A key difference is that the BODIPY concentrations between solution and thin film are dramatically different. Significantly micromolar concentrations are typically used in solution experiments compared to molar concentration within an undiluted self-assembled film. The high molar concentrations found in a film may limit the overall ECL efficiency, due to self-quenching.[39] Other effects include the change in the dielectrics the molecule experiences in the thin film compared to solvent, the increased rigidity of the environment in the thin film and the possibility of direct surface interactions.[40] The photoluminescence studies were conducted on the BODIPY films in solvents that have different polarity/dielectric constant; *i.e.* water, ethanol, dimethyl sulfoxide and acetonitrile. The photoluminescence investigation was carried for the following reasons; firstly to evaluate whether BODIPY remained luminescent or does it get quenched when it is in a tightly packed film on the electrode surface, because when the film is applied in ECL studies it needs to remain luminescent as a film. Furthermore, the solvent dependence was evaluated to identify the best solvent for ECL, *i.e*., the solvent in which the BODIPY thin

film exhibits the strongest luminescence. For the thin films, in each case, the samples were excited at 488 nm, using an argon ion laser line and the resulting emission spectra are presented in Figure 2.23.

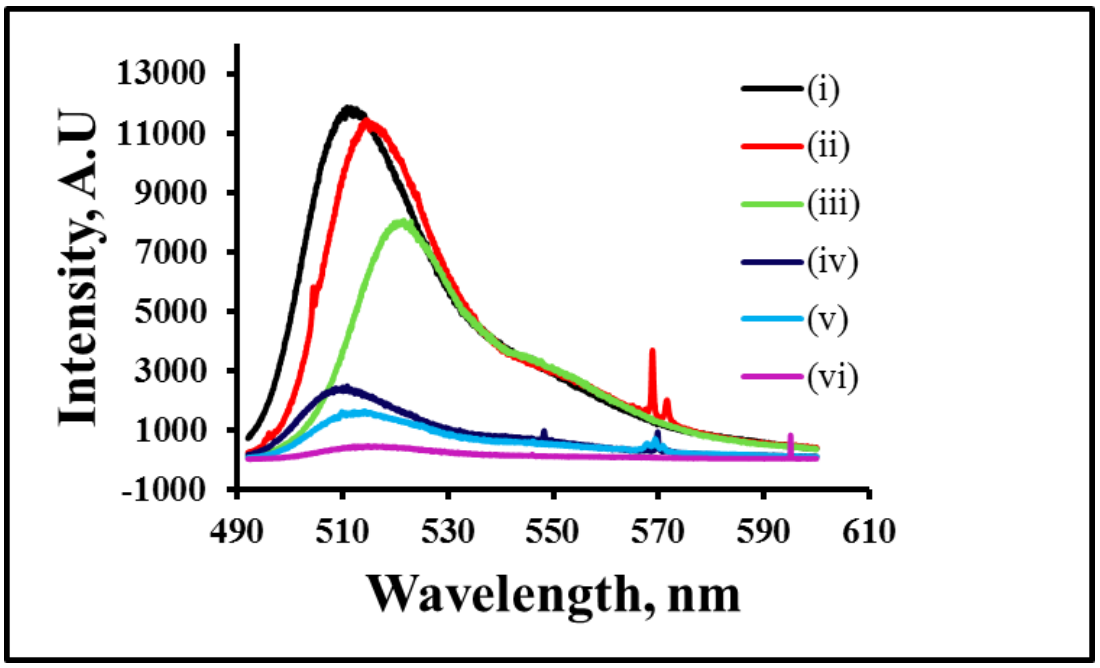

Figure 2.23: Photoluminescence spectra of BODIPY thin film in (i) H_2O, (ii) DMSO, (iv) EtOH, (v) MeCN, and (vi) Dry BODIPY-thin film (No Solvent). (iii) Solution BODIPY in DMF, The surface coverage of the monolayer is 4.2 x 10^{-9} mol cm^{-2}. Samples were irradiated using argon laser excitation at 488 nm, the laser power was 0.020 mW.

It shows that the dry BODIPY thin film (curve vi) and the film which was analysed in contact with H_2O, DMSO, MeCN and EtOH displayed similar luminescence properties. Upon excitation at 488 nm, one emission maxima centred approximately at 510 ± 5.00 nm is observed in all samples which is typical of BODIPY dyes. The results indicate BODIPY remains luminescent within a thin film at the electrode. This is in spite of the fact that the film is undiluted and therefore present at possibly molar concentrations. This

confirms that any self-quenching present is not complete and thus it may have useful ECL properties. Interestingly, the emission spectra are relatively strongly affected by the dielectric or polarity of the contacting solvent, suggesting that solvent can penetrate the film effectively. The results show that the emission intensity is affected by the polarity of the contacting solvent. The laser power and the detector settings were kept identical for all sample, therefore emission of the samples can be directly compared. From Figure 2.23, it can be observed that dry BODIPY-film (curve vi) which was analysed with no solvent present, exhibits the weakest luminescence intensity as compared to all the other samples. In contrast, the BODIPY-thin films analysed in the presence of different solvents with different solvent polarities, displayed higher luminescence, with the luminescence intensity increasing with the increasing solvent polarity. Water is the most polar, while ethanol is the least polar solvent among them all (based on their dielectric constants). Interestingly, the BODIPY-COOH thin film that was analysed in water displayed the strongest luminescence intensity, and the one analysed in ethanol displayed the weakest luminescence, the observed trend is demonstrated in Table 2.3 below. It should be noted that the sequence of exposing the BODIPY to different solvents did not affect the final intensity, as the dry film was always the first measurement, and after the film was exposed to the different solvents, the dry film was measured again to see if there any change in the film, and no change was observed and the same intensity of dry film was recovered. Furthermore, the measurement was reproducible as it was repeated on three electrodes and the same behaviour was observed all cases.

Table 2.3: Photoluminescence intensity of BODIPY thin films in different solvents.

Sample and solvent BODIPY	Curve	Polarity: Dielectric constant	Emission Wavelength (nm)	Luminescence Intensity
H_2O	(i)	80.0	510 ± 5	11700 ± 200
DMSO	(ii)	46.7	515 ± 5	11500 ± 195
DMF (in solution)	(iii)	38.0	525 ± 5	7900 ± 134
MeCN	(iv)	37.0	510 ± 5	2100 ± 36
Ethanol	(v)	24.5	510 ± 5	1650 ± 28
No solvent (Dry film)	(vi)	None	515 ± 5	200 ± 3

The highest intensity that is observed in water is particularly interesting as water can sometimes be an effective quencher.[41] The observation that ethanol and water give same wavelength emission at 510 ± 5 but have very different dielectric suggests H-bonding is playing a role in the photophysics in these solvents. The origin of the significant enhancement of the emission intensity in water is unclear, but potentially useful if applying these materials in ECL applications in biological media. The results suggest that solvent exclusion from the thin film is not taking as the luminescence seems to be influenced by the dielectric constant of the solvent rather than that of the film itself. Solution BODIPY (curve iii) exhibited emission maxima at 520 ± 5 nm in DMF, which is red shifted compared to of emission observed in the thin film. The emission wavelength for the BODIPY thin film in different solvents does not exhibit any significant shift.

2.3.4.3. Electrochemiluminescence of BODIPY-COOH thin film

Electrochemiluminescence of the BODIPY-COOOH thin films was investigated in the same experimental conditions as the solution ECL studies which were carried previously. The applied potential was swept linearly from an initial potential of 0.00 to -2.00 V in MeCN and DMSO in the presence of either BPO or H_2O_2 as coreactant while measuring the current and light emitted intensity. ECL from the BODIPY thin film was only detected in DMSO in the presence of BPO as coreactant, and no ECL was detected in MeCN. The result of lack of ECL from the BODIPY thin film in MeCN can be associated with the luminescence behaviour observed in Figure 2.23 above, the emission intensity of the film was significantly less in MeCN, compared to in DMSO. Furthermore, when hydrogen peroxide was used as a coreactant, no ECL was generated from the BODIPY-COOH thin film in either solvent.

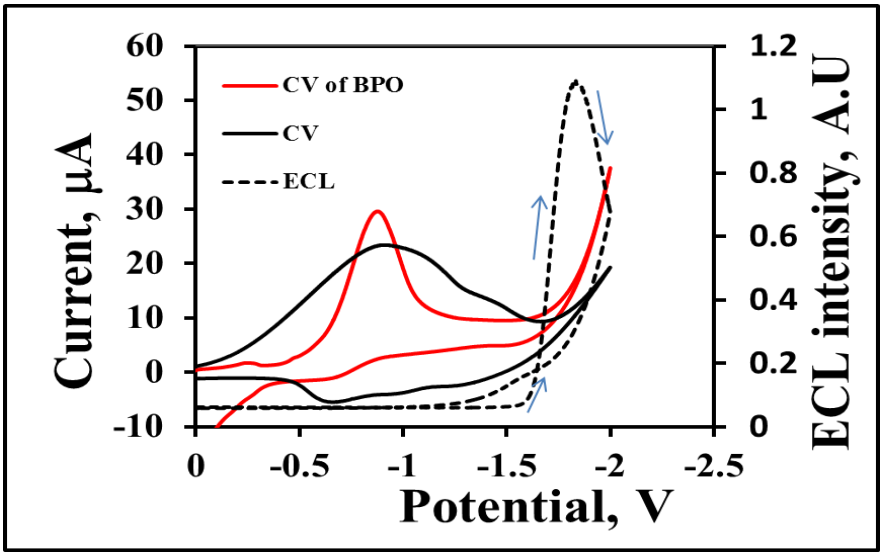

Figure 2.24: Cyclic voltammogram (solid line) and ECL spectra (dotted line) of Pt electrode modified with BODIPY-COOH thin film in DMSO with 0.1 M TBATFB supporting electrolyte in the presence of 90 mM BPO and 0.1 V s^{-1} scan rate.

ECL from the BODIPY-thin film modified platinum electrode was generated via coreactant pathway, in the presence of BPO coreactant dissolved in DMSO containing 0.1 M TBATFB. Upon applying a potential to the platinum electrode modified with BODIPY-COOH thin film from an initial potential of 0.00 V towards -2.00 V, BODIPY-COOH is reduced at E_{pc} = -0.677 V forming its radical anion BODIPY-COOH$^{\bullet-}$ and BPO is reduced at E_{pc} = -0.98 V. Although, the ECL of the luminophore and the coreactant are reduced before -1.00 V, no ECL is observed until potentials equal to or greater -1.60 V are applied as illustrated in Figure 2.24 above. It was previously explained in the solution studies that in the reaction sequence the reduced benzoate radical anion BPO$^{\bullet-}$ reacts with BODIPY-COOH$^{\bullet-}$generating excited state ^{1}BODIPY-COOH*. In the case of ECL generation from BODIPY thin films, the concentration of BPO used was relatively higher *i.e.* 90 mM compared to 3 mm which was used in solution ECL studies conducted previously. This implies that higher concentrations of benzoate radical anions will be produced to react with the BODIPY radicals to yield the excited state ^{1}BODIPY-COOH*. The light generation in Figure 2.24 is turned on from the onset potential of -1.65 V and it continues to increase reaching a maximum emission at -1.75 V, and relaxes back to the ground state on the reverse scan. The onset potential of -1.65 V in the BODIPY thin films is observed at more negative potentials compared to -1.00 V which observed in the BODIPY-COOH solution (DMSO) ECL. Successful ECL generation from BODIPY-COOH thin film confined to the surface of the electrode, suggests that the excited state is not strongly electronically coupled to the surface of the platinum electrode.

2.3.4.3.1. Dependence ECL intensity on BPO concentration

Previous ECL studies have demonstrated that the ECL emission intensity is proportional to the concentration of the coreactant.[42] To evaluate the effect of BPO concentration on ECL of BODIPY-COOH thin films modified electrodes, ECL was probed in the presence of various levels of BPO concentrations. The concentrations ranged from 10, 60, 120, 180 and 240 mM in DMSO and TBATFB scanning from an initial potential of 0.00V to -2.00 V at 0.1 V s^{-1} and the results are presented in Figure 2.25(a). In this system no ECL was observed at concentrations below 10 mM BPO. The ECL profiles depicted in Figure 2.25(a) show weak intensity starting at 10 mM, which increases progressively with increasing BPO concentration and this is also demonstrated in Figure 2.25(b) a plot of ECL intensity versus BPO coreactant concentrations. The plot shows that as BPO concentration increases, the ECL intensity increases linearly until peak intensity is reached at 180 mM BPO beyond this concentration and a decrease in the ECL intensity is observed, and almost no ECL is observed at 300 mM BPO. This suggests relatively high concentrations of BPO produced excess $BPO^{\bullet -}$ which quenched the excited state ^{1}BODIPY-COOH* and caused a drop in ECL intensity. Though, not investigated, it appears that BPO behaves as a solvent at high concentration and binds to (solvates) BODIPY-COOH and prevents the formation of ^{1}BODIPY-COOH* excited state. It is also possible that the ^{1}BODIPY-COOH* excited state is stabilised at high BPO concentration thereby preventing the emission of light.

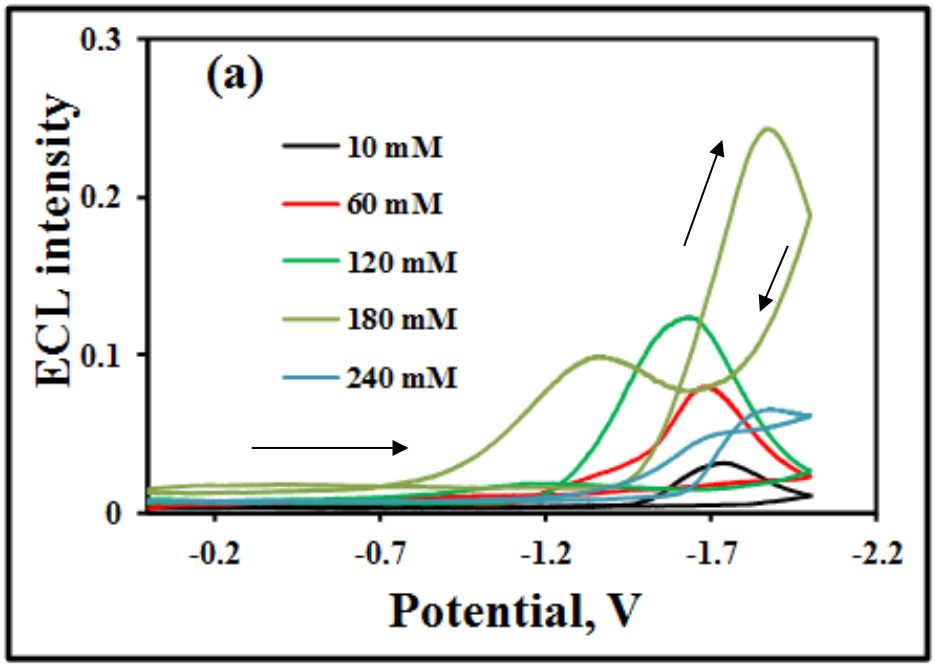

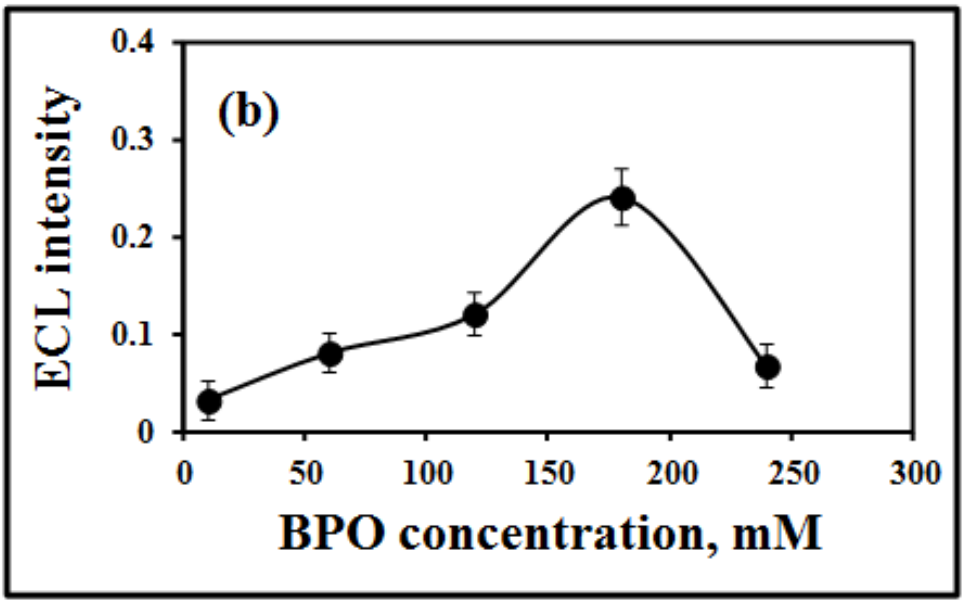

Figure 2.25: (a) ECL profiles of BODIPY-COOH thin film in DMSO solvent and in different BPO co-reactant concentrations at 0.1 V s^{-1} scan rate, the arrows indicate the progression of the ECL response and (b) Dependence of ECL intensity of the BODIPY-thin on BPO concentration at a fixed potential of -1.75 V. The error bars represent the standard deviations from three separate experiments (n = 3).

A particularly interesting feature in the ECL profiles presented in Figure 2.25 (a) is the remarkably different shapes they assume at different concentrations of the coreactant. Moreover, as the BPO concentration is varied, there is a significant shift in the potential at which the light is turned on. The shift of the onset potential can be ascribed to the exchange of electrons between BODIPY radical anion which reacts with the $BPO^{\bullet -}$ to produce the excited state. Formation of the BPO radical is the rate determining step, and when the concentration of BPO is varied it can be deduced that the time at which BPO radical is formed also changes and this is reflected by the onset potential.

2.3.4.3.2. ECL Scan rate dependence

The ECL dependence on BPO concentration studies showed that the optimum BPO concentration for generation of maximum ECL intensity is 180 mM and concentrations lower or beyond this exhibit lower ECL intensity. Thus, to carry out ECL scan rate dependence studies of the BODIPY-COOH thin films the coreactant concentration was kept constant at 180 mM BPO as it had proved to give the highest ECL intensity and only the scan rate was varied from 0.005 to 0.100 V s^{-1}. The ECL profiles obtained are presented in Figure 2.26 (a) and (b) below and a plot of ECL intensity vs scan rate is represented in Figure 2.27.

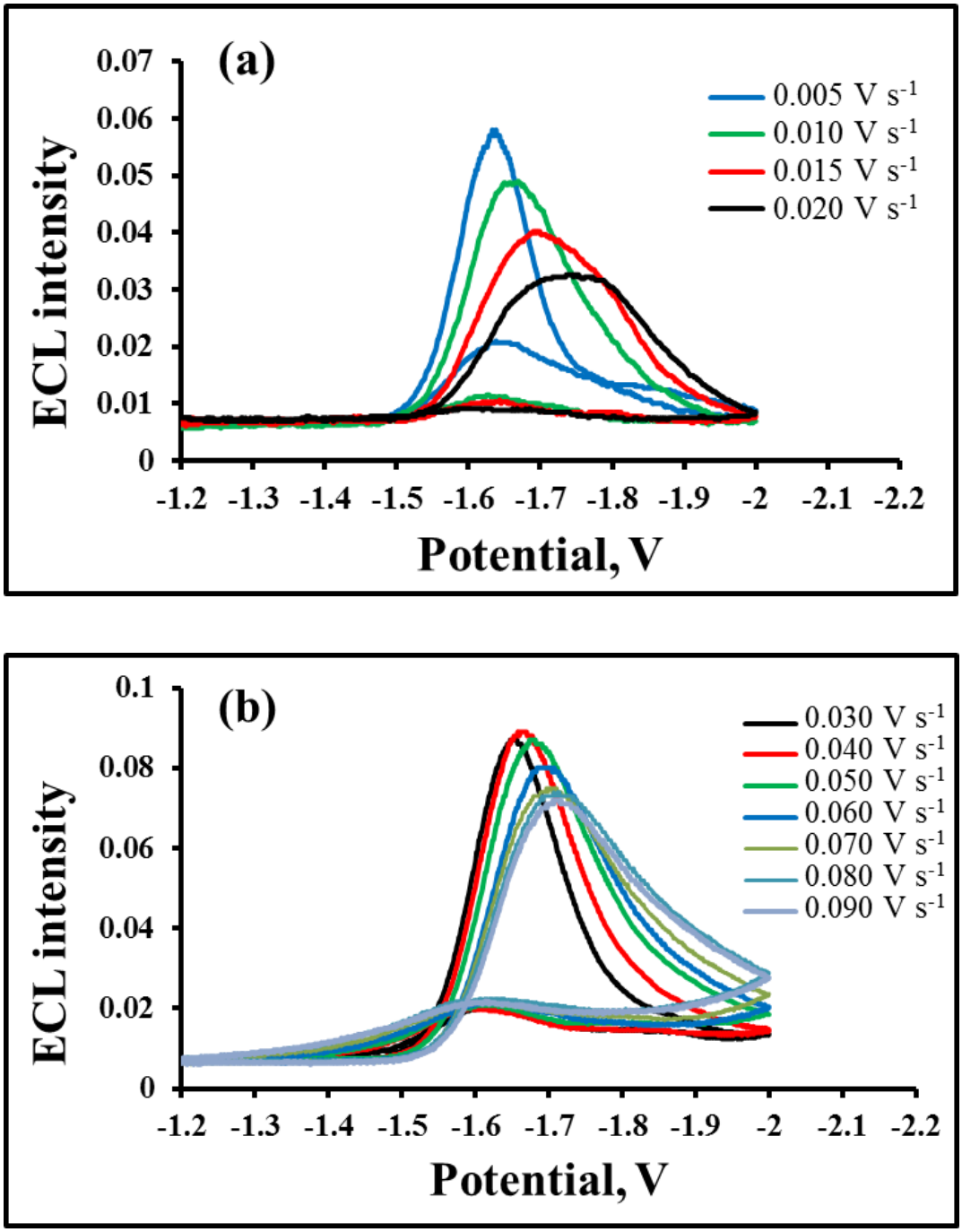

Figure 2.26: ECL responses of the BODIPY-COOH thin film modified Pt electrode in DMSO and 0.1 M TBATBF in the presence of 90 mM BPO. The initial potential was 0.000 V and the potential was initially scanned in the negative potential direction (a) at low scan rates (0.005 to 0.020 V s^{-1}), (b) high scan rates (0.030 to 0.090 V s^{-1}).

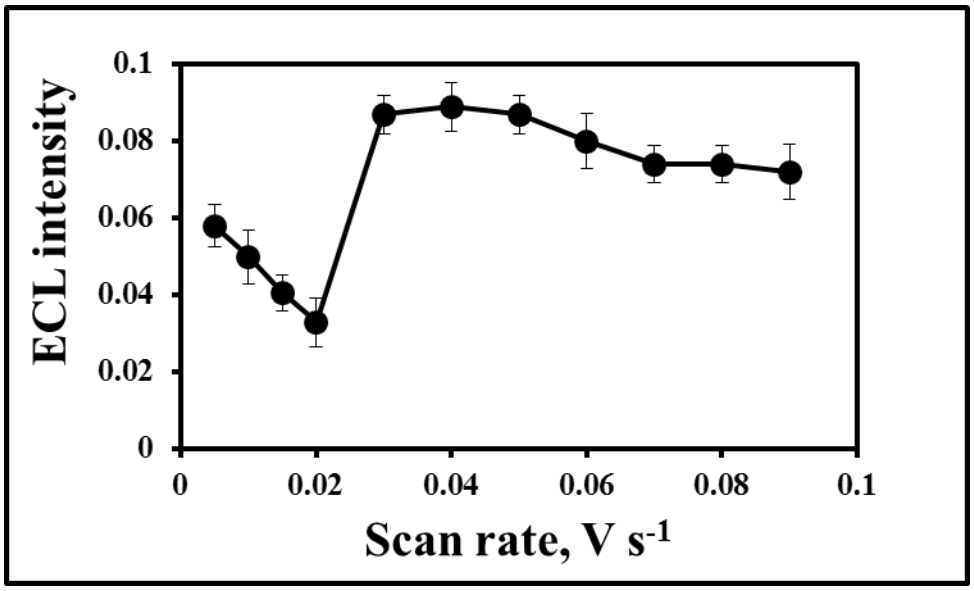

Figure 2.27: Dependence of maximum ECL intensity of the BODIPY thin film on the scan rates. The experimental conditions are as in Figure 2.26.

At low scan rates (0.005 to 0.020 V s^{-1}) in the presence of 180 mM BPO, ECL intensity is high (0.06 au at 0.005 V s^{-1}) and it decreases as the scan rate is increased scan rate is increased to 0.020 V s^{-1} as shown in Figure 2.26 (a) and Figure 2.27. This is accompanied with a shift in the potential at which the maximum intensity is observed from -1.6 V (0.005 V s^{-1}) to -1.8 V (0.02 V s^{-1}). The decrease in ECL with increasing scan rate is observed because at low scan rates process 3 mentioned in Scheme 2.1, i.e., the cross reaction of $BODIPY^{\bullet-}$ and $BPO^{\bullet-}$, have sufficient time to produce high concentrations of the excited state ^{1}BODIPY* which luminesces.

At high scan rate (0.03-0.09 V s^{-1}, Figure 2.26(b)), in the presence of 180 mM BPO, ECL intensities are higher than at low scan rates. However, the ECL intensity also decreases from 0.083 au (0.03 V s^{-1}) to 0.043 au (0.09 V s^{-1}) with increasing scan rate (Figure 2.26(b) and Figure 2.27). Figure 2.27 shows

that at scan rates (0.03 to 0.06 V s^{-1}), the intensity of ECL is relatively unchanged within limits of experimental error (average ECL = 0.087 ± 0.005 AU). Furthermore, that the ECL intensities observed in the case of BODIPY thin film are not significantly different from those observed in the previous solution studies, suggests that ECL of BODIPY is not significantly sensitive to the change of environment.

The cyclic voltammograms recorded during the ECL for low scan rates (0.005 - 0.020 V s^{-1}) display two peaks (see Figure 2.28(a)). The first peak is observed at -0.650 V corresponds to the reduction of BODIPY to its radical anion and the second peak is observed at -0.980 V corresponding to the reduction of BPO. At the high scan rates (0.030 - 0.090 V s^{-1}) shown in Figure 2.28(b), the two peaks which were observed at the slow rates merge into one single peak indicating that the charge transfer reaction is under kinetic control.

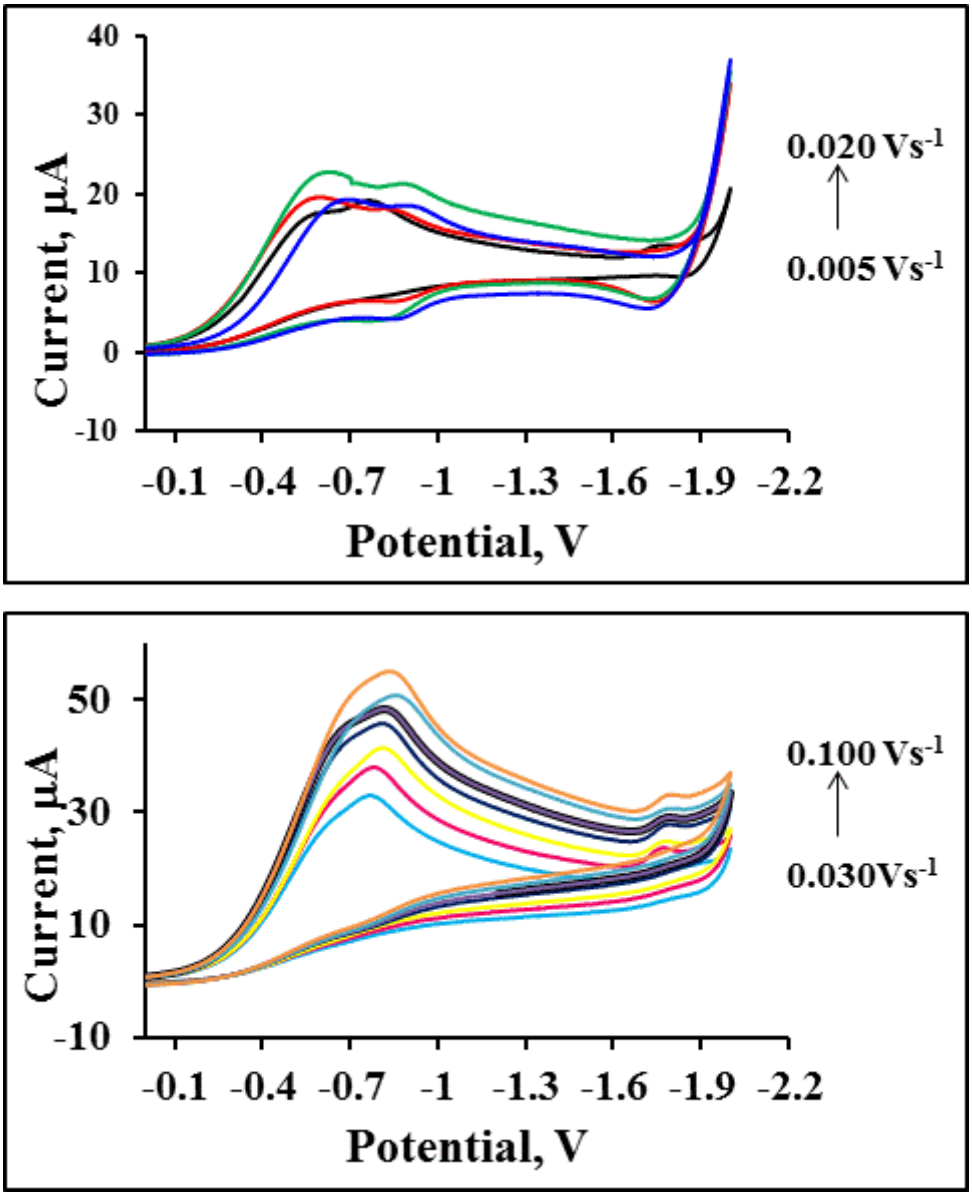

Figure 2.28: Cyclic voltammogram measured simultaneously with ECL of BODIPY-COOH thin films in the presence of 180 mM BPO in DMSO at low scan rates (a) 0.005 - 0.020 V s^{-1} and (b) high scan rates (0.030 - 0.090 V s^{-1}). The supporting electrolyte is 0.1 M TBATFB, using a 2 mm platinum working electrode. The initial potential was 0.00 V and the potential was initially scanned in the negative potential direction until it reached -2.00 V and it was reversed back to the initial potential 0.00 V.

2.3.4.3.3. Cyclic Voltammetry studies before and after ECL

To evaluate the effect of benzoyl peroxide on the BODIPY-COOH thin film, the cyclic voltammogram of the thin film was measured before ECL and its surface coverage was determined as 2.5 x 10^{-10} and 2.4 x 10^{-10} mol cm^{-2} for reduction and oxidation, respectively. Subsequently, the thin film was exposed to BPO for 20 ECL scans in DMSO and TBATFB.

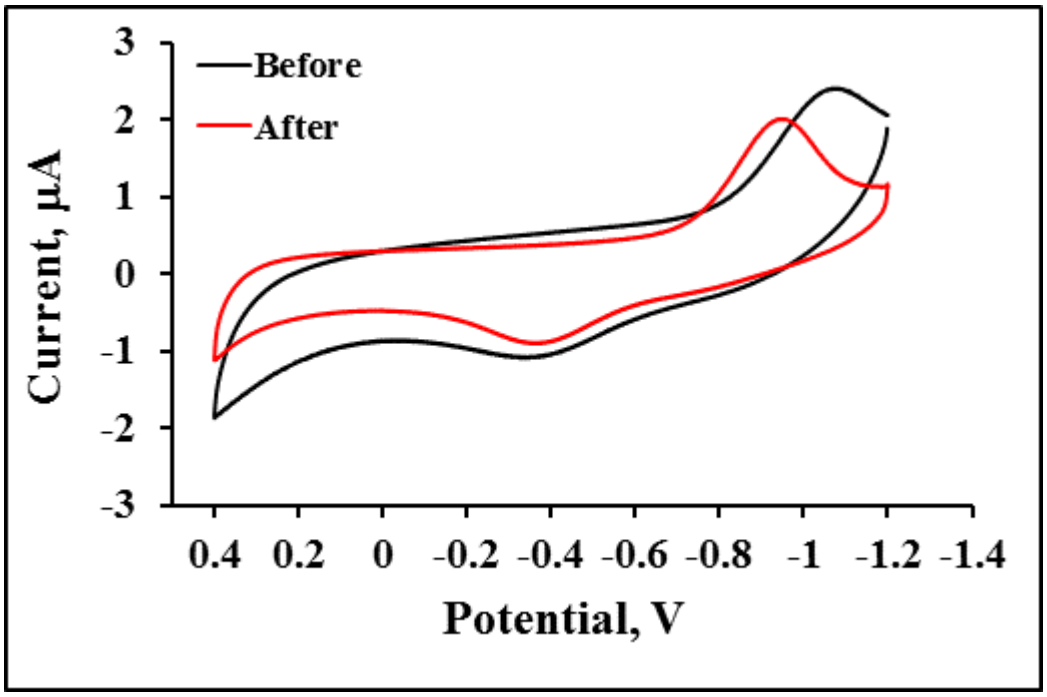

Figure 2.29: Cyclic voltammograms of the same BODIPY-COOH thin film modified Pt electrode, before and after ECL measurements, in DMSO and 0.1 M TBATFB at 0.1 V s^{-1}. The reductive surface coverage before and after ECL is 2.5 x 10^{-10} and 1.5 x 10^{-10} mol cm^{-2}, respectively.

The BODIPY-COOH thin film modified electrode was then placed in a BPO free DM8SO and TBATFB solution, and its CV was measured and reduction and oxidation surface coverage were determined as 1.5 x 10^{-10} and 2.2 x 10^{-10} mol cm^{-2}, respectively, and the CVs are presented below in Figure 2.29 above. The results demonstrate that exposing the BODIPY thin film to BPO during ECL destroys the monolayer and this is evident in the decrease in surface coverage of BODIPY.

2.3.4.3.4. Comparison of BODIPY-COOH adsorbed directly on the electrode and BODIPY-COOH confined to the electrode via a cysteamine layer

To investigate the effect which the cysteamine layer has on the electrochemical properties BODIPY-COOH, the dye was directly adsorbed on the platinum electrode without the cysteamine layer by immersing the electrode in a solution containing 5 mM BODIPY in DMSO for 3 h and its CV is depicted as Figure 2.30(a). This was compared to an electrode which was firstly modified with a cysteamine layer and then coupled to the dye (Figure 2.30(b)). The cyclic voltammogram showed that BODIPY-COOH can be directly adsorbed to the surface of a platinum electrode, and it displays electrochemical characteristics similar to those which were previously observed for a BODIPY-COOH in solution with a reduction peak at E_{pc} = -1.03 V and oxidation at E_{pa} = -0.79 V.

The physical adsorption of BODIPY most likely takes place via the binding between the nitrogens of the naphthyridine substituent and the platinum electrode. However, the dye was not stable on the electrode and cysteamine was used to crosslink BODIPY to the electrode.

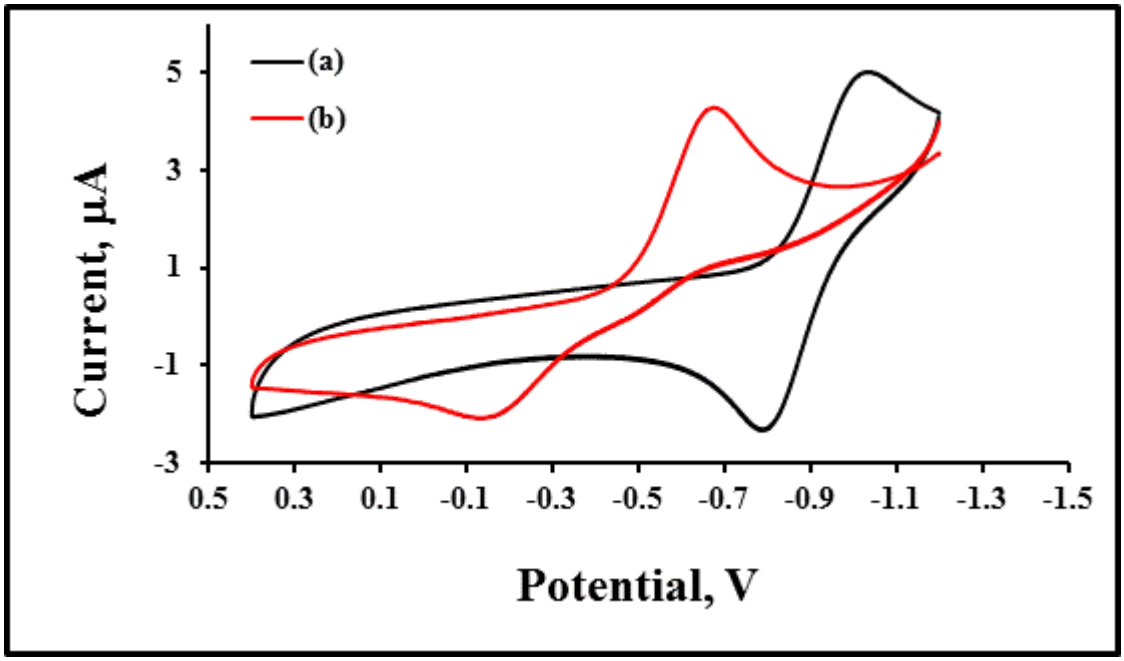

Figure 2.30: CV of BODIPY adsorbed directly to the electrode (a) for 3 h by immersing the Pt electrode in a solution of 5 mM BODIPY COOH in DMSO, with a Γ_{red} = 1.07 x 10^{-9} mol cm^{-2}. (b) The BODIPY thin film which the BODIPY is confined to the electrode via a cysteamine layer which was formed over 16 h and coupled to BODIPY-COOH via EDC coupling through for 3 h in DMF and its Γ_{red} = 9.31 x 10^{-10} mol cm^{-2}. The voltammetry was measured at 0.1 V s^{-1} in DMSO and TBATFB.

When comparing the directly adsorbed BODIPY to the one coupled to the cysteamine, the results show that the introduction of the cysteamine layer decreases the surface coverage of BODIPY from 1.07 x 10^{-9} mol cm^{-2} to 9.31 x 10^{-10} mol cm^{-2}. It also shifts the reduction potential observed at E_{pc} = -0.766

V and oxidation observed at E_{pa} = -0.163 V to less negative potentials, resulting in an increased peak to peak separation of -0.603 V. There are two possible reasons for increase of peak separation in the BODIPY that has been confined to the electrode through a cysteamine linker. The first reason is that the local environment that BODIPY experiences when it is attached to a cysteamine linker is very different from what it experiences when it is absorbed directly on the electrode by physisorption. Secondly, the coupling of BODIPY to cysteamine through EDC coupling changes the electron density of BODIPY resulting in the observed potential shifts.

2.3.4.4. ECL of BODIPY-COOH thin film, formed from a cysteamine layer with a decreased surface coverage

2.3.4.4.1. Electrochemiluminescence of BODIPY–COOH thin film with holes in the cysteamine layer

When a film is formed on the electrode surface, the coreactant may have limited diffusion access through the film and less ECL may be generated.[21] Thus, it is expected that decreasing time for the deposition of the cysteamine linker on the electrode can cause the cysteamine molecules to be spaced apart from each other and this can create more area between the molecules. An increased area between the linker molecules can influence two factors which can contribute to the ECL response which were previously mentioned earlier in Scheme 2.1. Firstly, it will be easier for the coreactant to diffuse

through the BODIPY and cysteamine layer compared to when the film is tightly packed.

Secondly, the cross reaction between $BPO^{\cdot-}$ and $BODIPY^{\cdot-}$ will be less sterically hindered which may result in increased production of the emitting singlet excited state, and increased ECL intensity. To evaluate whether decreasing the surface area of the linker will affect the ECL intensity of a BODIPY thin film using from a cysteamine linker which was measured in the presence of BPO as a coreactant. The ECL (Figure 2.31) is consistent with what was observed previously. Although BODIPY and BPO were both reduced before -1 V, no light was observed until potentials that were approximately more negative than -1.5 V were applied. The cyclic voltammogram (Figure 2.30) that was measured during the ECL experiment displays one major peak between -0.6 and -1.4 V under which both BODIPY and BPO are reduced.

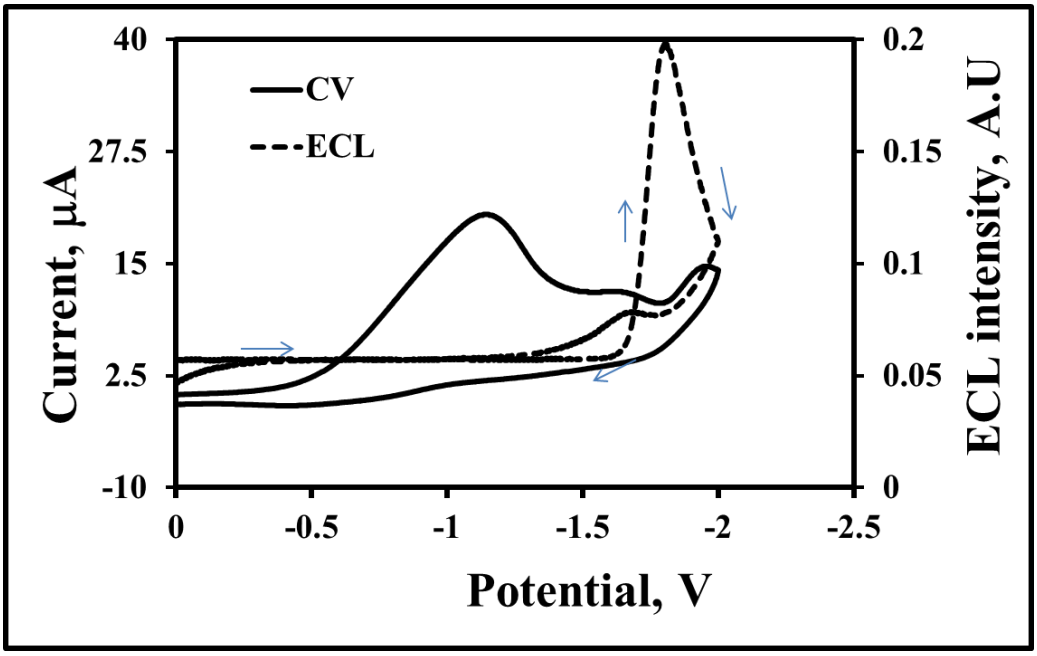

Figure 2.31: Cyclic voltammogram (solid line) and ECL spectra (dotted line) of BODIY-COOH thin film modified platinum electrode. The cysteamine layer was assembled on the electrode for 1 h and coupled to BODIPY-COOH. The ECL was evaluated in DMSO with 0.1 M TBATFB supporting electrolyte, in the presence of BPO as a coreactant at 0.1 V s^{-1}.

2.3.4.4.2. ECL dependence on BPO concentration

It was shown previously that ECL response is affected by concentration of BPO coreactant, which at saturated BPO concentrations result in quenching of ECL intensity. The dependence of ECL intensity on BPO concentration was studied with BODIPY-COOH thin film on cysteamine layer with a decreased surface coverage. Figures 2.32 (a) and (b) present the ECL responses of the BODIPY-COOH thin film at different BPO concentrations from 10, 60, 120, 180 and 240 mM.

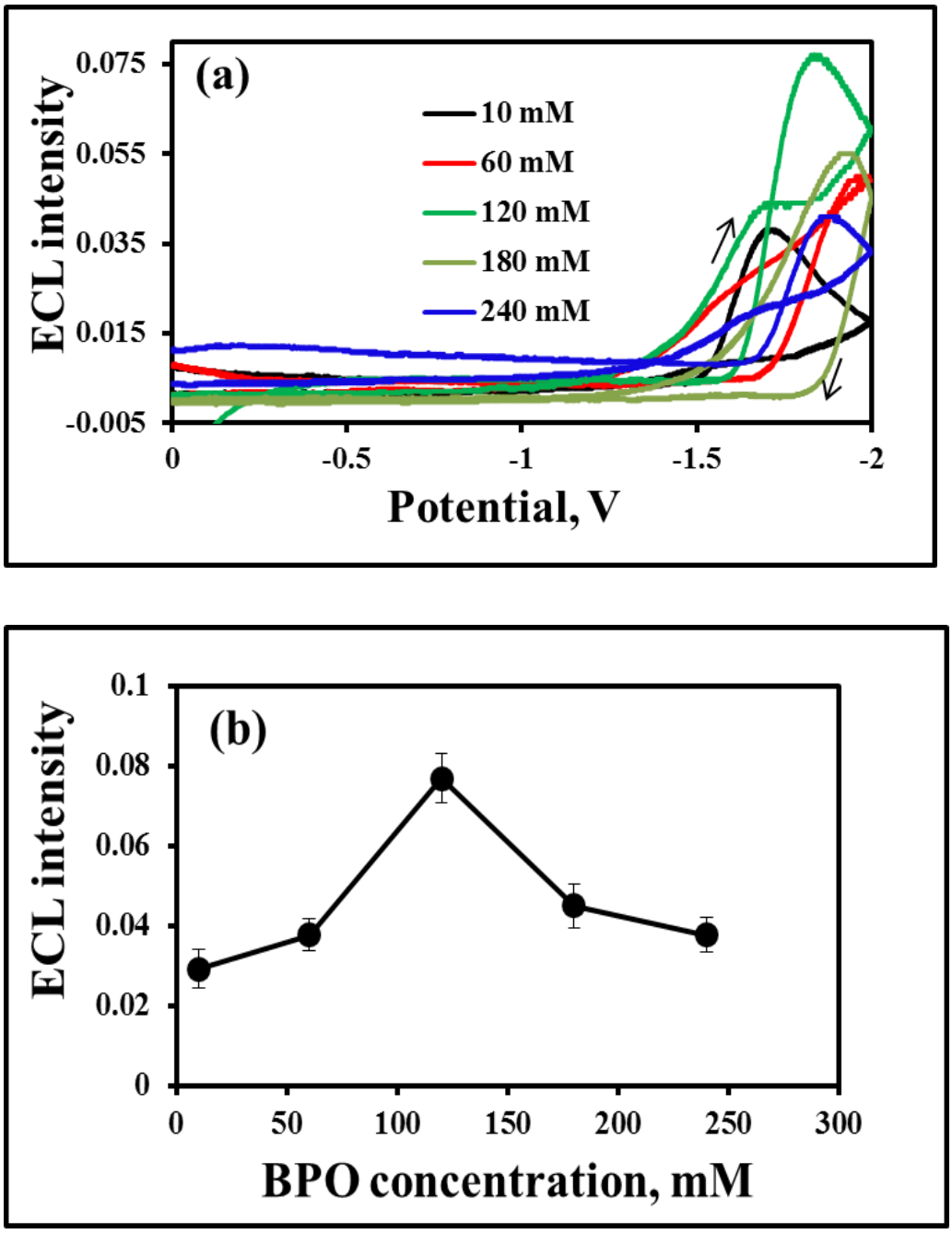

Figure 2.32: (a) ECL profiles where the arrows indicate the progression of the ECL response, and (b) dependence of ECL intensity of BODIPY-COOH thin film in DMSO and TBATFB on BPO (co-reactant) concentrations at 0.1 V s^{-1} and fixed potential of -1.83 V. The error bars represent the standard deviations from three separate experiments (n = 3). 0.1 M TBATFB was used as the supporting electrolyte.

The ECL intensity increases with increasing BPO concentration and the maximum ECL intensity is generated in the presence of 120 mM BPO. Beyond this concentration BPO becomes saturated and it results in a decrease in ECL intensity as illustrated in Figure 2.32 (a) and (b). The BPO concentration of maximum ECL intensity (120 mM) is lower that (180 mM BPO) observed for BODIPY-COOH thin film formed on cysteamine layer. The results suggest that BPO has increased diffusion access between the BODIPY film as the cysteamine molecules are spaced apart from each other, but with no concomitant increase in the production of the singlet excited state ^{1}BODIPY* from cross reaction process between the BODIPY radical anion and the benzoyloxy radical. ECL scan rate dependence studies in the presence of 120 mM BODIPY (as it was the optimum BPO concentration) were conducted in order to evaluate the behaviour of the film at different scan rates.

2.3.4.4.3. ECL scan rate dependent studies for 1 hour cysteamine films

ECL profiles of the BODIPY-COOH thin film modified Pt electrode in DMSO and 0.1 M TBATBF in the presence of 120 mM BPO. The initial potential was set to be 0.00 V scanned in the negative potential direction to a final potential of -2.00 V, and the potential scan was reversed to the initial potential. Figure 2.33(a) represents the low scan rates (0.005 to 0.040 V s^{-1}) and (b) the high scan rates (0.05 to 0.10 V s^{-1}). At the low scan rates, the ECL onset or turn-on

was observed at -1.6 V. The ECL peak potential was observed at -1.70 V (0.005 V s^{-1}) and shifts to -1.75 V (0.040 V s^{-1}). Furthermore, the ECL increased from 0.06 (0.005 V s^{-1}) to 0.16 (0.040 V s^{-1}). The result of the increase of ECL with increasing scan rate is not expected, because at the slowest scan rates the electron exchange process between reduced BPO and $BODIPY^{\cdot -}$ should have sufficient time to produce higher concentration of the singlet excited state ^{1}BODIPY*.

One can attribute the behaviour of ECL increasing with increasing scan rate to the instability of radicals produced. Scanning linearly from 0.00 V to -2.00 V, the first radical to be produced is the $BODIPY^{\cdot -}$, at -0.67 V. As soon as $BODIPY^{\cdot -}$, is produced its concentration decays before the BPO is reduced at -0.98 V to form the benzoyloxy radical. What is noticeable here is that at the high scan rates (Figure 2.33 (b)) the potential at which the ECL maxima is observed and peak intensity are independent of the potential scan rate showing that it is the cross reaction that determines the ECL intensity response.

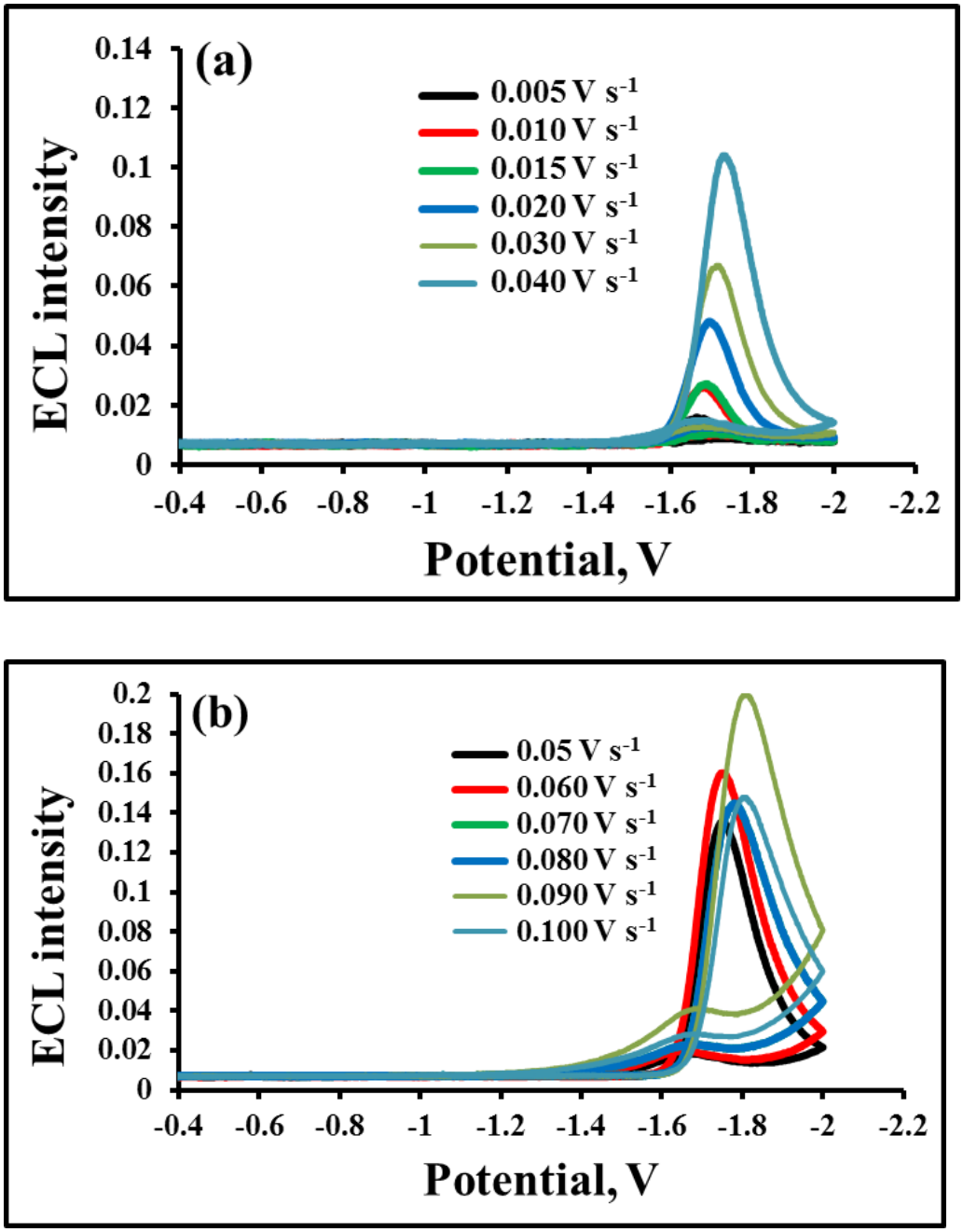

Figure 2.33: ECL profiles of the BODIPY-COOH thin film modified Pt electrode in DMSO in the presence of 120 mM BPO. The initial potential was 0.000 and initially scanned in the negative potential direction to a final potential of -2.00 V and the potential was reversed to the initial potential. (a) Represents the lower scan rates (0.005 to 0.040 V s^{-1}) and (b) the high scan rates (0.050 to 0.10 V s^{-1}).

2.3.4.4.3. Cyclic Voltammetry studies before and after ECL

To evaluate the effect of BPO on the surface coverage of BODIPY-COOH on the electrode, cyclic voltammetry of the BODIPY-COOH film was performed in DMSO with 0.1 M TBATFB before and after ECL measurements. The CVs are presented in Figure 2.34. The surface coverage was also evaluated prior to the ECL measurements, the reductive and oxidative surface coverage were determined to be 6.3 x 10^{-10} and 6.0 x 10^{-10} mol cm^{-2}, respectively.

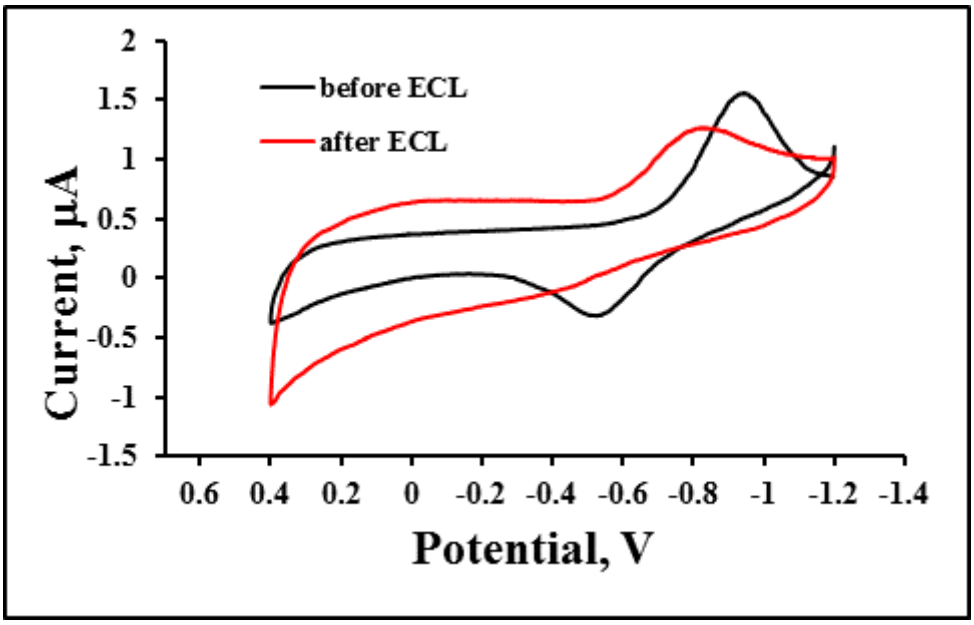

Figure 2.34: Cyclic voltammograms of BODIPY-COOH thin film modified Pt electrode, before and after ECL measurements in DMSO and 0.1 V s^{-1} scan rate.

The surface coverage was also evaluated after ECL measurements and was determined to be Γ_{red}: 4.2 x 10^{-10} mol cm^{-2} and Γ_{ox}: 4.8 x 10^{-11} mol cm^{-2}. The oxidative surface coverage decreased by one order of magnitude indicating that BPO has a destructive effect on the integrity of the film.[21] In the previous

studied densely packed BODIPY–COOH thin film, BPO also demonstrated a destructive effect, but it was not as significant as what is observed in the current case. The results suggest that an increased diffusion of the coreactant through the BODIPY film. This may be because the cysteamine molecule (within the film) are spaced apart from each other and a greater fraction of the film is active for ECL generation.

2.3.5. ECL OF BODIPY THIN FILM FORMED FROM AN L-CYSTEINE-PEG LAYER

2.3.5.1. Formation of a long chain layer which is coupled to BODIPY-COOH

The previous sections demonstrated that ECL can be generated from a BODIPY-COOH thin film formed from a cysteamine linker, which is a short chain alkyl thiol molecule containing two carbons. In this section ECL of a BODIPY thin film that has been formed from a longer linker instead of the short chain cysteamine and its ECL were investigated. Increasing the length of linker molecule can influence several parameters: firstly, it can change the electron transfer distance depending on the orientation of the molecule, thereby influencing the rate of heterogeneous electron transfer in Scheme 2.1. Furthermore, it can also influence the flexibility of the BODIPY molecule. Thus, ECL investigated was to evaluate whether changing the linker length will have any influence on the ECL intensity. The long chain linker was created by forming a L-cysteine layer on the surface of the electrode and increase the chain length of L-cysteine coupled to poly(ethylene glycol)bis(3-aminopropyl) [PEG] terminated with an amine functionality. Once this was achieved

BODIPY was joined to PEG via its carboxylic acid terminal group to the amine functionality of the PEG this is illustrated in Scheme 2.3 below.

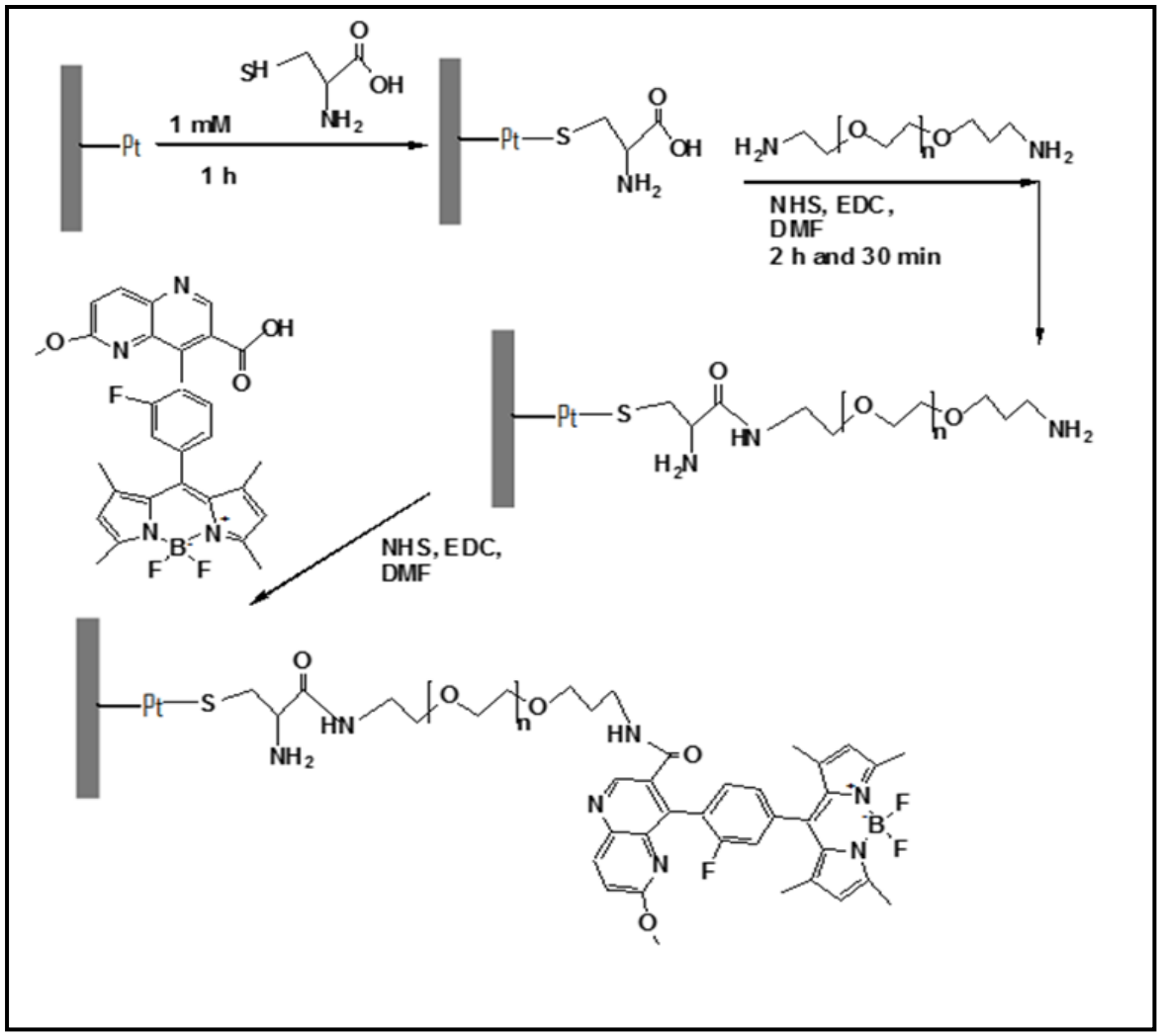

Scheme 2.3: Formation of BODIPY–COOH thin films produced by immersing the platinum electrode in ethanolic solution of 1 mM L-cysteine for 1 h. The L-cysteine layer was coupled for 2.5 h to PEG and BODIPY simultaneously via EDC coupling through a succinimide linker in DMF.

2.3.5.2. Blocking experiments, verifying the formation of L-cysteine-PEG on the platinum electrode

To verify whether the L-cysteine–PEG chain formed on the surface of the electrode, cyclic voltammograms of a bare platinum electrode were measured before and after the electrode was modified with L-cysteine, and PEG, respectively. The voltammetry was evaluated was in a solution of ferrocene methanol in DMSO in TBATFB and it is illustrated in Figure 2.35. DMSO is used in this case as it is the solvent which is used in the ECL experiments.

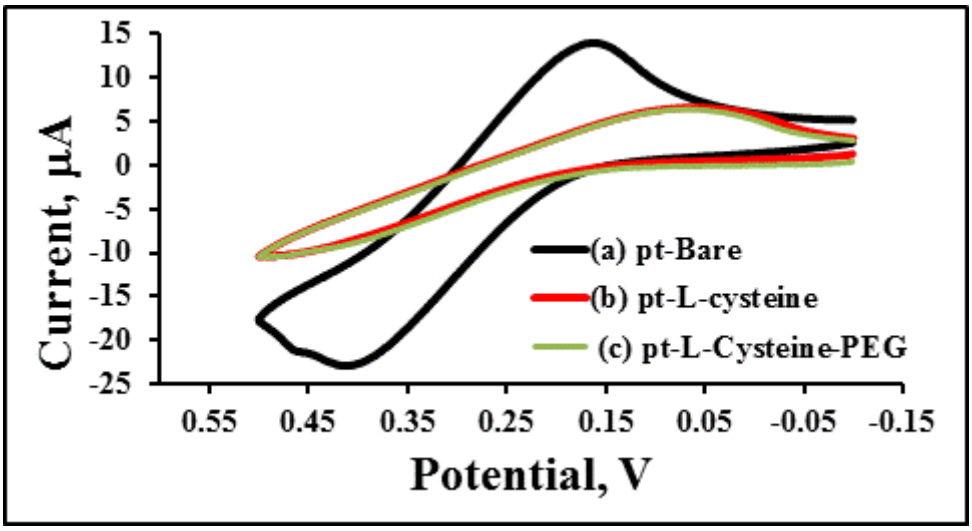

Figure 2.35: Effect of L-cysteine thin film formation on the cyclic voltammetry of ferrocene methanol (a) on bare platinum electrode Pt electrode, (b) Pt electrode after modification with L-cysteine for an hour and (c) Pt electrode after modification with L-cysteine-PEG. The voltammetry was assessed in DMSO and TBATFB as a supporting electrolyte at a scan rate was 0.1 V s^{-1}.

The bare electrode in ferrocene methanol in DMSO displays a cathodic reduction peak at 0.2 V, while oxidation take place at E_{pa} = 0.4 V, suggesting that the redox species has access to the electrode. When the Pt electrode is modified with L-cysteine-PEG the oxidation and reduction processes are considerably reduced, indicating that the redox species has reduced access to the electrode, as observed in Figure 2.35.

2.3.5.3. Electrochemiluminescence of L-cysteine-PEG- BODIPY-COOH thin films

Electrochemiluminescence of a BODIPY-COOH thin film, created by forming an L-cysteine-PEG layer (BODIPY-L-cysteine-PEG) on the surface of a platinum electrode and coupling it to BODIPY-COOH was investigated in the presence of BPO in DMSO and 0.1 M TBATFB solvent (Figure 2.36). The key issue was to evaluate whether changing the linker length will produce an increased ECL response.

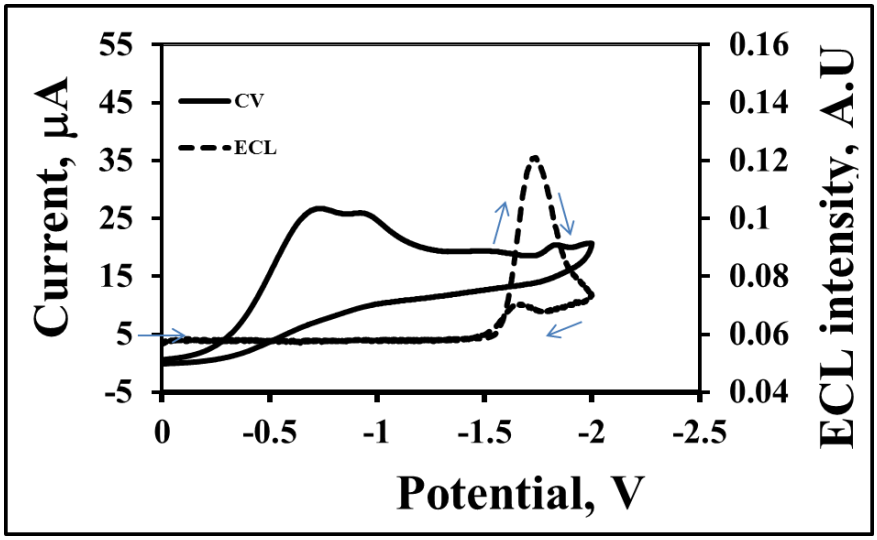

Figure 2.36: Cyclic voltammogram (solid line) and ECL spectra (dotted line) of prepared BODIY-COOH thin film modified platinum electrode. The L-cysteine layer was assembled on the electrode for 1 h and coupled to PEG and BODIPY-COOH. The voltammetry was evaluated in DMSO with 0.1 M TBATFB supporting electrolyte, in the presence of BPO as a coreactant at 0.1 V s^{-1}.

The ECL response here is consistent with what was previously observed, *i.e.*as the potential is scanned linearly from 0.00 to 2.00 V, no light was emitted at the observed potential until potentials more negative than -1.5 V were applied. The cyclic voltammogram measured during ECL displays a peak at E_{pc} = -0.75 V and it is ascribed to the reduction of BODIPY-COOH and second peak is observed at E_{pc} = -0.98 V and it is due to the reduction of BPO. Although both the coreactant and luminophore are reduced before negative -1.00 V and as the scan proceeded to a final potential for light generation is only observed at -1.58 V and the ECL maximum is observed at -1.85 V (Figure 2.36).

2.3.5.3.1. ECL dependence on BPO concentration

Electrochemiluminescence studies of BODIPY-L-cysteine-PEG thin films were investigated in the different concentration of BPO to evaluate the effect of BPO concentration on ECL. The concentrations ranged from 10, 60, 120, 180 and 240 mM in DMSO and TBATFB scanning from an initial potential of 0.00 to - 2.00 V at 0.1 V s^{-1} were used in the present study. The ECL profiles are depicted in Figure 2.37(a) and they show that ECL increases as the concentration of BPO is increased from 10 mM to 60 mM. However, it decreases slightly as soon as the concentration increased to 120 mM. The ECL maximum emission is observed when BPO concentration is 180 mM and this is the concentration that was used to carry out subsequent scan rate dependence studies. Concentrations higher than 180 mM resulted in a drop in ECL intensity as shown in Figure 2.37(b).

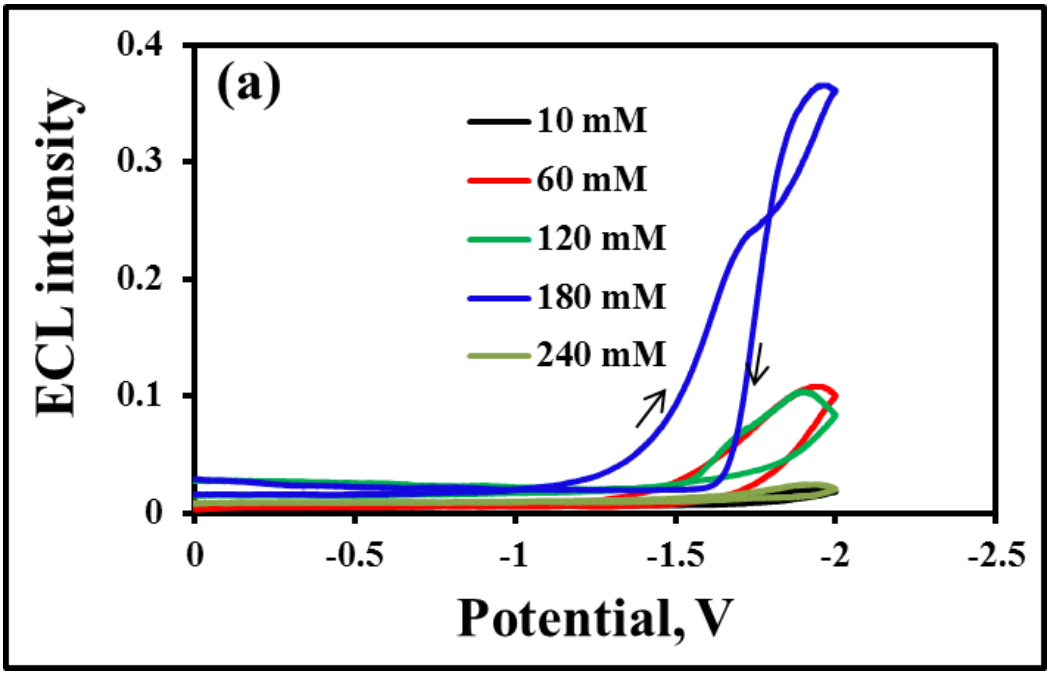

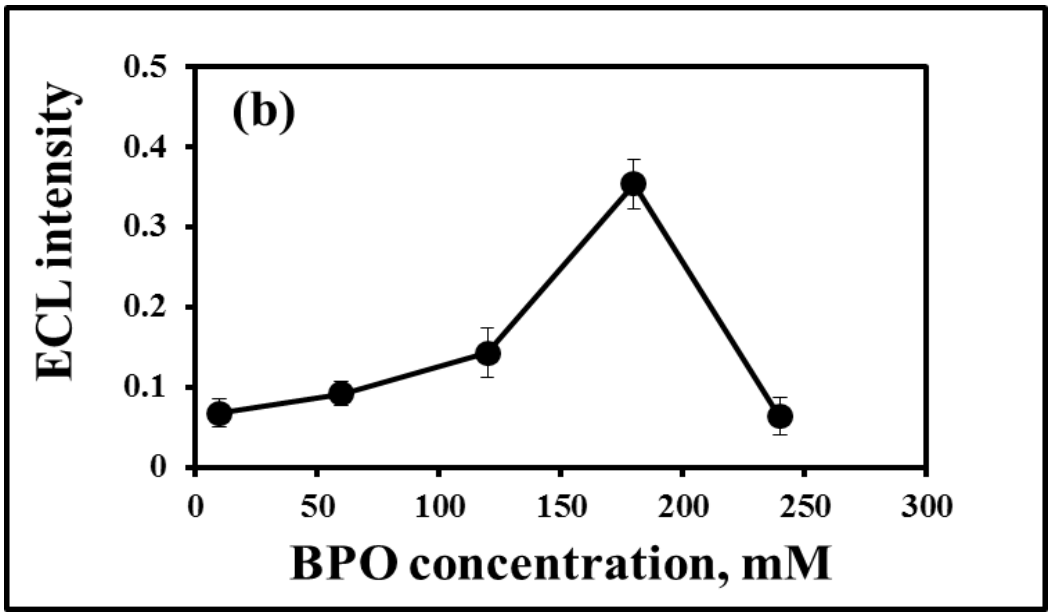

Figure 2.37: (a) ECL profiles of BODIPY-L-cysteine-PEG thin film in DMSO and TBATFB and in different BPO co-reactant concentrations: 10, 60, 120, 180 and 240 mM, in DMSO and TBATFB as a supporting electrolyte at 0.1 V s^{-1}. The arrows indicate the progression of the ECL response. (b) Dependence of ECL intensity of the BODIPY-COOH thin film on BPO concentration at a fixed ECL maximum potential of -1.85 V.

2.3.5.3.2. ECL Scan rate dependence

The electrochemiluminescence of the BODIPY-L-cysteine-PEG was investigated at different scan rates and the results are presented in Figure 2.38.

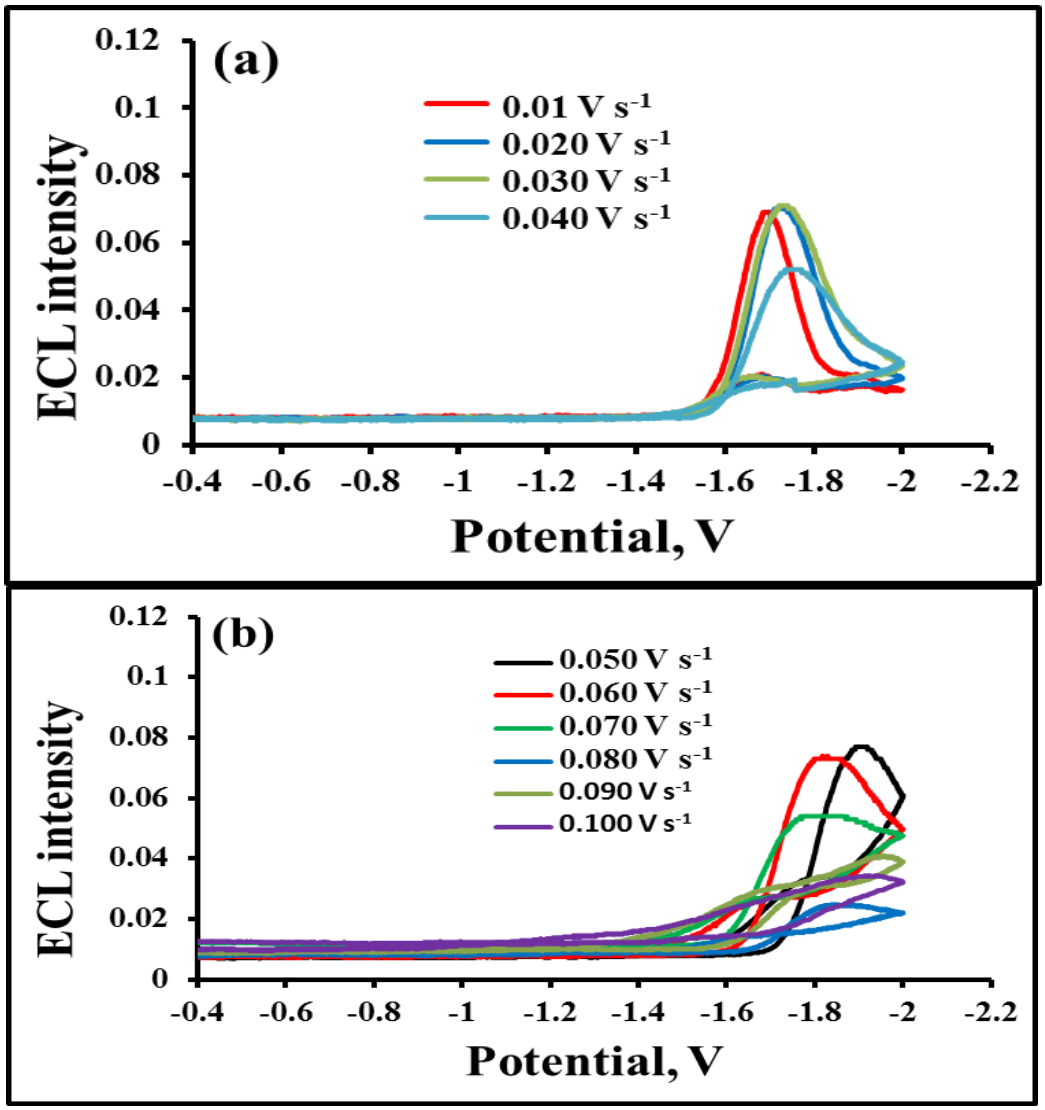

Figure 2.38: ECL profiles of the BODIPY-L-cysteine-PEG thin film modified Pt electrode in DMSO and 0.1 M TBATBF in the presence of 180 mM BPO. The initial potential was 0.00 V scanned in the negative potential direction to a final potential of -2.00 V and the potential reversed back to the initial potential. (a) Represents the low measured scan rates (0.010 to 0.040 V s^{-1}) and (b) the high scan rates (0.05 to 0.10 V s^{-1}).

As shown in Figure 2.38(a), at the low scan rates (0.010 to 0.040 V s^{-1}), the onset of the ECL in the presence of 180 mM is observed at -1.6 V, while the ECL intensity remains relatively unchanged as the scan rate was varied from 0.010- 0.030 V s^{-1}. The ECL intensity at high scan rates (0.050 to 0.10 V s^{-1}) decreased from 0.013 au (0.050 V s^{-1}) to 0.06 au (0.10 V s^{-1}). This ECL intensity response from the BODIPY thin film formed from the long linker (L-cysteine-PEG) is not different from the ECL behaviour of a BODIPY thin film formed with short linker (cysteamine). This observation suggests that both linker types bind the same amount of BODIPY.

2.3.6. ECL IN IONIC LIQUID

Ionic liquids (ILs) have been proposed as alternative solvents for a variety of applications, thus ILs offer unique chemical and physical properties, these include high thermal stability, low melting temperature and good electrochemical stability.[43, 44, 45] The previous solution and film BODIPY studies demonstrated that the rate which the radical anions react with each other, to produce the excited state is an important factor that contributes to the ECL output. Furthermore, the radical anions which are produced are during ECL are unstable resulting in low ECL intensities which are less than 0.1 AU. Thus because ILs offer good electrochemical stability it is of interest to investigate the ECL behaviour of BODIPY-COOH in ionic liquids. To investigate ILs as alternative solvent electrolyte systems for electrochemical and electrochemiluminescence measurements on planar electrodes, the

redox behaviour of BODIPY was investigated and the ionic liquid chosen for this study was 1-buty-1-methylpyrrolidinium bis-(trifluoromethylsulfonyl) imide ([BMP][Tf_2N]).

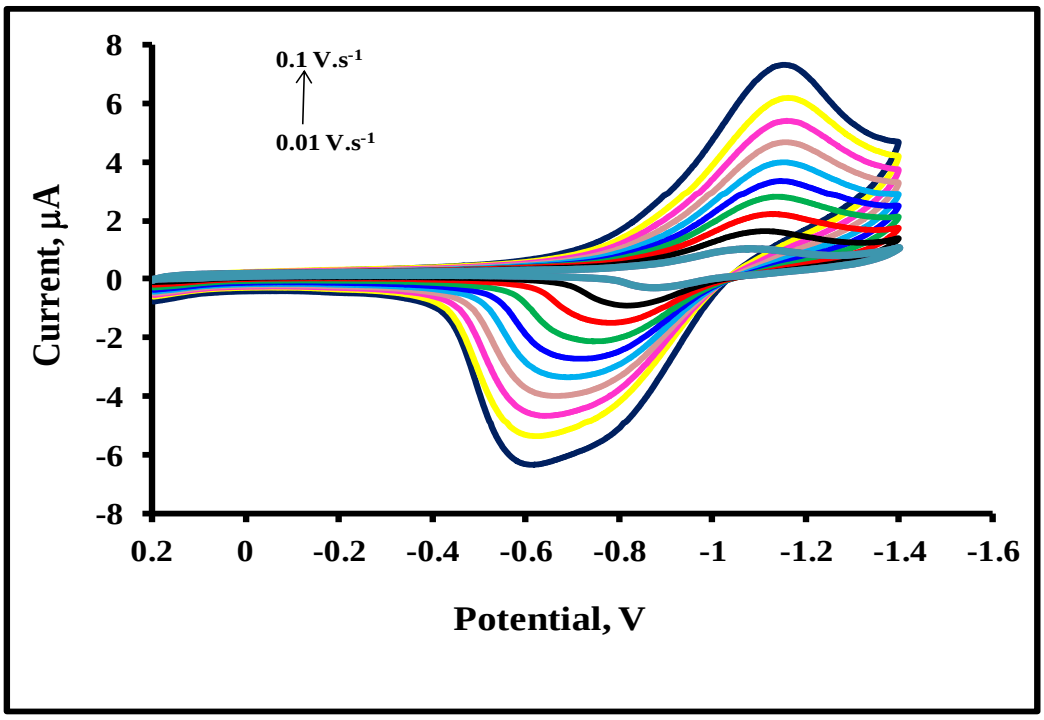

Figure 2.39: Scan rate dependence of the voltammetric response of 5 mM BODIPY-COOH in ([BMP][Tf_2N]) ionic liquid as the supporting electrolyte. The working electrode is 2 mm platinum electrode and the scan rates are 0.01 to 0.1 V s^{-1}.

The multi scan rate cyclic voltammetric responses of 5 mM BODIPY in ([BMP][Tf_2N]) ionic liquid are presented in Figure 2.39. As shown earlier in Figure 2.6, at 0.1 V s^{-1} BODIPY displayed reversible redox behaviour in DMSO with a reduction peak at E_{pc} = -0.965 V and oxidation peak at E_{pa} = -0.801 V. In contrast BODIPY exhibits quasi reversible redox behaviour in ([BMP][Tf_2N]) ionic liquid at 0.1 V s^{-1} producing a single wave associated with BODIPY reduction at E_{pc} = -1.16 V while the corresponding oxidation is

observed at E_{pa} = -0.641 V. Interestingly in the oxidation peak potentials shift negatively with increasing scan rate, indicating that it becomes increasingly difficult to drive oxidation of BODIPY in ([BMP][Tf_2N]) as scan rate increases.

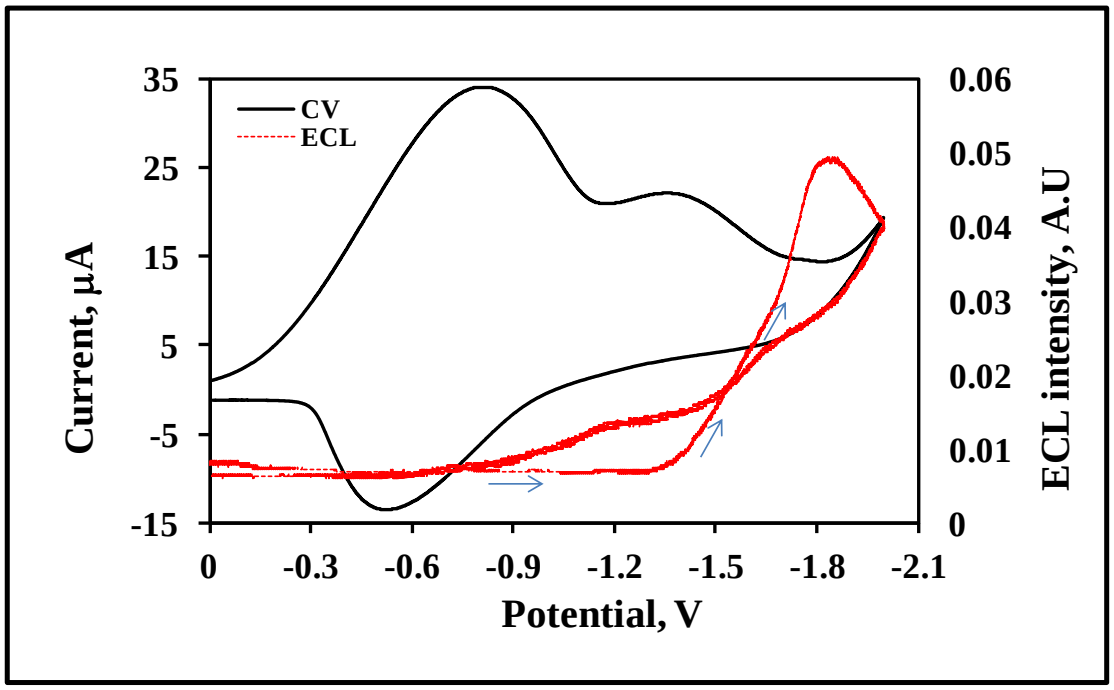

Figure 2.40: Cyclic voltammogram and ECL profile of 5 mM BODIPY-COOH dye in ([BMP][Tf_2N]) ionic liquid in the presence of 3 mM BPO on a platinum electrode. The scan rate is 0.1 V s^{-1} and the arrows show the direction of the scan.

Figure 2.40 above shows the CV and ECL response of 5 mM BODIPY in solution ([BMP][Tf_2N]) in the presence of 3 mM BPO. CV displays two reduction peaks, the first broad peak at -0.830 V and -1.37 V which are due to the reduction of BPO and BODIPY. The ECL onset is observed at -1.40 V and the emission maximum is observed at -1.85 V. The ECL light intensity of BODIPY in an ionic liquid is low and similar to what was previously in DMSO.

The ECL of the BODIPY thin film was also investigated in ([BMP][Tf_2N]). Figure 2.41 shows the CV and ECL response of BODIPY-COOH thin film modified platinum electrode in ([BMP][Tf_2N]) in the presence of BPO. ECL is observed at an onset potential of approximately -1.01 V corresponding to the reduction potential of BODIPY, to form the BODIPY-COOH$^{\bullet-}$ and the maximum is observed at -1.71 V in ([BMP][Tf_2N]).

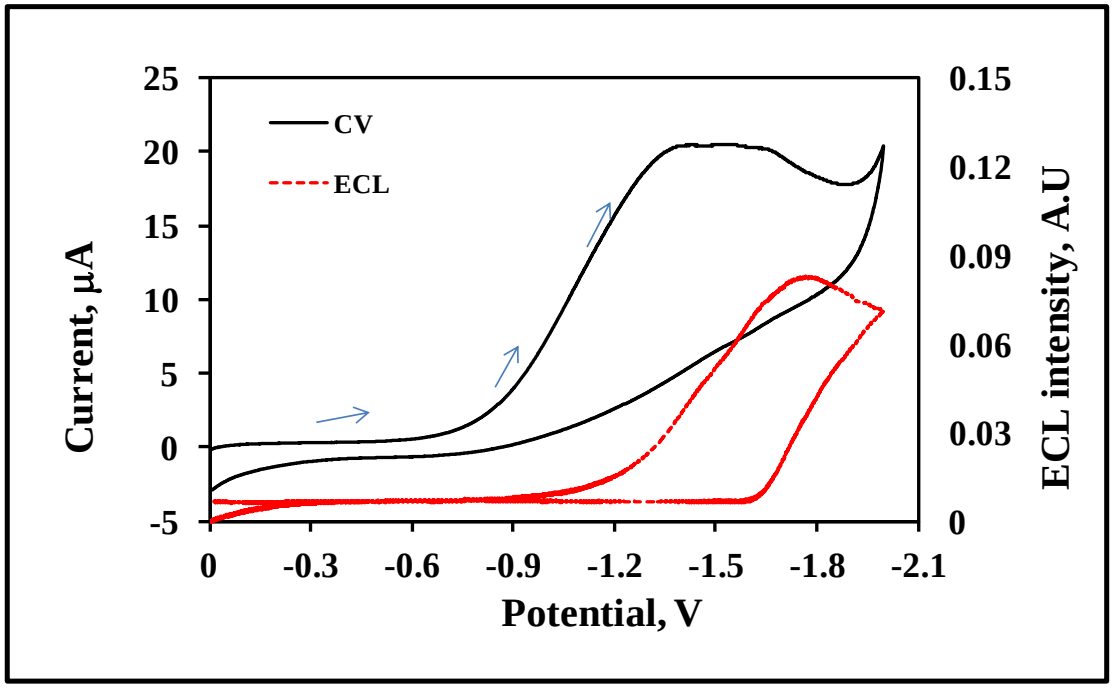

Figure 2.41: Cyclic voltammogram and ECL spectra of BODIPY-COOH thin film BPO on a platinum electrode. The scan rate is 0.1 V s^{-1} and the arrows show the direction of the scan.

The results show that ECL intensity generated both in solution or as thin film in an ionic liquid is also low (~0.083 au at -1.8 V), ultimately the ECL intensity output depends on the rate at which the BODIPY and the BPO radical react with each other within the reaction zone to produce the exited state species ^{1}BODIPY*. Thus it is concluded that the BODIPY radicals are unstable even in the ionic liquid ([BMP][Tf_2N]). that was used in this study.

2.3.7. ECL WITH INTERDIGITATED ELECTODES

In the previous sections the electrochemiluminescence experiments were conducted using macroelectrodes. However, one challenge experienced with using classic ECL with macroelectrodes in the present instance is that, BODIPY reduced radicals are the first to be generated and the cross reaction can only take place once BPO is reduced at later potentials. This suggests that there is a delay between the production of $BODIPY^{\cdot -}$ radicals, and their cross reaction with BPO radicals to produce the required excited state.[46] Furthermore, BODIPY radicals are short-lived and this type of behaviour suggests that only a fraction of the reduced BODIPY radicals are available to undergo the cross reaction with BPO to produce ECL and under these circumstances the resulting ECL intensity is limited. Previously reported studies of BODIPY linked the instability of the radicals to the absence of substitutions in positions 2, 6 on the BODIPY core also resulting in low ECL intensities.[47] To overcome this challenge of instability the electrogenerated radicals, IDA electrodes were used to generate ECL[48]. IDA electrodes have been used have been applied to fields like biosensing, trace electroanalysis and field flow fractionation separations.[49, 50] . Figure 2.42 shows a picture of the IDA electrode used in the current study , with 5 µm spacing between the working electrodes .The small gap between these array electrodes, in this case 5 µm makes them particularly convenient for generating ECL

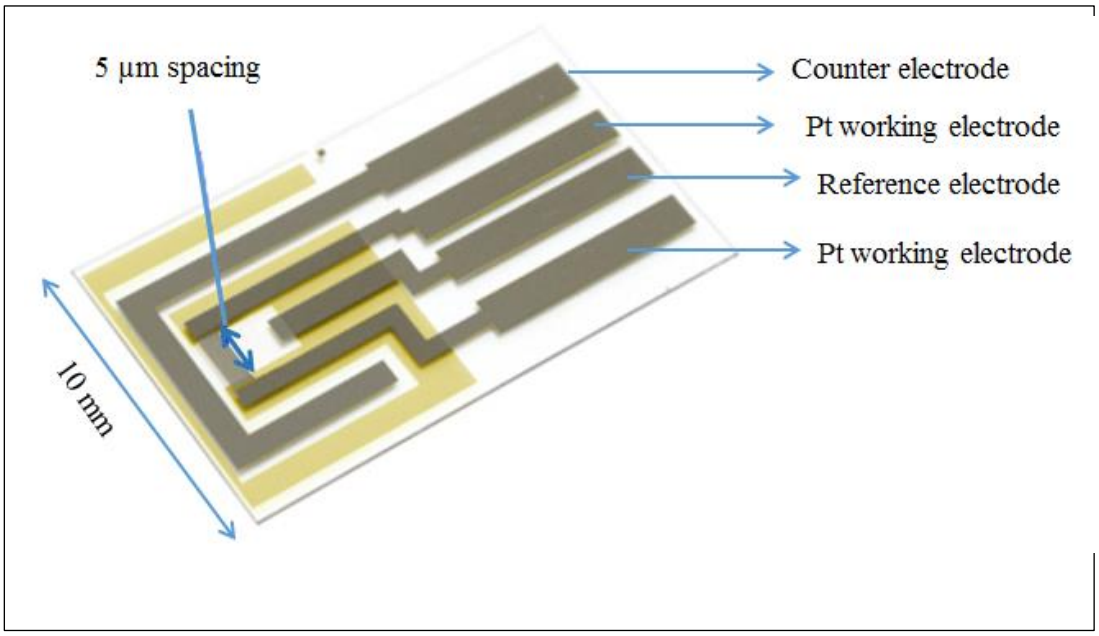

Figure 2.42: Interdigitated electrode, with two platinum working electrode with 5 µm spacing, counter and reference electrode.

Normally with a single macroelectrode, active species that are generated on the electrode surface move in and out of the double layer, while in IDA's redox cycling occurs inside the overlapped diffusion shroud of the adjacent electrodes. This results in an increase in the local concentration and flux of radicals and thereby generating high Faradaic currents.[51]

2.3.7.1. Electrochemical properties of BODIPY on IDA

Figure 2.43 illustrates the cyclic voltammograms of (a) blank IDA and (b) BODIPY-COOH thin film modified IDA electrode upon cycling in anhydrous DMSO with 0.1M TBATBF electrolyte at scan rate, 0.05 V s^{-1}.

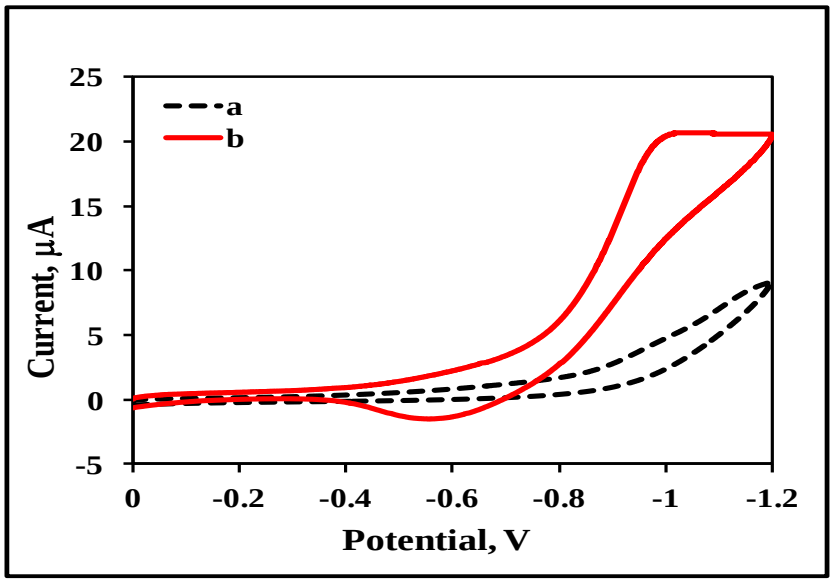

Figure 2.43: Cyclic voltammograms of (a) blank and (b) BODIPY-COOH thin film modified IDA electrode (b), in DMSO with 0.1 M TBATFB as supporting electrolyte, the scan rate is 0.1 V s^{-1}.

A single irreversible cathodic peak is observed at -0.988 V and it corresponds to the process of BODIPY reduction, while at the anodic side a peak for BODIPY oxidation is observed at -0.625 V in Figure 2.43 above. In comparison to the voltammetric behaviour of the thin film previously observed for BODIPY –COOH, the shape of the CV (Figure 2.18) of the thin film on IDA assumes a more sigmoidal shape, compared to the typical Gaussian peak shape previously observed on a macro electrode. The currents generated on IDAs are double and the redox peak potentials observed on IDA are shifted. For example, at the same scan rate 0.05 V s^{-1} on a Pt macroelectrode, the peaks for BODIPY reduction and oxidation where observed at -0.678 and -0.133 V respectively. The voltammetric responses of the thin film on an IDA electrode exhibit peak shapes that are not symmetrical and the peak to peak separation, ΔE, is large. For example at the slowest scan rate of 0.01 V s^{-1},

ΔE is 327 mV, as opposed to the theoretically expected ΔE of 0 mV where there are no lateral interactions between the immobilized species.

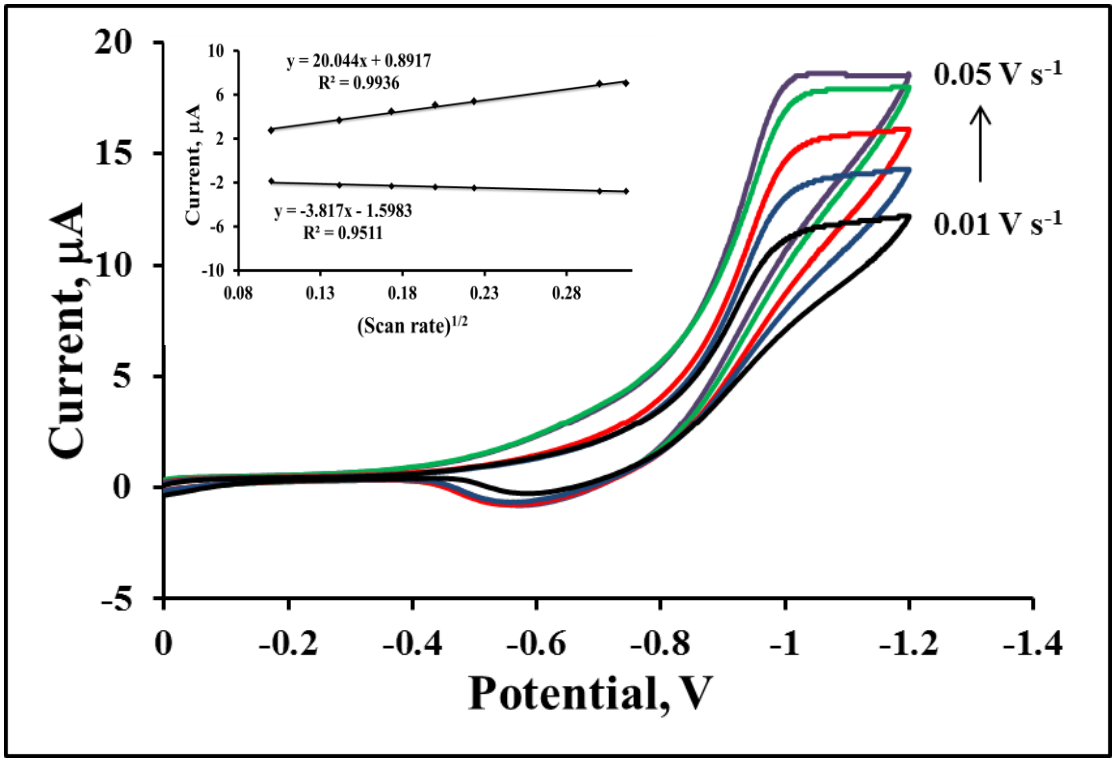

Figure 2.44: Scan rate dependence of the voltammetric response of thin film BODIPY-COOH in DMSO and 0.1 M TBATFB as a supporting electrolyte on a platinum IDA electrode, scan rates of 0.01 to 0.05 Vs^{-1}. The inset shows peak current dependence of the square root of scan rate.

Figure 2.44 illustrates the scan rate dependence of the voltammetric response of the BODIPY thin film on a Pt IDA. The inset shows the cathodic peak current, i_p , increases with v, which is consistent with a surface adsorbed redox species, rather than a diffusing reactant where i_p would be proportional to $v^{1/2}$. The quantity of the BODIPY complex immobilized on the IDA electrodes was determined by measuring the charge under the cyclic voltammetric peak

recorded at the slowest measured rate in DMSO and TBATBF, the surface coverage was determined to be 4.93 X 10^{-8} mol cm^{-2}.

2.3.7.2. Electrochemiluminescence of BODIPY on IDA

Figure 2.44 displays the ECL and CV response of BODIPY thin film on an IDA electrode. In the generator / collector ECL generating mode using interdigitated arrays, one of the working electrodes which serves as the generator, is scanned from an initial potential of 0.00 V to a final potential of -2.00 V to reduce BODIPY. While the second working electrode is the collector electrode and it held at a constant potential of -0.90 V, which is near the reduction potential of BPO. This type of set up allows for the simultaneous production of both radical anions of BODIPY and BPO, and since the radicals are continuously produced they are readily available to react with each other.[52]

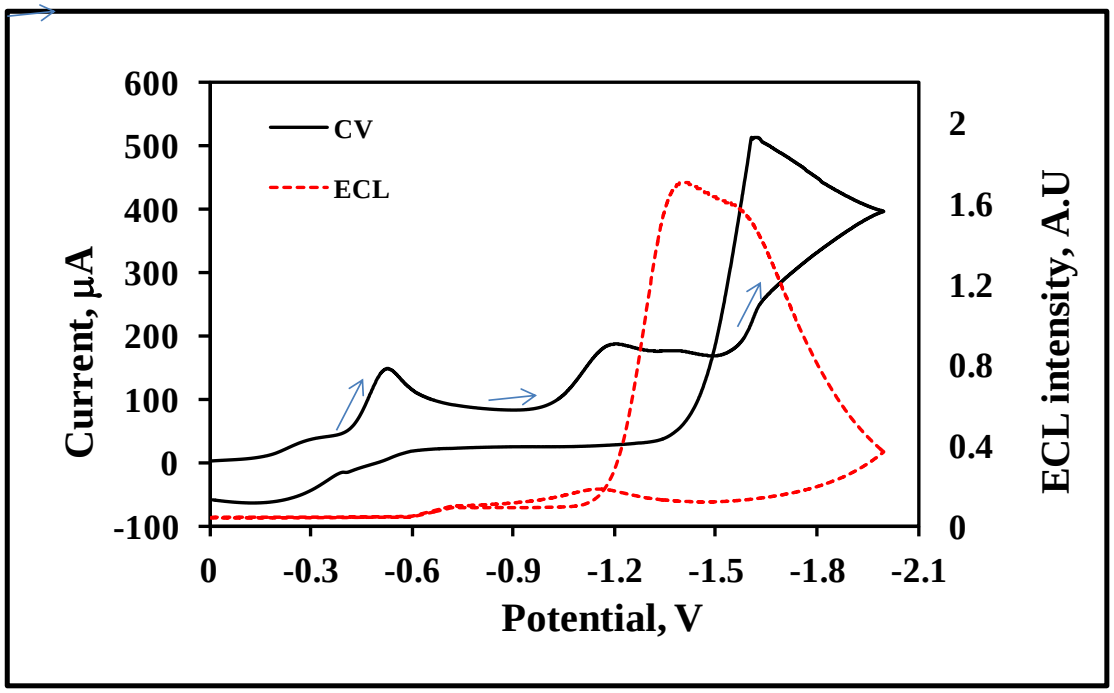

Figure 2.45: Cyclic voltammogram (solid line) and ECL spectra (dotted line) of BODIY-COOH thin film modified IDA platinum electrode, the scan rate is 0.1 V s^{-1}. The cysteamine layer was assembled on the electrode for 1 h and coupled to BODIPY-COOH. The ECL was evaluated in DMSO with 0.1 M TBATFB supporting electrolyte, in the presence of BPO as a coreactant. The scan rate is 0.1 V s^{-1} and the arrows show the direction of the scan.

In Figure 2.45, a constant potential of -0.90 V is maintained at the collector electrode, continuously producing BPO radicals, when generator electrode is swept between 0.00 to -2.00 V BODIPY is reduced to $BODIPY^{\cdot -}$. The radical species formed at the two electrodes diffuse together and react to form ^{1}BODIPY*. Strikingly on IDA electrodes there is 12 fold increase in currents generated during ECL, with increased ECL intensity output. ECL onset is tuned to less negative potentials, it is observed at -1.10 V and its maximum is

at -1.39 V. In contrast to ECL previously generated on macroelectrodes (Figure 2.32) at which the onset is observed at -1.65 V.

The enhanced ECL stability can be attributed to two advantages which IDA electrodes offer. This may be due to the fact that the spacing or gap between the electrodes is very small, the reduced BODIPY species produced on the generator electrode can diffuse across a small gap to the adjacent to collector electrode to react with BPO radicals, and then diffuses back to the original electrode to be reduced and form more BPO radicals.[53] This process is known as feedback loop redox cycling between the collector and generator electrodes, it results in an increase in the local concentration and flux of radicals and generating high faradaic currents.[54] In the classical approach of using a single macroelectrode, active generated species move in or out of the double layer, while in IDAs redox cycling occurs inside the overlapped diffusion shroud of the adjacent electrodes.

2.4. CONCLUSIONS

In this chapter the photophysics, electrochemical and electrochemiluminescence properties of a novel BODIPY-COOH in films are presented. One of the important objectives of the study was to investigate the ECL BODIPY-COOH dye in solution in the presence of a coreactant. BODIPY-COOH produced ECL responses when BPO or H_2O_2 were used as coreactants. A key finding from the ECL studies is that the ECL turn -on potential is dictated by the identity of the coreactant. When ECL was generated in the presence of BPO as the coreactant in solution the ECL turn-

on potential was -1.32 V. However, in the presence of H_2O_2, the ECL occurred at lower potentials -0.41 V. The use of two different coreactants which can turn on the ECL of a single luminophore at different electrode potentials, opens up possibilities for biological assay applications where analytes (important biomarkers) that can act as ECL coreactants can be individually detected in the same experiment.

Despite the significant results obtained from the solution studies, it has to be taken into consideration that solution ECL has its own limitations. Firstly solution ECL is limited when it comes to applications. Furthermore, there are other disadvantages such as the diffusion of the luminophore out of the detection zone and the constant need to supply the ECL reagent. To overcome these limitations, solid state ECL of BODIPY was investigated since the BODIPY-COOH has the carboxyl terminal group that can offer the opportunity to form thin film monolayer through coupling with linkers. The formation of BODIPY-COOH thin films via cysteamine and /or cysteine coupling were investigated. The ability to confine the BODIPY to electrode suggests that it could have potential applications in biological assays and biosensor design.

In form of thin film BODIPY remained luminescent in spite of the fact that the film is undiluted and, therefore, present at high molar concentrations. This confirms that self-quenching is not sufficient to interfere significantly with the film’s emission properties and thus the BODIPY thin films can be used in ECL applications. An important finding from the photoluminescence studies of BODIPY films is that BODIPY exhibits the strongest luminescence in water

and this is potentially useful in ECL application in biological media. The ECL was successfully generated from BODIPY thin film in the presence of BPO, and the ECL intensities observed for the thin film were the same as those observed when BODIPY was in solution. The cross reaction between the BODIPY radical anion and the reduced BODIPY radical is an important contributing process which influences the ECL intensity as reflected in the scan rate dependent studies.

Another objective of this study was to explore different methods of confining BODIPY to the electrode, with the aim of enhancing or achieving better ECL. This was carried out by using a short chain cysteamine or a long L-cysteine-PEG linker. An important outcome of the study was that ECL intensity of BODIPY-COOH thin film is not insensitive to the local environment. This is because changing the linker from a short chain cysteamine to a long L-cysteine-PEG linker did not increase or decrease the ECL (the intensities remained the same in both cases).

Electrochemiluminescence of BODIPY in solution and as a thin film on platinum electrodes was studied in an ionic liquid ([BMP][Tf2N]) as alternative solvents to DMSO and acetonitrile, because ILs are known to offer good electrochemical stability. However, results showed that the ECL intensity of BODIPY (for both solution and film based experiments) in ([BMP][Tf2N]) ionic liquid is low and not different from results obtained in DMSO. Thus from the ECL studies of BODIPY in solution or as thin film in DMSO, MeCN and ([BMP][Tf2N]), an important factor deduced is that the rate at which BODIPY

and BPO radical anions are produced as well as the rate which they react with each other to produce the excited state greatly influences the ECL intensity.

ECL of BODIPY thin films was investigated in IDA electrodes, where the $BODIPY^{\cdot -}$ and benzoyloxy radical can be generated on separate electrodes simultaneously. With IDA electrodes there was a 12-fold increase in currents generated during ECL and an increase in ECL intensity which was stable compared to when the ECL was generated on normal macroelectrodes

The overall conclusion of this chapter is the that the BODIPY-COOH dye investigated in this study does not exhibit better ECL when compared to the lead ECL reagent $[Ru(bpy)_3]^{2+}$ despite the fact that BODIPY-COOH exhibited higher quantum yield. However, the possibility of tuning the ECL of BODIPY-COOH can be very useful in multiplexing assays in which multiple analytes can be detected in one assay by just changing the coreactant.

2.5. REFERENCES

[1] Felix, F., Ferguson, J., Gudel, H. H., Ludi, A., *J. Amer. Chem. Soc.,* **1980**, 102, 4096-4102.

[2] Kalyanasundaram, K., Grätzel, M., Photosensitization and photocatalysis Using Inorganic and Organometallic Compounds, Kluwer Academic, Dordrecht, **1993**.

[3] Paris, J. P., Brandt, W. W., *J. Amer. Chem. Soc.,* **1959**, 81, 5001-5002.

[4] Nepomnyashchii, A. B., Bard, A. J., *J. Amer. Chem. Soc.,* **2011**, 45, 1844-1853.

[5] Krumova, K., Gonzalo, C., *J. Amer. Chem. Soc.*, **2010**, 132, 17560-17569.

[6] Ziessel, R., Ulrich, G., Harriman, A., *New J. Chem.*, **2007**, 31, 496-501.

[7] Qin, W., Rohand, T., Dehaen, W., Clifford, J. N., Drisen., K., Beljonne, D., Van Averbeke, B., Van der Auweraer, M., Boens, N., *J. Phys. Chem. A*, **2007**,111, 8588-8597.

[8] Strobl, M., Rappitsch, T., Borisov, S.M., Mayr, T., Klimant, I., *Analyst*, **2015**, 140, 7150-7153.

[9] Qin,W., Baruah, M., Van der Auweraer, M., De Schryver, F. C., Boens, N., *J. Phys. Chem. A*, **2005**, 109, 7371-738.

[10] Hesari, M., Lu, J., Wang, S., Ding, Z., *Chem. Commun.*, **2015**, 51,1081-1084.

[11] Venkatanarayanan, A., Martin, A., Keyes, T. E., Forster, R.. J., *Electrochem. Commun.*, **2012**, 21, 46–49.

[12] Loudet, A., Burgess, K., *Chem. Rev*., **2007**, 107, 4891-4932.

[13] Karolin, J., Johansson, L. B. A., Strandberg, L.., *J. Amer. Chem. Soc.*, **1994**, 116, 7801-7806.

[14] Martin, A., Long, C., Forster, R. J., Keyes,T. E., *Chem. Commun*., **2012**, 48, 5617-5619.

[15] Qin, W., Baruah, M., De Borggraeve,W. M., Boens, N., *J. Photochem. Photobiol. B,* **2006**, 183, 190–197.

[16] Prieto, J. B, Arbeloa, F. L., Martınez, V. M., Lopez, T. A., Amat-Guerri, F., Liras, M., Arbeloa, I. L., *Chem. Phys. Let*., **2004**, 385, 29-35.

[17] Lai, R. Y., Fleming, J. J., Merner, B. L.,Vermeij, R. J., Bodwell, G. J., Bard, A. J., *J. Phys. Chem. A.*, **2004**,108, 376-383.

[18] Qin, W., Rohand,T., Baruah,M., Stefan, A., Van der Auweraer, M**.**, *Chem. Phys. Let*., **2006**, 420, 562–568.

[19] Lai, R. Y., Bard, A. J., *J. Phys. Chem.,* **2003**, 107, 5036-5042.

[20] Bard, A. J., *Introduction in Electrogenerated Chemiluminescence,*ed. Bard. A. J., **2004**, New York: Marcel Dekker.

[21] Chandross, E., Sonntag, F., *J. Amer. Chem. Soc.,* **1966**, 88, 1089-1092.

[22] Forster, R. J., Bertoncello, P., Keyes, T. E., *Annu. Rev. Anal. Chem.*, **2009**, 2, 181-187.

[23] Gorman, A. A., Hamblett, I., King, T. A., Rahn, M. D., *J. Photochem. Photobiol. A.*, **2000**, 130, 127-132.

[24] Spehar-Deleze, A. M., Pellegrin, Y., Forster, R. J, Keyes, T. E., *Electrochem. Commun.*, **2008**, 10, 984-986.

[25] Batchelor–McAuley.,C., Dimov, I.B., Aldous ,L., Compton, R.G., *Proc Nat. Acad.Sci.,***2011**, 108, 19891-19895.

[26] Valenti, G., Bruno,C ., Rapino, S., Fiorani, A., Jackson, E. A., Scott, L. T., Paolucci, F., Marcaccio, M., *J. Phys. Chem. C.*, **2010**, 114, 19467-19472.

[27] Chandross, E. A.,Sonntag, F. I., *J. Amer. Chem. Soc.*, **1966**, 88, 1089-1095.

[28] Cruz, T. D. S., Atkins, D. L., Birke, R. L., *J. Amer. Chem. Soc.*, **1976**, 98, 1677-1682.

[29] Burghart, A., Kim, H., Welch, M.B., Thoresen, L.H., Reibenspies, J., Burgess, K., Bergstrom, F., Johansson, L.B., *J. Org. Chem.*, **1999**, 64, 7813-7819.

[30] Venkatanarayanan, A., Martin, A., Molapo, K. M., Iwuoha, E. I, Keyes, T. E., Forster, R. J., *Electrochem. Commun.*, **2013**, 31,116-119.

[31] Choi, J., Bard, A. J., *Anal. Chim. Acta.,* **2005**, 541, 143-150.

[32] Imamura, K., Tada, Y., Tanaka, H., Sakiyama, T., Nakanishi, K., *J. Colloid Interface Sci.*, **2002**, 250, 409-414.

[33] Velasco, J. G., Rubinstein, I., Crutchley, R. J., Lever, A. B. P., Bard, A. J., *Inorg. Chem.*, **1983**, 22, 822-825.

[34] Forster, R. J., Hogan, C. F., *Anal. Chem.*, **2000**,72, 5576-5582.

[35] Bertoncello, P., Forster, R. J, *Biosen. Bioelectron.*, **2009**, 24, 191-200.

[36] O'Reilly, E. M., Keyes, T. E., Foster, R. J.,Dennany, L., Analyst.,**2013** , 138, 677-682.

[37] Bertoncello, P., Kefalas, E. T., Pikramenou, Z., Unwin,P.R., Forster R. J,. *J. Phys. Chem. B.,* **2006**, 110, 10063-10069.

[38] Trama, K., Yan, H., Jemkins, H.A, Vassiliev, S, Bruce, D., Dyes Pigments., **2009**, 392-395.

[39] Dennany, L., Hogan, C. F., Keyes, T. E., Forster, R. J., *Anal. Chem.*, **2006**, 78, 1412-1417.

[40] Forster, R. J., Keyes T. E., Vos, J. G., Interfacial Supramolecular Assemblies, **2003**, England, John Wiley & Sons Ltd.

[41] Muino, P. L., Callis, P. R., *J. Phys. Chem. B.*, **2009**, 113, 2572-

[42] Miao, W., Choi, J., Coreactants, in Electrogenerated Chemiluminescence,ed. A.J Bard. **2004**, New York: Marcel Dekker.

[43] Roop, J., Nothnagel, M., Schnuriger, M., Richter, M., Baker., *J. Electrochem. Chem.*, **2011**,656, 34-40.

[44] Quinn, B., Ding, Z., Moulton, R., Bard, A. J., *Langmuir.,* **2002,** 18, 1734-1742

[45] Richter , M.M., Electrochemiluminescence , in Optical Biosensors Today and Tommorow , e.d. Ligler, S., Tait, C.R., **2008**, New York : Elservier

[46] Nepomnyashchii, A. B., Kolesov., G., Parkison., B. A., *Appl. Mater. Inter.,* **2013,** 5, 5931-5936.

[47] Nepomnyashcii, A. B., Boring, M., Ahrens, J. Bard, A. J., *J. Amer. Chem. Soc.,* **2011**, 133, 8633- 8645.

[48] Varshney, M., Li, Y., *Biosen. Bioelectron*., **2009**, 24, 2951-2960.

[49] Wang, X.B., Yang, J., Huang, J., Huang, Y., Vykoukal, J., Becker, F.F., Gascoyne, P.R.C., *Anal. Chem.,* **2000**, 72, 832-839.

[50] Lui, D., Perdue, R.K., Sun, L., Crooks, R.M., *Langmuir.*, **2004**, 20, 5905-5910.

[51] Fiaccabrino, G. C., Koudelka-Hep, M., Hsueh, Y., Collins, S. D., Smith., R.L, *Anal. Chem.*, **1998**,70, 4157- 4161.

[52] Amatore, C., Fosset., B., *Anal. Chem.*, **1993**, 65, 2311-2316.

[53] Liu, F., Kolesov., G., Parkison. B. A., *Anal. Chem.*, **2014**, 18, 7391- 7398.

[54] Tomcik, P., Sensors ., **2013,** 13, 13659-13684.

CHAPTER THREE:

ELECTROCHEMILUMINESCENCE FROM POLYANILINE RUTHENIUM METAL COMPLEX FILMS

3.1. INTRODUCTION

There is continues demand for inexpensive and selective sensors for analytical applications and especially in areas of clinical diagnostics.[1] While electrochemical methods have much to offer, however, designing electrode with surfaces which provide good sensitivity is a key challenge.[2] Electrochemiluminescence (ECL) involves light emission that arises when the energy liberated by the reaction of electrogenerated precursors is sufficient to generate a product in an electronically excited state.[3,4]

ECL offers advantages such as inherent sensitivity and selectivity, it also offers increased temporal and spatial control over the chemiluminescent reaction, making it a powerful analytical technique especially when the surface of the electrode is modified to fine-tune its ECL properties.[5] The majority of ECL systems that have been investigated involve solution detection, in which freely diffusing species with emission originating from a reaction layer near the electrode.[6] Despite the advantages of traditional solution ECL detection, their applications are limited because the ECL reagent must be continuously supplied to the reaction leading to higher reagent consumption and also diffusion of the ECL reagent out of the detection zone. To overcome these problems, different strategies to immobilize luminophores as films at the electrodes have been investigated.[7-9] These strategies include attaching the ECL emitting species to the electrode via a cation exchange polymer Nafion,[7] or self-assembled monolayers (SAMs),[8] or Langmuir Blodgett (LB). Covalent attachment to polymeric species such as polyvinyl pyridine,[9] conducting polymers (CPs) with redox centres attached or inserted

to their polymer backbone represent important novel materials that show high ionic and electronic conductivity. These properties are attractive in applications ranging from energy storage media,[10] electrochromic devices, light emitting diodes (LED),[11] and sensors.[12]

This chapter focuses on developing a method of surface confinement of a $[Ru(bpy)_2\ PIC]^{2+}$, bpy is 2,2'-bipyridyl and PIC is (2,2'-bipyridyl)-2(4-carboxylphenyl) imidazo [4,5][1,10] phenanthroline to the surface on an electrode. This is done by incorporating the charged metal complex within a conducting polymer polyaniline (PANI) through potentiostatic electropolymerization forming a composite film of PANI-Ru. Compared to the above mentioned immobilization method that have been used to confine luminophores, the present method explored in this chapter offers significant advantages including rapid, low cost in preparation procedures and good electrochemical, chemical and physical stability. The composite films have been characterized using cyclic voltammetry, AFM, Raman, and ECL.

3.2. EXPERIMENTAL SECTION

3.2.1. MATERIALS AND REAGENTS

The ruthenium (II) (bis-2,2-bipyridyl)-2(4-carboxylphenyl)imidazo[4,5-f][1,10]phenanthroline $[Ru(bpy)_2picH_2]^{2+}$ was synthesized by Dr Ciaran Dolan according procedure followed is described elsewhere.[13] Aniline (ANI > 99.5 %) and all other chemicals which were used in the experimental

procedures were all purchased from Sigma Aldrich and all spectroscopic measurements were carried out with solvents which were of HPLC grade.

3.2.2. POTENTIODYNAMIC POLYMERIZATION OF PANI-Ru

Aniline (ANI > 99.5 %) was distilled under nitrogen atmosphere into a conical flask covered with tin foil to keep out the light, and the monomer distillate was subsequently kept at -20°C prior to use. For electrosynthesis of PANI-Ru, a solution containing 0.2 M ANI, HCl (1 M) and 1 mM $[Ru(bpy)_2\ PIC]^{2+}$ was cycled between -0.2 (initial potential) to 1.2 V (final potential), at a potential scan rate of 0.1 V s^{-1}. The electropolymerization was stopped after 20 voltammetric cycles. The ITO-PANI-Ru modified electrode was then removed from the polymerization solution, and was rinsed off with deionized water to remove excess monomer.

3.2.2. POTENTIOSTATIC POLYMERIZATION OF PANI-Ru

Electrochemical measurements were used were conducted as described in Chapter 2. The PANI-Ru complex films were deposited at a fixed potential while measuring the charge passed. Briefly, ITO electrodes (1.25 cm^2) were cleaned by sonicating in deionized water for 5 min and followed by sonication in acetone for 5 min. The electrodes were then dried under a stream of nitrogen. The ITO electrodes were then placed in an electrochemical cell containing 0.1 M HCl, 0.2 M aniline and 1 mM $[Ru(bpy)_2\ PIC_2]^{2+}$ and electropolymerization was carried out at + 0.7 V for 1600 s. Following

electrodeposition, the modified electrodes were washed thoroughly with milli-Q water and were allowed to dry for 2 hours before use.

3.2.3. MORPHOLOGICAL CHARACTERIZATION OF THE COMPOSITE FILM

Atomic force microscope (AFM) was used to investigate the morphology of the PANI-Ru composite films on ITO. The measurements where performed on a Veeco Bioscope II instrument in tapping mode using FESP-V2 cantilever tips purchased from Bruker. The images were obtained by scanning an area of 5 μm^2 at a scan rate of 0.25 Hz.

3.2.4. ELECTROCHEMILUMINESCENCE

Electrochemiluminescence and electrochemistry experiments were performed as described in Chapter 2.

3.3. RESULTS AND DISCUSSION

3.3.1. POTENTIODYNAMIC POLYMERIZATION

Initially the voltammetry of $[Ru(bpy)_2PIC]^{2+}$ was measured in solution in order to have a benchmark of the electrochemical properties of the complex when its freely diffusing in solution, so that the properties can be compared when kthe luminophore incorporated in a polymer.

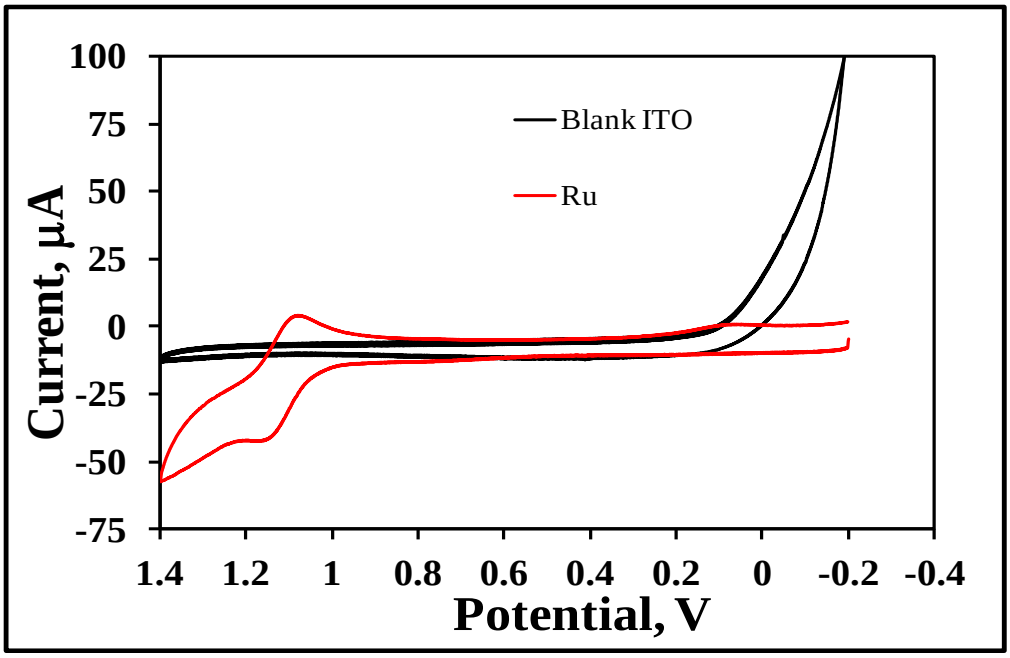

Figure 3.1: Cyclic voltammogram of 1mM $[Ru(bpy)_2PIC]^{2+}$ in 0.1 M HCl as a supporting electrolyte , the scan rate is 0.1 V s^{-1}. The working electrode ITO with an area of 1.25 cm^2.

Figure 3.1 shows the electrochemical characteristics of the ruthenium complex, $[Ru(bpy)_2\ PIC]^{2+}$, on its own was investigated in 0.1 M HCl using an ITO working electrode at 0.1 V s^{-1}. The $Ru^{2+/3+}$ couple with oxidation observed at 1.14 V and 1.09 V for reduction, consistent with typical characteristics of ruthenium trisbpy type complexes.Solution phase electrochemiluminescence of ruthenium complexes has been well investigated.[14,15] however, solution ECL has its own limitations such as higher reagent consumption and also diffusion of the ECL reagent out of the detection zone.[16,17] Here, an important objective was to confine $[Ru(bpy)_2PIC]^{2+}$ within an electropolymerised polymer film. Conducting polymers have been previously electrosynthesized under either potentiostatic[18,19] or potentiody-namic conditions.[20,21]

The first attempt to incorporate $[Ru\ (bpy)_2(PIC)_2]^{2+}$, was carried out by electrochemical deposition of PANI in the presence of Ru luminophore via potentiodynamic polymerization onto the surface of ITO. Potentiodynamic electropolymerization of conducting polymers is commonly used, because it allows control over several parameters, such as initial and final potential, number of scan cycles and the scan rate. These parameters may be important in the determination of the structure of the polymer that is produced.[22] Figure 3.2 illustrates the cyclic voltammogram recorded during polymerization, between -0.2 and 1.4 V, in an acidic medium, *i.e.,* 1M HCl in the presence of $[Ru(bpy)_2PIC]^{2+}$ at a scan rate of 0.1 Vs^{-1}.

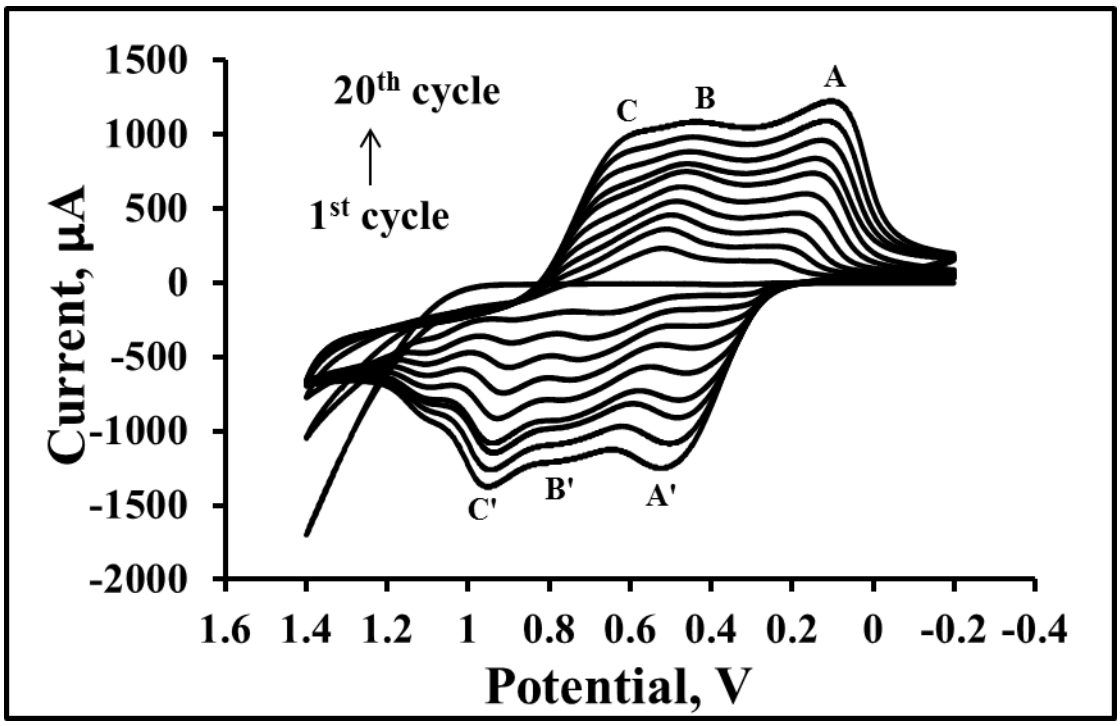

Figure 3.2: Electrosynthesis of PANI-Ru composite film in 1M HCl on an ITO electrode, area is 1.25 cm^2. The potential is cycled between -0.2 and 1.4 V in a solution containing 0.2 M Aniline, 1mM $[Ru(bpy)_2PIC]^{2+}$ and 1M HCl. Twenty successive cycles are shown and these cycles indicate the progressive increase in the thickness of the film as the electropolymerization proceeds.

Figure 3.2 illustrates a typical cyclic voltammogram obtained during electropolymerization of PANI in the presence of $[Ru(bpy)_2PIC]^{2+}$ at an ITO electrode by sweeping the potential from -0.2 to 1.1 V, successive polymerization cycles are shown. It is clear that PANI is redox active in this potential window, as the voltammetry of deposition exhibits three sets of redox peaks. The redox couple A/A' is attributed to the transformation from the reduced leucoemeraldine (amine units) to the partly oxidized emeraldine state (semiquinone radical cations) and the redox couple B/B' is due to the redox reaction of the benzoquinones .The redox couple C/C' which corresponds to the transition of PANI from leucoemeraldine (LE) to the pernigraniline (PE)

state. This process is accompanied by PANI oxidation at approximately 0.89 V, it results in the nucleation of PANI. During the electropolymerization process, an increase in the voltammetric peak current is observed as repetitive sweeping is carried out and this is indicative of an increase in thickness of film during the film deposition on the electrode.

An increase in both reductive and oxidation peak currents as the polymer is deposited on the electrode is observed and it indicates that the polymer is electroactive,[23] from Figure 3.2, there is an additional peak at 1.12 V. This peak is normally not observed during polymerization of PANI. On the basis of the solution phase voltammetry illustrated in Figure 3.1 Ru oxidation occurs at 1.14 V, this particular peak of interest is consistent with the presence of $[Ru(bpy)_2PIC]^{2+}$ in the polymerization solution. After potentiodynamic polymerization, the electrode was placed in fresh monomer free HCl electrolyte to characterize the electrosynthesized PANI-Ru film, using cyclic voltammetry as illustrated in Figure 3.3 .From the voltammetry presented in Figure 3.3, there is no evidence of the presence of $[Ru(bpy)_2PIC]^{2+}$ in the film electrosynthesized by cycling between potential -0.2 and 1.4 V. This is due to the absence of the oxidation and reduction Ru peaks which are expected at 1.14 and 1.09 V, respectively. This suggests that $[Ru(bpy)_2PIC]^{2+}$ was not successfully incorporated in the polymer backbone during the polymerization process.

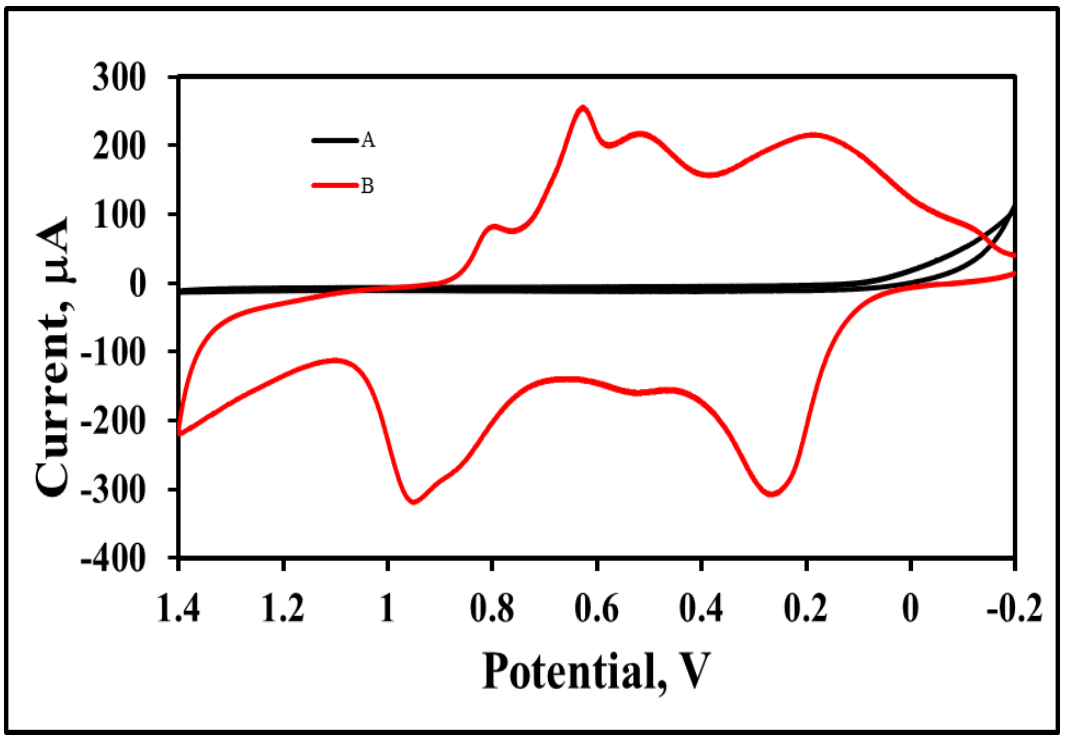

Figure 3.3: Cyclic voltammogram of (A) is blank ITO and (B) PANI-Ru film which was synthesised by cycling between -0.2 to 1.4 V on ITO working electrode, the supporting electrolyte is 0.1 M HCl and the scan rate is 0.1 Vs^{-1}. The working electrode area is 1.25 cm^2.

One reason that can be attributed to Ru not being incorporated in the polymer is that during the polymerization, when then potential reaches the oxidation potential at approximately 1.14 V, the $[Ru(bpy)_2PIC]^{2+}$ gets incorporated in the polymer. However in the reverse cycle, the Ru leaves the polymer. This essentially means that sweeping between a potential window encourages shuttling of Ru in and out of the polymer instead of its incorporation into the polymer. This suggests that the Ru oxidation peak that was observed at 1.14 V in Figure 3.2 was essentially due to the presence of Ru in polymerization solution and not necessarily due to its presence in the polymer during the electrosynthesis process. This leads to conclusion that for successful loading

of Ru in the polymer potentiodynamic polymerization is not an appropriate method that should be employed. In this regard, polymerization should rather be carried out by applying a constant potential using a potentiostatic technique such as amperometry (as presented in Figure 3.4).

3.3.2. POTENTIOSTATIC POLYMERIZATION

Potentiodynamic polymerization of the composite film was carried out by applying a constant potential of +0.7 V. It has been previously reported that over oxidation of PANI by applying higher potentials results in irreversible formation of quinonedimine structures which are electrochemically inactive.[24] When a constant potential of +0.7 V is applied at the electrode in a solution of 0.2 M aniline in 0.1 M HCl, in the presence of 1 mM $[Ru(bpy)_2PIC]^{2+}$, a polymeric film forms in which the metal complex is bound. This takes place when the negatively charged carboxyl sites of the Ru complex electrostatically interact with the positively charged nitrogen sites of PANI.[25] Figure 3.4 presents the formation of the PANI-Ru composite film using potentiostatic polymerization. The current-transient curve for the polymerizaton of the composite presented in (Figure 3.4) shows that the current falls to a minimum followed by an increase in the current. The linear current increase can be related to the growth of the bulk polymer layer.

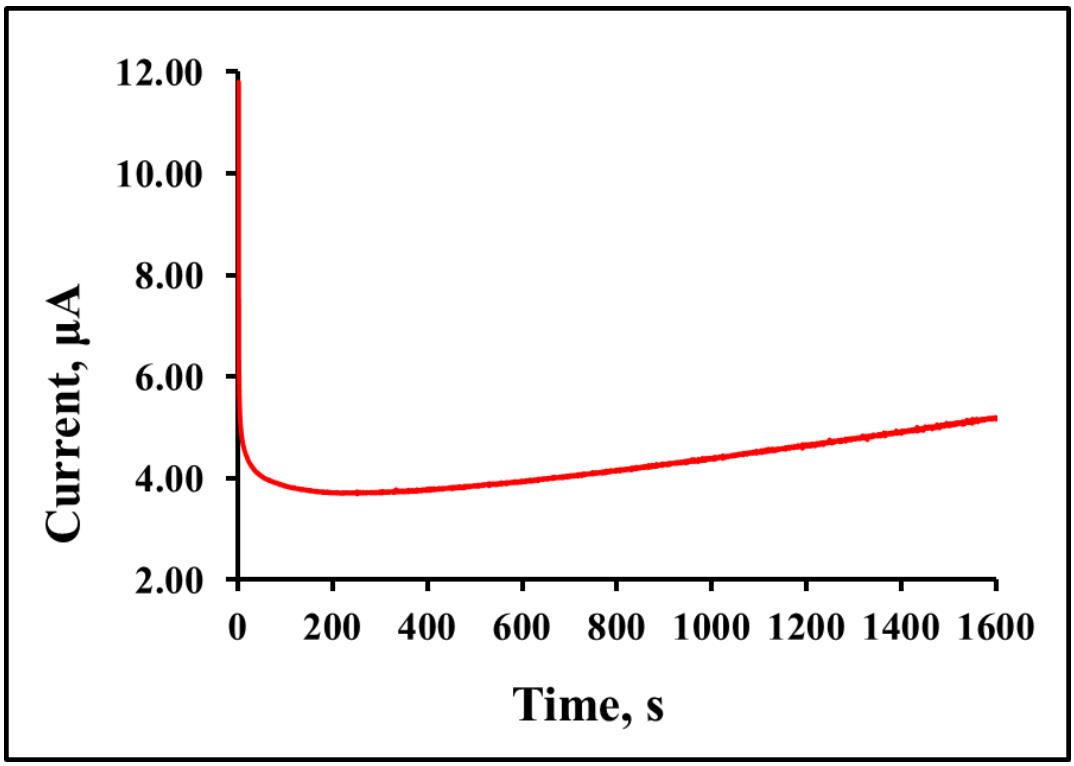

Figure 3.4: Potentiostatic electrosynthesis of PANI-Ru composite onto an ITO electrode from a solution containing 0.2 M Aniline, 1mM $[Ru(bpy)_2PIC]^{2+}$ and 1M HCl at an applied potential of + 0.70 V for 1600 s.

During the first 200 seconds of the polymerization process an initial decrease in current is observed, this decrease can be attributed double layer charging. It is well known that polymerization takes place in two stages, the first being nucleation and the second is polymer growth. The initial decrease in current observed is characteristic of both nucleation and growth kinetics.[26] Following the suddent decrease in current, from 200 s there is a steady constant increase in current, which indicates that the electropolymerization of the monomer *i.e* aniline is taking place. After the polymerization, the electrode was removed from the polymerization solution and was placed in fresh clean HCl electrolyte for characterization.

3.3.3. CHARACTERIZATION OF THE FILMS

3.3.3.1. Cyclic Voltammetry

A typical CV of the PANI-Ru composite film in 0.1 M HCL after potentiostatic polymerization is presented in Figure 3.5.

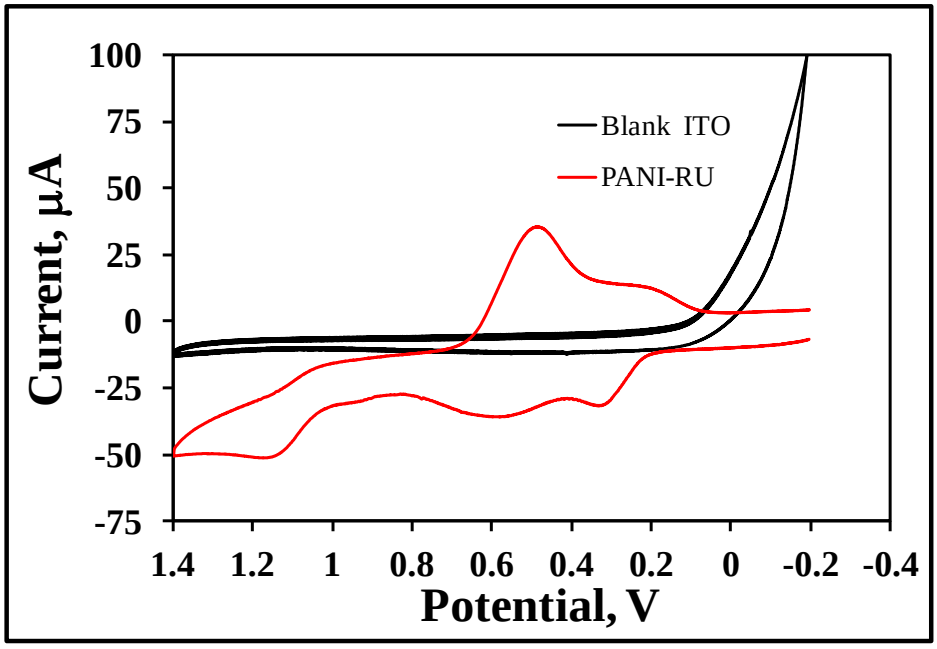

Figure 3.5: Cyclic voltammogram of PANI –Ru composite on ITO, electrode area is 1.25 cm^2. The supporting electrolyte is 0.1 M HCl and the scan rate is 0.1 V s^{-1}. The surface coverage of the ruthenium centres in the composite is 1.1 ± 0.1 x 10^{-10} mol cm^{-2}.

For comparison PANI prepared in the absence of $[Ru(bpy)_2PIC]^{2+}$ was synthesized employing the same method of potentiostatic polymerization. This was carried out to give insights into the difference in the voltammetric

behaviour of the polymer in the presence or absence of $[Ru(bpy)_2(PIC)_2]^{2+}$ and the CV showing the characterization of neat PANI in fresh 1M HCl is presented in Figure 3.6.

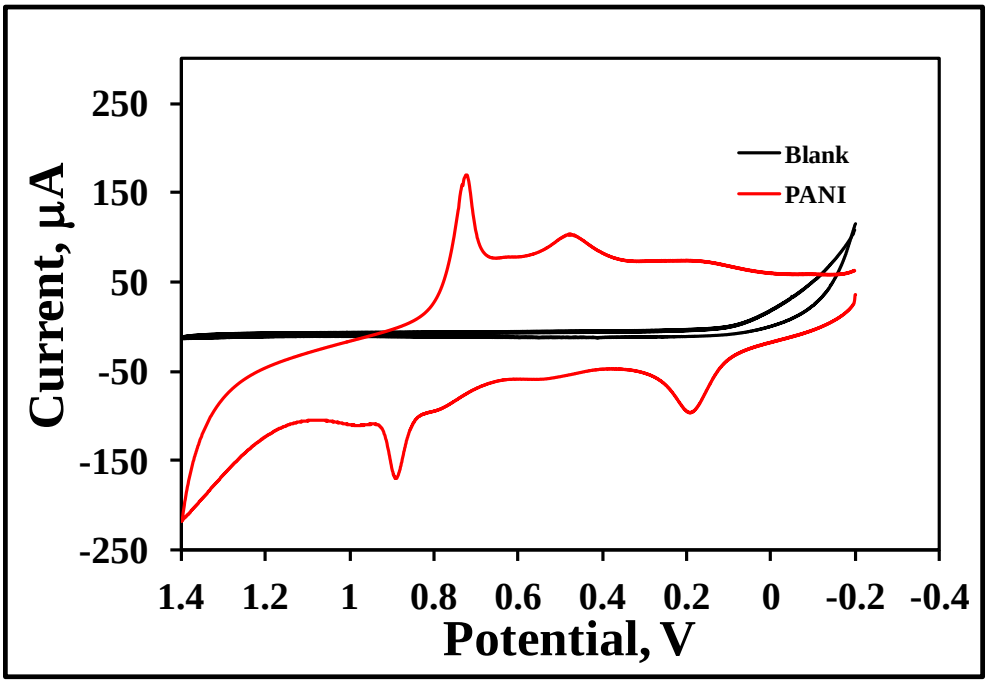

Figure 3.6: Cyclic voltammogram of neat PANI film on a ITO working electrode, the electrode supporting electrolyte is 0.1 M HCl and the scan rate is 0.1 V s^{-1}. The working electrode area is 1.25 cm^2, the surface coverage of PANI is 3.0 ± 0.2 x 10^{-10} mol cm^{-2}.

Figure 3.6 shows the voltammogram of a PANI film in the absence of incorporated $[Ru(bpy)_2(PIC)_2]^{2+}$ at a scan rate of 0.1 V s^{-1} where the supporting electrolyte is 0.1M HCl. The voltammogram exhibits the three redox couples typically associated with PANI.[27] The process with an anodic peak potential, $E_{pa,}$ of 0.19 V is due to the leucoemeraldine, LM, radical which

is subsequently converted to the emeraldine state with an E_{pa} of 0.55 V. The peak at 0.89 V is attributed to the formation of the pernigraniline, PE, salt. The voltammetric behaviour of PANI films in HCl has been previously reported and the electrochemical characteristics observed in this study are similar to those previously reported.[28] The surface coverage, Γ, was determined from the peak at 0.89 V by measuring the charge passed under in slow scan rate (< 0.01 V s^{-1}) background corrected voltammograms where the supporting electrolyte was 0.1 M HCl, yielding a value of 3.0 ± 0.2 x 10^{-10} mol cm^{-2}. This surface coverage is equivalent of 3 monolayers suggesting that the PANI film is very thin.

When comparing the voltammetric behaviour of PANI-Ru composite film in Figure 3.5 to that of neat PANI in Figure 3.6, it is clear that the three redox couples for the different oxidations states cannot be clearly identified in the PANI-Ru composite. Similar behaviour has been observed elsewhere in a study which involved PANI- [Ru (Cl_3 (dppb)-py)] (dppb= 1,4- bis diphenylphosphine butane, py = pyridine).[29] Where redox pair couples observed in pure PANI films were attributed to the inter-conversion between the leucoemeraldine and emeraldine oxidation states. However, when Rupy was introduced in the films, the peaks become less defined and this accompanied by a drop in the current.[29]

In the present study two redox couples are observed in the PANI-Ru at scan rate 0.1 V s^{-1} in Figure 3.5 and at slower scan rates only one redox couple is observed in Figure 3.7. However in PANI-Ru the $Ru^{2+/3+}$ couple is clearly observed and its formal potential is indistinguishable from that observed for the complex dissolved in aqueous electrolyte, see Figure 3.1. This suggests that Ru has been successfully incorporated into the polymer, the cyclic voltammogram of the PANI-Ru composite in Figure 3.5 shows that the pernigraniline redox reaction PANI is coupled to the Ru^{2+} to Ru^{3+} process which results in an irreversible oxidation wave from + 1.00 to 1.40 V at 0.1 V s^{-1}. Based on the on the pernigraniline peak ,the surface coverage of PANI in the composite is 7.5 ± 0.2 x 10^{-11} mol cm^{-2}, *i.e*., the PANI coverage is approximately 4 fold lower when the film is formed in the presence of the metal complex. The surface coverage of the ruthenium centres, 1.1 ± 0.1 x 10^{-10} mol cm^{-2}, i.e., the PANI-Ru film is approximately 60% mole percent ruthenium. However, the total number of moles of ruthenium immobilized is small and is equivalent to a monolayer of the metal complex. Figure 3.7 shows the slow, *i.e.,* 0.01 to 0.05 V s^{1} scan rate dependent voltammetry analysis of PANI-Ru composite and it can be observed that the current increases with increasing scan rate. From this the homogeneous charge transport diffusion coefficient, D_{CT}, can be determined as it can give more insights into the movement of the slowest species, ions or electrons.

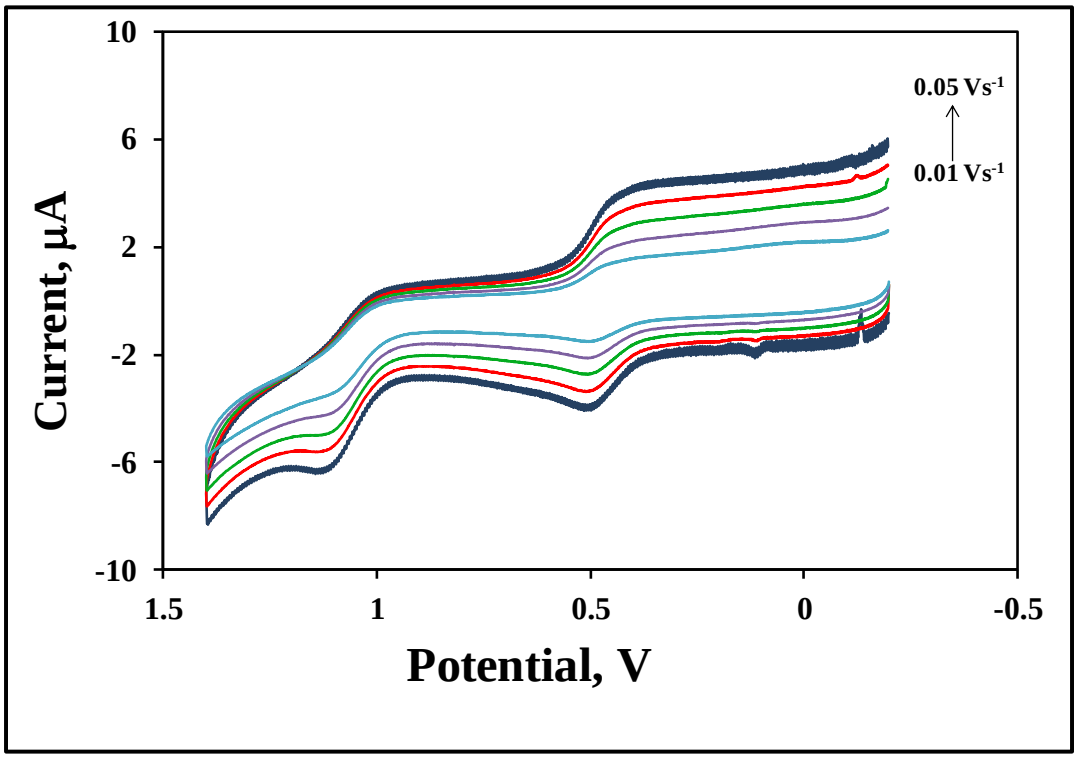

Figure 3.7: Scan rate voltammetric response of PANI –Ru composite on an ITO. The supporting electrolyte is 0.1 M HCl and the scan rate is from 0.01 to 0.05 V s^{-1}, the electrode area of 1.25 cm^2.

The diffusion coefficient was estimated from a plot of the peak current for the $Ru^{2+/3+}$ couple from, I_p versus the square root of the scan rate, $v^{1/2}$, under semi-infinite linear diffusion controlled conditions, as described by the Randles-Sevčik equation (Equation 1.33).

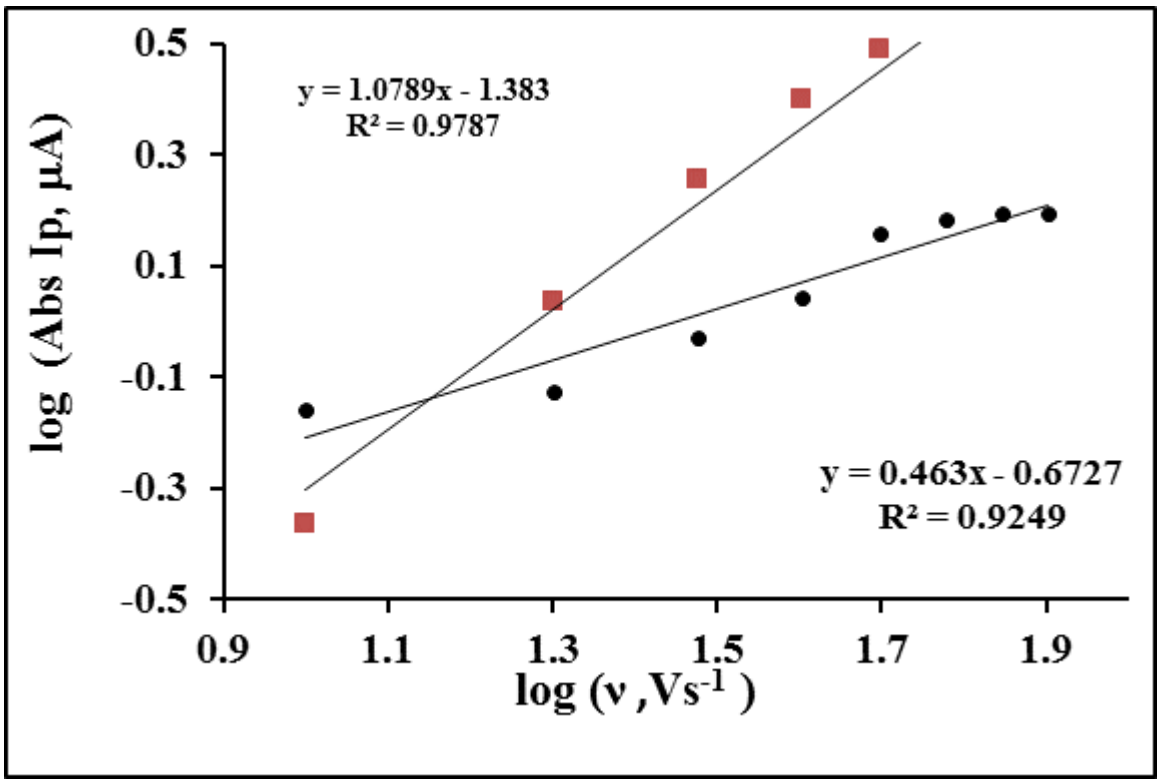

Figure 3.8: The plot of log-log of the absolute value of the peak and current for $Ru^{2+/3+}$ vs the scan rate for the composite film. The anodic currents are denoted ■ whilst ● denotes the cathodic peak currents.

A plot of log–log absolute value of the peak current Vs scan rate was plotted to determine D_{CT} value and it is presented in Figure 3.8. The plot shows that the anodic peak current is directly proportional to the scan rate, with a slope of 1.07 ± 0.08. From this result, it can be deduced that for the range of scan rates 0.01 to 0.05 V s^{-1}, the oxidation process is under finite diffusion control. In contrast, the slope of the reduction process 0.46 ± 0.05, is indistinguishable from that expected for semi-infinite diffusion control 0.5 and the depletion layer thickness is expected to be thinner than the layer thickness for all scan rates investigated.

The charge passed during they synthesis of composite film suggests the film is approximately 0.3 μm thick.[30] To determine the concentration, *C*, of the Ru centres within the PANI-Ru composite film the surface coverage of the ruthenium centres previously determined as $1.1 \pm 0.1 \times 10^{-10}$ mol cm^{-2}, was the divided by this film thickness and it yielded a value of 3.67 mM. Using the anodic slope from this plot, the number electrons =1 in conjunction with 3.67 mM concentration, the D_{CT} for Ru^{2+} oxidation in PANI-Ru was determined to be $2.6 \pm 0.9 \times 10^{-10}$ cm^2 s^{-1} for Ru^{2+} oxidation. Previously reported studies which focused on structurally related ruthenium complexes bound to non-conducting polymers, such as nafion-$[Ru(bpy)_3]^{2+}$ and $[Ru(bpy)_2$(poly-4-vinyl pyridine$)_{10}]^{2+}$, reported D_{CT} values of $3 \pm 0.8 \times 10^{-11}$ and $9.2 \pm 1.1 \times 10^{-11}$ cm^2 s^{-1}, respectively.[5] Significantly, $2.6 \pm 0.9 \times 10^{-10}$ cm^2 s^{-1} value in this study is approximately an order of magnitude faster.

The 3.67 mM concentration of the ruthenium centres in the polymer is low, compared to similar studies where a positively charged $(Ru(bpy)_3]^{2+}$ was incorporated in poly(2-methoxyaniline-5-sulfonic acid) by electropolymerization, in which the Ru- centres in the film were 0.6 M. However in the present study, although the Ru loading in the polymer film is low, a faster D_{CT} is observed and this can be attributed to the composite film being very porous.[31] The porous film allows increased penetration of the electrolyte in the film, leading to increased contact with the Ru centres in the film.

3.3.3.2. Morphological characterization

The morphology of the PANI-Ru composite film confined to the electrode was investigated with Atomic force microscopy. Figure 3.9 (A) displays 3D AFM micrograph of the PANI-Ru composite film on an ITO electrode and (B) shows a micrograph of control blank electrode where the ITO is unmodified. The bare ITO surface is featureless, as displayed on Figure 3.9 (B) with a mean roughness (R_a) of 2.09 ± 0.5 nm and the surface roughness is 1.42 μm^2. As observed from Figure 3.9 (A) after deposition of the PANI-Ru composite on the ITO electrode the morphology on the surface displays well defined globular like structures, which have a mean roughness (R_a) of 43±10 nm and a surface roughness of 34 μm^2. Suggesting that the increase in the mean and roughness on the ITO electrode is due PANI-Ru on the electrode. The increase in the surface roughness is due to an increase of polymer layers deposited on the electrode surface. The morphological aspects of the composite film are in agreement with those previously published, that the PANI films exhibit globular morphology for thin films.[32]

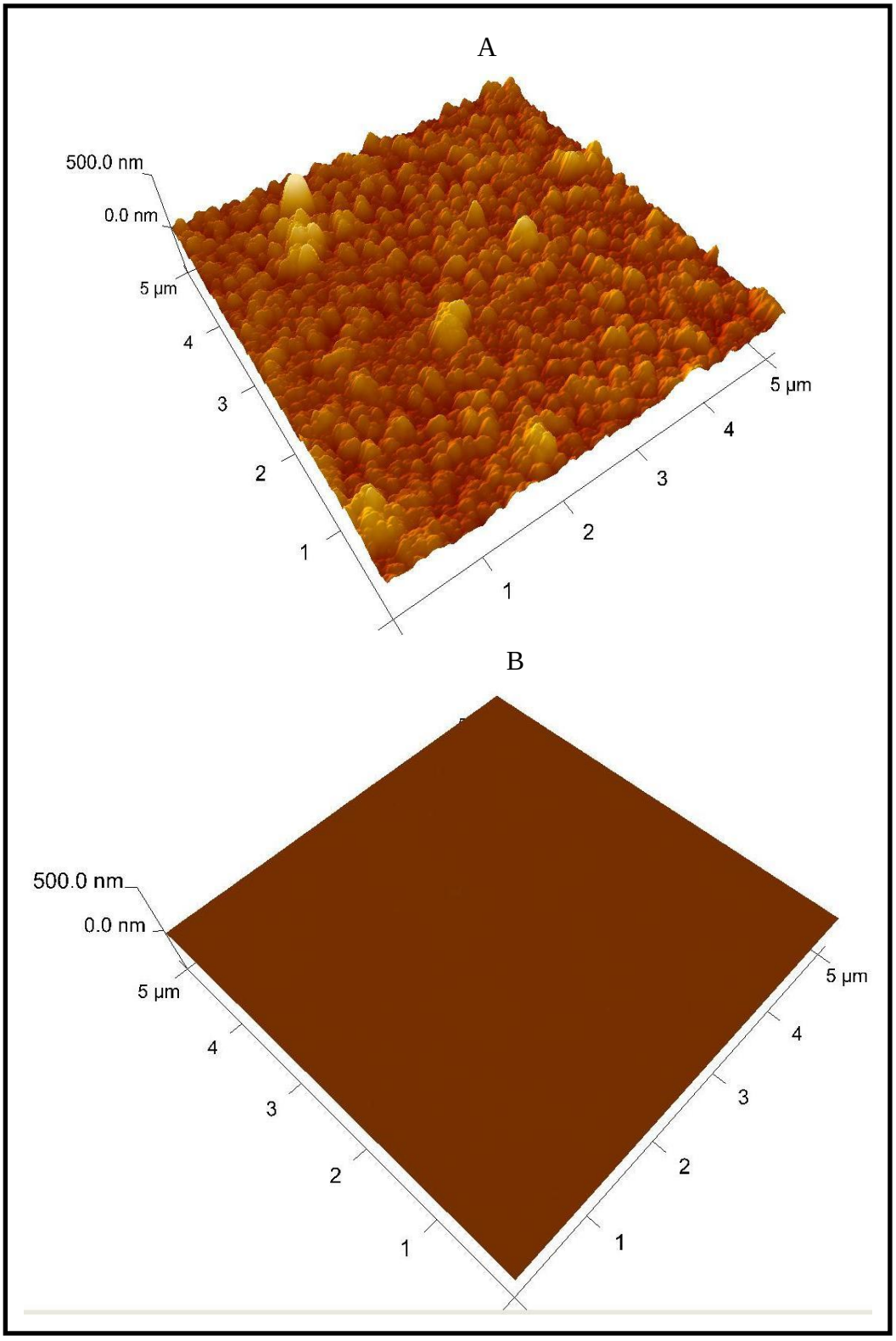

Figure 3.9 : 3D Atomic force microscope image of (A) modified with PANI-Ru composite film and (B) blank ITO electrode , obtained in tapping mode.

3.3.3.3. Raman spectroscopy

Raman spectroscopy was used to further characterize the layers since it can provide insights into both the PANI backbone and the incorporated metal complex. Comparative Raman spectra of $[Ru(bpy)_2PIC]^{2+}$, PANI and PANI-Ru are presented in Figure 3.10.

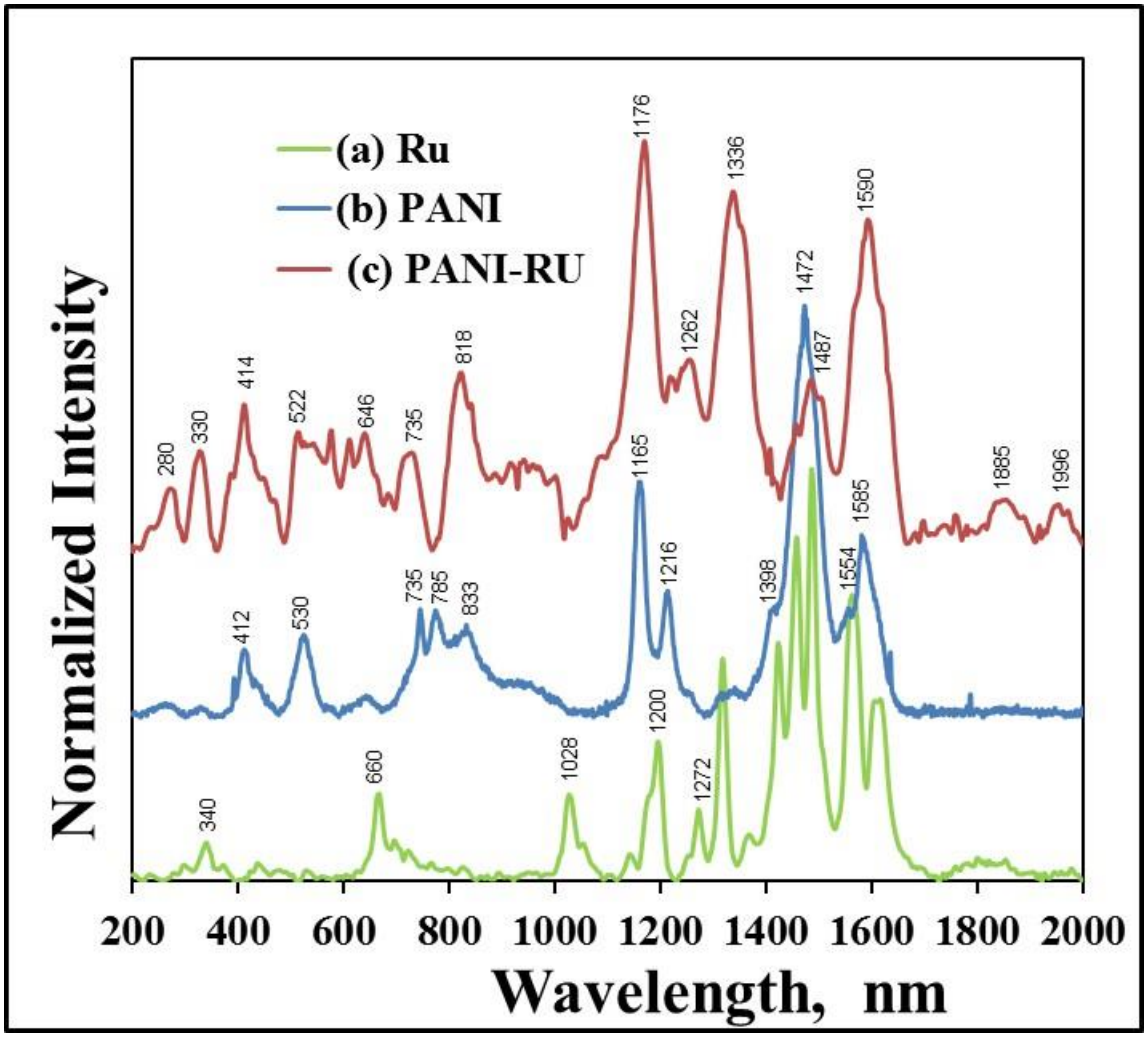

Figure 3.10: Raman spectra of $[Ru(bpy)_2PIC]^{2+}$, neat PANI, PANI-Ru modified ITO electrode, the samples were excited at 458 nm with an ion laser incident power of 20 Mw. The spectra were averaged over 2 acquisitions with an exposure time of 2s.

It was necessary to carry out RAMAN characterization of $[Ru(bpy)_2PIC]^{2+}$ and neat PANI to understand their structural characteristics separately. This would give insights into the modes observed for the composite material. The Raman spectrum obtained for $[Ru(bpy)_2 PIC]^{2+}$ is presented in Figure 3.10 (in green), signature modes are observed at 1554, 1488, 1313, 1272, and 1028 cm^{-1} that are all characteristic of bipyridyl ligand.[33] Furthermore, two weak vibration bands are observed in the lower frequency region, the first vibration mode observed at 340 cm^{-1} is due to the metal to ligand *i.e.* Ru-N bond[34, 35] and the second is at 660 cm^{-1} which is attributed to bipyridyl in plane twisting. Detailed assignments of vibrational modes are presented in Table 3.1.

The spectrum for neat PANI is presented in blue in Figure 3.10, what is immediately clear is modes of vibration at 1585, 1472, 1216, 1165 cm^{-1} which are characteristic of PANI are observed.[36] Here, the spectral positions of the vibrational modes have been assignment to typical vibrations of PANI as previously reported in literature as follows; the vibration band observed at 1585 cm^{-1} is due to the stretching modes of C=C vibrations of the quinoid structures.[37, 38] A relatively intense vibration band is observed at 1472 cm^{-1} and it is attributed to the C= N stretching in the quinoid units which are typically observed in PANI.[39] The vibration band that is observed at 1216 cm^{-1} is related to the C-N vibration modes of the benzene groups, while the vibration mode observed at 1165 cm^{-1} is due to the C-H bending vibration of semiquinone rings.[40] Other bands observed at 412 and 530 cm^{-1} out of plane

deformations of the ring,[41] while 833 cm^{-1} are due to the benzene ring deformations.

Figure 3.10 also shows the Raman spectra of PANI-Ru composite film (presented in red), the vibration modes attributed to the presence of PANI in the composite are observed at 1590, 1487, 1176, 818, 416 cm^{-1} and those of $[Ru(bpy)_2PIC]^{2+}$ are observed at 1337, and 1258 cm^{-1}. The raman band observed at 1590 cm^{-1}, can be attributed to C=C stretching modes from the quinoid structures of the polymer and bipyridyl structure of the ruthenium complex. The stretching modes observed at 1487 cm^{-1} are due to the C=N of the quinoid rings in the polymer. The symmetric C-H bending vibration of the PANI benzene rings are characterized by the vibration bands observed at 816 cm^{-1} while the amine deformation 1176 cm^{-1}.[42]

The presence of the $[Ru(bpy)_2PIC]^{2+}$ in the PANI-Ru composite is evident, due to the presence of the vibration modes observed at 1333, and 1258 cm^{-1}. The mode observed at 1337 cm^{-1} due to the C=N stretches of bpy in the PANI-Ru composite film shifted with 20 cm^{-1} to higher frequencies compared to 1313 observed from the $[Ru(bpy)_2PIC]^{2+}$. The band at 1258 cm^{-1} is attributed to the C=C inter ring bending of bipyridyl. The mode at 330 cm^{-1} is due to the metal ligand stretch in the PANI-Ru composite, however in neat $[Ru(bpy)_2PIC]^{2+}$ this band is observed at 340 cm^{-1}. This down shift of the metal stretch vibration in the composite film is caused by torsional strain between the polymer backbone and the metal ligand complex.

Table 3.1: General comparative assignments of Raman vibrational modes of $[Ru(bpy)_2PIC]^{2+}$, PANI and PANI-Ru the spectra were collected at an exciting wavelength 458 nm.

Sample	Raman band (cm^{-1})	Assignment
$[Ru(bpy)_2PIC]^{2+}$	~ 340	Metal ligand stretching
	~ 663	Pyridyl twisting
	~1028	Ring breathing
	~1200	C- CH bending
	~1313	C=N stretch
	~1272	C=C inter-ring bending
	~1488	C=N stretch
	~1554	C=C stretch
PANI	~415	out of plane ring deformation
	~ 522	out of plane ring deformation
	~831	Amine deformation
	~1165	C-H bending vibration
	~1216	Benzoid C- N stretching
	~1474	Quinoid C=N stretching vibration
	~1585	Quinoid C=C stretching vibration
PANI-Ru	~330	Metal ligand stretching
	~414	out of plane ring deformation
	~522	out of plane deformation
	~646	Pyridyl twisting
	~818	Benzoid ring deformation
	~1176	Benzoid C-H in plane bending
	~1262	C-C inter ring bending in bpy

	~1333 ~1487 ~1590	C=N stretching vibration in bpy Quinoid C=N stretching vibration C-C stretching modes

3.3.4. ELECTROCHEMILUMINESCENCE

As discussed in Chapter 1, ECL has two dominant pathways to generate ECL light. The first pathway is by potential step annihilation experiments where the electrode is alternated between values sufficiently positive to generate the Ru^{3+} form and sufficiently negative to generate the Ru^{+} form of the complex. The other pathway involves application of a single potential in the presence of a suitable coreactant. In the present instance, the annihilation approach did not give ECL and under these circumstances one might expect to generate ECL in the presence of a co-reactant. The ECL response of the electrodeposited PANI-Ru thin film generated by the oxidative co-reactant pathway using TPA as the co-reactant was investigated.

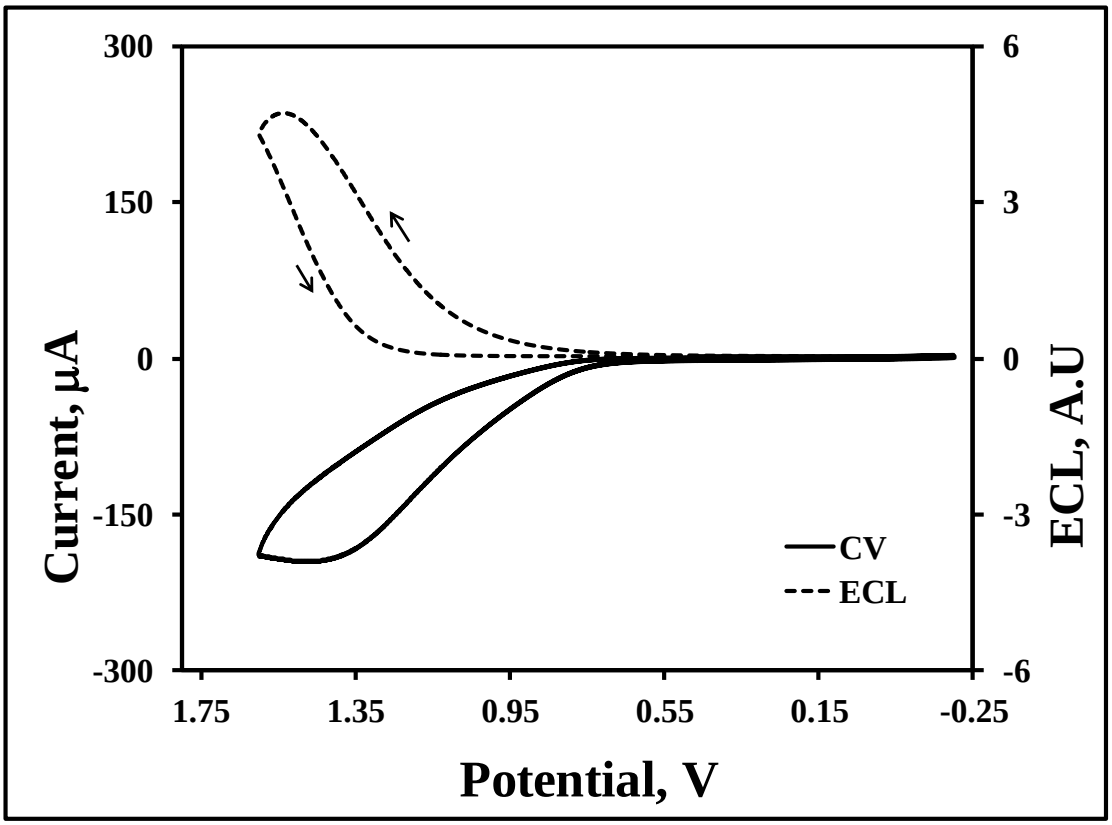

Figure 3.11: Cyclic voltammogram (solid line) and ECL response (dashed line) of a PANI-$[Ru(bpy)_2PIC]^{2+}$ where the contacting solution contains 50 mM TPA and 0.1 M phosphate buffer and the scan rate is 0.1 V s^{-1}. The working electrode is ITO with an electrode area of 1.25 cm^2.

Figure 3.11 shows the voltammetric (solid line) and the ECL (dashed line) responses of a PANI-Ru thin film on ITO, while the inset shows the ECL response of Ru in the absence of the polymer in 0.1 M HCl in the presence of 50 mM TPA, scanning from -0.3 to 1.6 V. The voltammogram of PANI-Ru reveals that in the presence of TPA, a broad irreversible oxidation wave is observed starting from + 0.8 V and the maximum current is observed at 1.4 V. TPA oxidation at the electrode surface results in the production of a short lived radical cation, $TPA^{\bullet}$, which is a highly reducing intermediate.[43] The Ru^{2+}

centres are oxidised to Ru^{3+} at the electrode which are then chemically reduced by the $TPA^{\bullet}$ to an electronically excited state, Ru^{2+*}, resulting in an enhanced oxidation current. The mechanism for production of the emitting excited state $Ru(bpy)_2^{2+*}$ is reminiscent of the one previously reported[44] as shown in Equation 3.1-3.5.

$$[Ru(bpy)_2]^{2+} \longrightarrow [Ru(bpy)_2]^{3+} + e \quad \textbf{[3.1]}$$

$$[Ru(bpy)_2]^{3+} + TPA \longrightarrow [Ru(bpy)_2]^{2+} + TPA^{+\bullet} \quad \textbf{[3.2]}$$

$$TPA^{\bullet +} \xrightarrow{-H^+} TPA^{\bullet} \quad \textbf{[3.3]}$$

$$[Ru(bpy)_2]^{3+} + TPA^{\bullet} \longrightarrow [Ru(bpy)_2]^{2+*} + \text{products} \quad \textbf{[3.4]}$$

$$[Ru(bpy)_2]^{2+*} \longrightarrow [Ru(bpy)_2]^{2+} + h\nu\ (610\ nm) \quad \textbf{[3.5]}$$

The enhanced current flow is accompanied by ECL and the maximum intensity is observed at 1.45 V. Pure PANI films do not generate any light under these conditions indicating that the ruthenium centres are responsible for the electrochemiluminescence. Throughout, the ECL analysis the films showed good stability, the ECL intensity does not significantly change, suggesting that the composite film is strongly bound to the electrode.

For comparison, the ECL of solution 1mM $[Ru(bpy)_2PIC]^{2+}$ alone was measured, under the same experimental condition as the PANI- Ru composite film to evaluate how its behaviour compares to when its entrapped in a polymer. Figure 3.12 shows the voltammetric (solid line) and the ECL (dashed line) responses. Significantly, the ECL analysis of Ru without PANI revealed that the ECL onset and maximum intensity potential observed is

indistinguishable to that of the composite film under the same reaction conditions as presented in Figure 3.13 below.

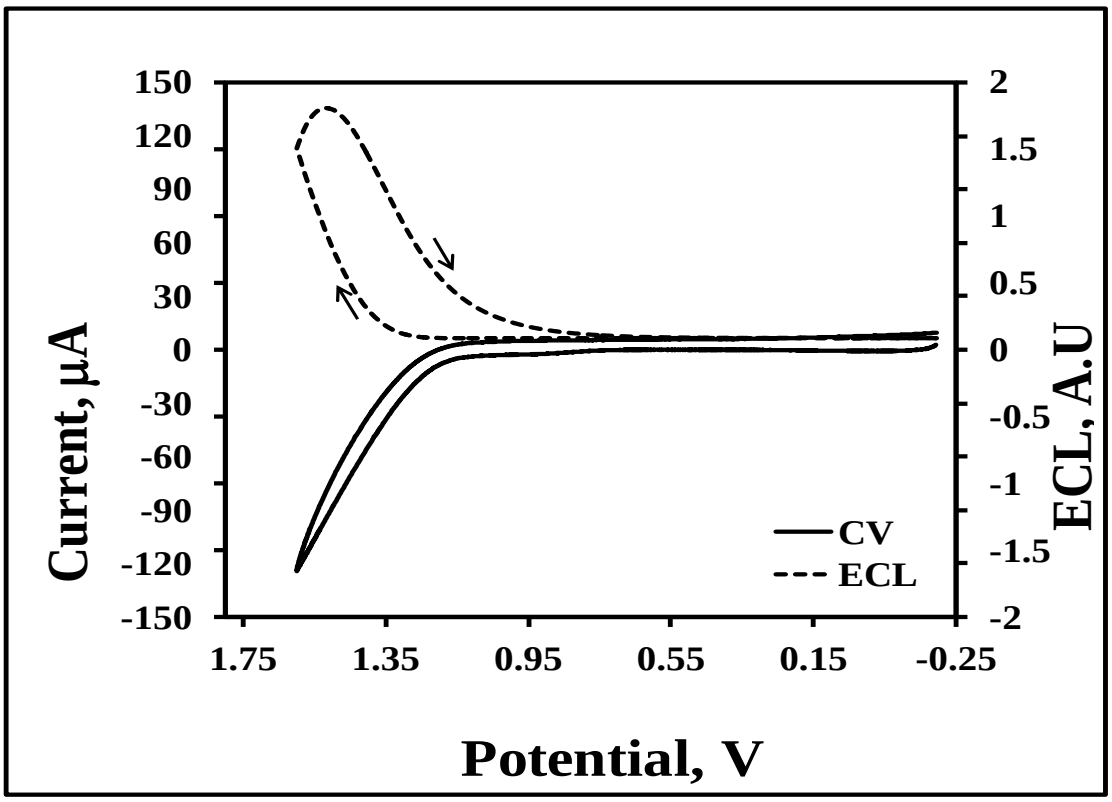

Figure 3.12: Cyclic voltammogram (solid line) and ECL response(dashed line) of solution 1mM $[Ru(bpy)_2PIC]^{2+}$ where the contacting solution contains 50 mM TPA and 0.1 M phosphate buffer and the scan rate is 0.1 V s^{-1}. The working electrode is ITO with an electrode area of 1.25 cm^2.

ECL of the PANI-Ru composite was also investigated by employing chronoamperometry using TPA as co-reactant. The potential of the electrode was stepped between -0.5 to 1.6 V for a period of 50 s. The potential is stepped from a negative potential to a sufficiently positive potential in order to generate the Ru^{3+} states as according to Equation 4.1. Figure 3.12 shows the ECL and current response of the PANI-Ru composite film on ITO electrode in contact 50 mM TPA as a co-reactant and 0.1 M phosphate buffer.

The ECL response in Figure 3.13 (a) increases when the potential is stepped towards the oxidative potential, hence, generating the Ru^{3+} which is subsequently converted to the excited Ru^{2+*}, and the signal decreases when this excited state relaxes back to the ground state. However as time passes, the ECL light emission signal steadily decays, this behaviour can be attributed to the presence of a relatively high concentration of TPA co-reactant compared to the concentration of Ru^{3+} states available. Since the TPA concentration in is solution is high, the catalytic Ru^{3+} are consumed faster than they can be regenerated by homogeneous charge transport through the composite film layer.

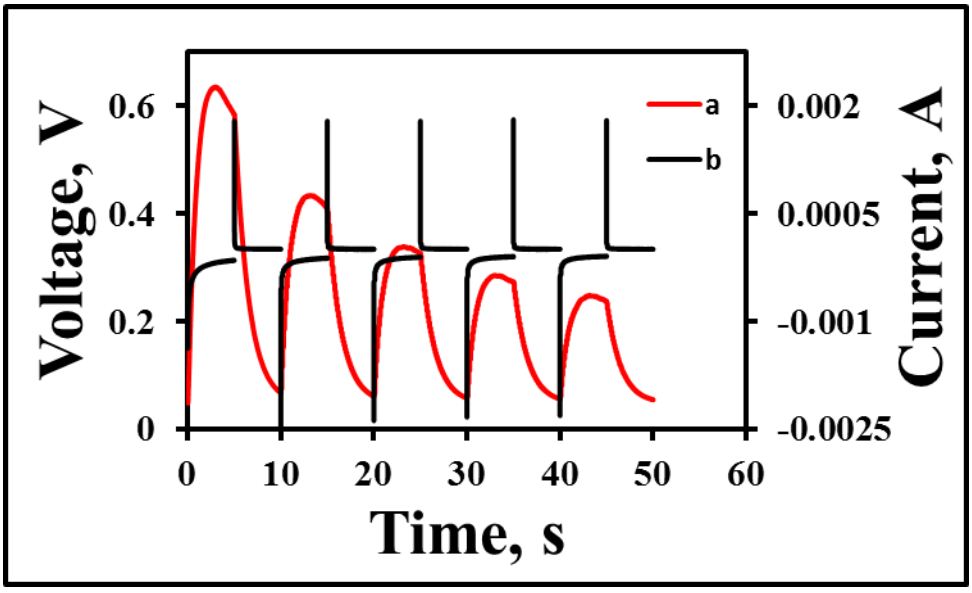

Figure 3.13: Shows the potential waveform of (a) ECL and (b) current response for PANI-Ru composite on the ITO electrode.The potential was stepped between -0.5 to 1.6 V for a period of 50 s, in 10 seconds intervals, The supporting electrolyte is PBS that contains 50 mM TPA.

There are two main processes that ultimately influence the ECL intensity observed for PANI-Ru films. Firstly, the rate of homogeneous charge transport

through the film, since this controls the rate at which the ECL luminophores are electrochemically regenerated. Secondly, the efficiency of the emitting photons once the excited state Ru^{2+*} is generated. In the PANI-Ru material, the PANI can mediate electron transfer to the ruthenium metal centres augmenting their intrinsic, distance dependent, and electron self-exchange rate. In seeking to understand these processes that contribute to the dynamics of the PANI-Ru composite, it is important to consider the role of mass transport of reactants moving to the interface of the electrode surface. The characteristic time, t, for the diffusion process, can be determined as per Equation 3.6.[45]

$$t = \frac{\delta^2}{\pi . D_{CT}} \qquad \textbf{[3.6]}$$

Where is δ is the film thickness, *D* is the homogeneous charge transport diffusion coefficient and π is 3.14. This equation gives the time for complete regeneration of the ruthenium centres to be 1.1 s. One potential difficulty with using conducting polymer backbones is that electron transfer to / from the polymer to the electronically excited ruthenium centres may be thermodynamically feasible leading to quenching and loss of the ECL. The Gibbs free energy, ΔG, for electron transfer can be calculated once the excited state oxidation potential is known which can be estimated from the Rehm- Weller Equation 3.7. [46, 47]

$$E(A^+/A^*) = E(A^+/A) - E^{0\text{-}0} \qquad \textbf{[3.7]}$$

where $E^{0\text{-}0}$ is the energy difference between the lowest vibration levels of the ground and electronically excited states. This quantity has been determined as 2.03 eV from the wavelength of maximum emission intensity recorded at 77 K, 610 nm. Therefore, the excited state oxidation potential (donor) for $Ru^{2+*/3+}$ is approximately -0.93 V. The first reduction potential for PANI (acceptor) is approximately -0.80 V[48] giving a ΔG of -0.13 eV, indicating that oxidative quenching of the electronically excited state is weakly exergonic. However, despite the PANI being thermodynamically capable of oxidizing the ruthenium excited state, Figure 3.11 shows that ECL is generated from PAN-Ru in the presence of TPA, i.e., not all the Ru^{2+*} species are oxidatively quenched. Therefore, it is important to establish the overall ECL efficiency.

3.3.5. ELECTROCHEMILUMINESCENCE EFFICIENCY

The ECL efficiency, ϕ_{ECL}, is defined as the number of photons emitted per Faradaic electron passed during the chemiluminescent reaction. It is the product of the efficiency of populating the excited state and the quantum yield of emission from that excited state. Equation 3.7 was used to determine ϕ_{ECL} of the composite film using tris 2, 2' bipyridylruthenium ($[Ru(bpy)_3]^{2+}$) in solution as a relative standard as shown in Figure 3.15.

$$\phi_{ECL} = \phi^{\circ}_{ECL} \frac{I}{Q} \frac{Q^{\circ}}{I^{\circ}} \qquad \textbf{[3.8]}$$

where ϕ_{ECL} is the ECL efficiency of $[Ru(bpy)_3]^{2+}$, taken as 5.0%, [49,50] *I* and *I*° are the integrated photomultiplier tube responses for the PANI-Ru film and $[Ru(bpy)_3]^{2+}$ respectively, and *Q* and *Q*° are the corresponding faradaic charge passed. It is important to note that the experimental parameters for the ECL analysis of both PANI-Ru composite and the $[Ru(bpy)_3]^{2+}$ standard (Figure 3.14) has to be kept constant, *i.e.* the type of electrodes, solvent, electrolyte, co-reactant, scan rate should be kept the same.

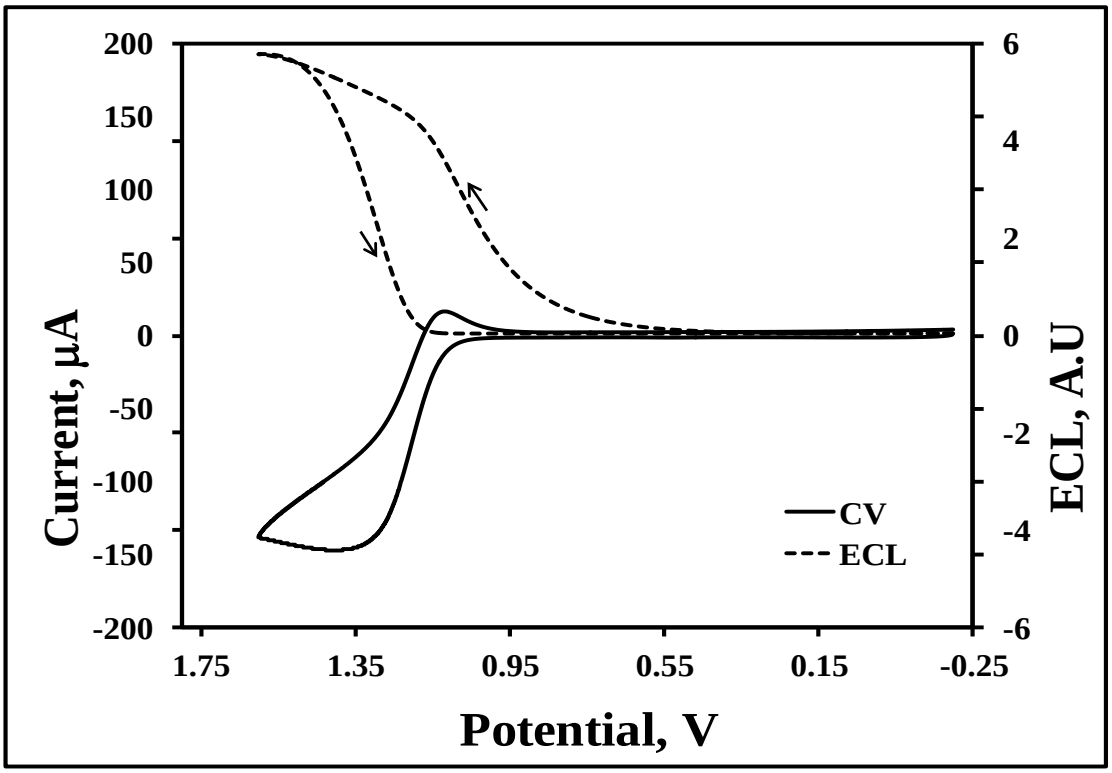

Figure 3.14: Cyclic voltammogram (solid line) and ECL response (dashed line) of a 1 µM $[Ru(bpy)_3]^{2+}$, where the contacting solution contains 50 mM TPA and 0.1 M phosphate buffer and the scan rate is 0.1 V s^{-1}. The working electrode is ITO with an electrode area of 1.25 cm^2.

Figure 3.14 shows the voltammetric (solid line) and the ECL (dashed line) responses of a $[Ru(bpy)_3]^{2+}$ standard in PBS, in the presence of 50 mM TPA, scanning from -0.3 to 1.6 V. The ECL onset potential is observed at 0.8 V corresponding to the oxidation potential of TPA, the maximum potential is observed at 1.4. Strikingly, the overall ECL efficiency for PANI-Ru obtained is 1.00 ± 0.1 % which is significantly higher than previously reported systems.[51] For example, the ECL efficiency of nafion-$[Ru(bpy)_3]^{2+}$ and $[Ru(bpy)_2(poly\text{-}4\text{-}vinylpyridine)_{10}]^{2+}$, of about 0.089 % and 0.152 %, respectively.[5] This is the highest efficiency obtained for an immobilized ruthenium metal complex. While the higher ECL intensity is due to rapid homogeneous charge transport, the increased efficiency arises because the PANI provides a more rigid matrix around the ruthenium complex[52] compared to those found in nafion and the $[Ru(bpy)_2(poly\text{-}4\text{-}vinylpyridine)_{10}]^{2+}$. In systems such as $[Ru(bpy)_2(PVP)_{10}]^{2+}$ films, the ruthenium centres are electrochemically isolated, while in the PANI-Ru composite the electrochemically active backbone of the conducting polymer provides a means of communication between adjacent ruthenium centers which then facilitates a faster production of the Ru^{3+}.

3.4. CONCLUSION

In summary, a novel rapid and effective method of confining a ruthenium ECL luminophore to the surface of an electrode has been developed by incorporating it within a film of the conducting polymer polyaniline during electropolymerization to form PANI-Ru. The studies showed that to load $[Ru(bpy)_2PIC]^{2+}$ in PANI backbone, potentiostatic polymerization is the

method which should be employed rather than potentiodynamic polymerization. AFM characterization of the composite film displayed well defined globular like structures, which are typical characteristic of PANI films. The homogenous charge transfer for the composite film was found to be 2.6 ± 0.9 x 10^{-10} cm^2 s^{-1}. Significantly, the rate of luminophore regeneration is approximately an order of magnitude more rapid than that observed for traditional non-conducting metallopolymers, the large D_{CT} facilitates more rapid regeneration of Ru^{3+}. The polymer provides a rigid microenvironment for $[Ru(bpy)_2PIC]^{2+}$, and this results in high ECL intensities in the presence of tripropylamine. Strikingly, the ECL efficiency of the PANI-Ru composite was determined to be 1%, which is the highest reported for a surface confined ruthenium complex. The increased luminophore regeneration rate and high ECL efficiency makes the PANI-Ru composite attractive for constructing ECL based sensing devices.

3.5. REFERENCES

[1] Dennany, L., Forster, R.J., *ECS Transactions*., **2007**, 3, 1-8.

[2] Bertoncello, P., Dennany, L., Forster, R.J., Unwin, P. R., *Anal.l Chem.*, **2007**, 79, 7549-7553.

[3] Bard, A. J., *Electrogenerated Chemiluminescence*, 1st ed. Bard, A. J., **2004,** Marcel Dekker, United States of America.

[4] Forster, R. J., Bertoncello P., Keyes T. E., *Annu. Rev. anal. Chem. 2.*, **2009**, 18.1-18.7

[5] O'Reilly, E. M., Keyes, T. E., Foster, R. J., Dennany, L., *Analyst.*, **2013**, 138, 677-682.

[6] Barbante, G. J., Hogan, C. ., Mechler, A., Hughes, A. B., *J. Mater. Chem.*, **2009**, 20, 891-899.

[7] Kharamov, A., Collinson, M., *Anal. Chem.*, **2000**, 72, 13, 2943-2948.

[8] Venkatanarayanan, A., Martin, A., Molapo, K. M., Iwuoha, E. I, Keyes, T. E., Forster, R. J., *Electrochem. Commun.*, **2013**, 31,116-119.

[9] Foster, R. J., Hogan, C.F., *Anal. Chem.*, **2000**, 72, 5576-5582.

[10] Yin, Y., Liu, C., Fan, C., *RSC; Adv.,* **2014**, 4, 26378-26382.

[11] Jang, J., Ha, J., Kim, K., *Thin Film Solids.*, **2008**, 3152-3156.

[12] Stamenov, P., Madathil, R., Coey, J. M., *Sens. Actuators.***, 2012**, 989-999.

[13] Pellegrin, Y., Keyes, T. E., Forster, R. J., *Inorg. Chim. Acta*., **2009**, 362, 1715-1722.

[14] Bruce, D., Richter, M. M., *Analyst.*, **2002**, 127, 1292-1494.

[15] Zhou, M., Robertson, G. P., Roovers, J., *Inorg. Chem.*, **2005**, 44, 8317-8325.

[16] Cooke, M.M., Doeven, E.H., Hogan ,C.F., Adocock, J.L., McDermott, G.P., Conlanc, X.A., Barnett, N.W., Pfeffer, F.M., Francis, P.S., *Anal. Chim. Acta.*, **2009**, 635, 94-101.

[17] Li, M., Chen,Z., Zhu, N., Yam, V.W., Zu, Y., *Inorg. Chem.*, **2007**, 47,1218-1223.

[18] Efimov, I., Winkels, S., Schultze, J.W., *J. Electroanal. Chem.*, **2001**, 499, 169-175.

[19] Ruiz, V., Colina, A., Heras, A., Lopez- Palacios, L., Seeber, R., *Electrochem. Commun.*, **2002**, 4, 451-456.

[20] Casalbore -Miceli, G., Camaioni, N., Geri, A., Cristani, M., Fichera, A.M., Berlin, A., *Synthetic Met.*, **2000**, 108-, 47-56.

[21] Ruiza, V., Colina, A., Heras, A., Lopez-Palacios, J., *Electrochim. Acta.*, **2004**, 50, 59-67.

[22] Xavier, M. G., Venancio, E. C., Pereira, E. C., Leite, F. L., Leite, E. R., MacDiarmid, A. G., Mattoso, L. H. C., *J. Nanosci. Nanotechnol.*, **2008**, 8, 1-4.

[23] Sarac, A.S., Ates, M., Kilic, B., *Inter. J. Electrochem.*, **2008**, 3, 777-786.

[24] Song, E., Choi, J.W., *Nanomater.*, **2013**, 3, 498-523.

[25] Dennany, L., Wallace, G. G., Forster, R. J., *Electrochim. Acta.*, **2008**, 53, 4500-4605.

[26] Molina, J., del Rio, A.L., Bonastre, J., Cases, F., *Euro. Pol. J.*, **2009**, 45, 1302-1315.

[27] Dennany, L., Innis, P. C., McGovern, S. T., Wallace, G. G., Forster, R. J., *Phys. Chem. Chem. Phys.*, **2011**, 13 , 3303-3310.

[28] Mathebe, N. G. R., Morrin, A., Iwuoha, E. I., *Talanta.*, **2004,** 64 ,115- 120.

[29] Ferreira, M., Wohnrath, K., Torresi, R.M., Constantino, C.J.L., Aroca, R.F., Oliveira, O, N., Giacometti, J.A., *Langmuir.*, **2002**, 18,540-546.

[30] Paul, E. W., Ricco, A. J., Wrighton, M. S., *J. Phys. Chem.*, **1985**, 89, 1443-1450.

[31] Cui, M., Siang, W. Wang, X., Darmawan, P., Lee, P.S., *Adv. Func. Mater.*, **2015**, 25, 401-408.

[32] Venancio, E. C., Costa, C. A. R., Machado, S. A. S., Motheo, A. J, *Electrochem. Commun.*, **2001**, 3, 229-301

[33] Keyes, T. E., Jayaweera, P. J., McGarvey, J. J., Vos, J. G., *J. Chem. Soc., Dalton Trans.,* **1997**, 7, 1627-1632.

[34] Webb, M.A., Knorr, F. J., McHale, J.L., *J. Raman Spectrosc.*, **2001**, 32, 481-485.

[35] Poizat, O., Sourisseau, C., *J. Phys. Chem.*, **1984**, 88, 3007-3014

[36] Rohom, A. B., Londhe, P.U., Mahapatra, S.K., Kulkarni, K., Chaure, N.B., *High Perform. Polym.*, **2014**, 26, 641-646.

[37] Trchovà, M., Maràvkovà, Z., Blàha, M., Stejskal, J., *Electrochim. Acta.*, **2014**, 122, 28-38.

[38] Bernard, M.C., Goff, H., *Electrochim. Acta.*, **2006**, 52, 595-603.

[39] Da Silva, J.E.P., De Torressi, S.I.C., De Faria, D.L.A., Temperini, M. L. A., *Synthetic Metals*, **1999**, 101, 834- 835

[40] Shakoor, A., Rizvi, T. S., *J. Raman Spectrosc.*, **2010,** 41, 237-240.

[41] Rohom, A.B., Londhe, P.U., Mahapatra, S.K., Kulkarni, S.K., Chaure, N.B., *High Perform. Polymers*, **2014**, 26, 641-646.

[42] Shreepathi, S., Holze, R., *Langmuir.*, **2002**, 22, 5196 -5204.

[43] Molapo, K. M., Venkatanarayanan, A., Dolan, C. M., Baker., P.G.L., Iwuoha, E. I., Keyes, T. E., Forster, R. J., *Electrochem. Commun.*, **2013**, 31, 116-118.

[44] Wang, H., Xu, G., Dong, S., *Electroanal.*, **2002**, 14, 853-858.

[45] Hogan, C.F., Forster,R. J., *Anal. Chim. Acta.*, **1999**, 396, 13-21.

[**46**] Rehm, D., Weller, A., *Isr. J. Chem.*, **1970**, 89, 259-262.

[47] Forster, R. J., Keyes, T. E., *J. Phys. Chem. B.*, **1998**,102, 10004-10012.

[48] Mallick, K., Witcomb, M., Scurrell, M., *Plat. Metal. Rev.*, **2007**, 51, 3-5.

[49] Wallace, W. L., Bard, A. J., *J. Phys. Chem.,* **1979**, 8, 1350-1355.

[50] Pyati, R., Richter, M. M., *Annu. Rep. Prog. Chem. Sect. C.,* **2007**, 103,12-78.

[51] Dennany, L., Hogan, C. F., Forster, R. J., *Anal. Chem.*, **2006**, 78, 1412-1417.

[52] Culvert, J. M., Meyer, T. Y., *Inorg. Chem.*, **1982**, 21, 3978-3982.

CHAPTER FOUR:

DNA BINDING INDUCED ECL GENERATION AT MONOLAYERS OF A MOLECULAR LIGHT SWITCH

4.1. INTRODUCTION

Polypyridyl complexes of Ru(II) and Os(II) have been widely studied in the context of DNA binding.[1,6] Where such complexes have been shown, depending on the structure of the polypyridyl ligands, to bind through intercalative and electrostatic interactions with the DNA duplex[6]. The intensive interest in Ru/Os DNA interactions, has focussed principally on the changes that DNA binding can induce in the metal complexes photophysics, where enhancement of emission intensity and lifetime of the probe and photoinduced damage to DNA have potential value from the perspectives of diagnostic probes,[7] in therapeutics in synthetic restriction enzymes, and new pharmaceuticals.[8] Ruthenium complexes containing ligands such as dipyrido [3, 2-a: 2-c] phenazine (dppz), [1, 4, 5, 8,9,12 –hexaazatriphenylene (HAT) [9] and 1,4,5,8-tetraazaphenanthrene[10,11] (TAP) ligands have in particular been extensively investigated for their DNA recognition and binding which is attributed to the extended aromatic structures which allow for extensive intercalative stacking in DNA. Among these ligands dppz has probably received most attention because of their molecular “light switch “capacity. That is, Ru(II) complexes containing this ligand show no photoluminescence in aqueous media, but intense photoluminescence in non-aqueous media or when they intercalate into the double helical structure of DNA.[12,13,14]. Figure 4.1 illustrates an example of this intercalation binding process of $[Ru(phen)_2(dppz)]^{2+}$ into DNA. The light switch effect for Ru (II) dppz complexes on DNA binding is attributed to the protection of the phenazine

nitrogen atoms from water when dppz is intercalated between the base pairs.[15] Phenazine ligands tend to show high affinity for DNA, For example, studies performed with $[Ru(phen)_2dppz]^{2+}$ demonstrated high affinity, with a binding constant to DNA of $K_{eff} \approx 10^8$.[16,17]

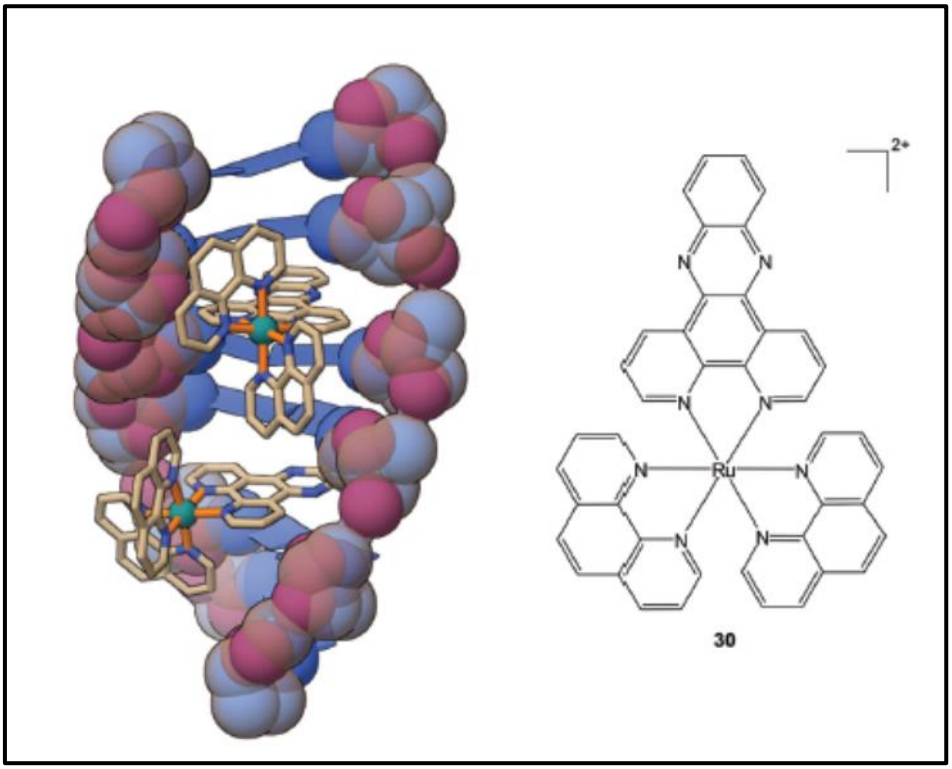

Figure 4.1: X-ray crystal structure of the complex rac $[Ru\ (phen)_2\ (dppz)]^{2+}$ intercalated with the DNA sequence $d(ATGCAT)_2$. Reprinted from Hall, J.P., Cook, D., Morte, S.R., McIntyre, P., Buchner, K., Beer, H., Cardin, D.J., Brazier, J.A., Winter, G., Kelly, J.M., Cardin, C.J., 2013, *J Amer. Chem Soc.,*135, 12652- 12659.

Common techniques that have been employed to establish and quantify binding of metal complexes to DNA, include UV-vis,[18] fluorescence spectroscopy,[19] electrochemistry and electrochemiluminescence. Although the least common of the methods applied, electrochemiluminescence offers

advantages such as rapid, sensitive, low background and low cost detection. Bard and colleagues pioneered the electrochemical and electrochemiluminescence method for studying the DNA interactions with metal complexes including ruthenium and osmium complexes.[20,21] Sensitive, selective detection of DNA binding is important to many clinical tests, including pathogen detection and other methods utilizing polymerase chain reaction, including genetic disease screening based on oligonucleotide hybridization and to molecular genotoxicity studies.[22]

However, most reports to date of electrochemiluminescence originating from metal complexes bound to DNA have been from solution based studies. There are a number of key advantages to immobilizing the ECL probe as outlined in Chapter 1.However it should be noted that the ECL properties of a ruthenium metal complex containing a dppz ligand have been recently reported for the first time by Xu and co–workers,[23] wherein the ECL switch by DNA was applied to investigate the interaction of $[Ru(bpy)_2dppz]^{2+}$ with DNA in solution. Using oxalate as co-reactant in aqueous media the ECL output of the complex was found to be negligible due to the well-known aqueous quenching effect observed in DPPZ containing complexes. However in the presence of DNA, ECL increased significantly.

The present study is the first report involving an immobilized ECL reagent containing an intercalating light switch complex. Rusling and co-workers have reported on interfacial binding of DNA to an immobilized ECL probe.[24] Their study examined ECL from thin films of $[Ru(bpy)_2(PVP)_{10}](ClO_4)$ and

oligonucleotides on electrodes which can generate direct ECL signals that are sensitive to hybridisation and the chemical damage of DNA. The present chapter focuses on an investigation into the interactions between surface immobilized molecular light switch; $[Ru(dppz)(bpyArCOOH)_2]^{2+}$ and contacting solutions of DNA. We demonstrate that $[Ru(dppz)(bpyArCOOH)_2]^{2+}$ forms stable monolayers on ITO and in the presence of Salmon Testes DNA, both emission and ECL from the monolayer were observed to increase very significantly compared with the film in the absence of DNA. DNA binding was found to specific, and attributed to intercalation analogous to solution phase binding, as binding to a BSA control produced less than 10% of the ECL intensity than DNA. This preliminary study indicates such immobilised light switch molecules may be useful sensors for DNA hybridization detection.

4.2. EXPERIMENTAL

4.2.1. MATERIALS AND REAGENTS

The *bis*-(4-(4-carboxyphenyl)-2,2'-bipyridine) dipyridophenazineruthenium(II) dichloride $[Ru(dppz)(bpyArCOOH)_2]^{2+}$ was synthesized by Mr Christopher Burke following a synthetic method that is yet to be published (The synthesis method and the NMR is presented in Appendix 4). Salmon testes (stDNA), Polydeoxyguanylic acid polydeoxycytidylic (Poly (dG).Poly (dG)) and Polydeoxyadenylic acid Polydeoxythimidylic acid sodium salt Poly(dA). Poly (dT) DNA were all purchased from Sigma Aldrich. All stock solutions of the DNA's were prepared in the Dulbecco's phosphate buffer. The concentrations of the Salmon testes DNA and the polynucleotides were determined

spectroscopically by measuring the absorbance at 260 nm, the absorption coefficient, ε of Salmon testes DNA[25] at 260 nm was taken as 6600 $M^{-1}cm^{-1}$. For the determination of the polynucleotide concentrations, ε at 262 nm was taken as 6600 $M^{-1}cm^{-1}$ for (Poly(dA-T)) and for (Poly(dG-C))[26] ε at 254 nm was taken as 8400 $M^{-1}cm^{-1}$. All other reagents used in this study were purchased from Sigma and used as provided unless stated otherwise.

4.2.2. PREPARATION OF $[Ru(dppz)(bpyArCOOH)_2]^{2+}$- DNA MONOLAYER

The ITO electrodes (1.25 cm^2) were cleaned by sonicating in in deionised water and acetone successively for 5 minutes and the electrodes were dried under a stream of nitrogen. The $[Ru(dppz)(bpyArCOOH)_2]^{2+}$-monolayer was assembled on ITO electrode by immersing the ITO electrode in a 1 mM solutions of $[Ru(dppz)(bpyArCOOH)_2]^{2+}$ dissolved in ethanol / water (1:1 volume) for 48 h. The carboxyl terminus of the dye spontaneously adsorbs onto the ITO electrode. Following dye assembly, the electrodes were rinsed with deionised water to remove any unbound material. To achieve saturation coverage of DNA the modified electrode was incubated in 100 µM Salmon Testes DNA solution for 3 h. To ensure that saturation binding of DNA had been achieved the ECL of $[Ru(dppz)(bpyArCOOH)_2]^{2+}$ -DNA electrodes were monitored at 1 h intervals , until no further change was observed in the ECL signal intensity. For the electrochemiluminescence concentration dependent studies, Salmon Testes DNA solutions of concentrations from 5 to 100 µM were prepared, and ITO electrodes modified with $[Ru(dppz)(bpyArCOOH)_2]^{2+}$

were incubated in these solutions for 3 h. Following this incubation the electrodes were washed with deionized water and used for the ECL measurements.

4.2.3. PHOTOPHYSICS

The optical absorbance and fluorescence measurements of $[Ru(dppz)(bpyArCOOH)_2]^{2+}$ were investigated in DPBS acetonitrile and water, as described in experimental, Chapter 2.

4.2.4. INTERFACIAL RAMAN AND FLUORESCENCE SPECTROSCOPY

Raman spectroscopy was used to confirm surface binding of $[Ru(dppz)(bpyArCOOH)_2]^{2+}$, and to evaluate DNA intercalation at the monolayer on ITO electrode. Raman spectra were collected on a Horiba Jobin-Yvon Labram HR 2000 confocal Raman microscope set at a power of 2 mW. A 100 x microscope objective was used to focus the laser (488nm) onto samples. The x-axis was calibrated versus the Rayleigh line at 0 nm and the photon mode from a silicon wafer at 520 cm^{-1}. Typical acquisitions were 5 seconds in length and accumulated four times. The spectral data was acquired and analysed using LabSpec software. The luminescence spectra of $[Ru(dppz)(bpyArCOOH)_2]^{2+}$ monolayer before and after intercalation into DNA were also collected with Horiba Jobin-Yvon Labram HR 2000 confocal Raman microscope set at a power of 0.015 mW. The luminescence spectra were

measured using a 473nm laser to excite the samples, with acquisitions collected for 5 s.

4.2.5. ELECTROCHEMILUMINESCENCE

Electrochemiluminescence and electrochemistry experiments were performed as described in the experimental Chapter 2.

4.3. RESULTS AND DISCUSION

4.3.1. UV AND FLUORESCENCE SPECTROSCOPY

The absorbance and emission spectra of $[Ru(dppz)(bpyArCOOH)_2]^{2+}$ are compared in water and acetonitrile in Figure 4.2.

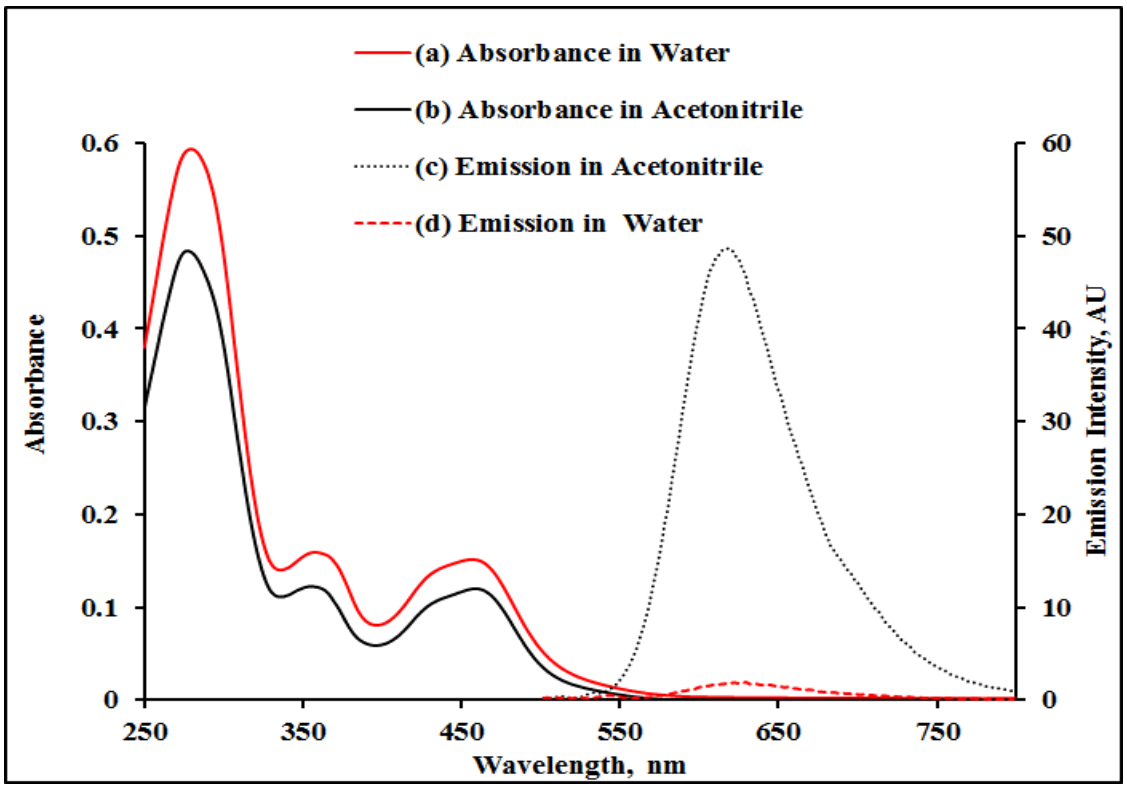

Figure 4.2: UV-Vis absorbance and emission spectra of 10 μM $[Ru(dppz)(bpyArCOOH)_2]^{2+}$ in water and acetonitrile. The emission spectra were collected with a slit width of 2.5 nm, excitation wavelength was 470 nm.

The UV-vis absorption spectra shows three bands at 285, 365 and 466 nm. The visible absorbance is attributed to a metal to ligand charge transfer (MLCT), *i.e.* Ru^{II} (dπ) to dppz (π*) transitions, centred at approximately 466 nm which occurs at a characteristic wavelength similar to other ruthenium complexes (II).[27]

The absorption band at 360 nm is assigned to π-π-*intra ligand transitions, localized on the dppz ligand.[28] There are no significant differences in the absorption spectra of $[Ru(dppz)(bpyArCOOH)_2]^{2+}$ in water or acetonitrile. In contrast, the emission behaviour, is strongly influenced by the solvent. $[Ru(dppz)(bpyArCOOH)_2]^{2+}$ displays very weak luminescence in water, whereas an intense emission centered at approximately 610 nm is observed in acetonitrile. This behaviour is similar to those of other similar complexes of Ru(II) containing the DPPZ ligand and the water response is similarly attributed to the light switch effect related to H-bonding interactions in water with the phenazine nitrogens which are believed to quench the emission of the complex.[4]

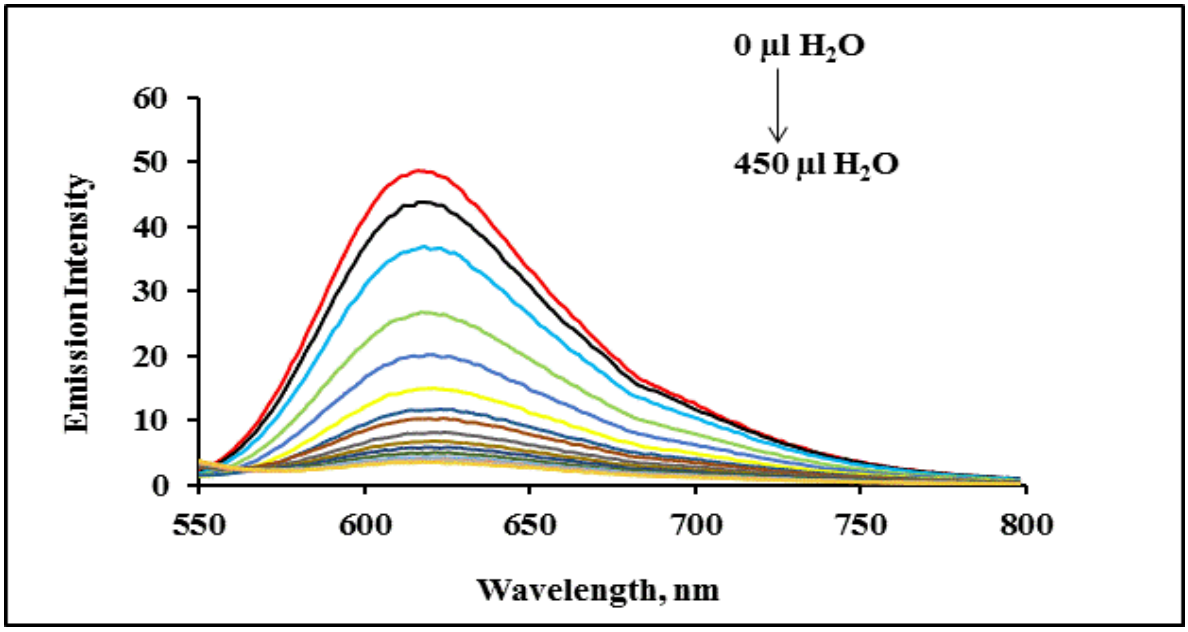

Figure 4.3: The emission spectra of 10 uM $[Ru(dppz)(bpyArCOOH)_2]^{2+}$ free dye in aerated acetonitrile solution, 450 µl of water was titrated in 30 µl aliquots to the 3ml $[Ru(dppz)(bpyArCOOH)_2]^{2+}$ acetonitrile solution.

Figure 4.3 shows the effect of addition of water on the emission of $[Ru(dppz)(bpyArCOOH)_2]^{2+}$ in solution acetonitrile and clearly demonstrates that the emission is quenched by the presence of water. Specifically, the light switch effect has been attributed to the variation in population of two closely lying dppz localized metal to ligand charge transfer excited states. Effectively population of the non-emissive state is favoured in H bonding solvents as the formation of the hydrogen bonds between the water and the nitrogens on the phenazine portion of the dppz ring stabilize the dark state.[29,30] As seen in Figure 4.3 complete extinction of the emission occurs at approximately 15 % v/v water. This is important confirmation that the light switch effect occurs in this complex as we wish to exploit it to report on DNA binding by ECL.

4.3.2. ELECTROCHEMICAL CHARACTERIZATION OF $[Ru(dppz)(bpyArCOOH)_2]^{2+}$

4.3.2.1 Electrochemical behaviour of $[Ru(dppz)(bpyArCOOH)_2]^{2+}$ in solution

Interestingly, in spite of their interesting solvent dependent photophysics the solvent dependent electrochemical behaviour of dppz containing Ru (II) complexes have not yet been reported. Given that we wish to exploit the ECL response in aqueous media, and exploit the light switch effect, it was important to investigate the cyclic voltammetry in both aqueous and non-aqueous media. For $[Ru(dppz)(bpyArCOOH)_2]^{2+}$ .Figure 4.4 shows the scan

rate dependent voltammetry of the complex in acetonitrile containing $LiClO_4$ as a supporting electrolyte at an ITO working electrode.

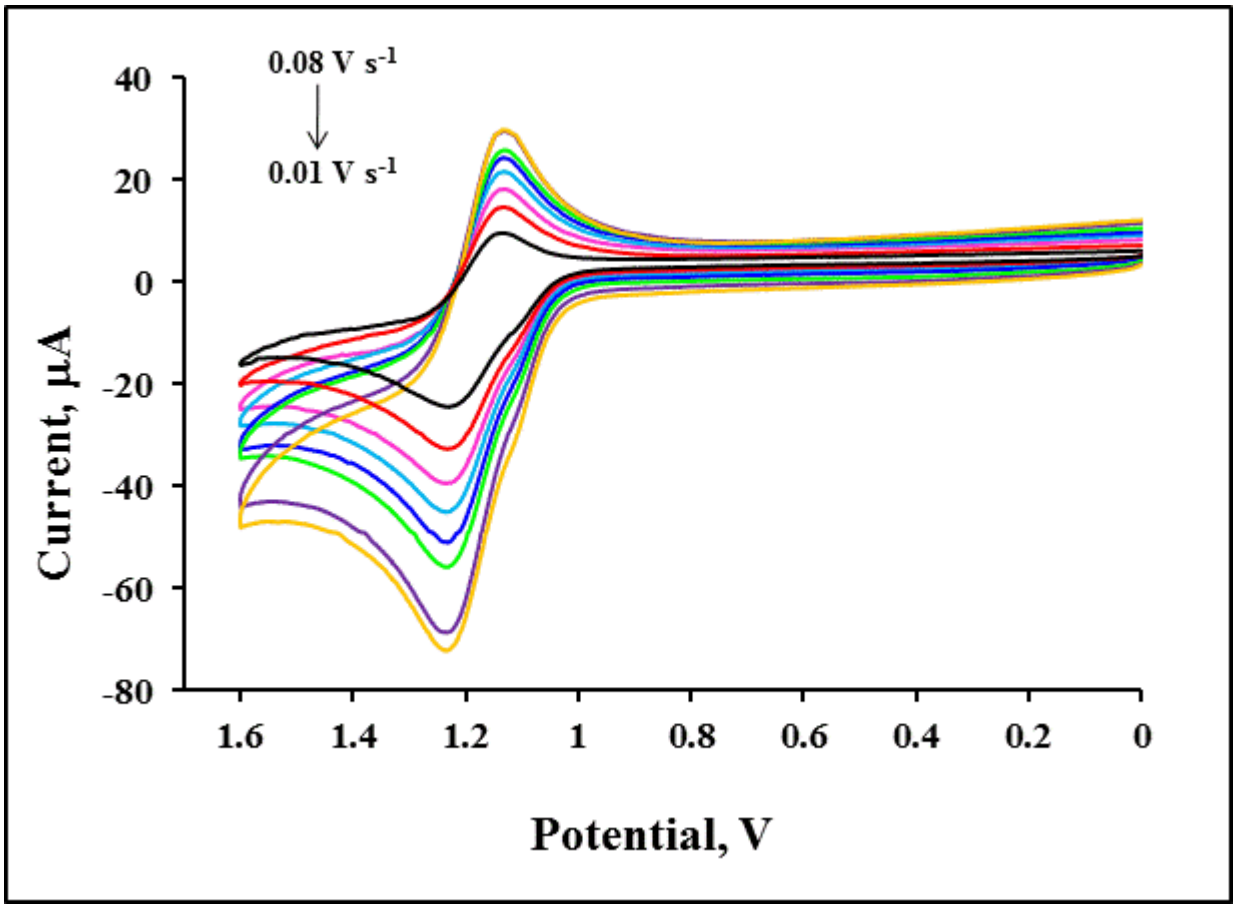

Figure 4.4: Scan rate dependence of voltammetric responses of 1 mM $[Ru(dppz)(bpyArCOOH)_2]^{2+}$ in acetonitrile solution and 0.1 M $LiClO_4$ as a supporting electrolyte. The working electrode is ITO (1.25 cm^2) electrode, the reference electrode is Ag /AgCl (1 M NaCl). The CVs are plotted incrementally for scan rates of 0.01 V s^{-1} (innermost CV) to 0.08 V s^{-1} (outermost CV) at 0.01 V s^{-1} intervals.

Notably in acetonitrile the voltammetric redox response of $[Ru(dppz)(bpyArCOOH)_2]^{2+}$ is well behaved, the dye exhibits a redox couple with a formal potential $E°$ of 1.18 V attributed to the metal based $Ru^{2/3+}$ oxidation reaction as observed from Figure 4.4. The voltammograms exhibit

features of a quasi-reversible response. For example at all scan rates the ratio of the anodic current to the cathodic peak current was found to be unity, the peak to peak separation is 98± 1.5 mV and classical diffusional tails are observed. The *ΔEp* observed here is larger than the 57 mV expected for a reversible one electron transfer under semi-infinite linear diffusion control. However, it is important to note that *ΔEp* does not increase with increasing scan rates suggesting that slow heterogeneous electron transfer or ohmic drop are not responsible for the larger than expected peak splitting observed.[31,32]

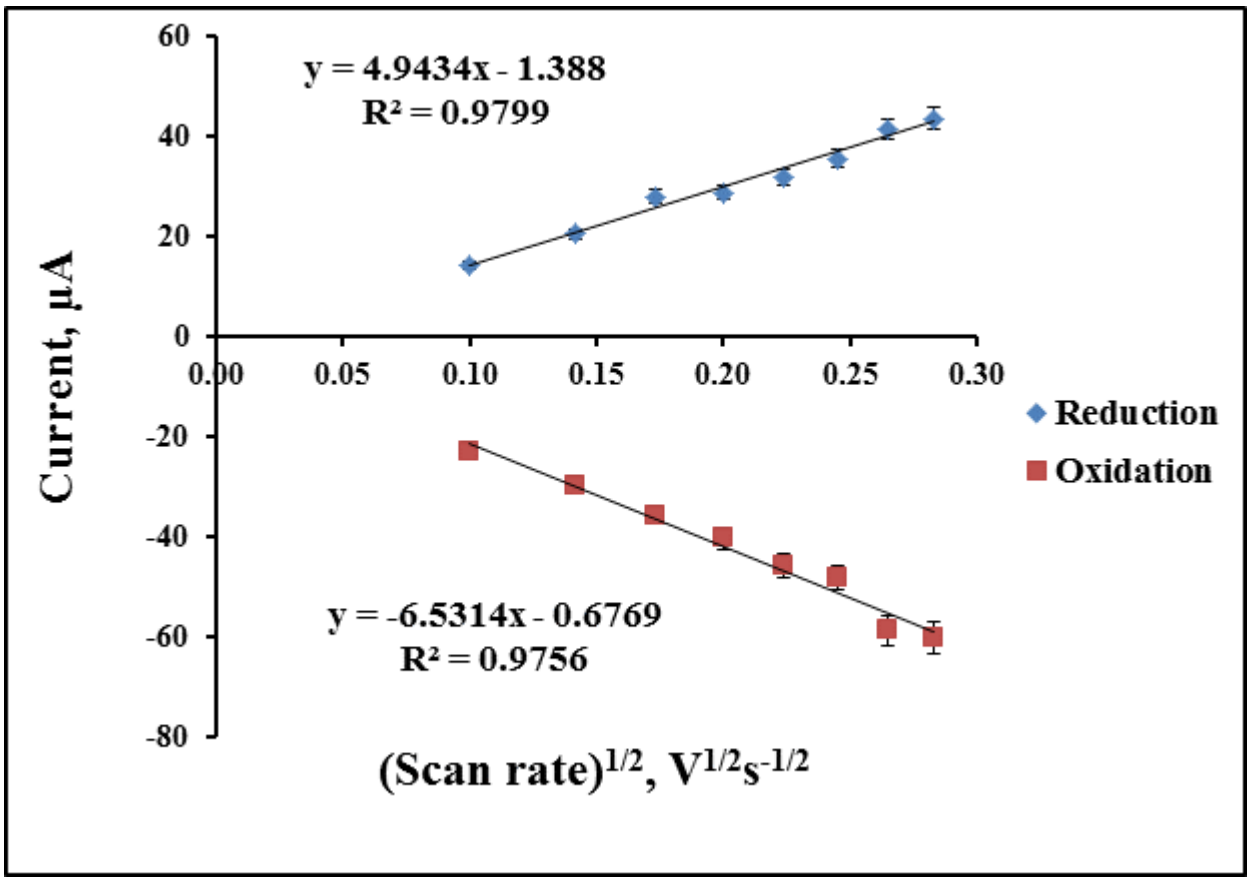

Figure 4.5: Scan rate dependence of solution 1 mM $[Ru(dppz)(bpyArCOOH)_2]^{2+}$ in acetonitrile and LiClO4 as a supporting

electrolyte. The working electrode is ITO (1.25 cm^2) and the reference electrode is Ag /Ag Cl .The scan rates are 0.01 to 0.08 V s^{-1}.

Figure 4.5 shows the peak current varies linearly with the square root of the scan rates, this behaviour is consistent with semi-infinite linear diffusion. From plot of peak current vs root of scan rate the effective homogeneous charge transport diffusion coefficient D_{CT} can be estimated from the Randles- Sevcik equation: [1.23].

$$i_P = (2.69x10^5)n^{3/2}AD_{CT}{}^{1/2}Cv^{1/2} \qquad [\mathbf{1.23}]$$

Where *n* is the number of electrons, *A* is the electrode area is (1.25 cm^2) and *C* is the concentration of $[Ru(dppz)(bpyArCOOH)_2]^{2+}$ in solution. The diffusion coefficient obtained is 3.77 ± 0.4 x 10^{-6} cm^2 s^{-1} and this fast D_{CT} is in agreement with other related Ru complexes in solution, for example Song *et al.* [33] reported a D_{CT} of 1.60 x 10^{-6} cm^2 s^{-1} for a carboxylate bipryridine Ru (II) complex in solution. The results in the current study suggests that the charge transport is slower than expected.

It should be noted also from the voltammetry of $[Ru(dppz)(bpyArCOOH)_2]^{2+}$ in MeCN that a small shoulder is evident at 1.1 V. The origin of the shoulder is unclear was deemed likely to be due to the adsorption of the complex through the carboxyl groups of the dye attaching to the ITO electrode. To investigate whether adsorption is an issue which dictates the voltammetric response of the complex in solution and possibly the subsequent ECL experiments, the electrode was checked for film formation by repeated cycling of $[Ru(dppz)(bpyArCOOH)_2]^{2+}$ in MeCN and $LiClO_4$. After repeated cycling in the

1mM $[Ru(dppz)(bpyArCOOH)_2]^{2+}$ solution the electrode was transferred into blank electrolyte, the electrode was checked and its resulting CV is presented in Figure 4.6. From the CV two oxidation peaks are observed at 1.1V and 0.5 V, suggesting that an electroactive film forms on the electrode. The peak at 1.1 V corresponds to the potential at which the shoulder was observed in the scan rate voltammetric response, confirming that it was due to adsorption of the complex.

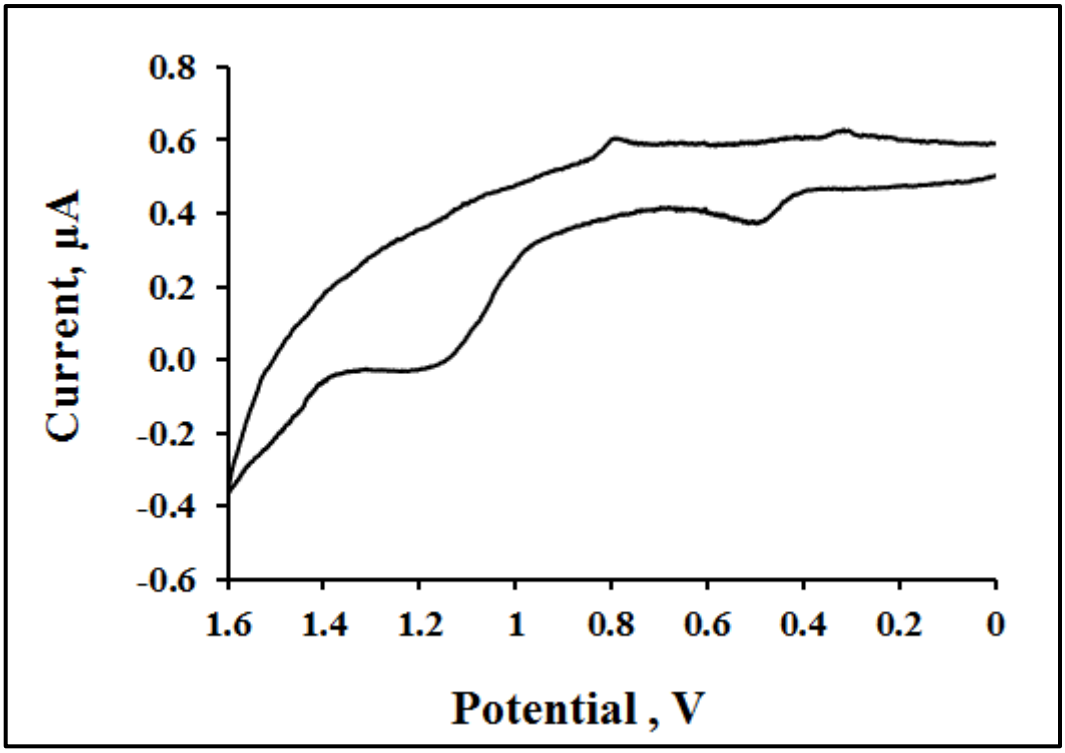

Figure 4.6: CV of the film formed on the electrode ITO (1.25 cm^2) electrode after the repeated cycling in 1 µM $Ru(dppz)(bpyArCOOH)_2]^{2+}$. The acetonitrile solution with 0.1 M $LiClO_4$ is a supporting electrolyte, The reference electrode is Ag/ AgCl and the scan rate 0.1 V s^{-1}.

The electrochemistry of the $[Ru(dppz)(bpyArCOOH)_2]^{2+}$ was then investigated in solution in DPBS, and the results are presented in Figure 4.7. Notably, the

voltammetric behaviour of the dye is significantly different to behaviour in acetonitrile across the same potential range. In DPBS the complex exhibits an irreversible oxidation peak at 1.21 V at the slowest measured scan rate 0.01 Vs^{-1}. Xu and co –workers[23] reported a single oxidative peak in this potential range for related compound $[Ru(bpy)_2dppz]^{2+}$ in PBS. This peak is attributed to the metal centre, and the anodic shift in its potential is not unexpected since H-bonding of water to the phenazine ligands will reduce the electron density at this site and therefore their donor capacity to the metal complex. Interestingly, for $[Ru(dppz)(bpyArCOOH)_2]^{2+}$ in DPBS, a new oxidation peak appears at 0.82 V such a feature which was not observed in acetonitrile. The origin of this process in aqueous media is not immediately clear, but its irreversibility may suggest it is a $Ru^{2/3+}$couple. The presence of two carboxyl groups may complicate the electrochemistry and it is possible that at this pH (7.2) there is a contribution from partially protonated complex in solution. As the objective is to examine the surface bound species this was not investigated further in solution.

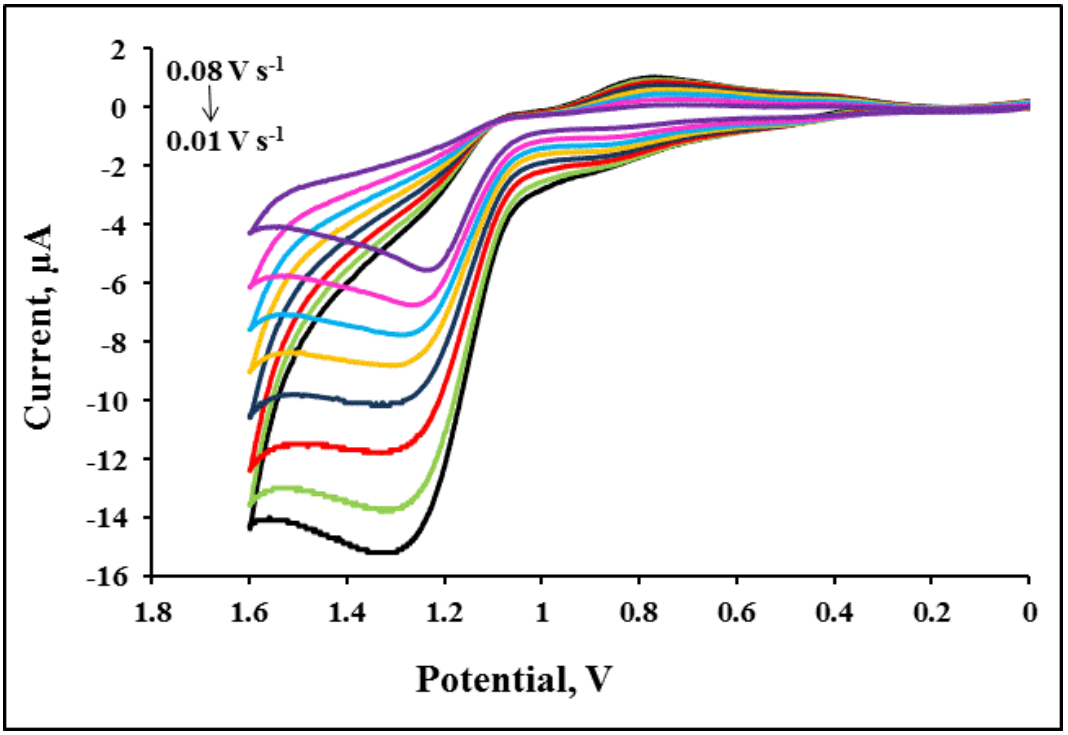

Figure 4.7: Scan rate dependence of solution 1 µM $[Ru(dppz)(bpyArCOOH)_2]^{2+}$ in DPBS , pH 7.2 .The working electrode is ITO (1.25 cm^2) and reference electrode is Ag / Ag Cl . The CVs are plotted incrementally for scan rates of 0.01 V s^{-1} (innermost CV) to 0.08 V s^{-1} (outermost CV) at 0.01 V s^{-1} intervals.

4.3.2.2. Electrochemical behaviour of $[Ru(dppz)(bpyArCOOH)_2]^{2+}$ as a monolayer

Scheme 4.1 shows a scheme of the anticipated assembly of $[Ru(dppz)(bpyArCOOH)_2]^{2+}$ and the DNA on the ITO electrode. Carboxyl functionalities are known to adhere to ITO.[34] Correspondingly the ITO electrode was immersed in 1 mM $[Ru(dppz)(bpyArCOOH)_2]^{2+}$ for 48 hours and the complex binds directly on the electrode. The negatively charged DNA is then anticipated to bind to the positively charged Ru monolayer through both electrostatic and intercalative binding.

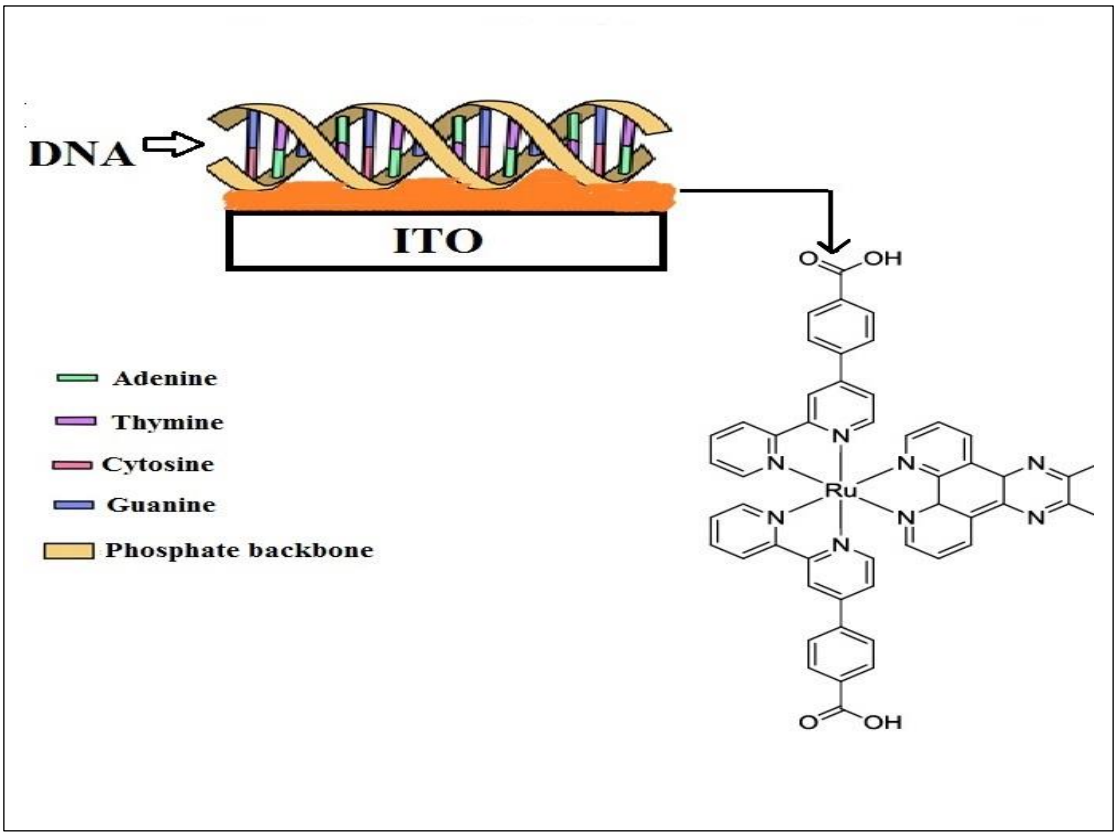

Scheme 4.1: Illustrates the $[Ru(dppz)(bpyArCOOH)_2]^{2+}$-monolayer modified with DNA on an ITO electrode.

Following assembly of the monolayer at ITO, the voltammetry of the $[Ru(dppz)(bpyArCOOH)_2]^{2+}$ was investigated in contact with MeCN and DPBS and the results are presented in Figure 4.8 and 4.9 respectively. In MeCN, the $[Ru(dppz)(bpyArCOOH)_2]^{2+}$ monolayer exhibits a single reversible oxidation with a formal potential of 1.307 V attributed to the $Ru^{2+/3+}$ couple. Interestingly, this peak has shifted by ~100 mV to a more positive potential compared to the dye in solution, suggesting binding to the electrode reduces the electron density at the metal centre forcing the oxidation of $[Ru(dppz)(bpyArCOOH)_2]^{2+}$ to higher potential. In an ideal voltammetric response, for a surface confined

species where there are no lateral interactions between adsorbates, the anodic and cathodic peaks are anticipated to be symmetrical, with zero peak to peak splitting and a full width at half maximum of 90.6 mV for a one electron transfer process.[35] The $[Ru(dppz)(bpyArCOOH)_2]^{2+}$ monolayer exhibits non- zero peak to peak splitting, when scanned voltammetrically at 0.01 Vs^{-1} where the *Δ Ep* is 15 ±4.5 mV and *ΔEp* increases with increasing scan rates. Such non-ideal behaviour is attributed to lateral interactions between the adsorbates of the monolayer.

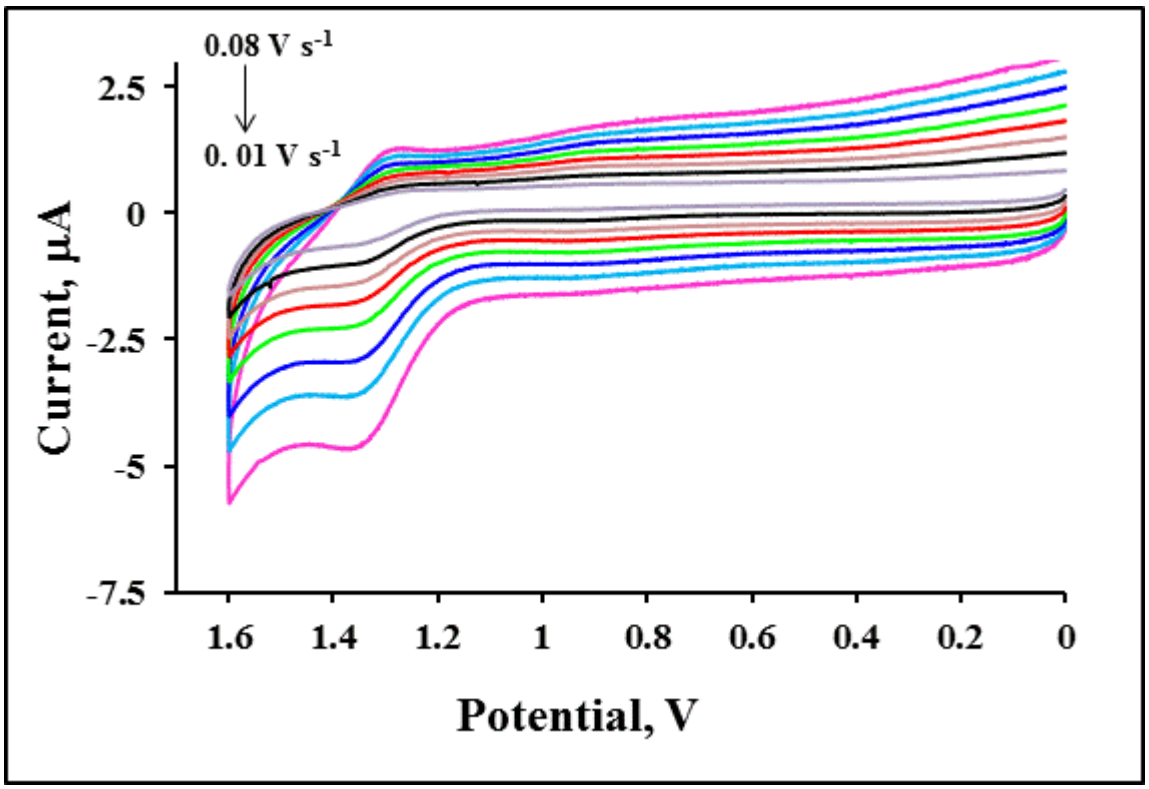

Figure 4.8: Scan rate dependent voltammetric responses of $[Ru(dppz)(bpyArCOOH)_2]^{2+}$ monolayer following 48 hour assembly on ITO electrode (1.25 cm^2) . The reference electrode is Ag/ Ag Cl and the supporting electrolyte is 0.1 M $LiClO_4$ in acetonitrile. The CVs are plotted incrementally for scan rates of 0.01 V s^{-1} (innermost CV) to 0.08 V s^{-1} (outermost CV) at 0.01 V s^{-1} intervals.

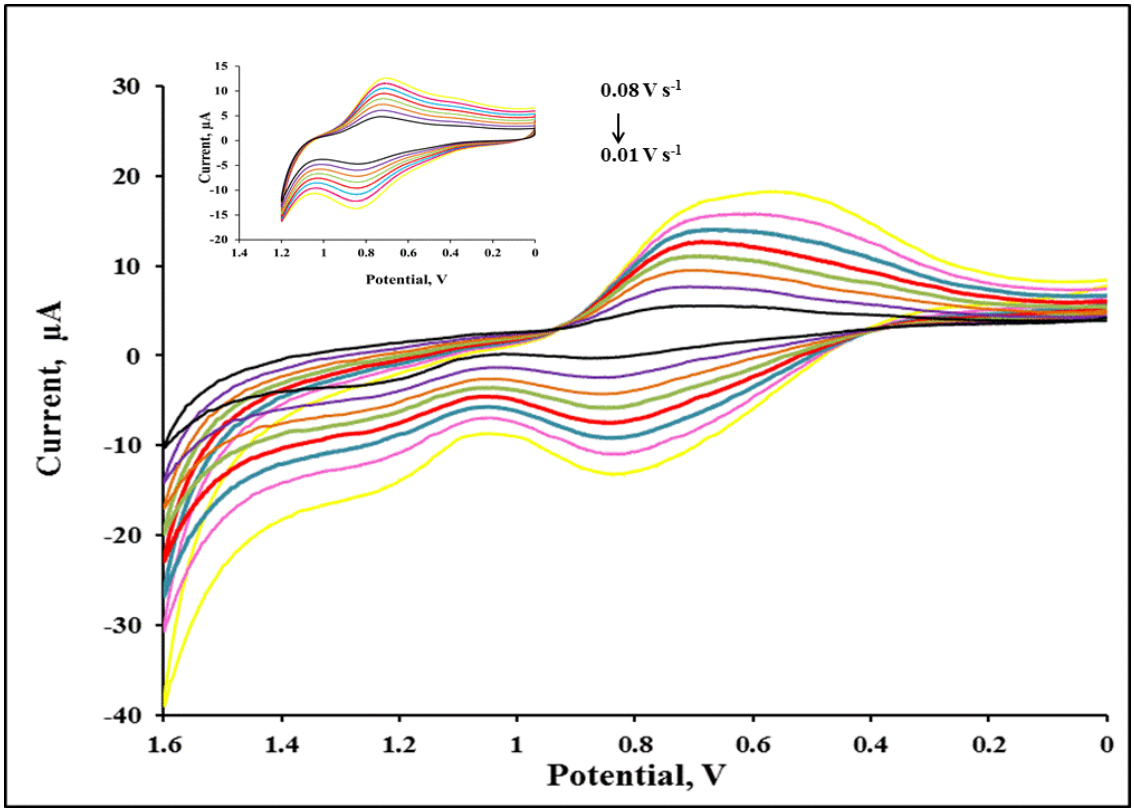

Figure 4.9: Scan rate dependent voltammetric responses of $[Ru(dppz)(bpyArCOOH)_2]^{2+}$ monolayer following 48 hour assembly on ITO (1.25 cm^2). The reference electrode is Ag/AgCl and the electrolyte is DPBS. The surface coverage of the monolayer is 1.29 ± 0.3 x 10^{-10} mol cm^{-2}. The CVs are plotted incrementally for scan rates of 0.01 V s^{-1} (innermost CV) to 0.08 V s^{-1} (outermost CV) at 0.01 V s^{-1} intervals.

As observed in solution, the voltammetric behaviour of the $[Ru(dppz)(bpyArCOOH)_2]^{2+}$ monolayer also exhibits strong solvent dependent responses. Typical scan rate dependent CVs of a $[Ru(dppz)(bpyArCOOH)_2]^{2+}$ monolayer on an ITO electrode in contact with PBS are presented in Figure 4.9. Interestingly, as observed in aqueous solution, the voltammograms exhibit two anodic peaks at 0.82 V while the second is 1.22 V, at the slowest measured scan rate 0.01 Vs^{-1}. This behaviour is similar to $[Ru(dppz)(bpyArCOOH)_2]^{2+}$ in DPBS Figure 4.7, although the relative

intensities of the peaks have changed, in the monolayer the lower potential process dominates the response. Conversely, the redox process at lower potentials; 0.82 V and the associated reduction peak at 0.69 V were not evident in MeCN.

The difference in the behaviour of the monolayer in contact with buffer and acetonitrile and the similarities of their potentials with the solution studies suggests that the monolayer is fully solvated in the buffer. The irreversible peak observed at 1.21 V is similar to the peak observed in acetonitrile which is attributed to the metal based $Ru^{2+/3+}$ redox. However, as observed from the inset in Figure 4.9 the dominant feature in the voltammetry is the quasi oxidation peak centred around 0.82 V. Its reversibility and scan rate dependence indicates that it is a metal based process but the potential at which it appears is surprising. The voltammetry of $[Ru(dppz)]^{2+}$ has not been reported in detail in aqueous media. Fees *et al.*[36] reported the effect of water on reduction potentials of this complex but not its oxidation. As it was not commented on, the presumption is that the oxidation is not significantly affected. In solution phase the dominant process was the 1.2 V oxidation, attributed to the $Ru^{2+/3+}$ couple and the lower potential process attributed tentatively to presence of different ionisation states of the complex in PBS. This suggest that the origin of the change is with the bpyArCOOH, deprotonation of the carboxyl would be expected to shift the oxidation of the metal to more cathodic potentials. Such shifts in oxidation potential have been observed previously in Ru(II) complexes on deprotonation of triazoles.[37] And

it is possible that lateral H-bonding in the monolayer or ITO binding reduces the pKa of the carboxyl groups in the complex.

Nonetheless, the anodic and cathodic peak potentials are independent of scan rate, thus confirming that the $[Ru(dppz)(bpyArCOOH)_2]^{2+}$ is surface confined. Using the Faradaic charge associated with the dominant oxidation peak centred at 0.82 V after background correction, together with the area of the electrode we were able estimate the surface coverage, of the complex at ITO, and it was determined to be 1.29 ± 0.3 x 10^{-10} mol cm^{-2} which is consistent with monolayer formation. However, when the surface coverage is calculated from the Faradaic charge associated with the peak centred at 1.22 V which is responsible for the converting the monolayer from 2+ to 3+ a lower surface coverage of 5.41± 0.2 x 10^{-11} mol cm^{-2}. Assuming each peak corresponds to a different protonation state of the complex, the surface coverage are additive, and even taking the values in total that is 1.83 x ± 0.1 10^{-10} mol cm^{-2}, corresponding to an area occupied molecule, A_{mol} of 90.7 $Å^2$ the surface coverage suggests that this is a closely packed monolayer, when compared to previously reported Ru monolayers. For example a surface coverage of related, but pyridine bound monolayer; $[Ru(bpy)_2Qbpy]^{2+}$ was determined as 1.05 x 10^{-10} mol cm^{-2} corresponding to A_{mol} of 158 $Å^2$ which was said to be a closely packed monolayer.[35]

4.3.2.3. Electrochemical behaviour of $[Ru(dppz)(bpyArCOOH)_2]^{2+}$ as monolayer after DNA intercalation

The impact of the interaction of the $[Ru(dppz)(bpyArCOOH)_2]^{2+}$ monolayer with DNA on the voltammetry of the complex was then studied by examining the cyclic voltammograms of the metal complex before and after exposure of the electrode to DNAintroduced to the contacting solution. The voltammetric profiles of the modified electrode before and after 3 hours incubation in 100µM DNA are presented in Figure 4.10.

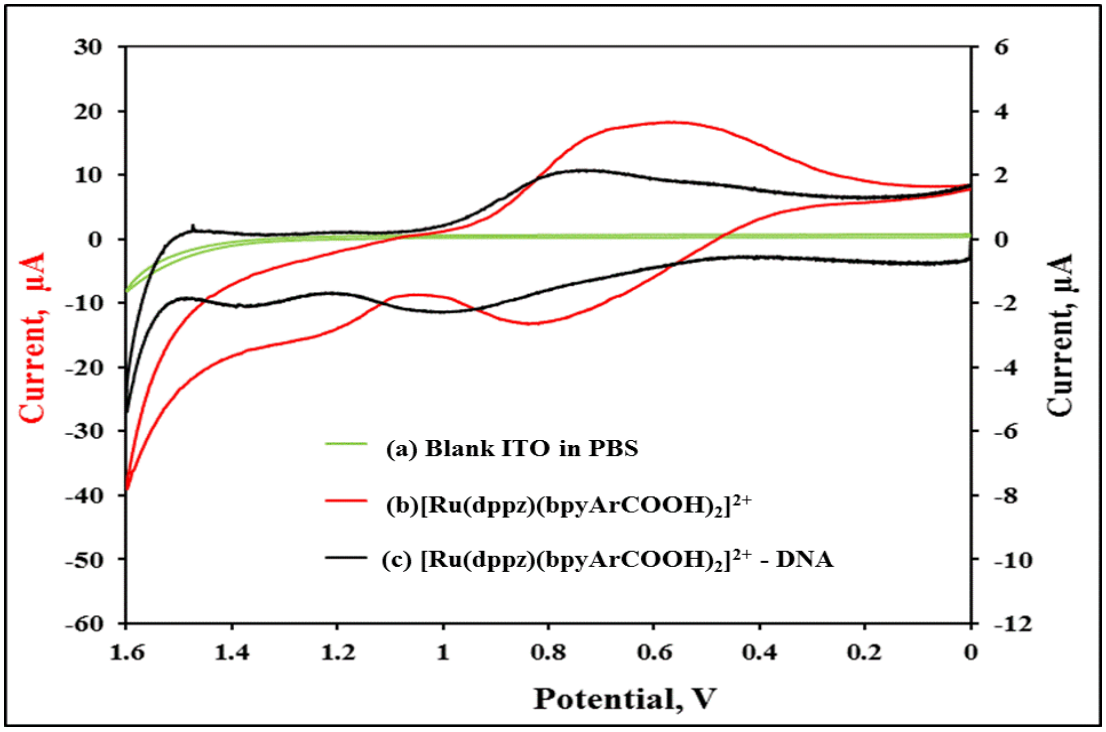

Figure 4.10: Cyclic voltammograms of (a) Blank ITO electrode (b) ITO modified with $[Ru(dppz)(bpyArCOOH)_2]^{2+}$ monolayer and (c) $[Ru(dppz)(bpyArCOOH)_2]^{2+}$ - DNA in DPBS. The scan rate is 0.08 Vs^{-1}.

Strikingly, after DNA binding has taken place, there is a significant decrease in peak current and an anodic shift in the voltammetric peak potentials. As observed from Figure 4.10 (b) after DNA binding the oxidative peak observed at 0.82 V in $[Ru(dppz)(bpyArCOOH)_2]^{2+}$ shifts to 1.00 V and the second peak which is at 1.22 V to 1.35 V. In other words, the first and second oxidation peaks shifted by 180mV, while the latter shifted by 143 mV to more positive potentials after DNA binding. The appearance of the shift and its magnitude upon exposure to DNA suggests strongly that the DNA is binding to the $[Ru(dppz)(bpyArCOOH)_2]^{2+}$ modified electrodes. The anodic potential shift and its magnitude indicate that it is thermodynamically more difficult to oxidise the metal centre on DNA binding indicating a reduction in electron density at the redox centre when it is DNA bound.

The scan rate dependent voltammetry of $[Ru(dppz)(bpyArCOOH)_2]^{2+}$-DNA modified electrodes are presented Figure 4.11. In addition to changes in the peak potentials, there is a substantial decrease of both the anodic i_{pa} and cathodic i_{pa} peak current compared to when the DNA is absent. Significantly they both decrease by approximately 80%. This is further confirmation that DNA strongly interacts with $[Ru(dppz)(bpyArCOOH)_2]^{2+}$ sites on the electrode. Similar behaviour was reported by Bard and co-workers[38] in were they observed a decrease in voltammetric current to a small fraction of its original magnitude upon addition of DNA to $[Co(phen)_3]^{3+}$ complexes in solution.

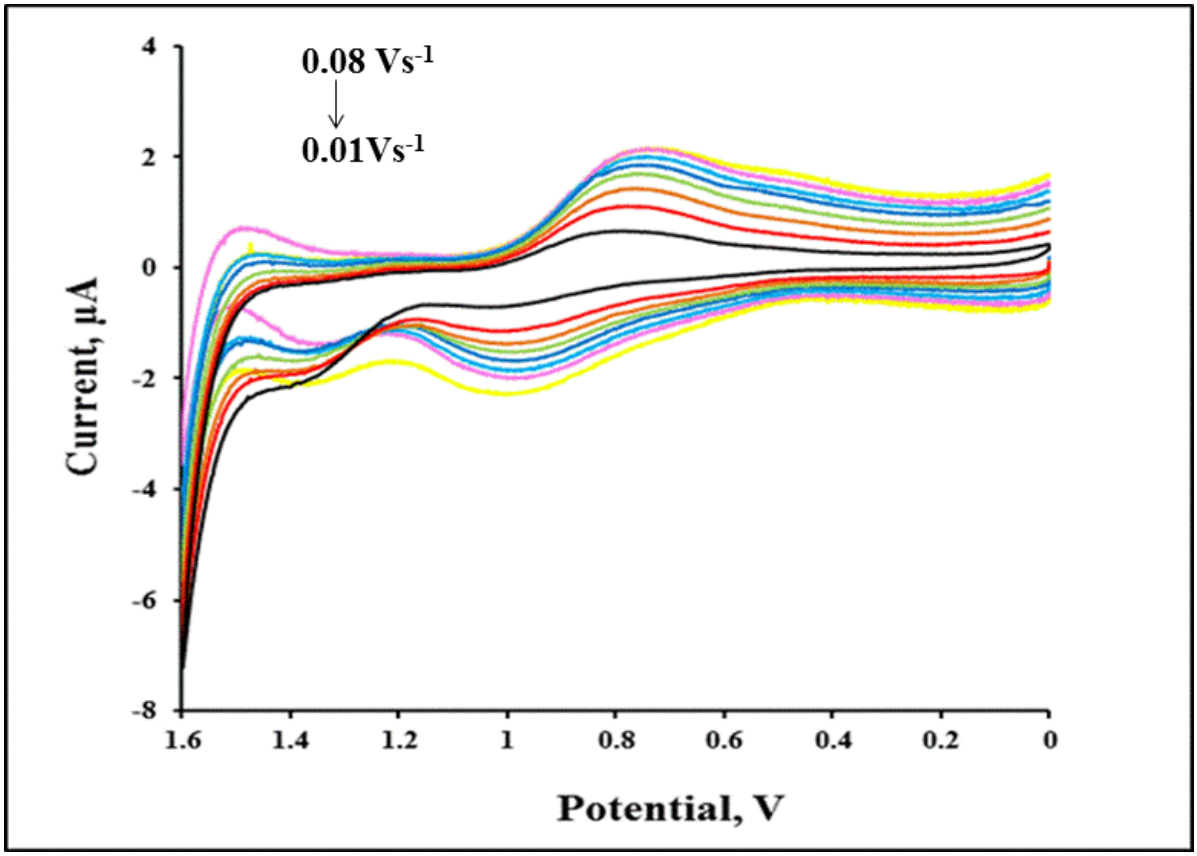

Figure 4.11: Scan rate dependence CVs of $[Ru(dppz)(bpyArCOOH)_2]^{2+}$-DNA monolayers after incubation of 100 uM DNA on ITO electrode (1.25 cm^2) for 3 hours. The reference electrode is Ag/AgCl. The surface coverage of $[Ru(dppz)(bpyArCOOH)_2]^{2+}$ is 1.85±0.2 x10 $^{-11}$ mol cm^{-2}. The CVs are plotted incrementally for scan rates of 0.01 V s^{-1} (innermost CV) to 0.08 V s^{-1} (outermost CV) at 0.01 V s^{-1} intervals.

Possible explanations for the observed decrease in voltammetric current upon DNA binding are; firstly the oxidation and reduction reactions of $[Ru(dppz)(bpyArCOOH)_2]^{2+}$ are impeded due to the formation of a DNA film at the monolayer which impedes ion transport. Secondly slower electron transfer mediated through DNA bound metal complex to the electrode surface.[39]

4.3.3. RAMAN SPECTRA OF $[Ru(dppz)(bpyArCOOH)_2]^{2+}$ MONOLAYER BEFORE AND DNA INTERCALATION

To further confirm the assembly of a $[Ru(dppz)(bpyArCOOH)_2]^{2+}$ monolayer at the ITO electrode and then latterly to assess any structural impact of DNA binding on the monolayers of $[Ru(dppz)(bpyArCOOH)_2]^{2+}$ resonance Raman spectroscopy (RRS) was carried out on the electrodes. In RRS the excitation wavelength that is employed is coincides with an optical absorbance of the material under interrogation.

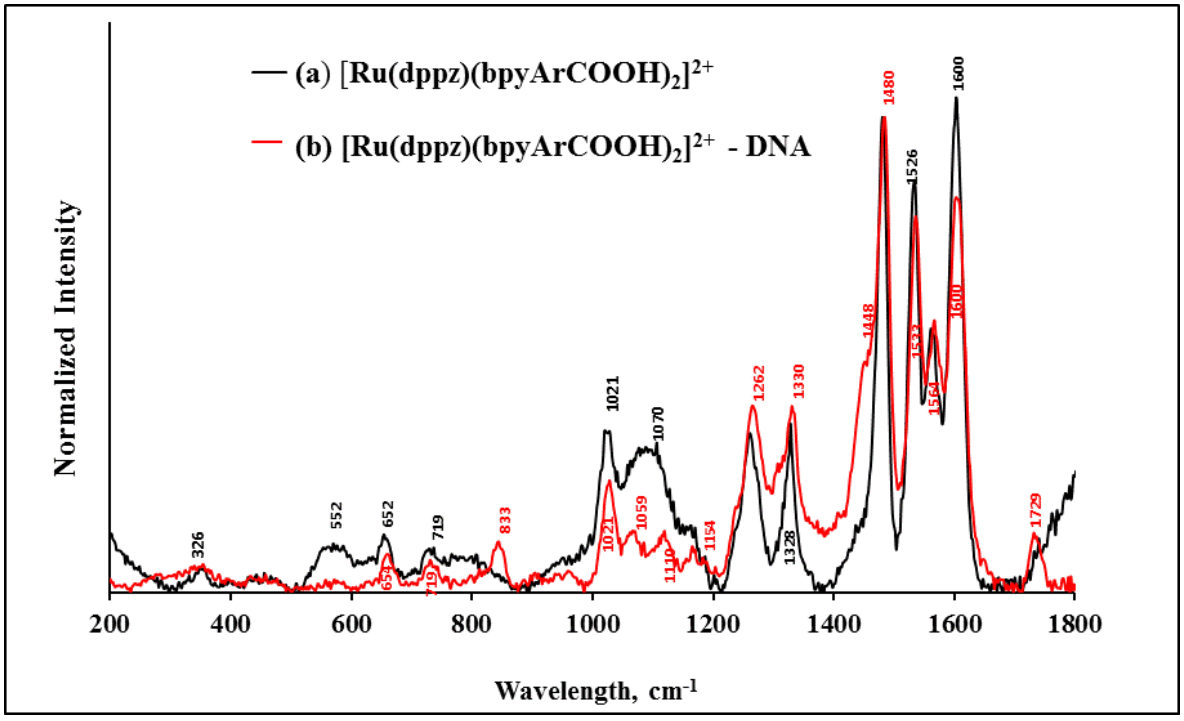

Figure 4.12: Normalized Raman spectra of the (a) $[Ru(dppz)(bpyArCOOH)_2]^{2+}$ monolayer and (b) $[Ru(dppz)(bpyArCOOH)_2]^{2+}$ monolayer after DNA intercalation on ITO electrodes. Samples were irradiated using argon laser excitation at 488 nm the laser power was 0.015 mW. The spectra were

averaged over 4 acquisitions with an exposure time of 2 s. The spectra was normalized to the 1480 cm^{-1} mode.

Under such conditions the, Frank-Condon modes of the chromophore are resonantly enhanced, giving selective increases in intensity of Raman modes associated with moieties in the complex participating in the electronic transition. Under Frank Condon enhancement, the intensity of such modes can be enhanced up to 7 orders of magnitude compared with normal Raman. Although selective this provides a valuable insight into origin of the optical transition the excitation is resonant with and also, provide sufficient enhancement in sensitivity so that collection of a Raman spectrum from a monolayer of material is feasible.[40] Figure 4.12 shows the resonance Raman spectra of $[Ru(dppz)(bpyArCOOH)_2]^{2+}$ monolayers at ITO collected (a) before and (b) after DNA binding. Spectra were collected using an excitation wavelength of 478 nm. This wavelength was selected for excitation as it is resonant with the dppz ligand centered metal to ligand charge transfer (MLCT) transitions which is centered at approximately 466 nm, as previously described from the UV/ Vis spectra. The spectrum for the monolayer alone, shown in Figure 4.12 (a), is dominated by vibrations attributable to the dppz ligand with some contributions arising from the BpyArCOOH ligand features. Raman vibrations are observed at 326,550, 652, 719, 833, 1021, 1070, 1258, 1328, 1480, 1533, 1560, 1600 cm^{-1}. The modes specifically associated with dppz ligand are observed at 1258, 1328, 1493, 1526, 1560, 1600 cm^{-1},[41]·Schoonover *et al*.[42] reported that the transitions associated with the dppz

ligand can be separated into contributions from the 1,10-phenanthroline (phen) [43] and the phenazine (phz)[44] parts of the ligand.

Introduction of DNA to the monolayer causes small shifts to some of the vibrational modes, on the order of approximately 5 cm^{-2}. These changes are limited to the modes associated with the dppz ligand, modes associated with the bpy ligand. For example modes at 1021cm^{-1} and 1480 cm^{-1} are unaffected by DNA binding, a blue shift in the dppz mode to 1526 cm^{-1} from 1533 cm^{-1} on DNA binding. This mode was identified previously as a marker signature band for the light switch DNA effect.[45]

There are also significant reductions in relative intensity of the dppz modes, with respect to the bpy modes on DNA binding. Turro and co-workers[45] reported an analogous response in the rR spectrum of related Ruthenium complexes on DNA binding in solution. They rationalised that the intercalation between the phz part of the dppz ligand leads to strong π-π stacking of the dppz ligand and the cofacial DNA bases which reduces the intensity of the aromatic C=C and related coupled modes for the dppz containing complex.[44] Thus it is concluded that the same effect is occurring here and that $[Ru(dppz)(bpyArCOOH)_2]^{2+}$ at the monolayer interacts with DNA through intercalation. It is important to note however that overall, the absolute Raman intensity from the ITO immobilised $Ru(dppz)(bpyArCOOH)_2]^{2+}$ is essentially unchanged following DNA exposure. This is important as it indicates that DNA

is not displacing the complex at the electrode and so the possibility that the current reduction observed in voltammetry on DNA binding is due to loss of the complex can be excluded. Interestingly, new Raman spectral features appear on DNA exposure at, 833, 1059, 1110, 1729 cm^{-1}. The mode at 833 cm^{-1} is attributed to phosphate, and the modes at 1059 and 1100 cm^{-1} are attributed to cytosine.[46] The feature at 1729 cm^{-1} is characteristic of C=O of guanine or thamine.[4748] There are also shoulders apparent around 1448 cm^{-1} and around 1250 cm^{-1} which are also attributable to DNA.

4.3.4. LUMINESCENCE OF $[Ru(dppz)(bpyArCOOH)_2]^{2+}$ MONOLAYER BEFORE AND DNA INTERCALATION

The luminescence of the monolayer of this material on the ITO electrode before and after DNA binding was investigated under dry conditions, that is when the monolayer is not in contact with solvent. The $[Ru(dppz)(bpyArCOOH)_2]^{2+}$ monolayer was found to be luminescent. The emission spectrum of the dry monolayer (before DNA exposure) is shown in Figure 4.13. The emission shows a broad spectrum with a maximum at 645 nm. The emission maximum of the monolayer is approximately 35 nm blue shifted compared to solution (Figure 4.2(b)). The shift in wavelength may be attributed to the rigidity of the bilayer due to lateral interactions between the dppz ligands or may simply be due to the difference in the dielectric constant of the dry monolayer compared with solution. Figure 4.13(b) illustrates the impact of introduction of DNA to its emission spectrum. In this experiment the

monolayer was incubated with DNA 100 µM for 3 hours and then the layer dried before running the spectrum. Significantly, even when dry, DNA exposure has a significant effect on the monolayer emission, as luminescence intensity from the monolayer is increased by >50% compared with the dry film with no DNA present in (Figure 4.13). This indicates, in agreement with Raman and electrochemical studies, that DNA binding is occurring at the monolayer and that the monolayer remains intact after such binding despite the decrease in current observed from electrochemistry.

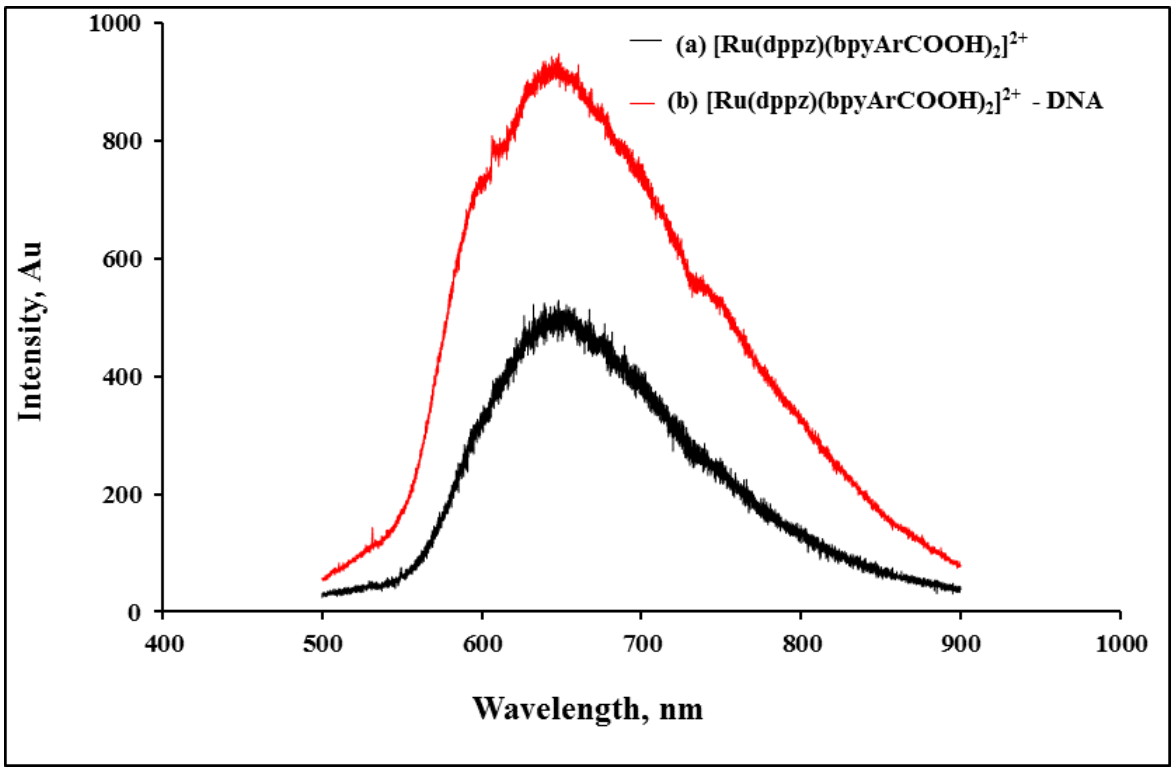

Figure 4.13: Luminescence spectra of the dry (a) [Ru (dppz)(bpyArCOOH)$_2$]$^{2+}$ monolayer and [Ru(dppz)(bpyArCOOH)$_2$]$^{2+}$ monolayer after DNA intercalation on ITO electrodes. Samples were irradiated using argon laser excitation at 488 nm the laser power was 0.015 mW. The spectra were averaged over 5 acquisitions with an exposure time of 0.5 s.

4.3.5. ELECTROCHEMILUMINESCENCE

Given the switching on of luminescence observed in the monolayer on DNA binding, it was necessary to investigate whether the film gives any ECL and if this signal is influenced by DNA binding to the monolayer. Since the interest is in ECL of the monolayers in aqueous media, co-reactant ECL was employed, to enable ECL generation by either applying a potential step or one directional potential scan. Ru- oxalate systems been previously shown to undergo oxidative-reductive ECL,[49] thus oxalate was chosen as co-reactant for these investigations. ECL of the $[Ru(dppz)(bpyArCOOH)_2]^{2+}$ monolayer was investigated at an ITO working electrode in contact with aqueous buffer containing 10 mM oxalate as the co-reactant. The ECL and voltammetric data are presented in Figure 4.14.

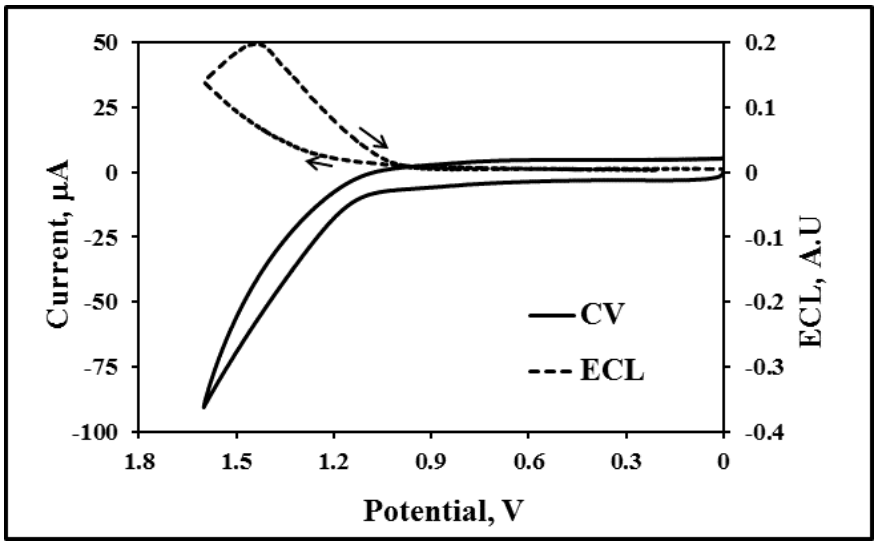

Figure 4.14: ECL profiles of $[Ru(dppz)(bpyArCOOH)_2]^{2+}$ monolayer on ITO electrode (1.25 cm^2) in DPBS, in 10 mM Oxalate. The reference electrode is Ag/AgCl and the scan rate 0.1 Vs^{-1}.

Interestingly, the monolayer $[Ru(dppz)(bpyArCOOH)_2]^{2+}$ generates ECL before DNA intercalation, Furthermore the ECL onset potential of the $[Ru(dppz)(bpyArCOOH)_2]^{2+}$ is observed at 1.20 V as shown in Figure 4.14. This peak potential corresponds to the second oxidative wave in the voltammetry of the monolayer in DPBS in Figure 4.9 and not to the more intense process observed at 0.82 V. There are a few explanations for this, firstly the lower oxidation potential process at 0.82 V, as described in (Figure 4.2), originate from a protonation state of the complex which is non-luminescent or for which the potential is too low for the oxalate co-reactant. The presence of ECL from the monolayer indicates its phenazine moieties are sufficiently protected from the aqueous solution in the film to prevent extinguishing of the excited state luminescence.

For a quantitative interpretation of the ECL intensity we measured the ECL emission efficiency ϕ_{ECL}, this value describes the number of photons emitted per faradaic electron passed during the chemiluminescent reaction of the $[Ru(dppz)(bpyArCOOH)_2]^{2+}$ monolayer. It was determined, according to equation 3.8, to be 0.018 %. This ϕ_{ECL} is very low compared to the 5% ECL efficiency previously reported for the $[Ru(bpy)_3]^{2+}$ in solution.[50] The low ECL efficiency for the monolayer is not surprising as the emission from the film is weak due to at least partial quenching of the excited state in aqueous media.

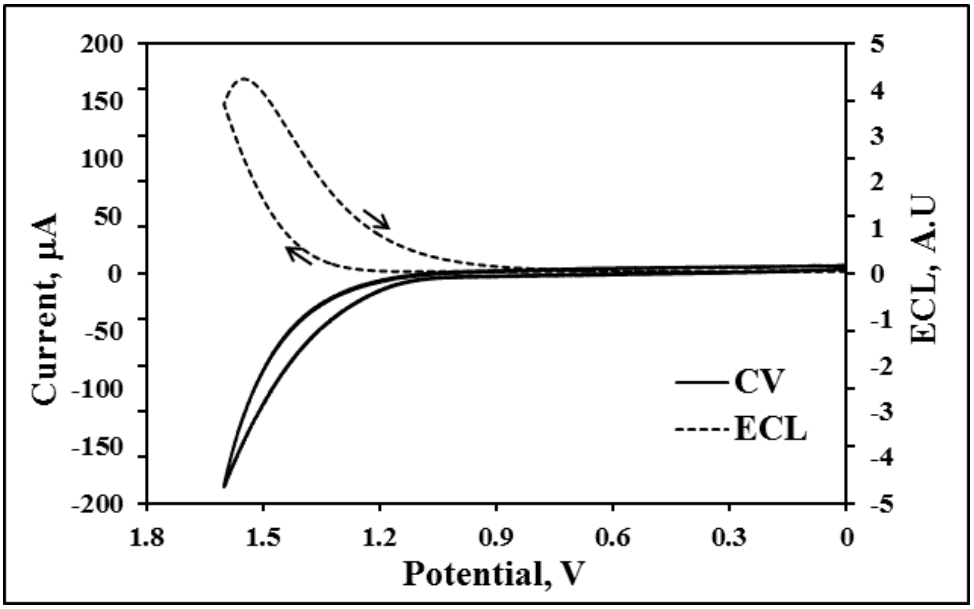

Figure 4.15: ECL and voltammetric profiles of $[Ru(dppz)(bpyArCOOH)_2]^{2+}$ following incubation with 100 µM DNA on ITO electrode and the reference electrode is Ag/AgCl, the coreactant is 10mM Oxalate in DPBS. The scan rate is 0.1 V s^{-1}.

Figure 4.15 shows the ECL and CV of a $[Ru(dppz)(bpyArCOOH)_2]^{2+}$ monolayer following incubation of the film with a 100 µM DNA for 3 h in the presence 10 mM sodium oxalate used as co-reactant. The $[Ru(dppz)(bpyArCOOH)_2]^{2+}$ bound to the DNA monolayer is oxidized at the electrode, to form $Ru(dppz)(bpyArCOOH)_2]^{3+}$ -DNA, which is capable of oxidizing oxalate as indicated in equation 4.2. It should be noted that oxalate coreactant is not expected to directly interact with the DNA as it is $C_2O_4^{2-}$ negatively charged and the phosphates in the DNA backbone are also negatively charged.[51] However oxalate reacts with Ru sites at the electrode to form the oxalate radical anion $C_2O_4^{-\bullet}$ which is capable of reducing $[Ru(dppz)(bpyArCOOH)_2]^{3+}$ to generate the excited emissive state as

indicated in Equation 4.4. In the presence of DNA the ECL turn on potential was observed to occur at1.30 V in Figure 4.15), suggesting that upon DNA intercalation the ECL onset potential shifts to more positive potentials. This shift of ~100 mV is consistent with the voltammetry of $[Ru(dppz)(bpyArCOOH)_2]^{2+}$ – DNA films in PBS which showed similar peak shifts in the second $Ru^{2+/3+}$ couple shifts to positive potentials when DNA is present. Again, the lower potential process does not seem to participate in ECL generation. The ECL mechanism equations for the $[Ru(dppz)(bpyArCOOH)_2]^{2+}$-DNA monolayer is given in equations [4.1-4.6], and is rationalized on the basis of previously reported studies which employed oxalate and ruthenium polypyridyl ECL pair.[52,53]

$$Ru\ (II)\text{- DNA -e} \longrightarrow Ru\ (III)\text{-DNA} \qquad [\mathbf{4.1}]$$

$$Ru\ (III)\text{- DNA} + C_2O_4^{2-} \longrightarrow Ru\ (II)\text{-DNA} + C_2O_4^{\bullet -} \qquad [\mathbf{4.2}]$$

$$C_2O_4^{\bullet -} \longrightarrow CO_2^{\bullet -} + CO_2 \qquad [\mathbf{4.3}]$$

$$Ru\ (II)\text{- DNA} + CO_2^{\bullet -} \longrightarrow Ru\ (I)\text{- DNA} + CO_2 \qquad [\mathbf{4.4}]$$

$$Ru\ (III)\text{- DNA} + CO_2^{\bullet -} \longrightarrow Ru\ (II)^*\text{- DNA} + CO_2 \qquad [\mathbf{4.5}]$$

$$Ru\ (II)^*\text{- DNA} \longrightarrow Ru\ (II) – DNA + hu \qquad [\mathbf{4.6}]$$

Importantly the presence of DNA instigates over an order of magnitude enhancement in the electrochemiluminescence efficiency, wherein the ϕ_{ECL} increases to 0.20 ± 0.01 % compared to 0.018± 0.02% when DNA is absent at the $[Ru(dppz)(bpyArCOOH)_2]^{2+}$ monolayer. Combined, the Raman, luminescence and ECL data suggests that the $[Ru(dppz)(bpyArCOOH)_2]^{2+}$

monolayer interacts strongly with DNA. The luminescence and ECL data from the monolayer alone, indicates that the packing of the complex at the interface offers some but not complete immunity from water quenching but DNA binding is effective in protecting the phenazine nitrogen atoms from the buffer in a way that is analogous to the complex-DNA binding in solution, indicating ECL is potentially useful way of reporting DNA binding.

To further explore the nature of the DNA- monolayer binding, i.e. to assess whether DNA intercalation, analogous to dppz interactions rather than just nonspecific coating of the electrode with DNA is responsible for the enhanced ECL. We examined the effect of exposing the $[Ru(dppz)(bpyArCOOH)_2]^{2+}$ monolayer to bovine serum albumin (BSA) on its ECL and luminescence. BSA is expected to bind non-specifically to the complex[54] and this would be expected to affect the emission intensity of the phenazine ligand complex but BSA is known in solution to bind more loosely to DNA with far less protection of the ligand from water.[54] The voltammetric and the ECL behaviour of $[Ru(dppz)(bpyArCOOH)_2]^{2+}$ after incubation of the monolayer in BSA dissolved in DPBS, for 3 hours was evaluated and compared to that of unmodified $[Ru(dppz)(bpyArCOOH)_2]^{2+}$ monolayer and the data are presented in Figure 4.17. Interestingly, as observed for DNA binding there is a significant decrease in the voltammetric current is observed after BSA exposure and the anodic peak potential which was observed 0.82 V before binding in the pure monolayer shifts to 0.86 V. Luzuriaga and Creda, also obtained similar shifts in voltammetry upon incubating $[Ru\text{-}(phenanthroline)_3]^{2+}$ with BSA in solution.[55] However, this shift of the oxidation potential upon BSA binding to

the Ru monolayer is smaller than that induced by DNA, which caused the oxidation potential of the monolayer shift by more than 100 mV (Figure 4.10).

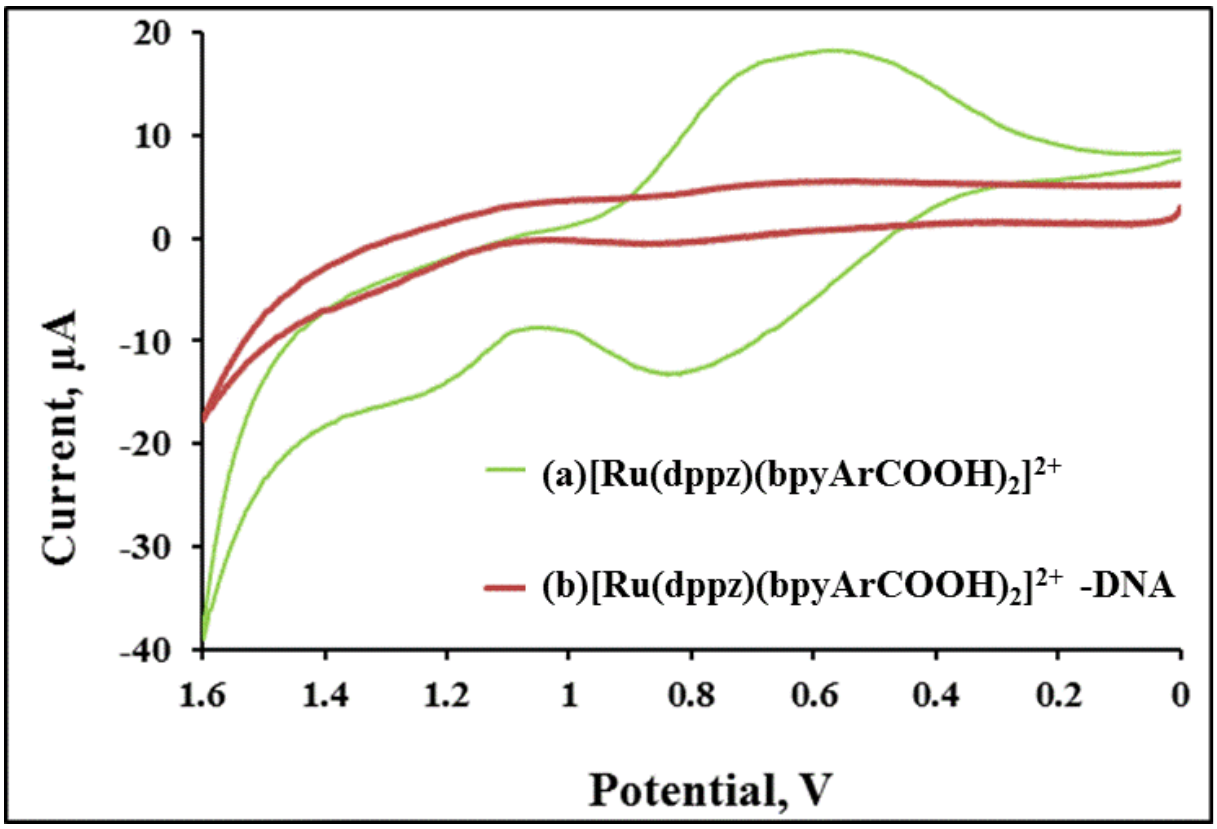

Figure 4.16: Cyclic voltammograms of (a) $[Ru(dppz)(bpyArCOOH)_2]^{2+}$, with surface coverage 1.83 x ± 0.1 10^{-10} mol cm^{-2} and (b) $[Ru(dppz)(bpyArCOOH)_2]^{2+}$–BSA 0.7 x 10^{-12} mol cm^{-2} on ITO electrode (1.25 cm^2), the reference electrode is Ag/AgCl. The supporting electrolyte is DPBS and the scan rate is is 0.08 Vs^{-1}.

The ECL of $[Ru(dppz)(bpyArCOOH)_2]^{2+}$–BSA exhibited an onset potential of 1.2 V again, corresponding to the second anodic process and consistent with the mechanism which is similar the one described above in Equations 4.1 - 4.6. The ECL emission efficiency of the $[Ru(dppz)(bpyArCOOH)_2]^{2+}$- BSA

modified electrode was determined to be 0.023 ± 0.01% which is a small increase compared with 0.018 ± 0.02% obtained from the pure $[Ru(dppz)(bpyArCOOH)_2]^{2+}$ monolayer. and approximately and order of magnitdue less efficient than ϕ_{ECL} of $[Ru(dppz)(bpyArCOOH)_2]^{2+}$ on interaction with DNA is 0.20 ± 0.01%. This is good indication that it is DNA intercalation and not non-specific binding that is responsible for the enhanced ECL observed on monolayer interaction with DNA.

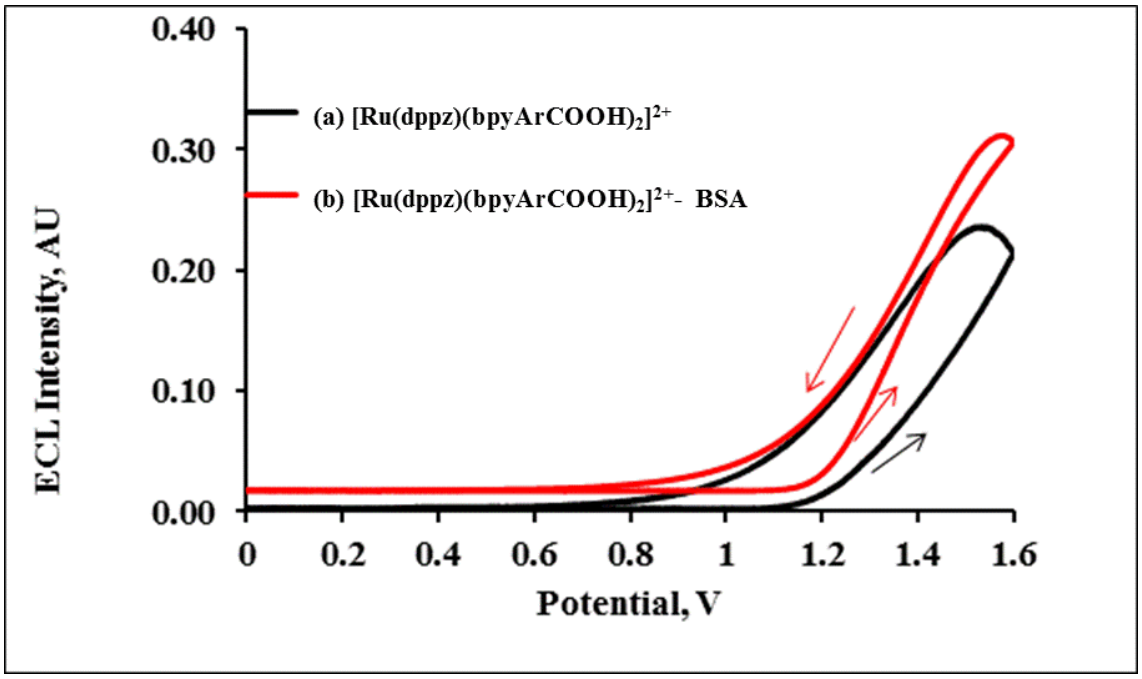

Figure 4.17: ECL profiles of (a) $[Ru(dppz)(bpyArCOOH)_2]^{2+}$ and (b) $[Ru(dppz)(bpyArCOOH)_2]^{2+}$–BSA on ITO electrode and the reference electrode is Ag./AgCl in DPBS, in 10mM Oxalate. The reference electrode is Ag / AgCl scan rate is 0.08 Vs^{-1}.

4.3.5.1. Electrochemiluminescence concentration dependence

To investigate the time it takes for the DNA binding process to reach equilibrium. The time dependence of the ECL signal intensity was followed as

a function of DNA incubation time with the monolayer and the data is presented in Figure 4.18.

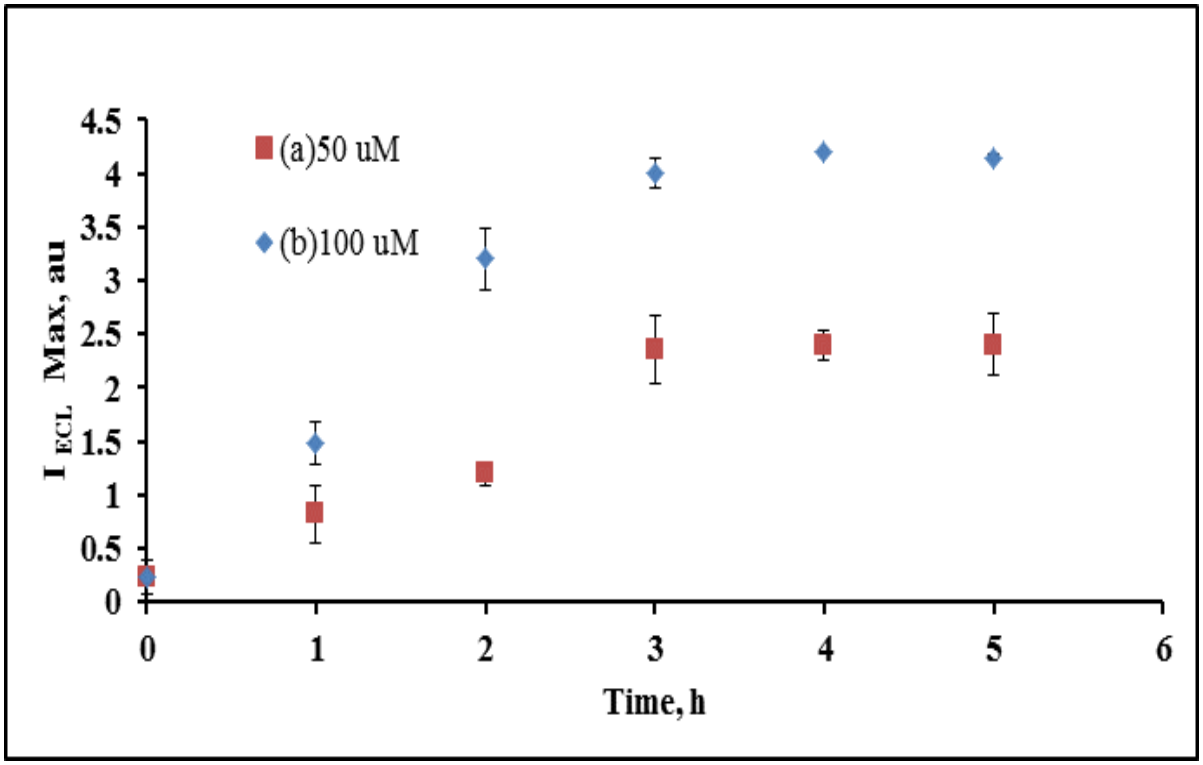

Figure 4.18: ECL maximum intensity of $[Ru(dppz)(bpyArCOOH)_2]^{2+}$ -DNA on ITO. The DNA concentrations used are (a) 50 µM and (b)100 µM. The ECL scans were conducted at 0.1 Vs^{-1}.

The results show that the ECL intensity of $[Ru(dppz)(bpyArCOOH)_2]^{2+}$ - DNA, increases linearly between 0 to 3 h. At 3 h the ECL signal reaches a maximum and undergoes no further change, which indicates that saturation coverage (for the given DNA concentration) is reached at this time and DNA binding reaction has equilibrated. To semi - quantitatively assess DNA binding and identify the concentration range over which DNA could be detected, DNA concentration dependent ECL studies were carried out under saturation

binding conditions, *i.e.* the electrodes were allowed to equilibrate with the contacting DNA solution for 3 h prior to measurement. The concentration of monolayer is kept constant (at saturation 1.83 x ± 0.1 10^{-10} mol cm^{-2}) on the electrode, and DNA concentrations were varied from 5 to 100 µM.

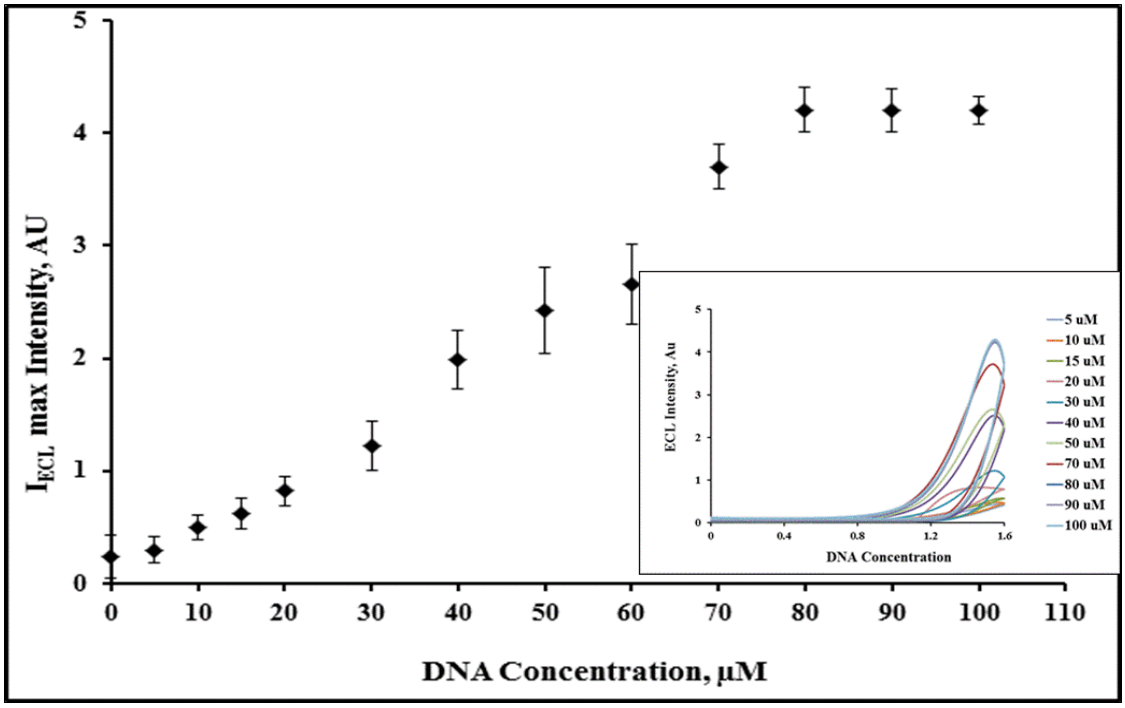

Figure 4.19: ECL intensity vs DNA concentration, the $[Ru(dppz)(bpyArCOOH)_2]^{2+}$ -DNA modified ITO electrodes , 5-100 µM of DNA concentrations, the inset shows the ECL profiles. The scan rate is 0.1 Vs^{-1} and the co-reactant is 10 mM oxalate in PBS, ionic strength 0.2 M and pH 7.

Figure 4.19 shows the resulting ECL intensity of $[Ru(dppz)(bpyArCOOH)_2]^{2+}$monolayer versus DNA concentration. The plot resembles a saturation binding curve, and assuming the ECL intensity is directly correlated with DNA binding indicates that the

$[Ru(dppz)(bpyArCOOH)_2]^{2+}$ monolayer saturation coverage by DNA occurs at 80 µM DNA. A previously reported study which investigated the interaction of 10 µM $[Ru(bpy)_2dppz]^{2+}$ and its interaction with DNA in solution, reported that the ECL intensity increased with DNA concentration linearly up to 20 µM where it reached a plateau at higher DNA concentrations.[23] Guo and co-workers reported that the plateau indicated the saturation of Ru dppz binding sites with DNA in their study which investigated the ECL of a similar complex $[Ru(bpy)_2dppz]^{2+}$ and its interaction with DNA in solution.[56] The detection limit for DNA in the current study is 5 µM, and below this concentration the ECL observed is equivalent to the ECL observed when the monolayer is alone (that is the intensity of 0.24 au). This sugguests that for molecular light switch effect to take place on the $[Ru(dppz)(bpyArCOOH)_2]^{2+}$ monolayer concentrations above 5 µM are required. A way to improve this response might be to co-adsorb the complex with second adsorbate, which does not recognise DNA but will separate the Ruthenium complex sites so as to better expose the phenazines to water and increase their availability for DNA binding. The results from Figure 4.20 saturation binding curve were analysed to determine the pseudo binding dissociation constant K_D which is a measure of the tendency of the DNA- to disassociate from the complex. The specific binding on the y axis is extrapolated at 50% of the x-axis, of its initial value where [DNA] = dissociation constant, K_D, at which 50 % of the Ru sites are occupied by the DNA and K_a is the reciprocal of this value. It is a pseudo K_D because such a model only typically applies to a single ligand complex binding site, but gives an indication of the binding constant.

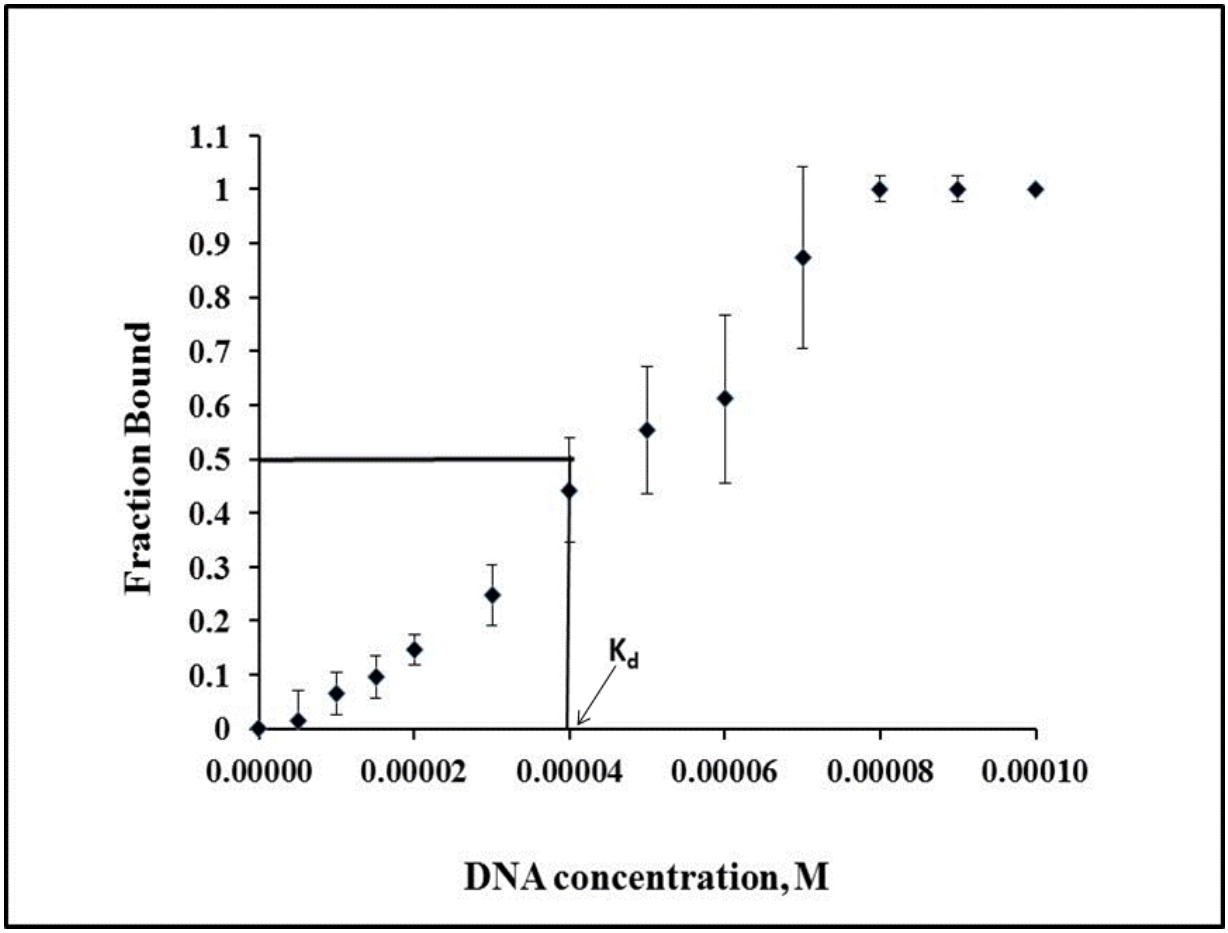

Figure 4.20: Saturation binding curve for, the $[Ru(dppz)(bpyArCOOH)_2]^{2+}$ - DNA modified ITO electrodes, 5 -100 µM of DNA concentrations.The scan rate is 0.1 Vs^{-1} and the co-reactant is 10 mM oxalate in PBS, ionic strength 0.2 M and pH 7. The estimated K_D value is 3.9 x 10^{-5}.

The K_D obtained from the saturation binding curve was determined as 3.9 x 10^{-5}, which yields an association constant of 2.56 x10^4. This K_a shows that the DNA binding to the $[Ru(dppz)(bpyArCOOH)_2]^{2+}$ monolayer is essentially irreversible. Solution studies on dppz containing ruthenium complexes binding to DNA in solution have reported K_a in the range 10^6 to 10^8. The lower association constant in this study is not surprising as the $[Ru(dppz)(bpyArCOOH)_2]^{2+}$ is expected to be less accessible in the close packed monolayer than in solution. As described above binding may be

promoted by reducing the packing density of the film by co-adsorbing a benign agent with the complex.

4.3.5.2. Effect of the ionic strength of the solution

The nature of DNA binding to dppz containing ruthenium complexes is still a point of significant discussion in the literature but a crystal structure of the Δ-[Ru(bpy)2dppz]$^{2+}$ shows a complex picture wherein binding involves a combination of major groove, intercalation or electrostatic association. The electrostatic element of the binding has the effect that, luminescence of DNA bound to dppz complexes is sensitive to ionic strength.[30,57] Indeed groove bound molecules have been shown to be released from the helix by increasing the ionic strength. Therefore, given ECL is carried out in electrolyte solution the effect of ionic strength on ECL intensity of [Ru(dppz)(bpyArCOOH)$_2$]$^{2+}$- DNA was examined. The effect of ionic strength on the ECL intensity of [Ru(dppz)(bpyArCOOH)$_2$]$^{2+}$- DNA was examined in high salt concentrations > 0.2 M, similar to physiological conditions see Figure 4.21.

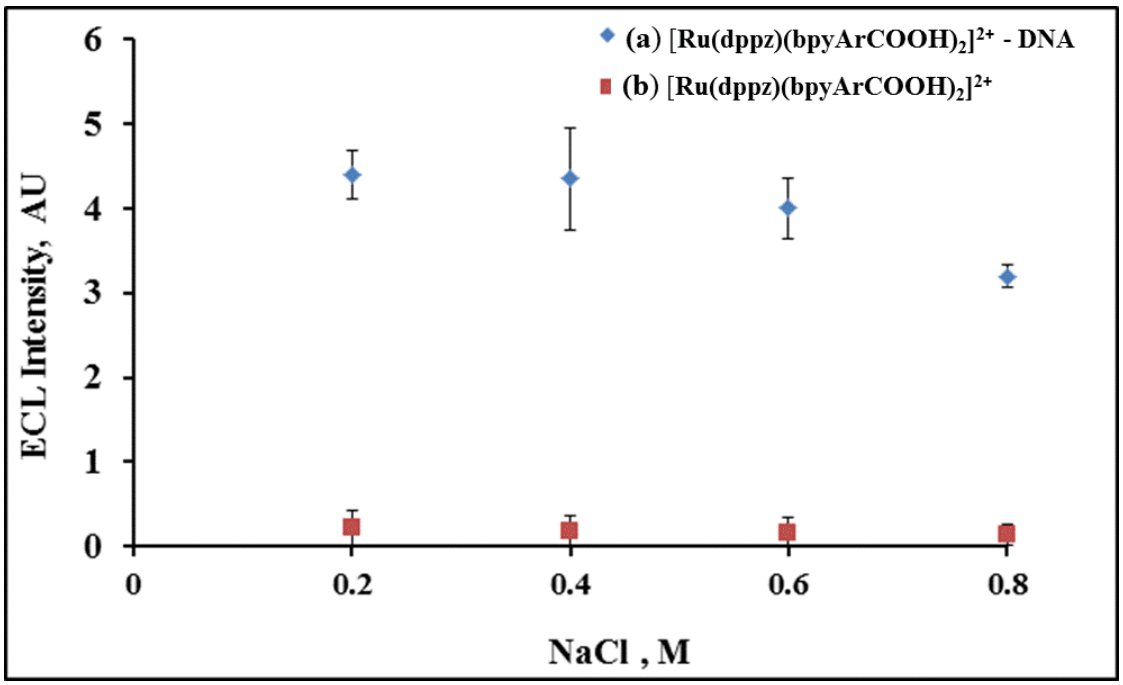

Figure 4.21: The effect of salt concentration on the ECL $[Ru(dppz)(bpyArCOOH)_2]^{2+}$ monolayer (a) in the presence of bound DNA(100 µM) (b) in the absence of DNA on ITO in 10mM oxalate with varying (0.2 , 0.4, 0.6, 0.8 M) NaCl concentrations in PBS and a constant pH = 7. The error bars in represent 3 repeats (n=3).

The results shown in Figure 4.21 indicate that the ECL of the $[Ru(dppz)(bpyArCOOH)_2]^{2+}$ monolayer -DNA complex is only modestly affected by increasing ionic strength of the buffer in the range 0.2 and 0.6 M. A control experiment conducted with the $[Ru\ (dppz)(bpyArCOOH)_2]^{2+}$ monolayer with no DNA present, showed that the change in the ionic strength does not an impact on the ECL of $[Ru(dppz)(bpyArCOOH)_2]^{2+}$ monolayer alone, as the ECL remained constant with increasing concentrations NaCl. Chaires and co-workers[17] investigated interaction of and $[Ru(phen)_2dppz]^{2+}$ with calf thymus DNA. In their study a sample of DNA-metal complex solution in which $[Ru(phen)_2dppz]^{2+}$ was 70% bound, was titrated with 0.2 M NaCl.

They observed a decrease in fluorescence intensity with increasing NaCl, which they attributed salt induced dissociation of the $[Ru(phen)_2dppz]^{2+}$ and DNA. A study conducted by Tabish and co-workers explained that strong dependence on ionic strength on the binding of DNA indicates that the binding is taking place by electrostatic interactions.[58]

According to the polyelectrolyte theory[59] interaction of a positively charged Ru (II) complex with nucleic acids would be influenced by the by the presence of cations or ionic strength of the solution. The sensitivity to ionic strength was reported to decrease in the order of DNA binding modes; electrostatic> groove> intercalative, thus this, can be a qualitative manner to give insights into the DNA binding mode. The modest effect of ionic strength on ECL intensity for the $[Ru(dppz)(bpyArCOOH)_2]^{2+}$ monolayer -DNA complex is again consistent with specific/intercalative binding between the DNA and the monolayer.[17]

4.3.6. INFLUENCE OF NUCLEIC ACID SEQUENCE

Previous studies suggest that some dppz containing ruthenium complexes exhibit enhanced emission in the presence of specific DNA sequences. For example, $[Ru(phen)_2(dppz)]^{2+}$ has been shown to emit more strongly when bound to AT rich than to GC-polynucleotides.[60,61] Also, Ortmans and co-workers reported that when no G-C pairs are present in the sequence, *i.e.* for $[poly(dA\text{-}dT)]_2$ a strong luminescence enhancement is observed.[62,63] This effect was attributed to the decrease of the efficiency of the non-radiative

decay of the ^{3}MLCT exited state induced by the double helix micro environment and protection from oxygen quenching. Also guanine which is the most easily oxidized of the DNA bases, with an oxidation potential of approximately 1.3 V, it may act as an electron transfer donor a leading to Ru emission quenching when the complex has the appropriate excited state reduction potential. We were therefore interested to see, if ECL intensity from the monolayer is influenced by the identity of the polynucleotide sequence. We therefore compared ECL intensity generated on binding of nucleotides composed of either only adenine-thymine (A-T) or cytosine–guanine (C-G).

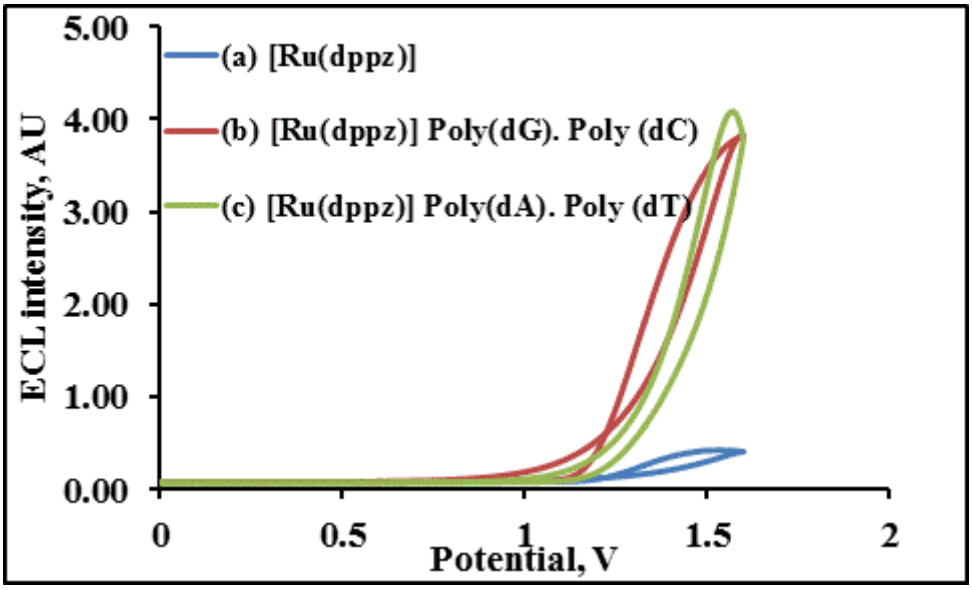

Figure 4.22: ECL of a) $[Ru(dppz)(bpyArCOOH)_2]^{2+}$-Ploy(dG). Poly(dC), b) $[Ru(dppz)(bpyArCOOH)_2]^{2+\cdot}$- Poly(dA).Poly (dT) on ITO (1.25 cm^2), the reference electrode is Ag/AgCl. The co-reactant is 10 Mm oxalate in PBS ionic strength 0.7 M and pH = 7. The DNA concentration used to modify the monolayer is 100 µM.

The $[Ru(dppz)(bpyArCOOH)_2]^{2+\cdot}$monolayer was incubated with nucleotide sequences 100 µM Poly(dA). Poly (dT) or Poly(dG).Poly (dG) for 3 h, and the

results are presented in Figure 4.22. The results were consistent with those for $[Ru(dppz)(bpyArCOOH)_2]^{2+\cdot}$monolayers incubated with the Salmon Testes DNA; There is a significant enhancement of ECL upon binding of either Poly(dA).Poly (dT) or Poly(dG).Poly (dG). However the peak ECL intensity was approximately the same irrespective of the identity of the oligonucleotide, and was the same as observed for stDNA. Quantitatively, the ECL efficiency obtained from the $[Ru(dppz)(bpyArCOOH)_2]^{2+\cdot}$-Poly(dA).Poly (dT) is 0.17± 0.02 %, while for $[Ru(dppz)(bpyArCOOH)_2]^{2+}$-Poly(dG). Poly(dC) ϕ_{ECL} is 0.18%± 0.01 which are indistinguishable from the value obtained for stDNA. However the ECL onset was observed to be slightly less positive at 1.24 V for Poly(dG). Poly(dC) containing compared to the 1.3 V previously seen from stDNA results. The origin of this difference is unclear, but in the case of guanine may suggest that it can directly participate as a co-reactant, this will be investigated in future studies. Overall it can be concluded that ECL observed is not significantly influenced by the nucleotide sequence. This indicates it is principally the DNA or oligonucleotide binding that is responsible for ECL enhancement with no significant discrimination between binding.

4.4. CONCLUSIONS

$[Ru(dppz)(bpyArCOOH)_2]^{2+}$ DNA interaction studies have been carried out using Electrochemiluminescence, electrochemistry, luminescence and Raman spectroscopy.Here a switchable ECL surface has been investigated, which can useful in determining DNA binding and hybridization events. Evidence of DNA binding to $[Ru(dppz)(bpyArCOOH)_2]^{2+}$ was observed from the

voltammetry and the Raman studies. The voltammetric response of the monolayer upon DNA binding showed a shift to more positive potentials, was also accompanied by a significant decrease in the current.

The luminescence studies of $[Ru(dppz)(bpyArCOOH)_2]^{2+}$ monolayer in the presence of DNA displays the light switch characteristic as in the presence of DNA, a 50% increase in the luminescence. Similarly ECL investigations also showed that DNA binding enhances the ECL of $[Ru(dppz)(bpyArCOOH)_2]^{2+}$ .The ECL efficiency of the monolayer alone is 0.018 ±0.02 % and upon DNA binding the ϕ_{ECL} it is significantly enhanced to 0.20 ± 0.01 %. The ECL light switch behaviour is ascribed to the intercalation that shields the phenazine nitrogens of $[Ru(dppz)(bpyArCOOH)_2]^{2+}$ from the solvent.

One of the key finding from the work is that intercalative binding takes place between the DNA and the monolayer, as the ionic strength studies showed increasing the NaCl concentration between 0.2 M to 0.6 M hardly changed the ECL intensity of the $[Ru(dppz)(bpyArCOOH)_2]^{2+}$ -DNA. The concentration dependent studies showed that ECL intensity increases linearly with increasing DNA concentration up to 80 µM, above this concentration the ECL plateaus indicating that Ru binding sites are depleted. The DNA saturation experiments also revealed that the association constant of 2.56 $x10^4$, which suggests that the DNA is not strongly bound to the complex on the electrode. Finally, it is clear from ECL studies that the 1.2 V process is the one responsible for proving ECL active Ru(III) complex. Future work will focus on identifying the set of conditions under which this complex dominates by

investigating in particular the effect of pH on ECL generation. Overall, though dppz complexes look extremely useful as ECL switches for DNA hybridization sensing and in diagnostics. It was recently shown that dppz complexes binds particularly strongly to DNA mismatches and ECL from such complexes may therefore be a means to monitor DNA damage.

4.5. REFERENCES

[1] Johnston, D. H., Glasgow, K. C., Thorp, H. H., *J. Amer. Chem. So*c., **1995**, 8901-8938.

[2] Weltch, T. W., Corbett, A. H., Thorp, H. H., *J. Phys. Chem.*, **1995**, 99, 11757-11763.

[3] Ontko, A. C., Armistead, P. M., Kircus, S. R., Thorp, H. H., *Inorg. Chem*., **1999**, 38, 1842-1846.

[4] Barton, J. K., Goldberg, J. M., Kumar, C.V.,Turro, N. J.,. *J. Amer. Chem. Soc*., **1986**, 108, 2028-2090.

[5] Barton, J. K., Olmon, E. D., Sontz, P. A., *Coord. Chem. Rev*., **2011**, 108, 619-634.

[6] Kumar, C. V., Barton, J. K., Turro, N. J.,. *J. Am. Chem. Soc.*, **1985**, 105, 5518- 5523.

[7] Barton, J. K., Sci., **1986**,233, 727-743.

[8] Shi, L. H., Liu, X. Q., Li, H. J., Xu, G. B., *Anal Chem.*, **2006**, 78, 7330-7334.

[9] Smith, J. A., Morgan, J. L., Turley, A. G., Collins, J. G., Keene, F. R., *Dalton Trans.,* **2006**, 26, 3179-31187.

[10] Jacquet, L., Kelly, J. M., Mesmaeker, A. K., *J. Amer. Chem. Soc. Commun*., **1995**, 9,. 913-914.

[11] Jacquet, L., Dak2vies, R. J. H, Mesmaeker, A. K., Kelly, J. M., *J. Amer. Chem. Soc.,* **1997**, 119, 11763-11768.

[12] Jenkins, Y., Friedman, A. E., Turro, N. J., Barton, J. K., *Biochem*., **1992**, 31, 10809-10816.

[13] Vasudevan, S., Smith, J. A., Wojdyla, M., McCabe, T., Fletcher, N. C., Quinn, S. J., Kelly, J. M., *Dalton Trans*., **2010**, 39, 3990-3998.

[14] Friedman, A. E., Chambron, J., Sauvage, J., Turro, N. J., Barton, J. K., *J. Amer. Chem. Soc*., **1990**, 112, 4960-4962.

[15] McKinley, A. W., Lincoln, P.,Tuite, E. M., Coord. *Chem. Rev.*, **2001**, 255, 2676-2692.

[16] Hiort, C., Lincoln, P., Norden, B., *J. Amer. Chem. Soc*., **1993**,115, 3448-3454.

[17] Haq, I., Lincoln, P., Suh, D., Norden, B., Chowdhry ,B. Z., Chaires, J. B.,. *J. Amer. Chem. Soc*., **1995**,117, 4788-4796.

[18] Nair, R. B., Teng, S. L., Kirkland, S. L., Murphy, C. J., *Inorg. Chem.,* **1998**, 37, 139-141.

[19] Shao, F., Elias, B., Lu, W., Barton, J. K., *Inorg. Chem.*, **2007**, 46, 10187-10199.

[20] Carter, M. T., Bard, A. J., *Bioconjugate Chem*., **1990**,1, 257-263.

[21] Rodriguez, M., Bard, A.J., *Anal. Chem.*, **1990**,62, 2658-2662.

[22] Cadet, J., Weinfield, M., *Anal. Chem.*, **1993**, 65, 675A-682A.

[23] Hu, L., Bian, Z., Li, H., Han, S., Yuan, Y., Gao, L., Xu, G.,. *Anal. Chem,* **2009**, 81, 9807-9811.

[24] Dennany, L., Forster, R. J., Rusling, J. F., *J. Amer. Chem. Soc.*, **2003**,125, 5213-5218.

[25] Lewandowska, H., Sadlo, J.,Meczynska-Wielgosz, S., Stepkowski, T., Wojciuk, G., Kruszewski, M., *Daltons Trans.*, **2015,** 44, 12640-12652.

[26] Wells, R. D., *J. Mol. Biol.*, **1970**, 54, 465-497.

[27] Hartshorn, R. M., Barton, J. K., *J. Amer. Chem. Soc*., **1992**, 114, 5919-5925.

[28] Coates, C. G., Jacquet, L., McGarvey, J. J., Bell, S. E., Al-Obaidi, A. H., Kelly, J. M., *J. Amer. Chem. Soc*., **1997**,119, 7130-7136.

[29] Brennaman, M. K., Alstrum-Acevedo, J. H., Fleming, C. N., Jang, P., Meyer, T. J., Papanikolas, J. M., *J. Amer. Chem. Soc*., **2002**, 124, 15094-15098.

[30] McKinley, A. W., Lincoln, P., Tuite, E. M., *Dalton Trans*., **2013**, 42, 4081-4090.

[31] Zheng, Q., McNally, A., Keyes, T. E., Forster, R. J., *Electrochem. Commun.,* **2006**,10, 466-470.

[32] Walsh, D. A., Keyes, T. E., Hogan, C. F., Forster, R. J., *J. Phys. Chem. B*, **2001**,105, 2792-2799.

[33] Song, N., Concepcion, J. J., Binstead, R. A., Rudd, J. A., Vannucci, A. K., Dares, C. J., Coggins, M. K., Myer, T. J., *Proc. Nat.l Acad. Sci*., **2007**, 112, 4935-4940.

[34] Schwartz, J., Bernasek, S.L., *Catalysis Today.*, **2001**, 66, 3-13.

[35] Forster, R. J., Keyes, T. E., *J. Phys. Chem. B.*, **1998**, 102, 10004-10012.

[36] Fees, J., Ketterle, M., Klein, A., Fiedler, J., Kaim, W., *J. Am. Chem. Soc. Dalton Trans.*, **1999**, 2, 2595-2599.

[37] Browne, W.R., Hage, R., Vos, J.G., *Coord. Chem. Rev*, **2006**, 250, 1653-1668.

[38] Carter, M. T., Rodriguez, M., Bard, A., *J. Amer. Chem. Soc*., **1989**, 111, 8901-8911.

[39] Maheswari, P. U., Rajendiran, V., Stoeckli-Evans, H., Palaniamdavar, M., *Inorg. Chem.*, **2006**, 45, 37-50.

[40] Keyes, T. E., Forster, R. J., Coates, C. G., McGarvey, J. J., Niewenhuyzen, M. N., Figgemeier, E., Vos, J. G., *Inorg. Chem*., **2002**, 41, 5721-5732.

[41] Coates, C.G., Callaghan, P.L., McGarvey, J.J., Kelly, J.M., Kruger, P.E., Higgins, M.E., *J. Raman Spectrosc.*, **2000**, 31, 283-288.

[42] Schoonover, J. R., Bates, W. D., Meyer ,T. J., *Inorg.Chem.,* **1995**, 34, 6421- 6422.

[43] Chang, Y. J., Xu, X., Yabe, T., Yu, S.C., Anderson, D. R. *J. Phys. Chem*., **1990**, 94, 729-736.

[44] Kessler, R. J., Fisher, M. R.,Tripathi, G. N. R., *Chem. Phys. Lett.*, **1984**, 112, 575-579.

[45] Chen, W., Turro, C., Friedman, L. A., Barton, J .K. Turro, N. J.,. *J. Phys. Chem.,* **1997**, 101, 6995-7000.

[46] Benevides, J. M., Thomas, G. J. *Nucleic Acids Res*., **1983**, 11, 5747-5761.

[47] Domke, K.F., Zhang, D., Pettinger, B., *J. Amer. Chem. Soc*., **2007,** 129, 6708-6709.

[48] De Gelder, J., De Gussem, K., Vandenabeele, P., Moens, L., *J. Raman Spectrosc.,* **2007**; 38, 1133-1147

[49] Wang, T., Fan, S., Erdmann, R., Shannon, C., *Langmuir.,* **2013**, 29, 16040-16044.

[50] Dennany, L., Keyes, T.E., Forster, R.J., *Analyst*, **2008**, 133, 753-759.

[51] Xiong, H., Zheng, X., *Analyst*, **2014**, 139, 1732-1739.

[52] Rubinstein, I., Bard, A. J., *J. Amer. Chem. Soc.*, **1981**, 103, 512-515.

[53] Chang, M. M., Saji, T., Bard, A. J., *J. Amer. Chem. Soc*., **1997**, 99, 5399-5403.

[54] Svensson, F.R., Abrahamsson, M., Stromberg, N., Ewing, A.G., Lincoln, P., *J. Phys. Chem.,* **2011**, 2, 397-401.

[55] Luzuriaga, L., Cerda, M.F., *Adv. Bio. Chem.,* **2012**, 2, 262-267.

[56] Huang, R., Wang, L. R., Guo, L. H., *Anal. Acta*, **2010**, 31, 41-45.

[57] Kanoufi, F., Bard, A. J., *J. Phys.Chem*., **1999**, 103, 10469-10480.

[58] Sarwar, T.,Husain, M.A, Rehman, S., ishqi, H.M., Tabish., *Mol. Biosyst.,* **2015**, 11, 522 -531.

[59] Mudasir, W.K., Wahyuni, E.T., Yoshioka, N., Inoue, H., *Biophys. Chem*., **2006**, 121, 44-50.

[60] Tuite, E., Lincoln, P., Nordén, B.,. *J. Amer. Chem. Soc*., **1997**, 119, 239-240.

[61] McKinley, A. W., Anderson, P., Lincoln, P., Tuite, E. M., *Dalton Trans.*, **2012**, 18, 15142-15150.

[62] Ortmans, I., Elias, B., Kelly, J.M., Moucheron, C., Krich-DesMesmaeker, A., *Dalton Trans*., **2004**, 4, 668-676.

[63] Haq, I., Lincoln, P., Suh, D.,Norden, B., Chowdhry, Z. B., Chaires, J. B., *J. Amer. Chem. Soc*., **1995**, 117, 4788-4796.

CHAPTER FIVE:

An ECL Method for Assessment of Metabolic Status of Live Cells

5.1. INTRODUCTION

Real time detection of biological molecules e.g., metabolites emitted by living cells is important in understanding cellular functions in physiology, pathology and in the development of applications for disease diagnosis and drug discovery.[1,[2] The emergence of the field of metabonomics for example has opened the demand for such detection even further.[3] ECL is a fast sensitive and selective means of detecting analytes in real times, so it has significant potential benefits for this field. ECL studies on live cells that have been reported in literature to date mainly focus on the detection and quantifying the cells.[4,5,6]

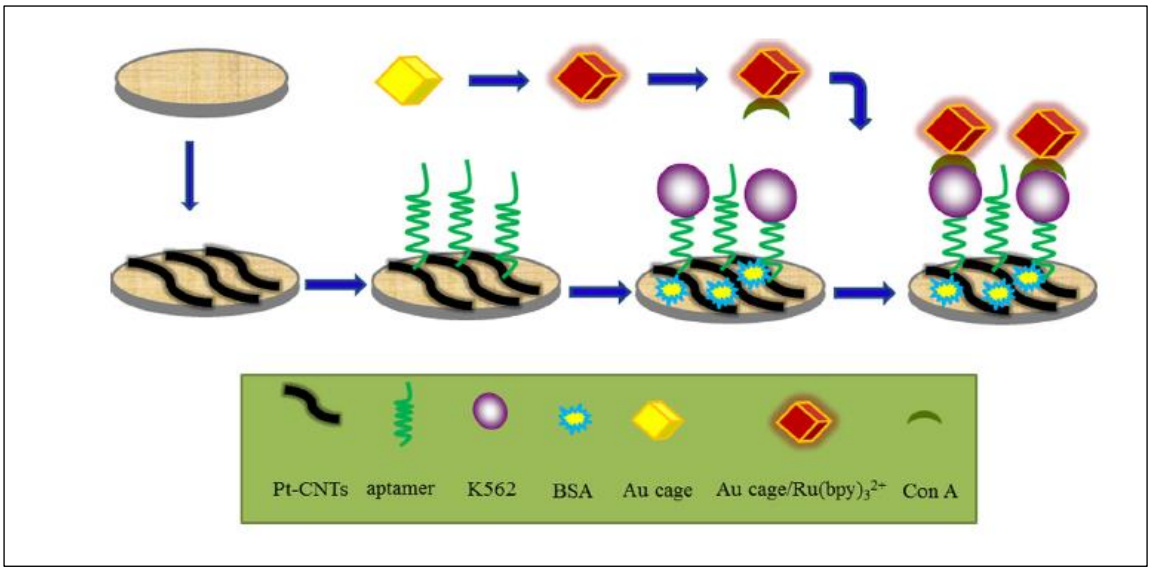

Figure 5.1: The fabrication and detection procedures of an ECL cytosensor. Reprinted from Ge, L., Sub, M., Gao, C., Tao, X., Ge, S., *Sens. Actuators B*, **2015**, 214,144-151.

For example, an ECL cytosensor for ultrasensitive and selective detection of K562 cancer cells was recently developed by Ge and co-workers.[7] As illustrated in Figure 5.1, their approach is analogous to a sandwich assay.

The working electrode was modified with Pt nanoparticles-decorated carbon nanotubes (Pt-CNTs) on which an aptamer was attached to capture the cells. Then Gold cages (with hollow structures) loaded with $[Ru(bpy)_3]^{2+}$ were employed to generate ECL. Using the cytosensor, K562 cancer cells were detected and the ECL intensity was observed to increase quantitatively with an increasing number of cells.[7] In a separate study Ding *et al.*[8] reported an ECL method of detecting Burkitt's lymphoma (RAMOS) cells by functionalizing signal DNA (which was complementary to the Ramos cell-specific aptamer) with $[Ru(bpy)_3]^{2+}$ on a gold electrode. The ECL intensity of the signal DNA that was replaced by the target cells from the ECL probes directly reflected the quantity of cells.[8] In another study an ECL cytosensing strategy was developed for the monitoring of carbohydrate expression in living cells. The cytosensing procedure involved the measurement of the changes in the ECL intensity of carbohydrate-modified CdSe quantum dots as a lectin binds to the carbohydrate.[9] In spite of strong interest in the literature on cell detection by ECL, none of the studies to date involved the investigation of endogenous agents released by living cells in solution and the determination of any analytical parameters of the cells. The present chapter investigates the possibility of using ECL to detect adenosine 5'triphosphate (ATP) from the extracellular matrix from cells.

The detection of such an endogenous metabolite could potentially be used as a marker of metabolic status or to quantitatively report on cell capture by ECL, without need for a coreactant. ATP, it is a ubiquitous energy rich compound in all cells of living organisms and the energy derived from ATP is essential for driving biochemical reactions that are fundamental for the survival of cells.[10] In addition to ATP's role in intracellular metabolism, it is also released by cells into the extracellular matrix where it functions as a primary signaling molecule.[11] It has been previously reported that endogenous ATP and ADP are released into the extracellular milieu through several mechanisms including cell lysis, opening of channel pathways and during the course of normal metabolism through exocytosis of secretory vesicles.[12] It is therefore potentially of value in monitoring metabolic status of living cells.

In animal cells, extracellular ATP is important for several physiological processes such as platelet aggregation; regulation of blood vessel tone; cell growth, aggregation and differentiation; and the functioning of immune cells.[13] The determination of the ATP released from the cells is useful as a quantitative measure of cell metabolism which in turn reports on the cell's health. This chapter reports on a primary investigation into establishing a protocol for the detection of ECL from whole, lysed and captured HeLa cells in solution. Furthermore, how ATP inhibition affects the viability of cells and the ECL detected from the cells will be examined. In this approach self-assembled monolayers of a surface active luminescent metal complex, $[Ru(bpy)_2Qbpy]^{2+}$ (where bpy is 2,2' bipyridyl and Qbpy is 2'2; 4,4"-quaterpyridyl), are formed on gold electrodes by self-assembly and the ATP

secreted by the cells acts as the coreactant.[14] Current methods to establish cell activity rely on chemical methods such as the AlamarBlue assay and this simple ATP assay has the potential to replace such methods providing a facile, reliable, non-invasive and quantitative way to measure cell activity.

5.2. EXPERIMENTAL SECTION

5.2.1. MATERIALS AND REAGENTS

The reagents used in this section were purchased from Sigma Aldrich. The $[Ru(bpy)_2Qbpy)]^{2+}$ shown in Figure 5.2 was synthesized and characterized by Dr Aaron Martin according to a previously reported protocol.[15]

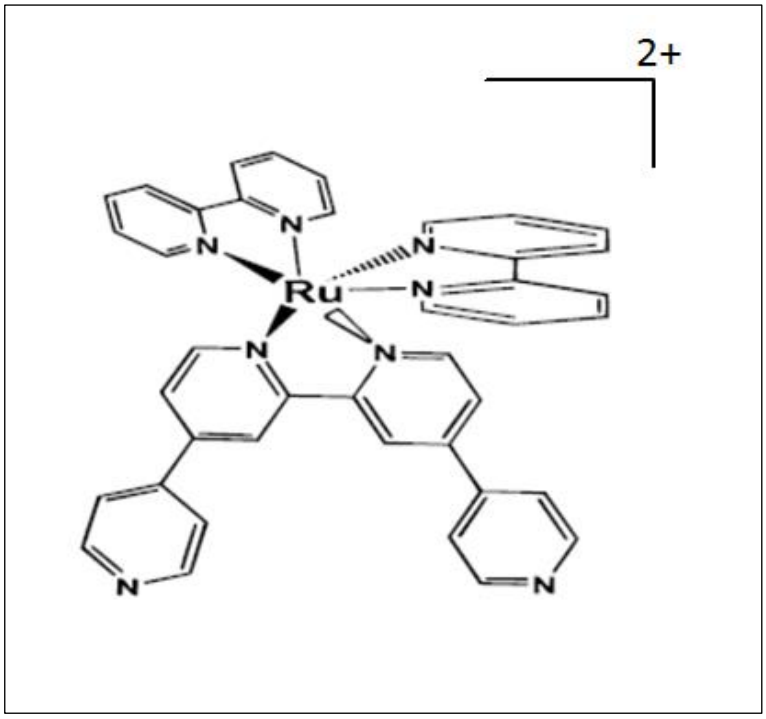

Figure 5.2: Structure of $[Ru(bpy)_2Qbpy)]^{2+}(PF6)_2$

5.2.2. MONOLAYER FORMATION

Monolayers of $[Ru(bpy)_2Qbpy)]^{2+}$ were formed by spontaneous adsorption on gold electrodes following a procedure previously published elsewhere.[16] It involved the immersion of the Au electrodes in a 1 mM $[Ru(bpy)_2Qbpy)]^{2+}$ ethanol/DMF (1:1 V/V) solution for 48 h. Prior to electrochemiluminescence or electrochemistry measurements the electrodes were rinsed with deionised water to remove any unbound material.

5.2.3. CELL CULTURE

HeLa cells, which are adherent human cervical cancer cell line, were kindly provided by Ms Aisling Byrne. The cells were cultured at 37 °C with 5% CO_2 in Dulbecco's modified Eagle's medium (DMEM) supplemented with 10% foetal bovine serum, 1% penicillin and streptomycin, and 2% L-glutamine. Cells were harvested or routinely spilt at 80% confluence in culture dishes. The cells were washed with PBS and 0.25% trypsin was added to the dish which was then placed at 37 °C for 5 min. After the cells were detached from the dishes and pre-warmed culture media was added, the cells were transferred to a falcon tube. The cells were then spun down and plated in new dishes with fresh culture medium prior to measurement.

5.2.4. CELL LYSING

100 µL of deionized water was added to 50000 HeLa cells and left for 15 min for the water to enter the cells. The cells were centrifuged at 4000 rpm for 15 min at room temperature. The lysates were then collected for use in ECL experiments.

5.2.5. CONFOCAL MICROSCOPY

For confocal fluorescence imaging, HeLa cells were seeded at 1.5 x 10^5 cells in 2 mL culture media on poly-L-lysine coated 16 mm cover slips in a 6-well plate and left for 48 h at 37 °C and 5% CO_2. Cells were washed with PBS (supplemented with 1.1 mM $MgCl_2$ and 0.9 mM $CaCl_2$). To enable visualization of the cells, DRAQ 7 (1:100) was added to the cell medium and the cells imaged immediately using a Zeiss LSM570 Meta Confocal Microscope. Cells stained with DRAQ 7 were imaged using a 633 nm HeNe laser and the emission was collected with a long pass 650 nm filter set.

5.2.6. ELECTROCHEMILUMINESCENCE DETECTION FROM CELLS

HeLa Cells were added to 1 mL Dulbecco's phosphate-buffer saline (DPBS) and ECL measurements were carried out at a $[Ru(bpy)_2Qbpy)]^{2+}$-modified gold working electrode. The ECL was monitored at 1 h intervals. In between the measurement, the cells were maintained at 37 °C.

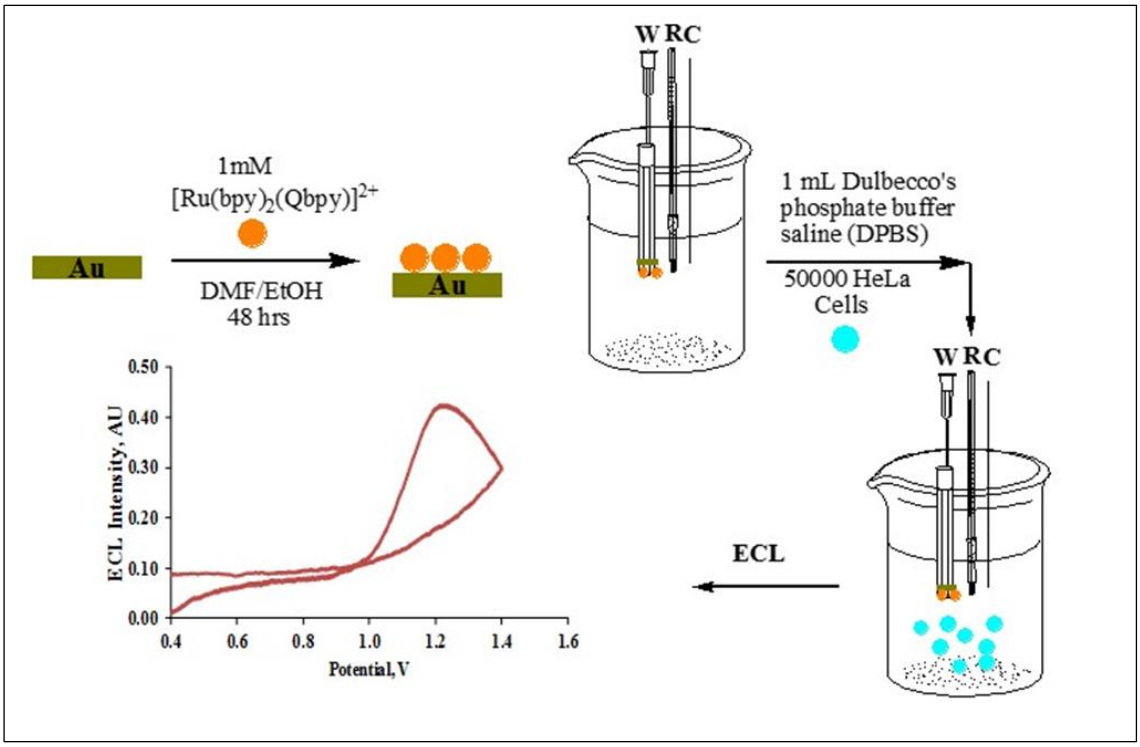

Scheme 5.1: ECL detection from HeLa cells in DPBS, W is the gold working electrode modified with $[Ru(bpy)_2Qbpy]^{2+}$, R is the Ag/AgCl reference electrode and C is the counter electrode.

5.2.7. VIABILITY STUDIES

The effects of the ATP inhibitors, Antimycin A (AMA) and carbonyl-cyanide-4-(trifluoromethoxy) phenylhydrazone (FCCP), on the cell viability were examined using Alamar Blue Assay protocol. HeLa cells were seeded in 96-well plates (Starstedt) at 1 x 10^4 in 100 µL media for 48 h at 37 °C with 5% CO_2. Stock concentrations of AMA and FCCP were made up in DMSO and cell culture to yield final concentrations of 200, 300, 400, and 500 µg/mL. 100

µL of AMA or FCCP was added to each well at 15 min intervals for a total exposure time of 2 h, after which the antibiotics solutions were pipetted out from the cell. For the alamar Blue Assay a 1:10 resazurin reagent was added to the cell media in each well to give a final volume of 100 µL, followed by incubation in the dark for 6 h at 37 °C. Resazurin, which is in its oxidized state in the AlamarBlue reagent, is a non-fluorescent blue coloured substance which gets reduced in the medium by cell activity (were cells are live) in the medium to form resorufin which is pink and fluorescent.[17] The intensity of the resorufin fluorescence is proportional to the number of living respiring cells. Absorbance was measured with a Tecan 96-well plate reader at 570 nm and 600 nm (the latter for background subtraction). Each assay was carried out in duplicate for both AMA and FCCP.

5.2.8. CELL CAPTURE

In preliminary work attempts were made to capture cells at the ECL surface using the approach described in Scheme 5.1 illustrates the chemistry carried out on the electrode surface prior to the capturing of the HeLa cells on the electrode surface. The gold electrodes were initially modified with $[Ru(bpy)_2Qbpy)]^{2+}$ dye for 48 h (as described in section 5.2.2). The electrode was rinsed with water to remove any loosely bound dye. Following metal complex modification, the electrode then back filled by incubating in 1 mM 11-mercapto-1-undercanoic acid (MUA) for 24 h. It was then treated with 0.01% poly-L-lysine (PL) solution which was left in contact with the surface for 1 h

before washing with water. Prior to cell capture, the cells were harvested and spun down at 1200 rpm for 4 min. They were then re-suspended in PBS (supplemented with 1.1 mM $MgCl_2$ and 0.9 mM $CaCl_2$) to yield a final concentration of 1 x 10^6 cells in 100 µL PBS. The Au-$[Ru(bpy)_2Qbpy)]^{2+}$-MUA-PL electrodes were exposed to 50000 cells for 3 h at 37 °C for cell capture.

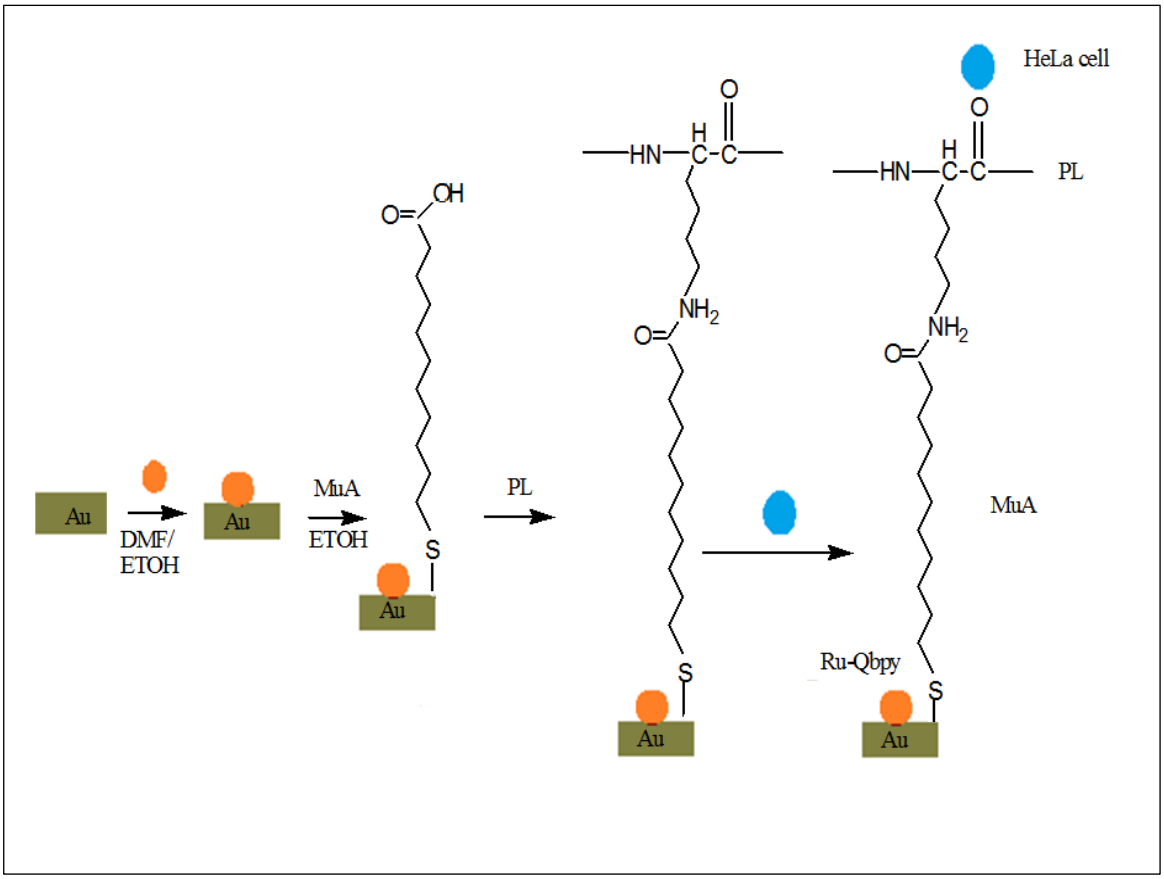

Scheme 5.2: The process of HeLa cell capture on a $[Ru(bpy)_2Qbpy)]^{2+}$-modified gold electrode.

5.3. RESULTS AND DISCUSSION

5.3.1. GENERAL ELECTROCHEMICAL PROPERTIES $[Ru(bpy)_2QBPY)]^{2+}$ MONOLAYERS

The electrochemical and spectroscopic properties of self-assembled monolayers of $[Ru(bpy)_2Qbpy)]^{2+}$ at both gold and Pt surfaces have been studied in our group previously.[18] This complex was selected for this study because of its appropriate oxidation potential and because the monolayers of this material have been shown to be strongly luminescent when bound to Au and Pt surfaces. Herein the complex was assembled at 2 mm gold electrodes and their electrochemical properties were studied before ECL investigations were performed to ensure its behavior conformed to the previous reports. Consistent with previous data the monolayers were formed for 48 h as it has been shown previously that this time scale is required to reach equilibrium surface coverage for micromolar concentrations of the complex. This length scale is required as the complexes have been shown to undergo extensive and slow rearrangement at the metal surface before reaching equilibrium over approximately 36 hours.[18]

Figure 5.3 shows the representative scan rate dependent voltammetric responses for a spontaneously adsorbed monolayer of $[Ru(bpy)_2Qbpy)]^{2+}$ at a gold electrode, where the supporting electrolyte is aqueous 0.1 M $LiClO_4$. The voltammograms display a single reversible redox couple with a formal potential, $E°$, of 1.16 V versus Ag/ AgCl. Typical of RuN_6 complexes, this redox couple with $E°$ value of 1.16 V is attributed to metal based $Ru^{2+/3+}$ redox reaction.[19]

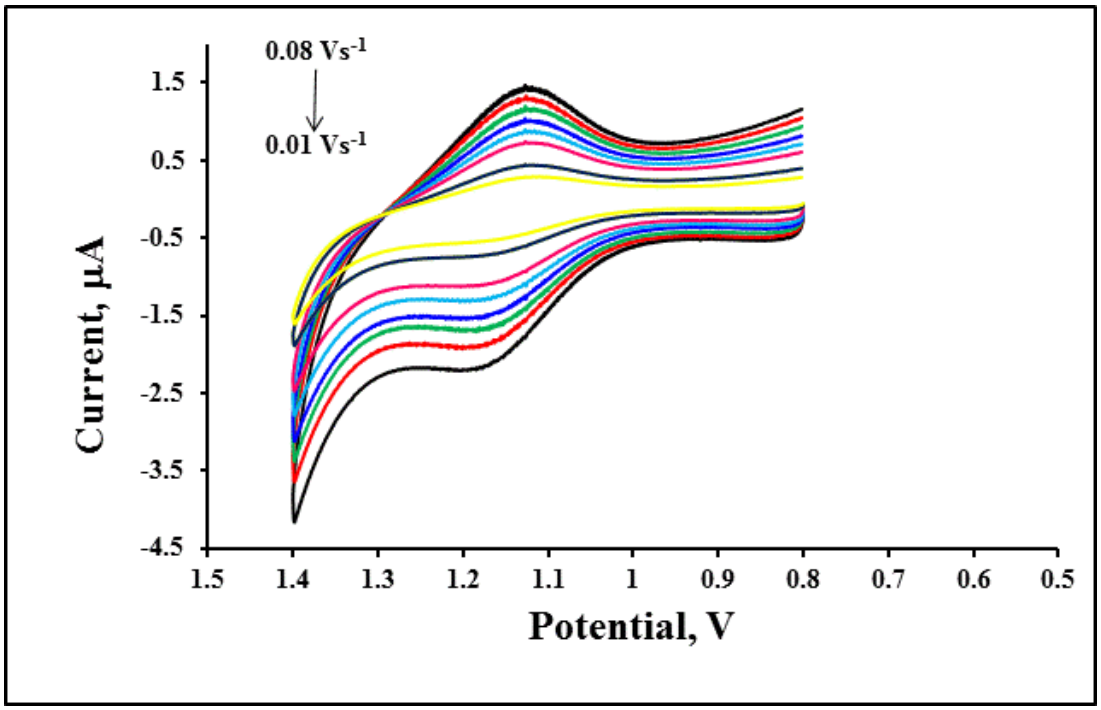

Figure 5.3: Scan rate dependent CVs of $[Ru(bpy)_2Qbpy)]^{2+}$ monolayer on a 2 mm gold electrode, the reference electrode is Ag/AgCl. The supporting electrolyte is 0.1 M $LiClO_4$ and the surface coverage is 4.1 x 10^{-10} mol cm^{-2}. The CVs are plotted incrementally for scan rates of 0.01 V s^{-1} (innermost CV) to 0.08 V s^{-1} (outermost CV) at 0.01 V s^{-1} intervals.

Forster *et al*.[14] previously performed the voltammetry of the $[Ru(bpy)_2Qbpy)]^{2+}$ monolayers and the redox potentials they reported are in agreement with those observed in the present study. From the oxidation peak at 1.15 V, after background correction, the Faradaic charge, *Q*, which originates from switching the $[Ru(bpy)_2Qbpy)]^{2+}$ monolayer from the +2 to +3 oxidation states was estimated and used to calculate the surface coverage, as per equation 1.39 (where *n* is the number of electrons transferred, *F* is the Faraday constant and *A* is the area of electrode).

$$\Gamma = \frac{Q}{nFA} \qquad \textbf{[1.39]}$$

The surface coverage was determined to be 4.1 x 10^{-10} mol cm^{-2} for the $[Ru(bpy)_2Qbpy)]^{2+}$ monolayer formed for 48 h on gold electrodes. Again this is consistent with previously reported surface coverage of this material 1.1 x 10^{-10} mol cm^{-2} has been previously reported for $[Ru(bpy)_2Qbpy)]^{2+}$ monolayers formed on platinum electrodes [15] after 24 h assembly. The increase in the surface coverage in this current study is attributed to better spontaneous adsorption of the dye on gold electrode compared to platinum.

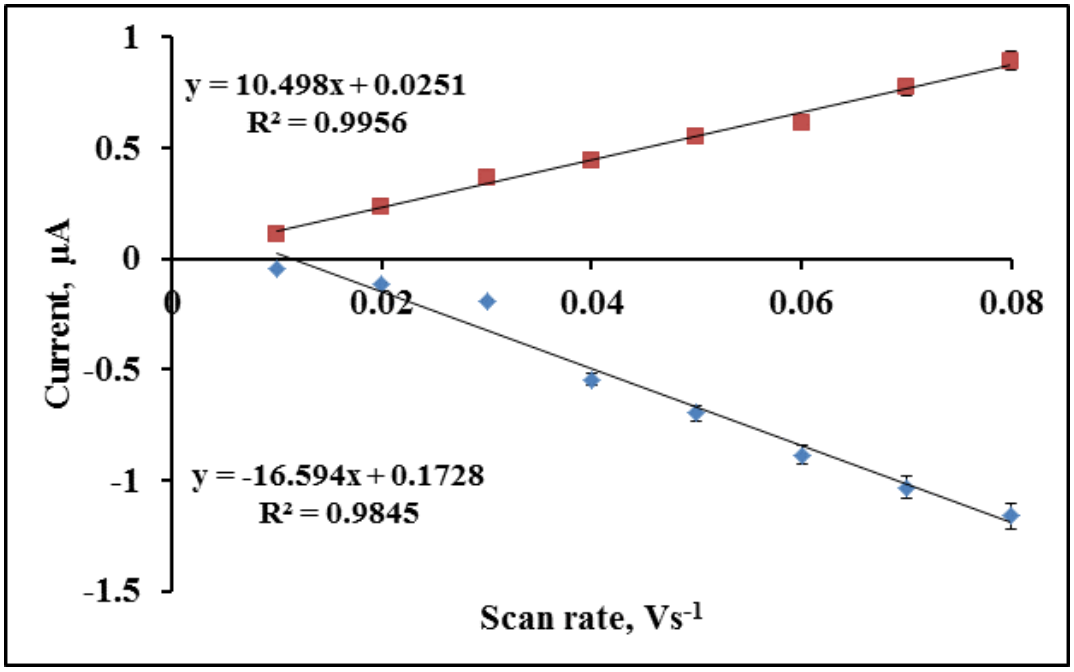

Figure 5.4: The scan rate dependence of the peak current the of adsorbed $[Ru(bpy)_2Qbpy)]^{2+}$ monolayer on a 2 mm gold electrode. The supporting electrolyte is 0.1 M $LiClO_4$.

The voltammetric responses of the monolayer exhibit characteristics of a redox system that is confined to the electrode surface. For example Figure 5.3 shows that at most scan rates, the peak shapes are almost symmetrical and are independent of the scan rate. Figure 5.4 shows that the peak current, i_p, has a linear dependence on scan rate, v, which is consistent with an adsorbed redox species rather than a diffusing reactant where i_p would be expected to have a linear dependence on $v^{1/2}$.

For an ideal redox system confined to an electrode surface, a peak to peak splitting, ΔE_p, of 0 mV and a full width at half maximum (FWHM) of 90.6/n mV (where n is the number of electrons transferred) are expected.[20] However, these conditions hold only when there are no lateral interactions between the adsorbates.[21] In the present instance, at the lowest scan rate of 0.01 V s^{-1}, the peak to peak separation of the cathodic and the anodic peak potentials, ΔE_p, is 26 mV. The monolayer displayed reversible electrochemistry and upon repeated voltammetric cycling for 30 min the peak height and area under the peak centred at 1.15 V do not change by more than 5%, thereby indicating that the monolayer is stable on the electrode.

5.3.2. ELECTROCHEMILUMINESCENCE

5.3.2.1. ATP Electrochemiluminescence

Solution phase ECL experiments were carried out initially to investigate whether adenosine triphosphate (ATP) could be used as an ECL coreactant

to generate excited state $[Ru(bpy)_2Qbpy)]^{2+*}$. To our knowledge this is the first investigation into direct detection of ATP as a coreactant with a ruthenium polypyridyl complex. In other reports of ECL detection ATP the focus has been on the indirect detection of ATP using additional reagents such as quantum dots, potassium persulfate ($K_2S_2O_8$)[22] and DNA aptamers[23] as coreactants. Herein the direct, *i.e.* reagent free, ECL-based detection of ATP was investigated on electrodes that were modified with $[Ru(bpy)_2Qbpy)]^{2+}$ to find out if ATP can be detected directly in PBS.

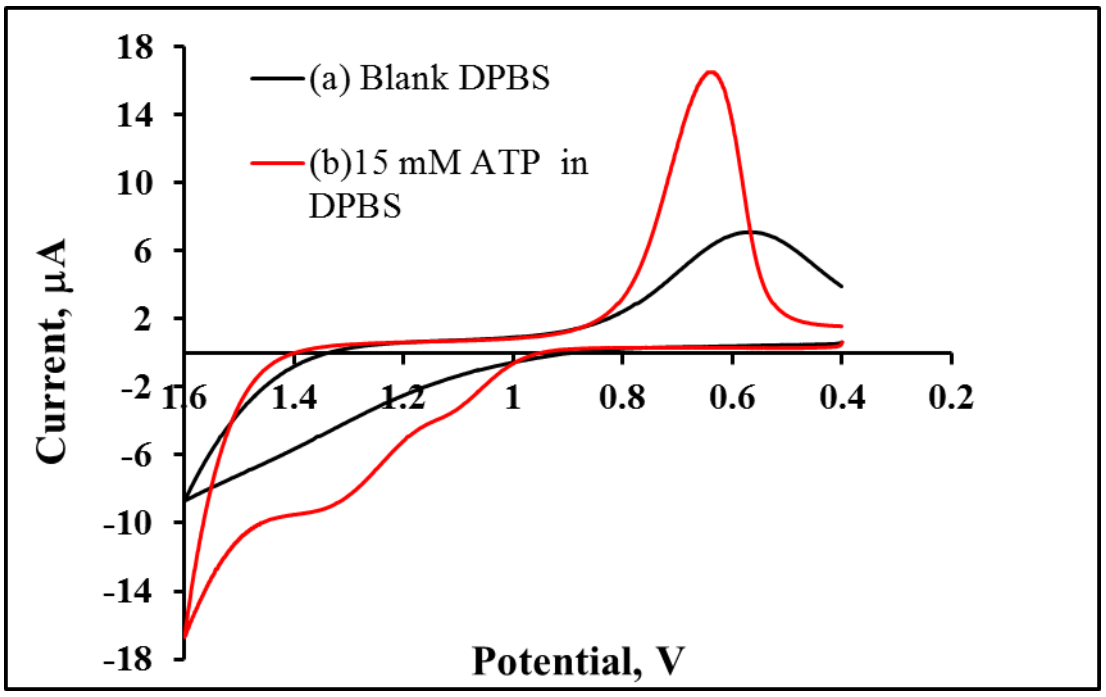

Figure 5.5: CV of (a) 2 mm gold electrode in DPBS and (b) in 15 mM ATP in DPBS at a scan rate of 0.1 V s^{-1}. The reference electrode is Ag/ AgCl

Figure 5.5 shows the cyclic voltammogram of (a) blank gold electrode in DPBS and of (b) 15 mM ATP in DPBS at a scan rate of 0.1 V s^{-1}. The reduction peak observed at 0.7 V is attributed the reduction of gold, while the

two irreversible oxidation peaks observed at 1.07 V and 1.30 V are due to ATP oxidation. Venton and co-workers[24] reported two oxidation peaks at 1.00 V and 1.5 V for cyclic voltammetric characterization of 5 µM ATP in Tris buffer on carbon microelectrodes at a scan rate of 400 mV s^{-1}. In a separate study, Blanco and co-workers[25] reported a single oxidation peak for ATP at 1.2 V in 0.1 M phosphate buffer using pyrolytic graphite working electrodes. They associated this peak to the irreversible oxidation of adenosine. It has been previously reported that the electrochemical signatures of adenosine triphosphate and adenosine are the same.[26] This is because ATP and adenosine have similar purine structures and the adenine moiety is present in both.[27]

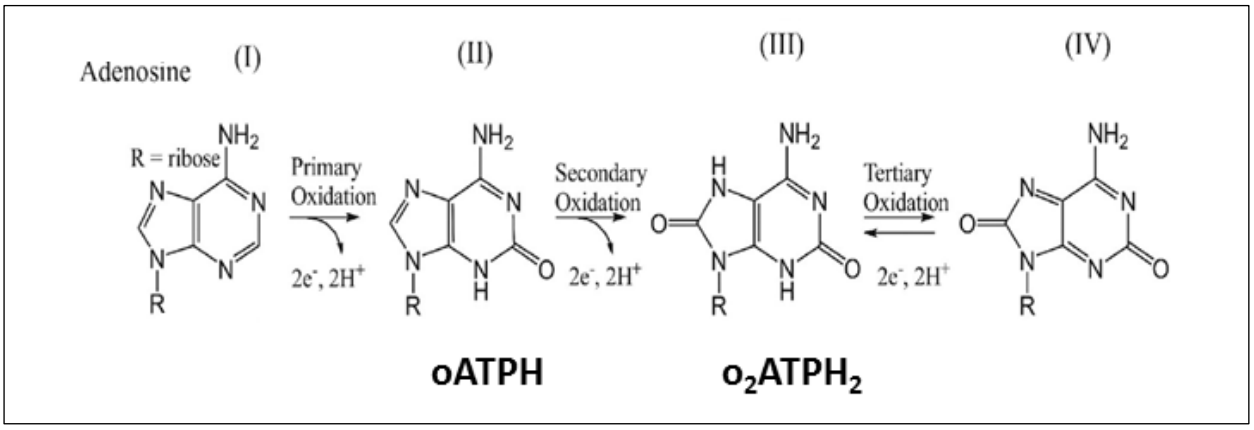

Scheme 5.3: A three step oxidation scheme for adenosine. Adapted from Nguyen, M.D., Venton, B.J., *Comput. Struct. Biotech. J.*, **2015**, 13, 47-54.

Scheme 5.3 presents a three-step reaction scheme that has been previously assigned to the electrochemical oxidation of adenosine and ATP. The two peaks (oxidation peaks at 1.07 V and 1.30 V) which are observed in the CV of

ATP in Figure 5.5 are due to the primary and secondary redox steps indicated in Scheme 5.3.

Figure 5.6 displays the CV of $[Ru(bpy)_2Qbpy)]^{2+}$ monolayer in DBPS, which is the buffer that would be used for investigating the ECL of ATP as a possible coreactant for the ruthenium complex. The CV observed in DPBS is similar to that obtained when the $[Ru(bpy)_2Qbpy)]^{2+}$ monolayer was characterized in aqueous $LiClO_4$. The CV obtained in DPBS has a single redox couple with a kformal potential of 1.14 V, which is not significantly different from the 1.16 V observed in $LiClO_4$.

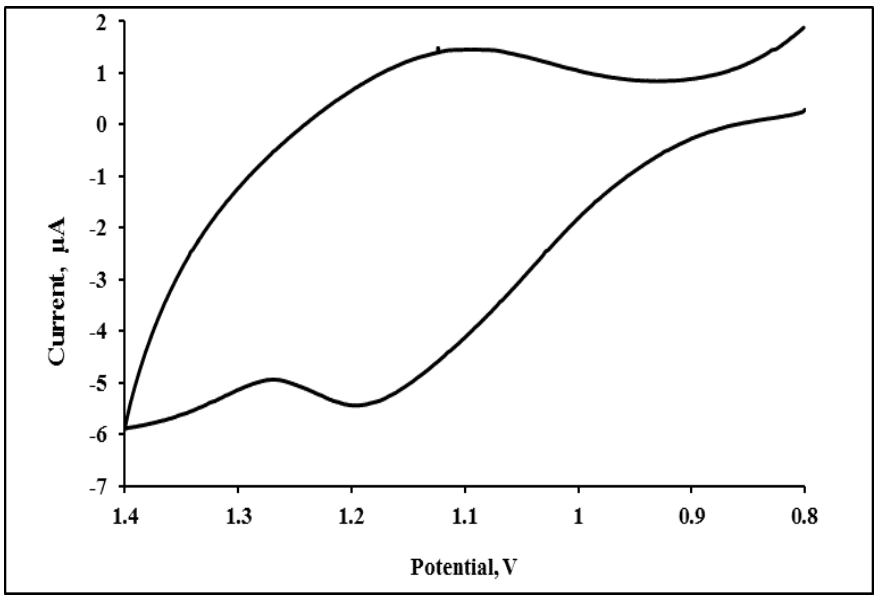

Figure 5.6: CV of $[Ru(bpy)_2Qbpy)]^{2+}$ monolayer on 2mm gold electrode in DPBS, the reference electrode is Ag/Ag Cl. The scan rate of 0.1 V s^{-1}.

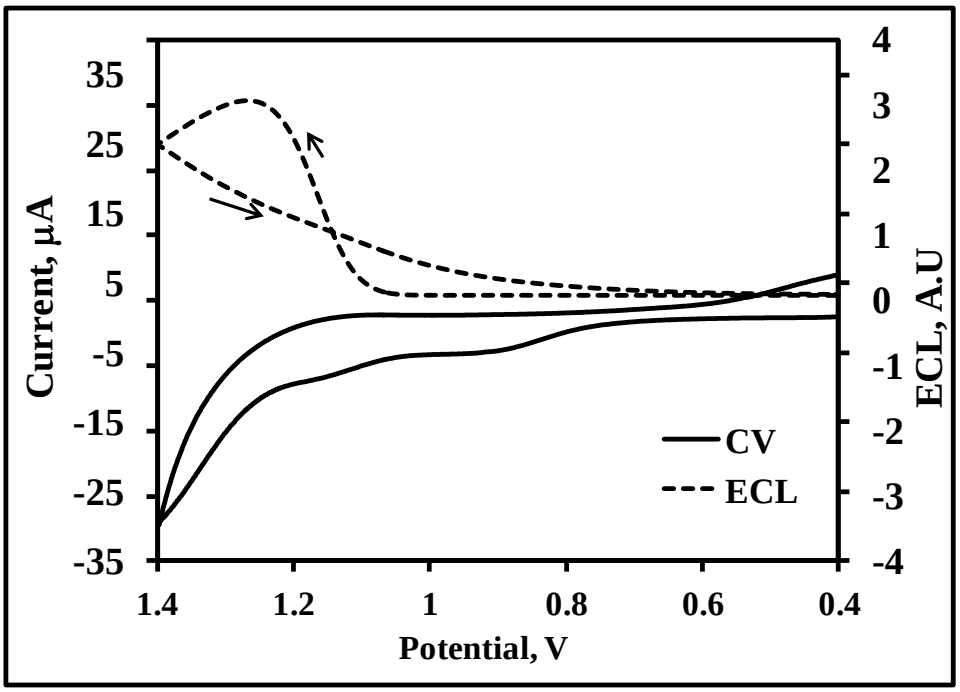

Figure 5.7: ECL and CV of 2mm gold electrode modified with $[Ru(bpy)_2Qbpy)]^{2+}$ monolayer in Dulbecco's phosphate buffer with 15 mM ATP as the coreactant. The reference electrode is Ag / AgCl and the scan rate is 0.1 V s^{-1} and the arrows show the direction of the scan.

Figure 5.7 shows the ECL and CV response from a $[Ru(bpy)_2Qbpy)]^{2+}$ monolayer-modified Au electrode in DPBS containing 15 mM ATP. Importantly intense ECL is generated from the $[Ru(bpy)_2Qbpy)]^{2+}$ in the presence of ATP. The ECL onset is observed at 1.10 V and the ECL maximum potential is observed at 1.25V. The CV indicates the oxidation of ATP at 1.07 V and Ru at 1.15 V, the latter being for the production of Ru^{3+} centers. The peak observed at 0. 91 V is due to the oxidation of ATP on the Au electrode modified with $[Ru(bpy)_2Qbpy)]^{2+}$ monolayer. This peak is equivalent to that observed for the primary oxidation of ATP (see Figure 5.5), but it shifted by ~200 mV to a lower oxidation potential, due to the catalytic effect of the ruthenium dye. It is important to note that there is no coreactant

other than ATP present in the reaction mixture (and the PBS alone does not generate ECL from the monolayer).

The effect of increasing the concentration of ATP on the ECL intensity was investigated. Figure 5.8 and 5.9 show the ECL responses of gold electrode modified with $[Ru(bpy)_2Qbpy)]^{2+}$ monolayer over the range 3 - 15 mM ATP. These concentrations were chosen to reflect the physiological range of ATP concentration which is found in cells.[28]

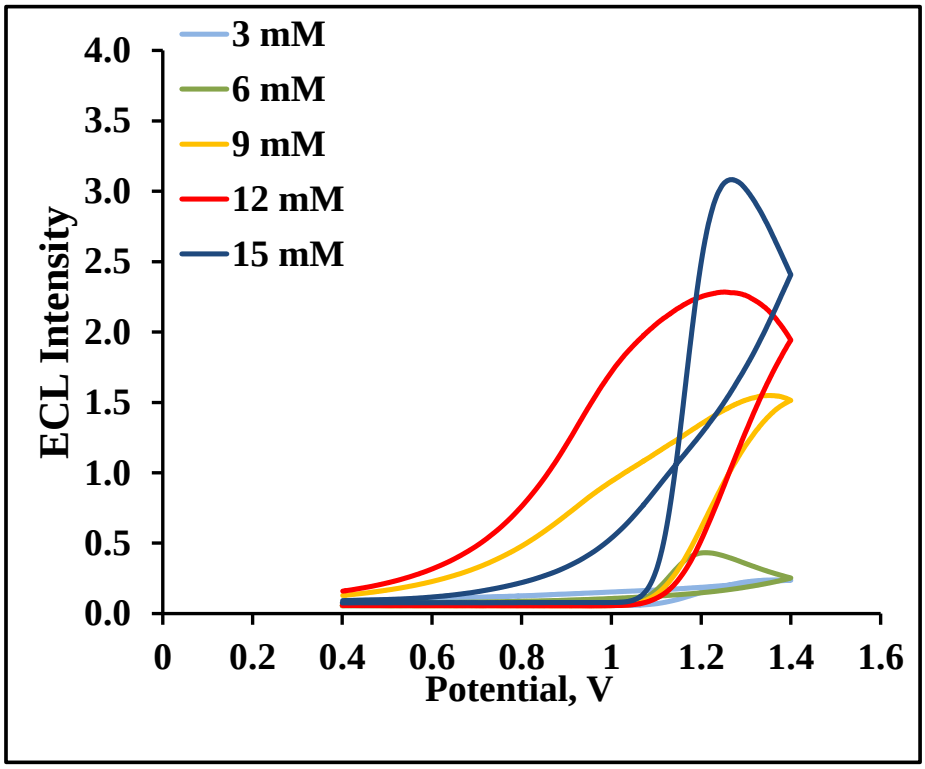

Figure 5.8: ECL of gold electrode modified with $[Ru(bpy)_2Qbpy)]^{2+}$ monolayer in Dulbecco's phosphate-buffer saline containing 3 - 15 mM ATP as the coreactant. The scan rate is 0.1 V s^{-1}.

From the concentration dependent ECL studies, it can be observed from Figure 5.8 that the ECL onset potential for all concentrations is 1.1 V. This suggests that although ATP undergoes three oxidation steps, as shown in

Scheme 5.3, the product of the primary oxidation step is the one which directly contributes to the generation of the $[Ru(bpy)_2Qbpy)]^{2*}$ excited state. This is because the second oxidation product of ATP is formed at a higher potential (1.30 V), and at this potential the ECL is seen to be to decreasing, which indicates the return of the excited state to thke ground state.

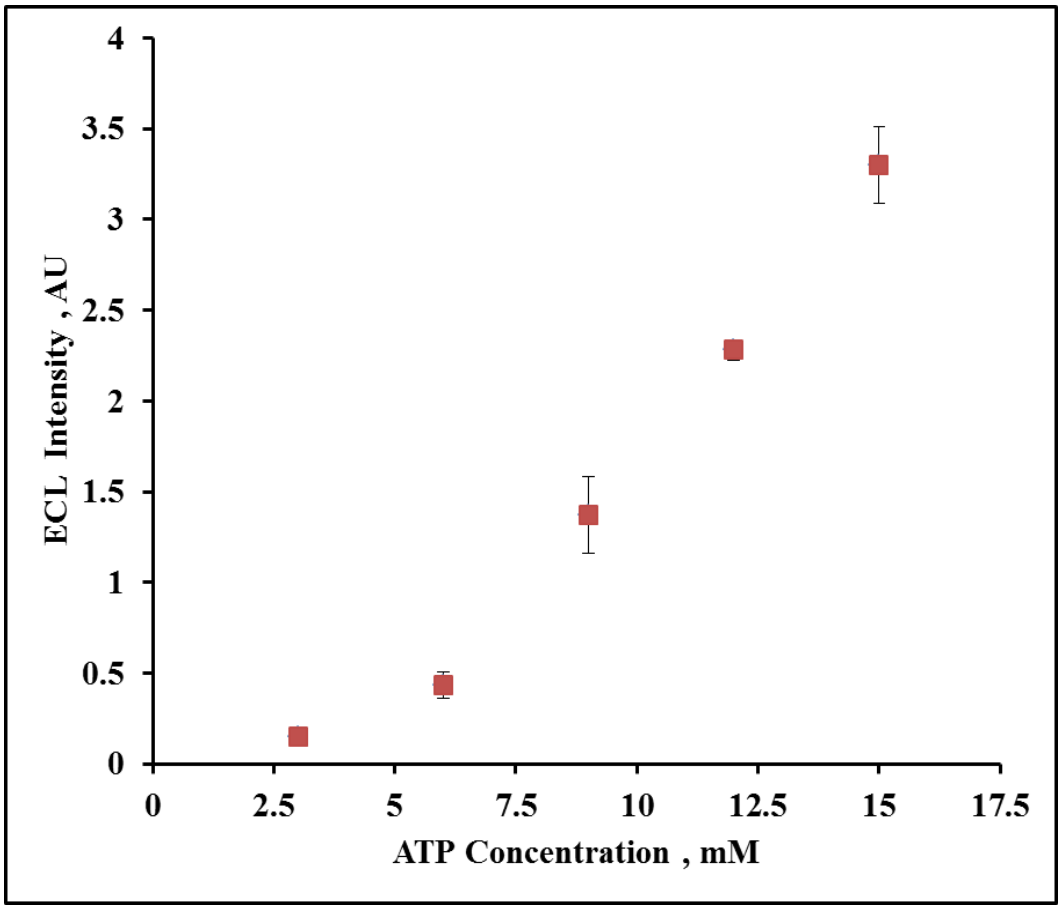

Figure 5.9: ECL maximum intensities of gold electrode modified with $[Ru(bpy)_2Qbpy)]^{2+}$ monolayer in Dulbecco's phosphate-buffer saline, for 3 - 15 mM ATP as the coreactant. The scan rate is 0.1 V s^{-1}. Error bars represent 3 repeats (n = 3).

The ECL intensity increased as ATP concentration increases (Figure 5.9), suggesting that the ECL intensity generated from $[Ru(bpy)_2Qbpy)]^{2+}$ and ATP as a coreactant is dependent on the ATP concentration. This means that the

ECL is driven by the availability of the oATPH (see Scheme 5.3) which react with $[Ru(bpy)_2(Qbpy)]^{3+}$ to generate the excited states, which eventually generate light. Scheme 5.4 represents a proposed mechanism which elucidates the process of how the electrochemiluminescence is generated at the electrode modified with $[Ru(bpy)_2Qbpy)]^{2+}$, with adenosine triphosphate as a possible coreactant. In the proposed mechanism ATP and $[Ru(bpy)_2(Qbpy)]^{2+}$ are both oxidized at the surface of an electrode.

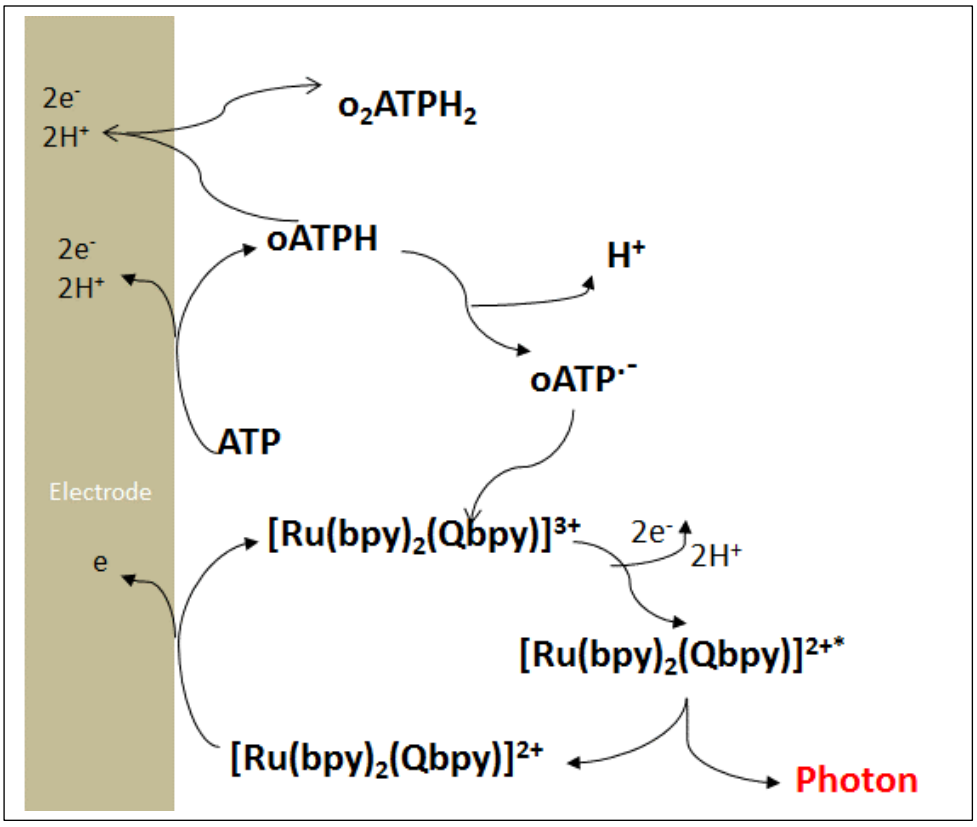

Scheme 5.4: Proposed mechanism for ECL generation on a $[Ru(bpy)_2(Qbpy)]^{2+}$-modified Au electrode using ATP as the coreactant.

Adenosine is an electroactive molecule in ATP structure that can undergoe a series of three two-electron oxidation reactions. Iinitially ATP oxidizes at the electrode to form the primary oxidized ATP structure (oATPH). The oATPH

can also undergo a secondary oxidation to form o_2ATPH_2. The $[Ru(bpy)_2(Qbpy)]^{2+}$ monolayer also oxidises at the electrode to generate $[Ru(bpy)_2(Qbpy)]^{3+}$ sites. The oATPH looses one hydrogen ion to generate the strongly reducing $oATP^{\cdot-}$ radical which reduces $[Ru(bpy)_2(Qbpy)]^{3+}$ to $[Ru(bpy)_2(Qbpy)]^{3+*}$ which emits a photon when it decays to the ground state and regenerates $[Ru(bpy)_2(Qbpy)]^{2+}$.

5.3.2.2. ECL investigation of adenosine diphosphate

Clearly from the study above ATP it is a useful coreactant for ECL generation

coreactant of $[Ru(bpy)_2(Qbpy)]^{2+}$ modified electrode, there are other agents that are released from cells that are redox active that are consired. It is thus important to consider that ATP is often hydrolysed into other adenine nucleotides.[29] ATP can be hydrolysed to adenosine diphosphate (ADP) plus inorganic phosphate, or adenosine monophosphate (AMP) plus pyrophosphate. Moreover ADP often co-exists with ATP in cells and biological tissues.[30] Therefore, these other nucleotides i.e ADP and AMP could possible be capable of acting as coreactants to the $[Ru(bpy)_2(Qbpy)]^{2+}$ monolayer. To explore this possibility, solution phase ECL of ADP, AMP and pyrophosphate were each investigated as possible coreactants with the $[Ru(bpy)_2(Qbpy)]^{2+}$ monolayer. The voltammetry of 15 mM solutions of each of the three nucleotides is compared in Figure 5.10.

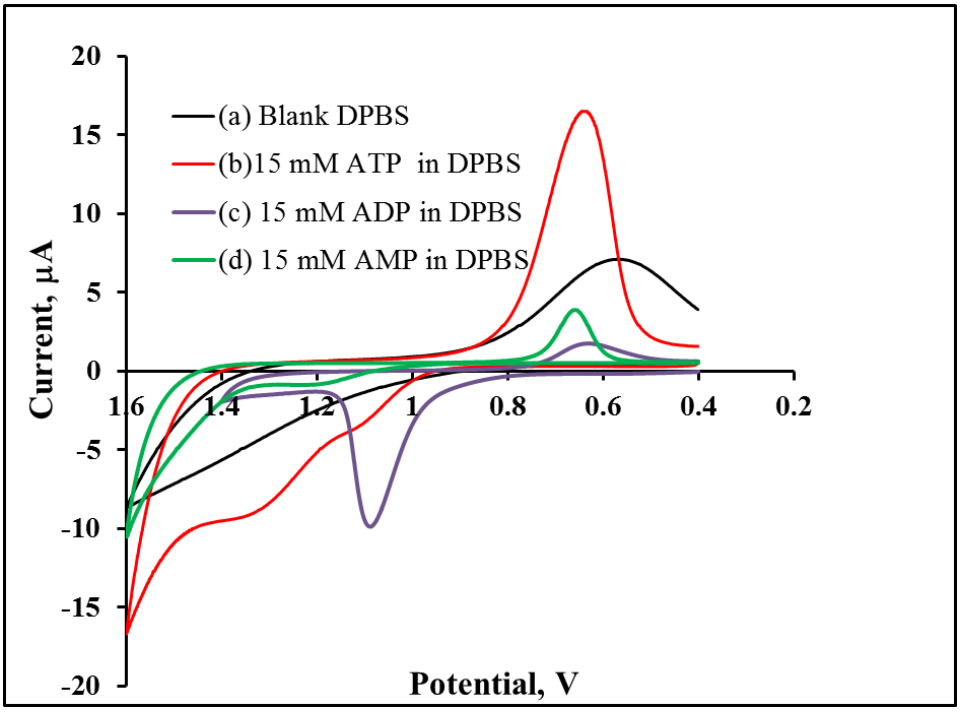

Figure 5.10: CVs of a) DPBS alone, b) 15 mM ATP, c) 15 mM ADP, and d) 15 mM AMP in DBPS at an unmodified 2mm gold working electrode. The reference electrode is Ag/AgCl and the scan rate is 0.1 V s^{-1}.

Figure 5.10 displays the CVs of the three nucleotides in solution using a gold working electrode. The CVs of the mono-, di- and tri-phosphate adenosine molecules indicate that their primary oxidation process occurs at 1.07 V and 1.09 V, 1.2 V, respectively, for ADP, ATP and AMP all leading to the formation of oxidized oATPH, as shown in Scheme 5.3. Adenosine diphosphate also gives ECL when it is used as a co-reactant with $[Ru(bpy)_2Qbpy)]^{2+}$. Figure 5.11 shows the ECL response of $[Ru(bpy)_2Qbpy)]^{2+}$ modified electrode in DPBS containing 15 mM ADP. The ECL onset is observed at 1.07 V, which corresponds to the oxidation potential of ADP as previously observed in Figure 5.10, and the potential for maximum ECL intensity is 1.24 V. A probable conclusion here is that the oxidized adenosine species (oATPH) is

the active co-reactant which drives the ECL in the ADP/ATP-related ECL. It is also important to note that the ECL intensity obtained when ADP is used as a coreactant is less than that obtained from ATP of the same concentration.

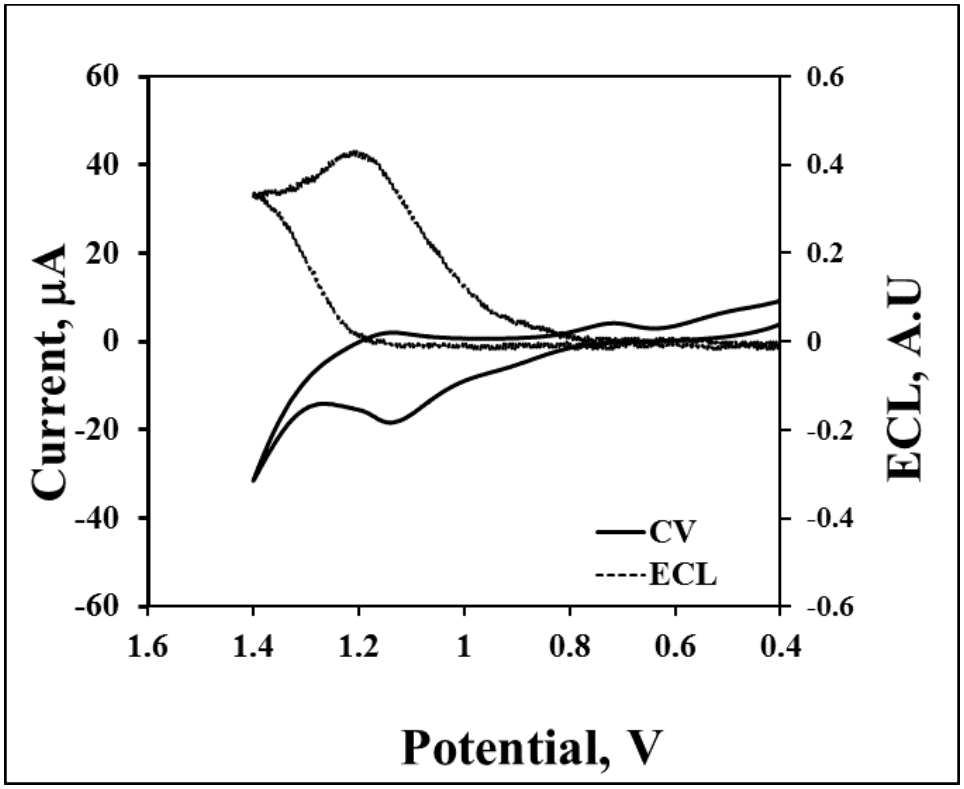

Figure 5.11: ECL and CV of 2mm gold electrode modified with $[Ru(bpy)_2Qbpy)]^{2+}$ monolayer in Dulbecco's phosphate buffer with 15 mM ADP as the coreactant. The reference electrode is Ag/AgCl and the scan rate is 0.1 V s^1.

Adenosine monophosphate did not produce ECL when it was tested as a coreactant with $[Ru(bpy)_2Qbpy)]^{2+}$. It is not clear why this is the case, as it has the adenine moiety which both ATP and ADP have, and the latter molecules have been shown to produce ECL in the presence of $[Ru(bpy)_2Qbpy)]^{2+}$ as a

luminophore. One possible explanation of this result is that the oxidation of AMP occurs at a higher potential value of 1.2 V compared to 1.09 V and 1.07 V, respectively, for ATP and ADP. Thus AMP could not produce ECL because it is oxidized after the oxidation of $[Ru(bpy)_2Qbpy)]^{2+}$ to $[Ru(bpy)_2Qbpy)]^{3+}$, thereby suggesting that the oxidized adenosine drives the ECL and it must be formed prior to the oxidation of $[Ru(bpy)_2Qbpy)]^{2+}$ for ECL to turn on.

The final product of ATP hydrolysis pyrophosphate was also investigated as a possible coreactant. In the current study sodium pyrophosphate was used and the CV is presented in Figure 5.12. The pyrophosphate CV has an oxidation peak at 0.82 V. However, when it was tested as a coreactant with $[Ru(bpy)_2Qbpy)]^{2+}$, it did not give any ECL. This confirms that the phosphate ion is not the species responsible for ECL generation, rather it is the presence of the adenosine moiety (as in both ATP and ADP) that produces ECL.

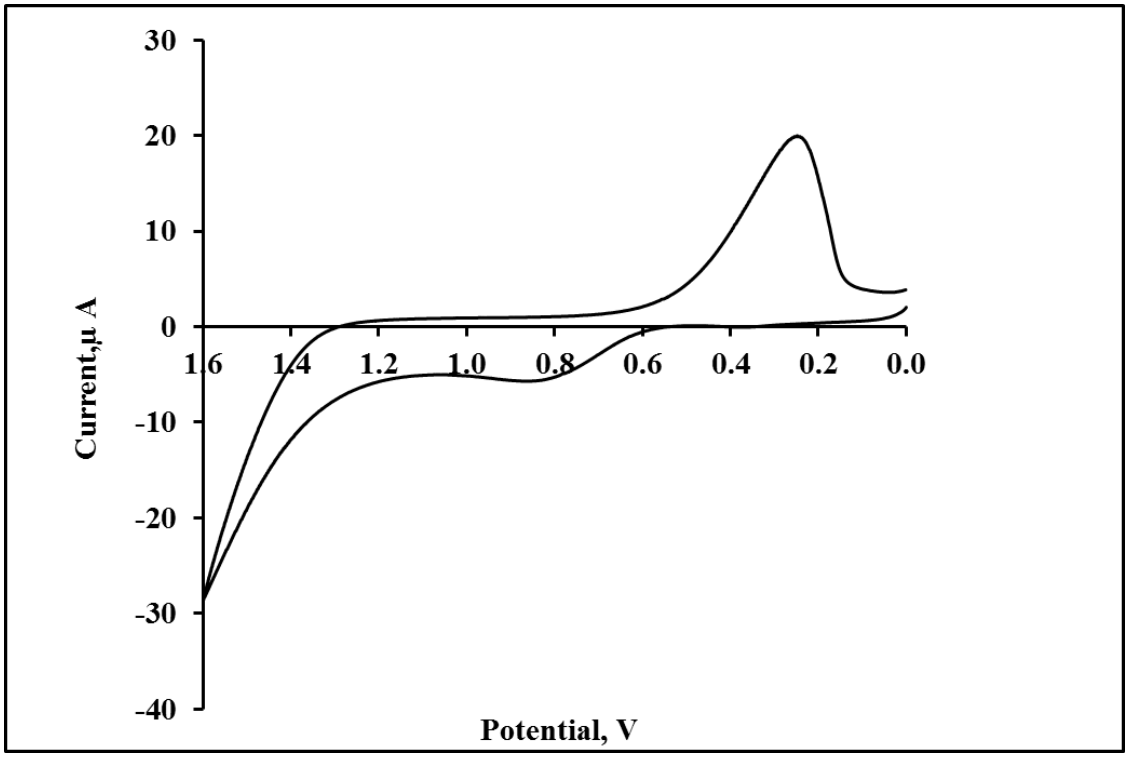

Figure 5.12: The CV of 15 mM sodium pyrophosphate in DBPS, the working electrode is a 2mm gold electrode, the reference electrode is Ag/ AgCl and the scan rate is 0.1 V s^{-1}.

5.3.3. ELECTROCHEMILUMINESCENCE DETECTION FROM CELLS

The solution phase experiments in Section 5.3.2.1 demonstrated that ATP is an effective coreactant for ECL generation $[Ru(bpy)_2Qbpy)]^{2+}$. This section (Section 5.3.3) deals with the detection of ATP-related ECL in living cells (which are known to produce and release ATP in the extracellular matrix). The ECL generated at $[Ru(bpy)_2Qbpy)]^{2+}$ from both lysed cells and living whole HeLa cells in buffer and in cell medium, in the absence of added coreactant is compared.

5.3.3.1. Electrochemiluminescence detection from lysed cells

Electrochemiluminescence was first investigated by lysing cells so that the ECL intensity from the cell content could be measured. Cell lysis was carried out by osmotic lysis whereby the cells were incubated in distilled water. Huguet and Keeling[31] have previously demonstrated that incubating cells in distilled water resulted in 100% lysis after 15 min of incubation with water. In the present The extent of cell lysis was monitored in intervals of 5 min post incubation with water for a total of 15 min by confocal microscopy and the images are presented in 5.13.

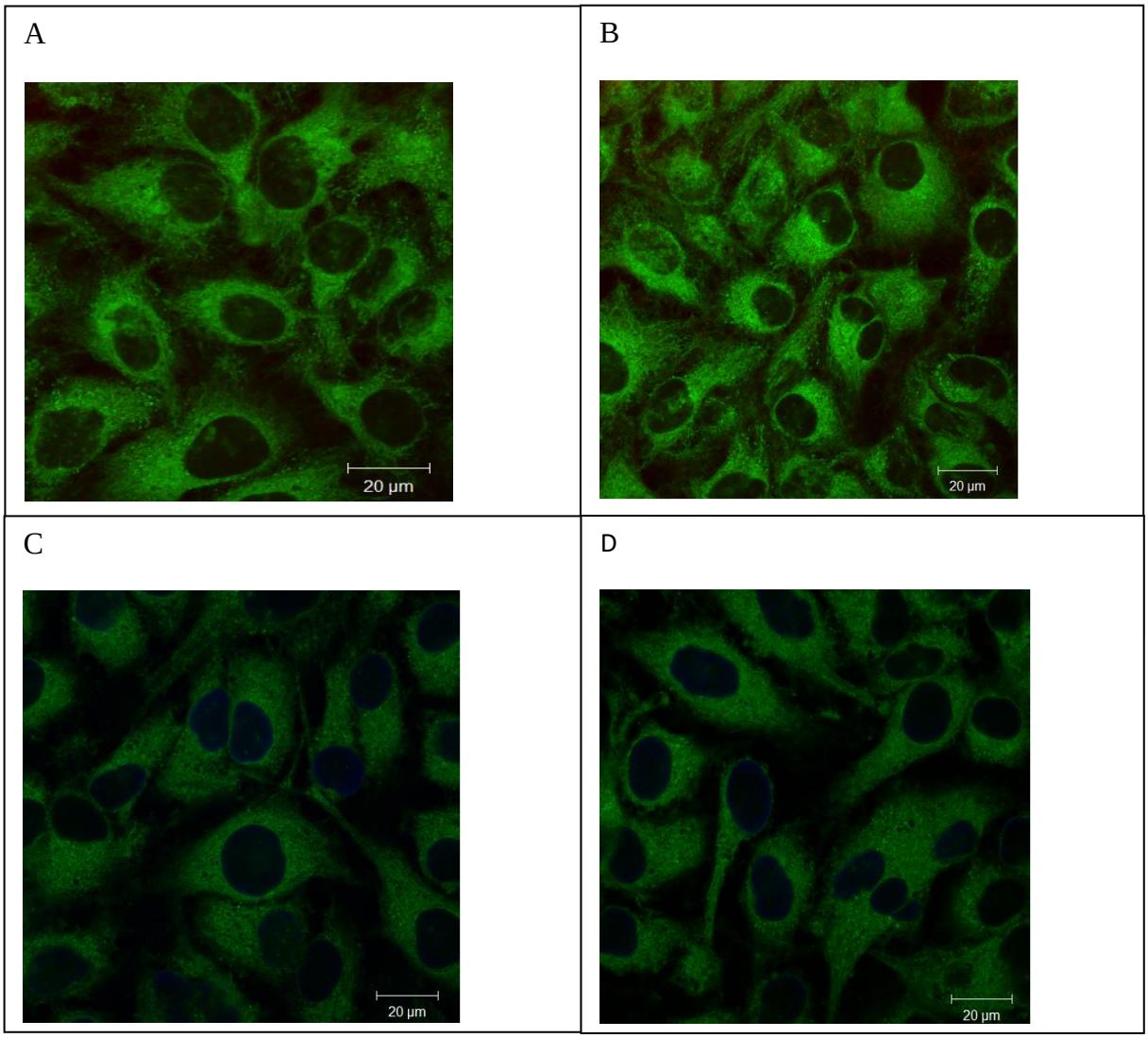

Figure 5.13: Confocal fluorescence imaging of HeLa cells during cell lysing. To visualize the cells on the confocal microscope, they were stained with DiOC6 for 30 min, DRAQ 7 and distilled water was added to the cells at the same time. DiOC6 was excited using 488 nm argon ion laser and the emission was collected using a 505-550 nm band pass filter. DRAQ 7 (1:100 dilution) was excited using a 633 nm HeNe laser and the emission was collected using a 650 nm long pass filter. Figure 5.13 are images of cells (A) before the addition of water; (B), (C) and (D) are images of cells at 5, 10 and 15 min, respectively, after incubation in deionized water.

Figure 5.13 shows the changes in the cells prior to and post exposure to water. It can be seen in Figure 5.13 (A) that before water was added to the cells they displayed characteristics of typical healthy HeLa cells with elongated shapes. The cells are unaffected within 5 min of their exposure to distilled water as shown in Figure 5.13 (B). However exposure to distilled water for 10 min and 15 min as shown in Figures 5.13 (C) and (D), respectively, the water enters the cells by osmosis and results in cell death. This is evident from the localization of the DRAQ7 in the nucleus, which is present in the contacting water. DRAQ7 is normally excluded from viable cells,[32] and it only stains the nucleus of dead and permeabilised cells, as it can only diffuse through the damaged cytoplasmic and nuclear membranes. Having established that it takes approximately 15 min for water to enter and kill the cells, the same lysing procedure was repeated, but this time without staining the cells with DiOC6 or DRAQ7. Once water entered the cells, they were centrifuged and the lysate was collected and added to 1 mL DPBS and their ECL responses were studied, the results are presented in Figure 5.13.

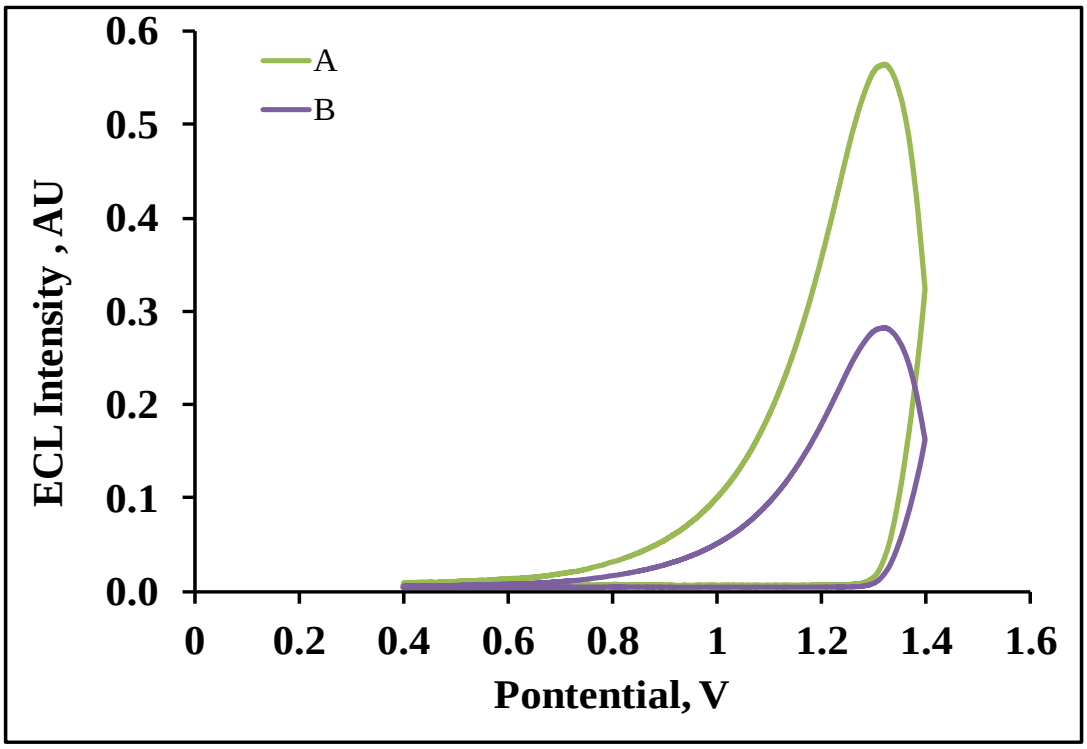

Figure 5.14: Electrochemiluminescence of (A) lysate from 100000 and (B) 50000 HeLa cells in DBPS. The working electrode is a 2 mm gold electrode modified with $[Ru(bpy)_2Qbpy)]^{2+}$. The reference electrode is Ag/ AgCl and the scan rate is 0.1 V s^{-1}.

The results shown in Figure 5.14 show the ECL of the lysate generated at $[Ru(bpy)_2Qbpy)]^{2+}$ modified electrode in contact with lysate from (A) 100000 cells or (B) 50 000 cells without requirement of coreactant. The ECL onset potential is observed at 1.10 V and the maximum ECL intensity is observed at 1.25 V. These result are consistent with the results obtained from the solution-phase ATP studies, suggesting it is ATP and also possibly ADP which is responsible for the ECL signal.

As it took 15 minutes to lyse the cells, the ATP from the lysate is not expected to reflect the ATP concentration of normally metabolizing HeLa cells. Furthermore the lysate has been diluted into 1mL DPBS decreasing the ATP concentration. It is interesting to note however, that the intensity of the ECL signal, at least from this preliminary data is increased proportionately when the number of cells have doubled, though it is important to note that ATP generation and use will have been switched off as the cells died. It would be interesting to compare the ECL intensity by instantaneously lysing cells, e.g. by detergent where metabolism has not slowly diminished as it did in this approach.

5.3.3.2. Electrochemiluminescence from whole cells in Dulbecco's phosphate buffer saline

In a second experiment ECL was measured from the $[Ru(bpy)_2Qbpy)]^{2+}$ modified gold electrode immersed in a solution in contact with live HeLa cells Figure 5.15 shows the resulting ECL signal collected at a scan rate of 0.1 V s^{-1}. The ECL onset potential is observed at 1.10 V and the maximum ECL intensity is observed at 1.25 V. Control experiments carried out with the gold electrode modified with $[Ru(bpy)_2Qbpy)]^{2+}$ in the absence of cells, or unmodified gold electrode in the presence of cells in DBPS did not generate ECL. This suggests that the ECL generation requires both the presence of the $[Ru(bpy)_2Qbpy)]^{2+}$ monolayer on electrode and the cells as the coreactant. The potential at which the ECL is detected, *i.e.* the potential of maximum ECL intensity (1.25 V) for the cells, is similar to the potential for the detection of

free ATP for which the ECL onset potential is 1.10 V and the ECL maximum potential is 1.25 V (see Figure 5.9). Thus the ECL signal obtained with HeLa cells should be due to the detection of the ATP released from the cells into the extracellular medium.

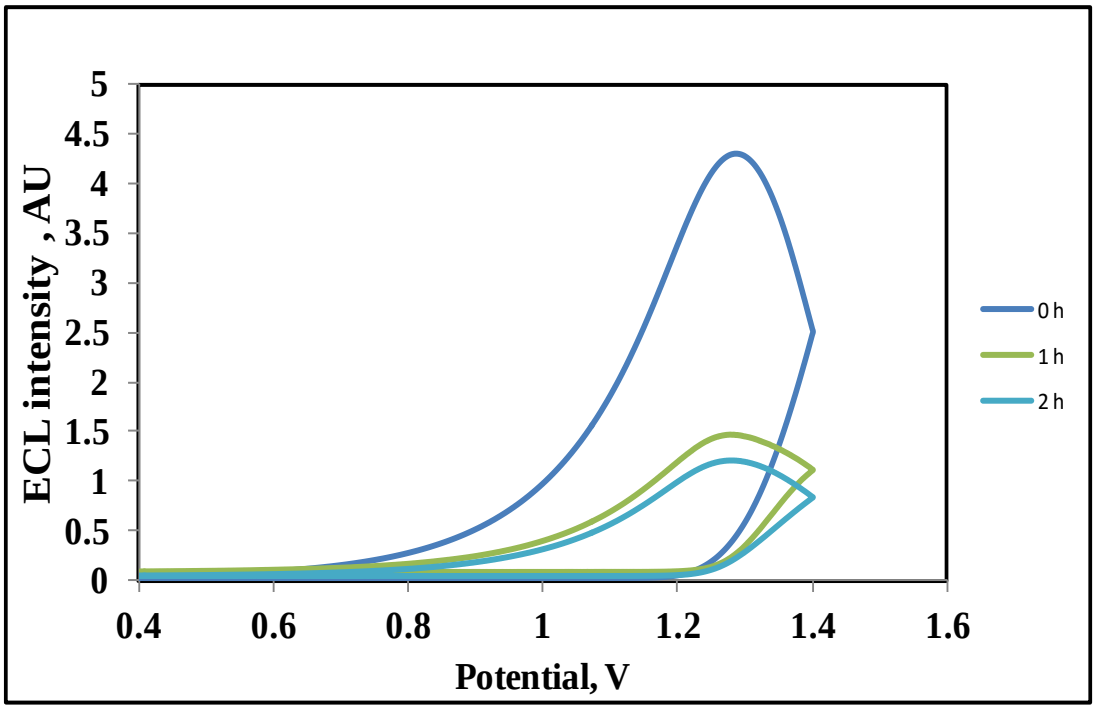

Figure 5.15: Electrochemiluminescence of 50000 intact whole HeLa cells in Dulbecco's phosphate buffer saline. The working electrode is a gold electrode modified with $[Ru(bpy)_2Qbpy)]^{2+}$. The reference electrode is Ag/ AgCl and the scan rate is 0.1 V s^{-1} and the ECL was monitored at 1 h intervals.

In Figure 5.15, the ECL of the HeLa cells in solution was monitored at 1 h intervals. By 1 h the ECL intensity had decreased to approximately 30 % initial intensity and at 2 h to about 20%. After 2 h no ECL was detected and there are two possible reasons to explain this behavior. Firstly, the monolayer on gold the electrode is unstable over the extended period over which these measurements were collected. Secondly the metabolic rate of the cells

decreases and thereby caused a decrease in the ATP output. To assess whether the monolayer was unstable at the electrode over time course of the experiments, the voltammetry and electrode was checked before and after ECL. This is unlikely to occur as $[Ru(bpy)_2Qbpy)]^{2+}$ forms monolayers which are stable on the electrode. This is evident from the cyclic voltammetry of $[Ru(bpy)_2Qbpy)]^{2+}$ in DPBS performed before and after ECL measurements which produced voltammograms (Figure 5.16), the surface coverage of the $[Ru(bpy)_2Qbpy)]^{2+}$ monolayer on the remained relatively unchanged, thereby suggesting that the luminophore was strongly bound to the electrode.

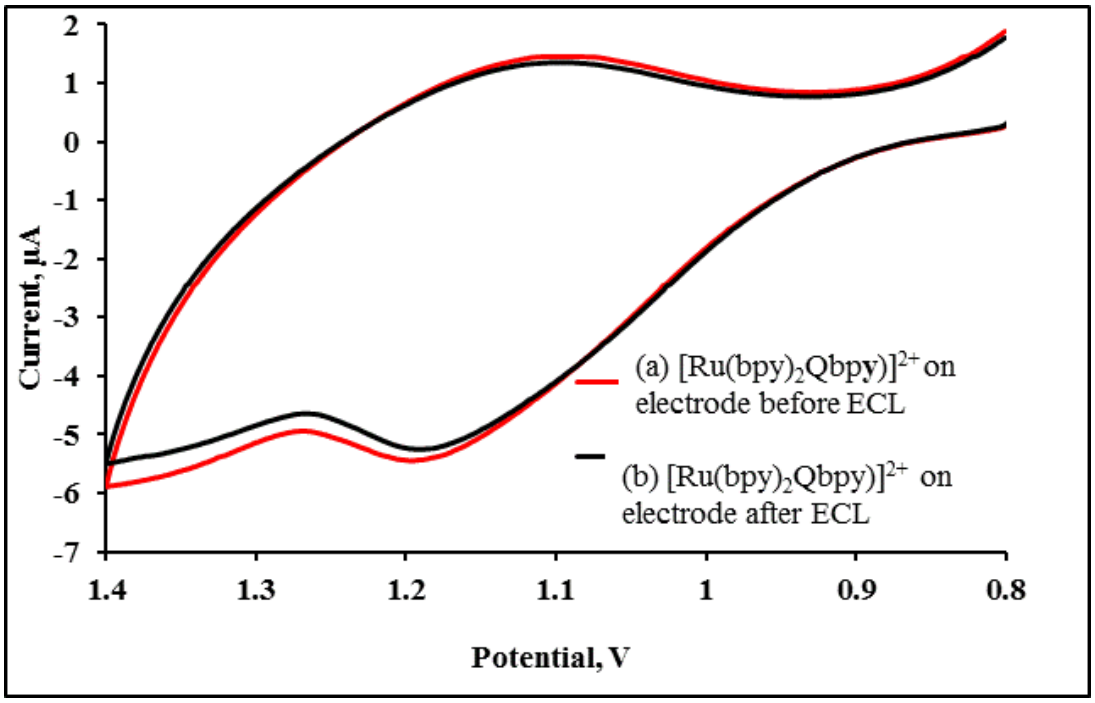

Figure 5.16: The CVs of spontaneously $[Ru(bpy)_2Qbpy)]^{2+}$ monolayer on a 2 mm gold electrode before and after ECL measurement, the is reference electrode Ag/ AgCl. (a) CV before with surface coverage 1. 48 ± 0.2 x 10^{-10} mol cm^{-2} and (b) CV after with surface coverage of 1. 43 ± 0.2 x 10^{-10} mol cm^{-2}. The supporting electrolyte is DPBS and the scan rate is 0.1 V s^{-1}.

To further asses that the monolayer is stable on the electrode Raman spectroscopy of the $[Ru(bpy)_2Qbpy)]^{2+}$ monolayer at the gold electrode was performed before and after ECL experiment described above in Figure 5.15 was compared. The resonance Raman spectroscopy data for the $[Ru(bpy)_2Qbpy)]^{2+}$ monolayer assembled on a gold electrode are presented in Figure 5.17. The sample was excited at 488 nm using an argon laser. This wavelength (488 nm) is resonant with the main metal ligand charge transition of the complex.

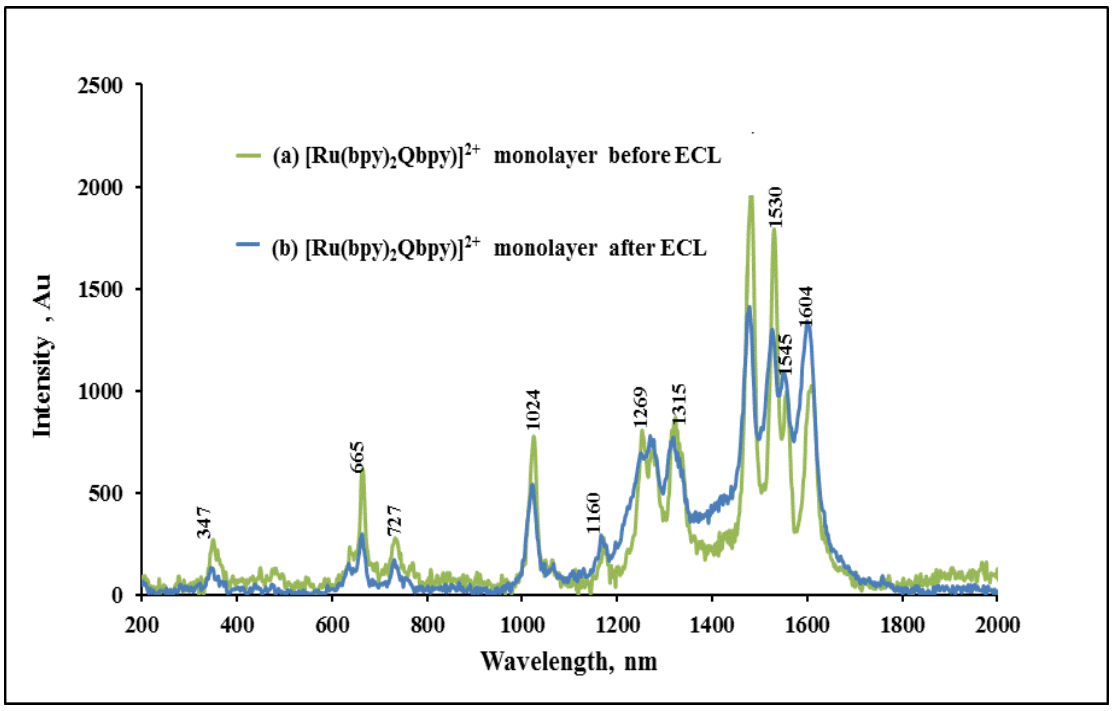

Figure 5.17: The Raman spectra of $[Ru(bpy)_2Qbpy)]^{2+}$ monolayer on a 2 mm diameter gold electrode. Samples were irradiated using argon laser excitation at 488 nm and the laser power was 0.015 mW. The spectra were averaged over 5 acquisitions with an exposure time of 2 s.

It has been previously reported that $[Ru(bpy)_2Qbpy)]^{2+}$ in solid powder form displays its most intense features which are attributed to C-C pyridine stretching modes at 1608, 1560, 1531, and 1487 cm^{-1}.[33] The Raman spectrum matches well to the reported powder correspondingly the most intense peaks from the monolayer are observed around 1604, 1545, 1530 and 1474 cm^{-1} and these are attributed to the pyridine C-C stretching modes. Two modes observed at 1248 and 1315 cm^{-1} are ascribed to C-H deformation, while the feature at 1160 cm^{-1} is attributed to C-H deformation and ring bend mode[34]. Ring vibration modes are represented by the weak modes observed at 1026, 727, and 665 cm^{-1}. Importantly there are no significant differences in the bands or peak intensity Raman spectra of the monolayer after ECL compared to the one acquired prior to the ECL. This indicates that the $[Ru(bpy)_2Qbpy)]^{2+}$ monolayer was stable at the electrode under the conditions of these experiments. Therefore both Raman combined with the CV results indicate that monolayer is stable and intact over the time period of the experiment. Thus it was concluded that it is likely that ATP concentration is decreasing over time.

Decreasing ECL is likely to therefore be related to the falling metabolic rate of the cells as they slowly die in the buffer. The results from this experiment prompted the probing of whether adding extra ATP to the DPBS would lead to an increase in ECL. The test was carried out by adding 15 mM ATP to DPBS and subsequently measuring the ECL response. The results obtained are presented in Figure 5.18 which shows the ECL responses of 50000 HeLa cells in DPBS containing 15 mM ATP.

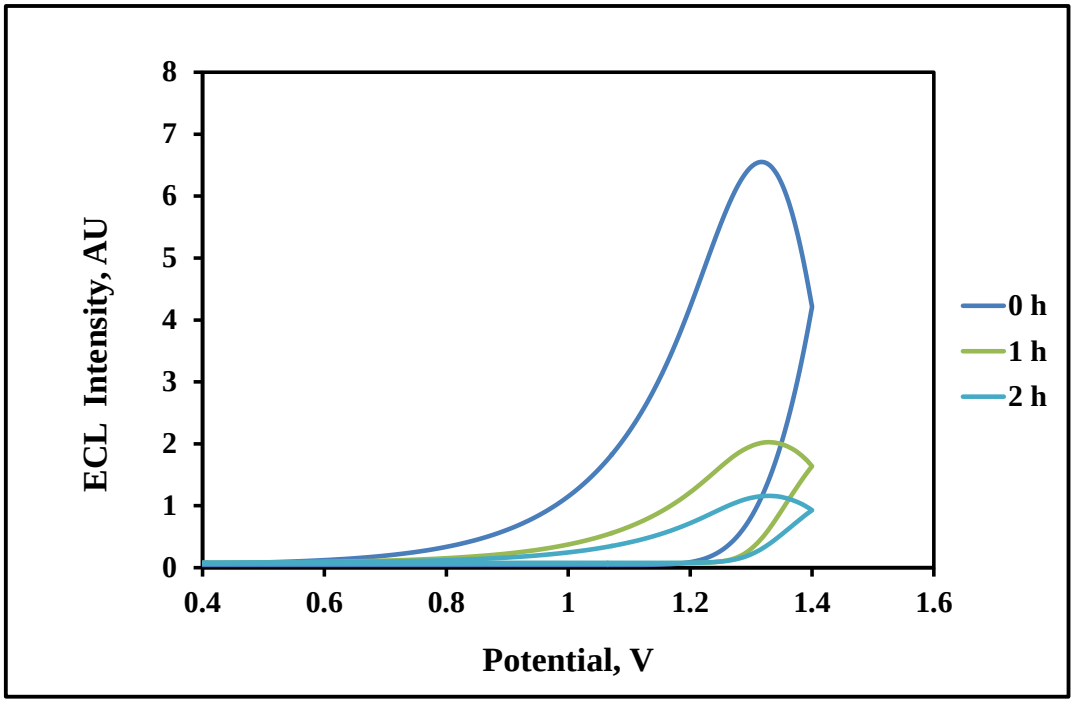

Figure 5.18: Electrochemiluminescence of 50000 whole HeLa cells in Dulbecco's phosphate buffer saline containing 15 mM ATP. The working electrode is a gold electrode modified with $[Ru(bpy)_2Qbpy)]^{2+}$ and the reference electrode is Ag/AgCl. The scan rate is 0.1 V s^{-1} and the ECL was monitored at 1 h intervals.

Figure 5.18 shows the ECL response of 50 000 HeLa cells in DPBS which contained 15 mM ATP. The results indicate that the addition of ATP to DPBS caused an initial increase in the ECL intensity. Furthermore the ECL onset (1.10 V) and maximum intensity (1. 25 V) potentials remained indistinguishable from the ones obtained when the ECL of the cells was measured in DBPS with no added ATP. This suggests that the ATP is the coreactant which is responsible for the observed ECL. However, the decrease in ECL intensity over time is still observed even with additional ATP in the system, and no ECL was observed beyond 2 h. This implies that adding exogenous ATP to DPBS containing HeLa cells does not result in the cells

recovering the ATP that was used up. A comparison of the ECL responses of the HeLa cells presented in Figures 5.15 and 5.18 shows that the addition of exogenous ATP resulted in an initial increase in the ECL intensity (compare the ECL intensities at 0 h). However, there was a clear decrease in ECL intensity with time in the presence and absence of exogenous ATP. One important question that is arises from these results is whether ATP is stable over time in solution.

5.3.3.3. Electrochemiluminescence from whole cells in growth medium

The ECL results above suggest that cellular metabolism and therefore ATP production is decreasing over time under the prevailing experimental conditions (including the use of DPBS as the electrolyte). In DPBS the HeLa cells are likely to be in a metabolically starved condition. Therefore metabolism and ATP production is decreases over time under these conditions. To explore this possibility, ECL of HeLa cells was investigated whilst they were suspended in cell growth media consisting of Dulbecco's modified Eagle's medium (DMEM) supplemented with 10% foetal bovine serum, 1% penicillin, 1% streptomycin and 2% L-glutamine normally used for cell culture. DMEM offers a growth medium environment to encourage cell health and allowing cells to metabolize.

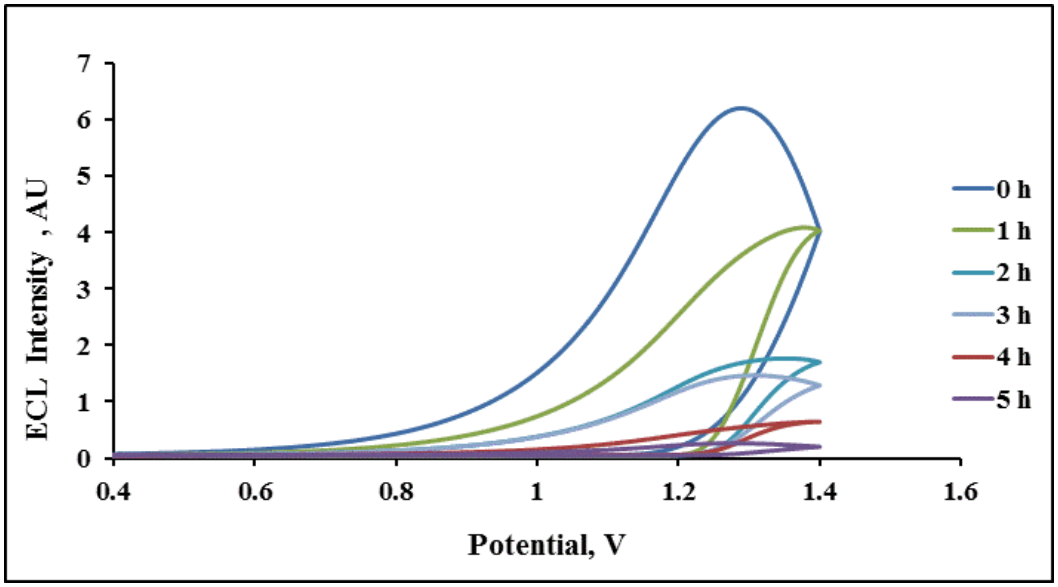

Figure 5.19: Electrochemiluminescence of 50000 HeLa cells in Dulbecco's modified Eagle's medium (DMEM) supplemented with 10% foetal bovine serum, 1% penicillin and streptomycin and 2% L-glutamine. The working electrode is a gold electrode modified with $[Ru(bpy)_2Qbpy)]^{2+}$ and the reference electrode is Ag/AgCl. The scan rate is 0.1 V s^{-1} and the ECL was monitored at 1 h intervals for a period of 5 h.

Figure 5.19 shows the ECL generated from $[Ru(bpy)_2Qbpy)]^{2+}$ monolayer at a gold electrode and whole cells in contact with DMEM (culture medium) at the scan rate of 0.1 Vs^{-1} in the absence of any added coreactant. The onset potential of ECL of the whole cells (Figure 5.19) in the DMEM media is 1.10 V and the maximum intensity occurred at 1.25 V. Again this is consistent with what was observed for the cells in DPBS. Significantly the period over which ECL was detected extended to 5h when the cells were maintained in contact with the culture medium. However, there was a gradual decrease in the ECL intensity with time. The results of the DMEM media experiments suggest that in the culture medium the cells are metabolically active for a longer period compared to when the cells are in contact with DPBS. Therefore culture

medium extends ECL detection from the cells which indicates that the ECL detected is a measure of metabolic activity from the cells. Comparison of the behavior of ATP with the ECL luminophore $[Ru(bpy)_2Qbpy)]^{2+}$ at a gold electrode strongly suggests that it is ATP released from the metabolizing cells into the medium that is acting as a coreactant. However cells are complex systems containing other redox active metabolites which can also act as possible coreactants, including amino acids such as proline and coenzymes such as nicotinamide adenine dinucleotide (NADH).[35]

The ECL responses obtained from HeLa cells originate from the ATP released from the cells. In order to investigate further the hypothesis that the ECL is a consequence of the metabolic activity and that the ATP is the primary coreactant, inhibition studies were carried out to investigate the effect of inhibiting ATP production in the cell. The inhibition experiment consisted of cell viability studies and ECL studies in the presence of an inhibitor in solution.

5.3.4. ATP INHIBITION STUIDES

5.3.4.1. Cell Viability

To investigate the effect of decreasing ATP levels in the cells inhibition experiments were carried by introducing of carbonyl cyanide 4-(trifluoromethoxy) phenylhydrazone (FCCP) or Antimycin A (AMA) to the cell culture medium. AMA and FCCP were chosen as the inhibitors because they target oxidative phosphorylation and thus reduce ATP production.[36]

In parallel cell viability tests were carried out using the the resazurin-based alamarBlue cell viability assay protocol which was applied with varying concentrations of FCCP or AMA.[37] The principle of the assay was described earlier in section 5.2.7, wherein the intensity of the fluorescence is proportional to the number of respiring cells, and this acts as a direct method to quantitatively measure cell viability. The first inhibitor which was is FCCP, which is an ionophore that is a mobile carrier that transports hydrogen ions across the mitochondrial membrane instead of the proton channel of ATP synthase. FCCP transports these hydrogen ions before they can be used to provide the energy for oxidative phosphorylation. Thus it is referred to as an uncoupling agent[38] and one of the major consequences of the uncoupling of oxidative phosphorylation by FCCP is a decrease in ATP concentration.

The cell viability results are presented in Figure 5.20. Cell viability of 85% is observed when cells are treated with 200 µg/mL FCCP after 120 min. The results show that prior to the addition of any inhibitor, *i.e.* at 0 min, the cells are 100% viable and the addition of FCCP exerts effects on the viability immediately. After 20 min of cells being exposed to FCCP, viability decreases to 80 ± 6.6% over the four different concentrations. The greatest cell death was observed for cells treated with 400 µg/mL FCCP, where 67% viable cells was observed after 120 min. The results from the cell viability assay using FCCP as an uncoupling agent in HeLa cells suggest that FCCP causes a limited decrease in ATP in the cells, which appears to be insufficient to cause a significant cell death compared to just leaving the cells alone.

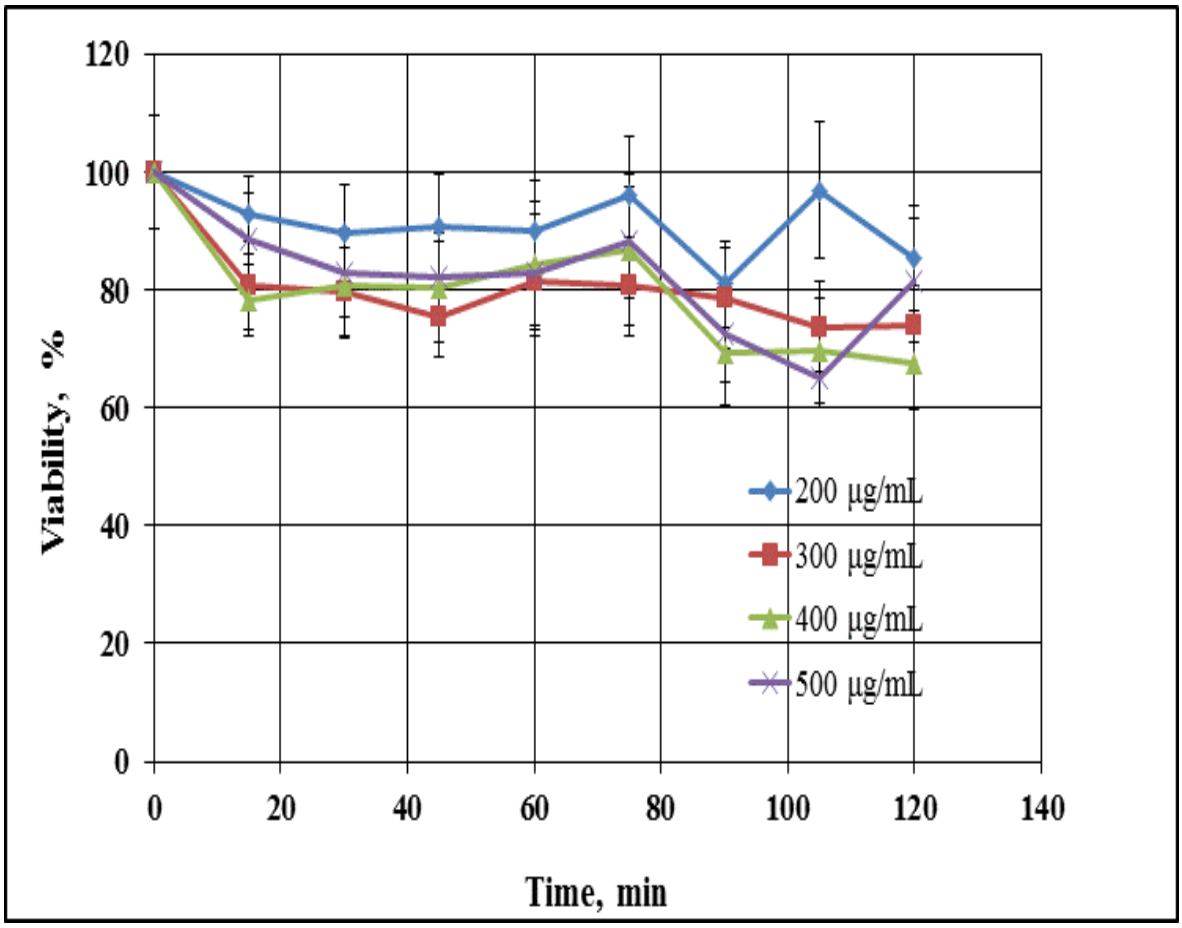

Figure 5.20: Effect of carbonyl-cyanide-4-(trifluoromethoxy) phenylhydrazone (200 - 500 µg/mL) on cell viability. AlamarBlue reagent was used to measure the viability of HeLa cells at intervals of 15 min over 2 h. The error bars represent the standard deviations from two separate experiments (n = 2).

The second inhibitor which was used is Antimycin A (AMA) made up of Antimycin A1 and A3 derived from *Streptomyces kitazawensis* which has been previously used in HeLa cells as an ATP depleting agent.[39,40] Antimycin works by binding to the Qi site of complex III (cytochrome C reductase) and this binding event results in the inhibition of the oxidation of ubiquinol in the electron transport chain of oxidative phosphorylation. As a direct

consequence of inhibiting cytochrome C reductase, proton translocation across the inner mitochondria and subsequently the synthesis of ATP is inhibited. This inhibition process is also known to induce oxidative stress which results in the generation of reactive oxygen species (ROS) that deplete ATP.[41]

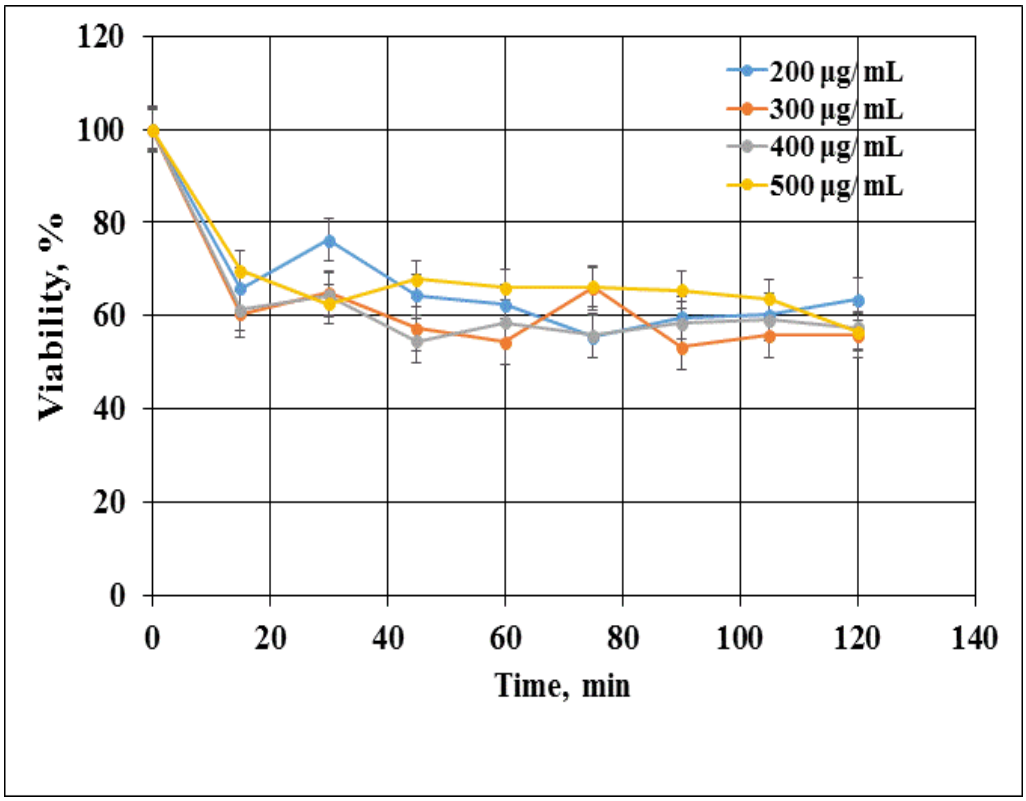

Figure 5.21: Effect of antimycin A (200 - 500 µg/mL) on cell viability. AlamarBlue reagent was used to measure the viability of HeLa cells at intervals of 15 min over 2 h. The error bars represent the standard deviations from two separate experiments (n = 2).

Figure 5.21 displays the viability of cells treated with Antimycin A after 120 min of exposure to increasing concentrations of AMA , 200, 300, 400, 500 ug/mL, there is a significant cell death which is which caused by the inhibition of ATP. The most extensive cell death was observed was 64 ± 5% viable cells

after 20 min for cells treated with and to 57 ± 3.3% after 120 min of incubation with AMA. Tzung *et al.*[42] reported that intracellular ATP levels are decreased by 70 - 75% in cells within 30 min of exposure to AMA. The lowest cell death is observed in cells treated with the lowest concentration of AMA i,e 200 ug/ mL were 63 % of the cells were viable after 120 min AMA exposure. Comparing the responses obtained for cells treated with FCCP (Figure 5.20) and AMA (Figure 5.21), it is clear that AMA is a faster acting and more effective ATP inhibitor, with cell viability being as low as 57% after 120 min. Thus AMA was chosen as the inhibitor for the ECL experiments.

Figure 5.22 shows the ECL responses of 50000 HeLa cells in DPBS in the presence of 400 µg/mL AMA, monitored at 15 min intervals until ECL could no longer be detected. It is expected that ECL will be detected from the AMA-treated cells even though the ATP levels are being depleted. This is because the viability experiments showed that although ATP levels are interfered with, more than 67% of cells are still viable after 1 h. Generally, there are three typical mechanisms of cell death; namely, necrosis, apoptosis and autophagy.[43] When ATP is in short supply autophagy is activated to isolate the damaged cell organelles and cytoplasmic materials in the autolysosomes. Autophagic degradation pathway produces fatty acids and amino acids that can be used to for ATP synthesis to sustain cell survival under ATP deficient conditions.[44] This is probably the reason why 57% of cells are still alive after 2 h under ATP-deficient conditions as demonstrated by the viability assays.

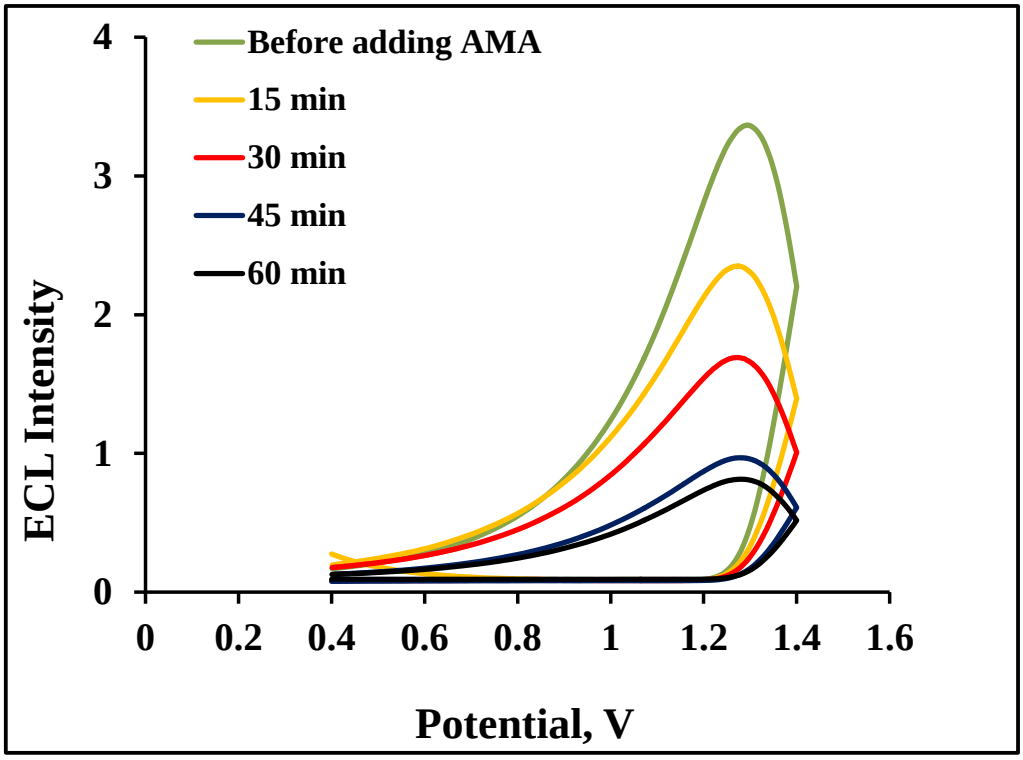

Figure 5.22: Electrochemiluminescence of 50000 HeLa cells in 400 µg/mL antimycin A in DPBS. The working electrode is a gold electrode modified with $[Ru(bpy)_2Qbpy)]^{2+}$, the reference electrode is Ag/AgCL and the scan rate is 0.1 V s^{-1}. The ECL was monitored at 15 min intervals for 1 h.

The ECL spectra in Figure 5.22 show that in the presence of AMA the HeLa cells can produce ECL for up to 1 h but it is characterized by a rapid decrease in the ECL intensity with time. After 1 h no ECL could be generated from the AMA-treated cells, which suggests that the ATP level is too low to be detected. These results confirm that there is a direct correlation between the intensity of ECL detected and the amount of ATP present in the cells and that ECL is not detected in the absence of ATP.

5.3.5. CELL CAPTURE

It was previously mentioned that ECL studies of cells reported in literature mostly focus on detection of cells using sandwich assays. These studies all employ a coreactant such as tripropylamine for the detection cells.[45] In the above studies the metal complex luminophore electrode was simply placed in contact with the cell solution. In this section of the work is a preliminary study that aims to investigate whether a non-sandwich ECL assay for the detection of cells can be implemented from cells which are captured on the electrode solid surface, without adding any coreactant. The first attempt to capture the cells on gold electrodes was carried out by modifying the surface with arginylglycylaspartic acid (RGD) and exposing the modified electrode to HeLa cells. Interestingly, no cells were captured on the surface, though the use of RGD peptide for human endothelial cell adhesion has been demonstrated by other researchers.[46] A possible explanation for the failure of the RGD cell capture protocol can be the effect of the net charge of the peptide and the cells. The cell membrane of HeLa cells and all other cells is negatively charged[47,48] and the RGD peptide is also negatively charged. This may lead to electrostatic repulsion of HeLa cells and the prevention of cell adhesion at pH 7.4. However, it should be noted that this did not prevent other cell lines such as human endothelial,[46] embryonic kidney (HEK293)[49] and human gastric carcinoma (BCG)[50] cells.

A second approach of capturing cells was therefore attempted. This involved using a polycation (poly-L-lysine) to enable cell capture. Kornguth *et al*.[51]

reported that poly-L-lysine binds tumor cells with high affinity. Poly-L-lysine promotes cell adhesion through the enhancement of the electrostatic interaction between the negatively charged phospholipids cell membrane and the surface at which the adhesion is intended to take place. Recently a study which involved the investigation of the adhesion and proliferation of HeLa and fibroblast cells on chemically modified gold surfaces, demonstrated that HeLa cells can adhere to surfaces modified with poly-L-lysine.[52] This approach involves an initial modification of the electrodes with 11-mercapto-1-undecanoic acid (MUA) followed by treatment with poly-L-lysine as shown in Scheme 5.1. Cell capture at gold the surface was evaluated by confocal microscopy using LysoTracker dye as a cellular stain. In order to achieve cell capture, the time at which the cells were exposed to the Au-$[Ru(bpy)_2Qbpy)]^{2+}$-MUA-(Poly-L-lysine) modified gold electrode had to be optimized. Initially the cells were exposed to the electrode for 1 h at 37 °C and the electrodes were evaluated by confocal microscopy. However no cells were observed on the electrode after this period. Figure 5.23 shows confocal microscopy images of the electrode incubated with HeLa cells after 2.5 h. The images confirm that HeLa cells are captured on the electrode after this period. From the 1 million cells which the electrode was incubated with approximately 30 cells were captured on the cell surface. The HeLa cells are healthy and appear to have spread out on the surface and they have assumed the elongated shape which is a typical characteristic of healthy HeLa cells. It should be noted that the cells were stained with LysoTracker green dye in these experiments only for the purpose of visualizing the cells during imaging,

and the cells were not stained with any dye for subsequent electrochemical and electrochemiluminescence experiments.

A

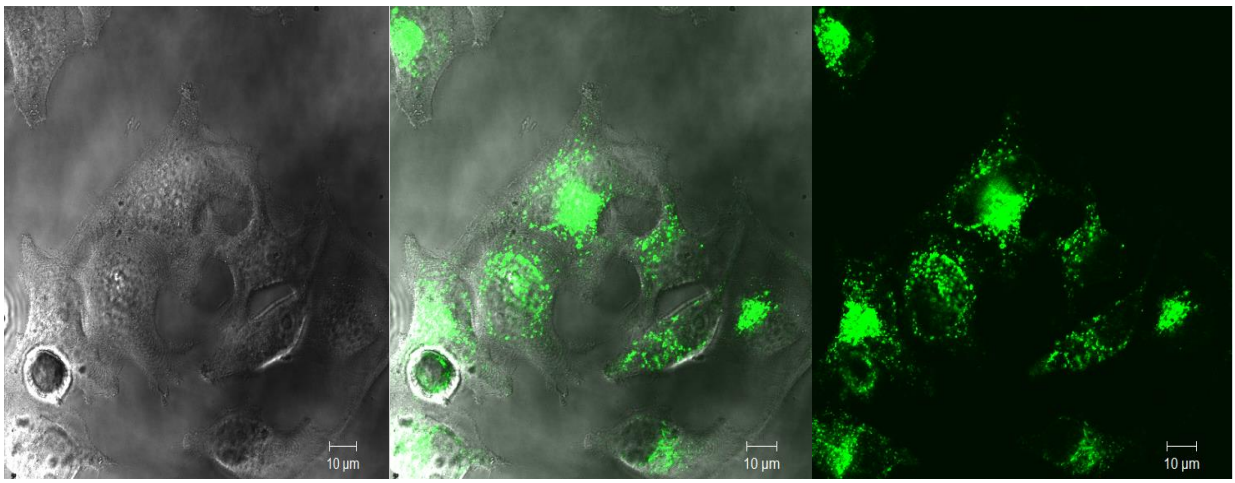

B

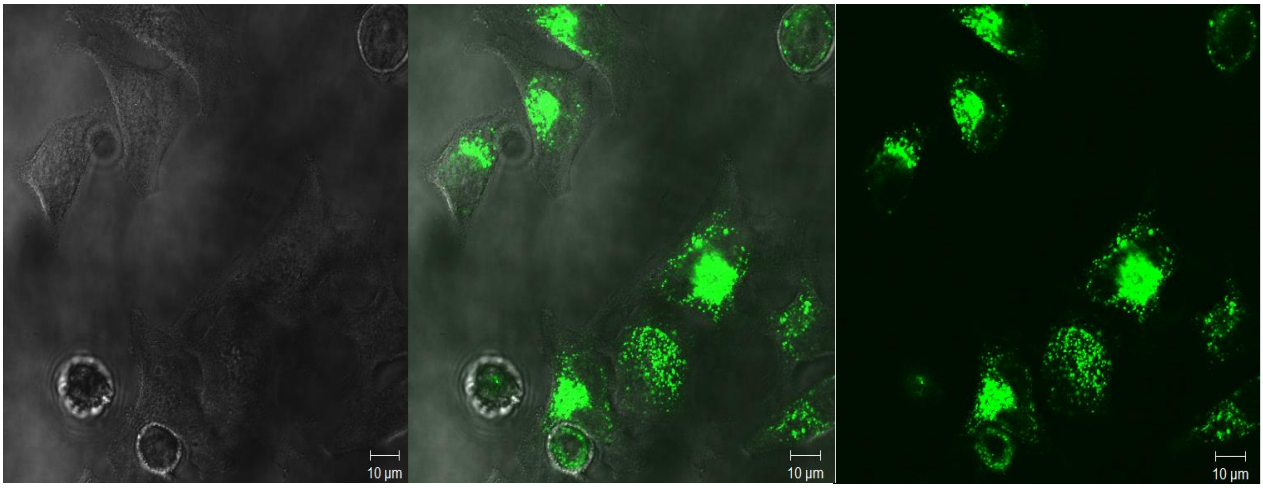

Figure 5.23: Confocal flourescence images of HeLa cells stained with LysoTracker green that are captured on two separate areas (A and B) of the gold electrode modified with MUA-PL. The white light image is shown on the left, the fluorescence on the right and the overlap of both in the middle. LysoTracker green was excited at 488 nm and emission was collected using 505 nm band pass filter. The cells were imaged with a 63 X oil immersion lens.

Having evaluated cell capture by confocal fluorescence imaging, cyclic voltammetry of the electrode systems was carried out to monitor the changes on the electrode prior to any modification and after each of the modification steps leading up to the cell capture. The voltammetry was performed in 1 mM ferrocene methanol (FeMeOH) as an electrochemical probe within a potential range of -0.15 to +0.55 V. Cyclic voltammetry of an electroactive probe solution such as FeMeOH can provide insights into the changes that takes place on the electrode upon surface modification and cell capture.[53] As such modifications reflect changing accessibility of the electrode probe.

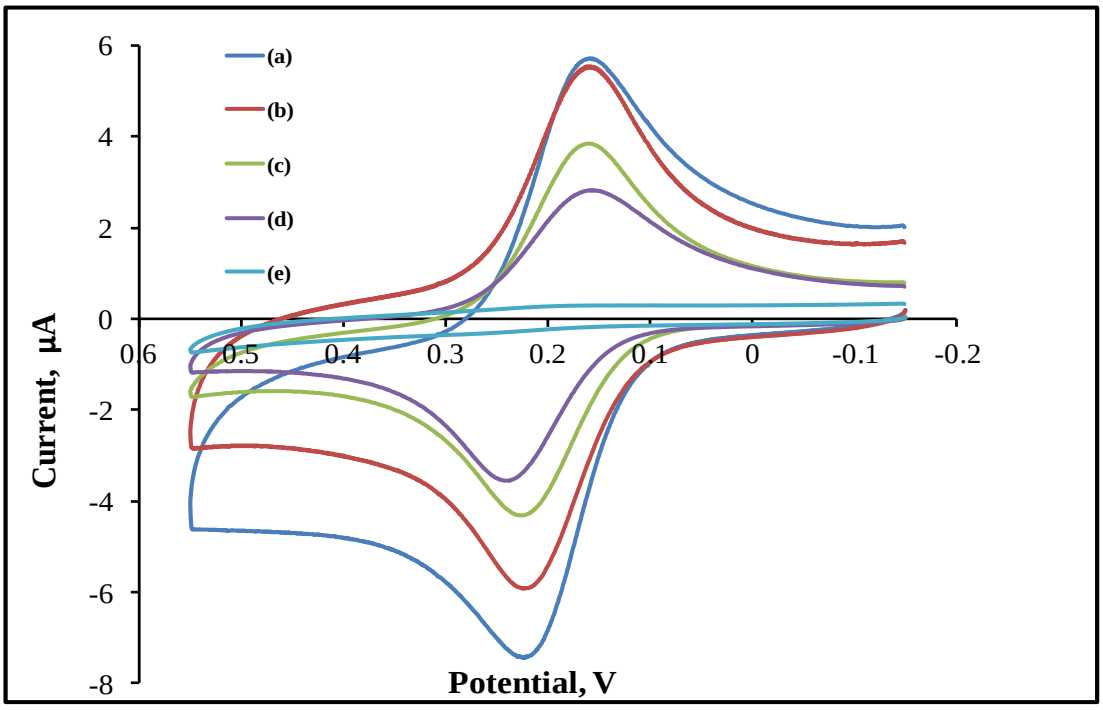

Figure 5.24: Cyclic voltammograms of 1 mM FeMeOH on (a) 2 mm Bare gold, (b) Au-$[Ru(bpy)_2Qbpy)]^{2+}$, (c) Au-$[Ru(bpy)_2Qbpy)]^{2+}$-MUA, (d) Au-$[Ru(bpy)_2Qbpy)]^{2+}$-MUA-(Poly-L-lysine), and (e) Au-$[Ru(bpy)_2Qbpy)]^{2+}$-MUA-(Poly-L-lysine)-cells in DPBS at a scan rate is 0.1 V s^{-1}. The reference electrode is Ag/AgCl.

Cell capture can affect voltammetric response by blocking the electron transfer to the electroactive probe solution. This would result in the reduction of the electrode area and the corresponding peak current, while maintaining a constant peak to peak separation.[54] Curve (a) in Figure 5.24 displays the CV of bare gold electrode in 1 mM FeMeOH which has a well-defined reversible redox couple, with a peak to peak separation (ΔE_p) of 64 mV. This ΔE_p is close to the theoretical value of 59 mV expected for a reversible one electron transfer process. Post modification with $[Ru(bpy)_2Qbpy)]^{2+}$ monolayer, the ΔE_p remains constant (64 mV). However, there is a decrease in the oxidation current which indicates that $[Ru(bpy)_2Qbpy)]^{2+}$ monolayer occupies some sites of the gold electrode. It also implies that the electrode surface is not completely blocked by the $[Ru(bpy)_2Qbpy)]^{2+}$ monolayer, rather there free intervening gold sites that can allow the formation of an alkanethiol self-assembled monolayer (SAM).

Figure 5.24 (c) presents the CV of Au-$[Ru(bpy)_2Qbpy)]^{2+}$ following subsequent modification of the electrode with mercaptoundecanoic acid (MUA). Both the oxidation and reduction peak currents were observed to decrease. This implies a decrease in the rate of electron transport to and from the gold sites because the monolayer acts as an impediment to the access of FcMeOH to the gold surface. Further decrease in the oxidation current of the CV for Au-$[Ru(bpy)_2Qbpy)]^{2+}$-MUA-(Poly-L-lysine)-cells in Figure 5.24 (d) confirms the immobilization of poly-L-lysine. Upon capture the HeLa cells at Au-

$[Ru(bpy)_2Qbpy)]^{2+}$-MUA-(Poly-L-lysine the CV response undergoes a dramatic change.

The ferrocene appears to be completely blocked from the surface as negligible faradaic current is observed in Figure 5.24 (e). This suggests that the cells form a barrier that affects electron transfer involving FcMeOH electro-oxidation on the gold surface. Overall these studies confirm each modification step was successful and consistent with the confocal fluorescence studies cells are effectively captured at the surface. Given the blocking of the electrode surface by cells, we were interested to see an ECL response would be observed. An initial ECL at the Au-$[Ru(bpy)_2Qbpy)]^{2+}$-MUA-(Poly-L-lysine) modified electrode in DPBS was carried out in order to ascertain whether any ECL can be obtained from the electrode without cells and in the absence of a coreactant. No ECL was observed for the electrode under the conditions of the potential, thereby confirming the solution studies which showed that cells have to be present for ECL to occur.

The ECL from the captured cells was also investigated in order to determine l2whether cells bound to the electrode would give any ECL. Figure 5.25 shows the ECL response of Au-$[Ru(bpy)_2Qbpy)]^{2+}$-MUA-(Poly-L-lysine)-cells electrode exposed to 1 million HeLa cells. The onset potential for the ECL of the HeLa cells captured on the electrode is 1.05 V and the ECL has a maximum intensity at 1.22 V as shown in Figure 5.25.

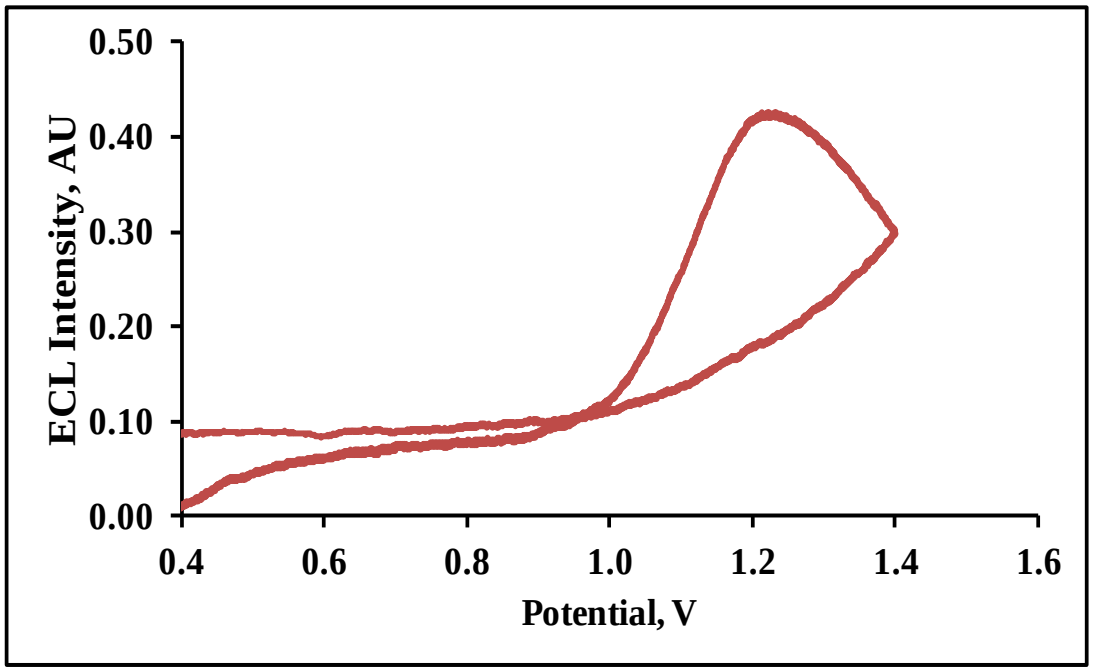

Figure 5.25: ECL response of a 2mm gold electrode modified with $[Ru(bpy)_2Qbpy)]^{2+}$-MUA-(Poly-L-lysine)-cells in DPBS at 0.1 V s^{-1}, with no ECL coreactant in the buffer.

However, the ECL intensity is low considering that 1 million cells were used for the capturing process. This can be attributed to the fact to the both that 30 cells are captured on the electrode at the electrode and that poly-L-lysine does not discriminate between cells which are alive or dead as non-specific binding occurs. This means that not all the cells that are captured on the surface of the electrode are necessarily alive to produce ECL. Furthermore, the density of cells captured at the electrode surface sufficiently high to block electrochemical access to ferrocene. This probably limits the electroactive area of the surface, e.g. blocking ion transport. In the future, means of reducing the capture efficiency may be sought to improve the ECL response.

5.4. CONCLUSIONS

In this chapter a reagent-less method for establishing the metabolic status Has been investigated using electrochemiluminescence from living cancer cells. Spontaneously adsorbed monolayers of ECL luminophore $[Ru(bpy)_2Qbpy]^{2+}$ were formed on gold electrodes and the presence and structuture of the monolayers were confirmed by cyclic voltammetry and Raman spectroscopy. The results showed that the monolayers are strongly coupled to the electrode and were stable under the conditions used for electrochemistry and ECL. The monolayers produced intense and concentration dependent ECL which is consistent with the release of adenosine triphosphate from the cells whereby ATP acts as a coreactant. Both lysed cells and media in contact with living cells produced measurable ECL from the electrodes without the need for a- coreactant and the onset and peak ECL potentials corresponded exactly in the latter to cases to values for ATP in solution. This strongly suggests that ATP, is the coreactant in both cases. However, control experiments performed with ADP in solution as coreactant showed that the potential at which the ECL maximum is observed from ADP is indistinguishable from what is obtained when ATP a coreactant. This suggests that the ECL that is observed from the cells is potentially due to the presence of both adenosine triphosphate and adenosine diphosphate.

The ECL intensity reduced over time from cells incubated in DPBS but it was found that ECL production can be extended by incubating the cells in DMEM media. Where the ECL output could be detected over 5 h compared to 2 h when the cells are in DPBS. There are two important conclusions that can be drawn from these experiments. Firstly, culture medium extends ECL detection

from the cells and secondly, ECL detected is a measure of the metabolic activity from the cells. This was further confirmed with inhibition studies involving AMA to inhibit ATP in HeLa cells. ECL intensity and the period over which it could be detected from the cell medium decreased by more than half when in the presence of AMA. Overall, our preliminary data indicate that ECL from ruthenium polypyridyl monolayers in contact with cell culture medium can be used as a simple measure of metabolic activity from the cells. Finally an attempt to capture living cells on the electrode was also carried out using poly-L-lysine as the binding agent. The objective was to evaluate whether analogus metal complex monolayers could be used as cell-capture substrates for label free detection of live cells. Although cells were captured, the ECL obtained from the captured cells was low. Low ECL production was attributed to low electroactivity of the cell modified electrode. Future work will focus on reducing the capture density to improve ion transport through the films.

5.5. REFERENCES

[1] Kirschmaum, S. E. K., Baeumner, A. J., *Anal. Bioanal. Chem.*, **2015**, 407, 3911-3926.

[2] Baba, K., Nishida, K., *Theranostics.*, **2012,** 7, 655-667.

[3] Nicholson, J. K., Lindon, J. C, *Nature.*, **2008**, 455,1054-1056.

[4] Jie, G., Wang, L., Yuan, J., Zhang. S., *Anal. Chem.,* **2011**, 83, 3873-3880.

[5] Li, C.,Lin, J., Guo, Y. ,Zhang, S., *Chem. Commun.,* **2011***,* 47, 4442-4444.

[6] Liu, Y., Zhu, L., Kong, J, Yang, P., Lui, B., *Electrochem. Commun.*, **2013**, 33, 59-62.

[7] Ge, L., Sub, M., Gao., C., Tao, X., Ge, S., *Sens. and Actuators.*, **2015**, 214,144-151.

[8] Ding, C.F., Ge, Y., Zang, S.S., *Chem. Euro. J.*, **2010**, 16, 10707-10714.

[9] Han, E., Ding, L., Lian, H.,Ju, H., *Chem. Commun.*, **2010**, 46, 5446 -5448.

[10] Chivasa, S., Ndimba, B.K., Simon, W. J., Lindsey, K., Slabas, A. R., *The Plant Cell.*, **2005**, 17, 3019-3034.

[11] Yegutkin, G.G., *Biochim. et Biophys.***2008**, 1783, 673-694.

[12] Yegutkin, G.G., Henttinen, T., Sirpa, J.*, The Faseb Journal*, **2001**, 15, 251-260.

[13] Redegeld, F.A., Caldwell, C.C., Sitkovsky, M.V., *Trends in Pharmaco. Sci.*, **1999**, 20, 453-359.

[14] Forster, R. J., O'Kelly, J. P., *J. Electrochem. Soc.,* **2001**, 148, E31-E37.

[15] Forster, R. J., Keyes, T. E., *J. Phys. Chem. B*., **1998**, 102, 10004-10012.

[16] Lordan, F., Rice, J. H., Jose, B., Forster, R. J., Keyes, T. E., *Appl. Phys. Lett.*, **2011**, 99, 0331041 – 0331043.

[17] Dolan, C., Moriarty, R., Lestini, E., Devocelle, M., Forster, R.J., Keyes, *J. Inorg. Biochem.,* **2013**, 119, 65-74.

[18] Forster, R. J., Pellegrin, Y., Leane, D., Brennan, J. L., Keyes, T. E., *J. Phys. Chem. C.,* **2007**, 111, 2063-2068.

[19] Brennan, J. L., Keyes, T. E, Forster, R. J., *Langmuir.,* 2006, 22, 10754 – 10761.

[20] Bertoncello, P., Kefalas, E. T., Pikramenou, Z., Unwin, P. R., Forster, R. J., *J. Phys. Chem. B*., **2006**,110, 10063-10069.

[21] Forster, R. J., Keyes T. E., Vos, J. G. *Interfacial Supramolecular Assemblies*, **2003**, England , John Wiley & Sons, Ltd.

[22] Huang, H., Tan, Y., Shi, J., Lianga, G., Zhu, Z., *Nanoscale.*, **2010**, 2, 606-612.

[23] Lie, Y., Lei, J., Huang, H., Ju, H*., Anal. Chem.*, **2014**, 86, 8735-8741.

[24] Xu, Y., Venton, B. J., *Electroanalysis*, **2010**, 22, 1167-1174.

[25] Alvarez , N. D, Ortea, P. M ., Paneda, A. M., Castanon, M. J., Ordieres, A. J., Blanco, P. T., *J. Electroanal. Chem.*, **2001**, 52, 109 -117.

[26] Swamy, B. E. K., Venton, B. J., *Anal. Chem.*, **2007**, 79, 744-750.

[27] Nguyen, M. D., Venton, B. J., *Comp. Struct. Biotech. J.*, **2015**, 13, 47-54.

[28] Schwiebert, E.M., Zsembery, A., *Biochim. Biophys.*, **2003**, 1615, 7-32.

[29] Meghi, P., Pearson, I.D., Slakey, L.L., *The Amer. J. Physio.*, **1992**, 263, H40-H47.

[30] Wang, C.,Huang, C.Y.C., Lin, W.C., *Biosens. Bioelectro.*, **2013**, 43, 355-361.

[31] Huguet, E. L., Keeling, N. J., *Diseases of the Colon and Rectum.*, **2004**, 47, 2114 -2119.

[32] Ware, M. J., Godin, B., Singh, N., Majithia, R., Shamsudeen, S., Serda, R. E., Meissner, K. E., Rees, P., Summers, H. D., *Amer. Chem. Soc. Nano.,* **2014**, 8, 6693-6700.

[33] Forster, R. J., Pellegrin, Y., Leane, D., Brennan, J. L., Keyes, T. E., *J. Phys. Chem.* C., **2007**, 111, 2063-2068.

[34] Jose, B., Mallon, C.T, Forster, R.J., Keyes, T.E., *Phys. Chem. Chem. Phys.,* **2011**, 13, 14705-14714.

[35] Devadoss, A., Dennany, L., Dickinson, C., Keyes, T. E., Forster, R. J., *Electrochem. Commun*., **2012**, 19, 43-45.

[36] Dott, W., Mistry, P., Wright, J., Cain, K., Herbert, K., *Redox Biology.*, **2014**, 2, 224-233.

[37] Bonnier, F., Keating, M., Wrobel, T., Majzner, K., Baranska, M., Garcia, A., Blanco, A., Byrne, H. J., *Tox. in Vitro*, **2015**, 29, 124-131.

[38] Wallace, K.B., Starkov, A.A., *Annual Rev. Pharm. Tox.,* **2000**, 40, 353-388.

[39] Drose S., Brandt, U.J., *J. Bio. Chem.*, **2008**, 31, 21649-21654.

[40] Han, Y. W., Moon, H. J., You, B. R., Kim, S. Z., Kim, S. H., Park, W. H., *Anticancer Res.* , **2009**, 29, 4423-4432.

[41] Martin, A., Byrne, A., Burke, C. S., Forster, R. J., Keyes, T. E., *J. Amer. Chem. Soc.*, **2014**, 136, 15300-15309.

[42] Tzung, S., Kim, K. M., Basanez, G., Giedts, C. D., Simon, J., Zimmerberg, J., Zhang, K. Y. J., Hockenberys, D. M., *Nature Cell Biol.*, **2001**, 3,183 -191.

[43] Edinger, A.L., Thompson, C.B., *Curr. Opi. Cell Biol.***2004**, 16, 663-669.

[44] Levine, B., Yuan J., *The J. Clinic. Inves.*, **2005**, 115, 2679-2688.

[45] Nie, G., Bai, Z., Yu, W., Chen, J., *Biomacromol.*, 2013, 14, 834-840.

[46] Guo, C. X., Ng, S. R., Khoo, S. Y., Zheng, X., Chen, P., Li, C. M., *Amer. Chem. Soc. Nano.*, **2012**, 8, 6944-6951.

[47] Hauck, T. S., Ghazani, A. A., Chan, W. C. W., *Small.*, **2008**, 1, 153-159.

[48] Slowing, I., Trewyn, B. G., Lin, V. S. Y., *J. Amer. Chem. Soc.*, **2006**, 128, 14792- 14793.

[49] Sandrin, L., Thakar, D., Goyer, C., Labbe, P., Boturyn, D., Coche-Guerente, L., *J. Mater. Chem. B.*, **2015**, 3, 5577-5587.

[50] Cheng, W., Ding, L., Lei, J. P., Ding, S. J., Ju H. X., *Anal. Chem.*, **2008**, 80, 3867-3872.

[51] Kornguth, S., Kalinke, T., Robins, H.I., Cohen, H.D., Turski, P., *Cancer Res.*, **1989**, 49, 6390- 6395.

[52] Santos, P. A., Rocha, C. S., Baptista, M. S., *Col. Surf. B: Biointer.*, **2014**, 123, 429-438.

[53] Venkatanarayanan, A., Keyes, T. E., Forster, R. J., *Anal. Chem.*, **2013**, 85, 2216-2222.

[54] Nwankire, C. E., Venkatanarayanan, A., Glenon, A. B., Keyes, T. E., Forster, R. J., Ducree, J., *Biosens. Bioelectron.,* **2015**, 68, 382-389.

CHAPTER SIX:

GENERAL DISCUSSION, CONCLUSIONS AND RECOMMENDATIONS

6.1. GENERAL DISCUSSION AND CONCLUSIONS

This chapter deals with general discussions and conclusions of the results presented in the study and makes further recommendations for ECL studies. This study has been directed towards exploring a number of novel materials and methods for the application of interfacial electrochemiluminescence in the detection of representative biological materials, which when extended beyond this thesis may be used in detection of disease. The overall goal of this thesis was to study, efficient and viable novel ECL generating luminophores in order to increase the scope of these materials for application in different areas such as; electrochemiluminescent sensors and detection assays. The luminophore materials studied were identified and were chosen on the basis of the excellent properties they offer. For example Ru Polypyridyl complexes exhibit chemical stability in different solvents and strong luminescence emission. It also exhibits favourable electrochemical redox properties such as being able to undergo electron transfer reactions at potentials that are accessible. BODIPY compounds offer remarkable photophysical and optical spectroscopic properties, when compared to the conventional fluorophores.

Chapter 2 focused on new class of fluorophores as potential ECL luminophores. The electrochemical and electrochemiluminescence properties of novel BODIPY-COOH bioconjugate in solution have been investigated. The photophysics and electrochemistry of a novel BODIPY derivative were investigated to estimate the thermodynamic and electrochemical parameters of the dye which would indicate their value as ECL reagents. ECL was successfully generated from BODIPY–COOH

in solution in the presence of either benzoyl peroxide or hydrogen peroxide coreactant. The ECL generated with hydrogen peroxide was approximately 50% less than when BPO was used as a coreactant. BODIPY-COOH thin films via cysteamine and/or cysteine coupling were also investigated. A careful engineering of the novel BODIPY-COOH with cysteamine linker; capable of being immobilized effectively onto a surface has been developed. The BODIPY-COOH dye has some potential to be used in ECL biosensor application as it can be easily coupled to biomolecules and transducer surfaces through straight forward bio-conjugation techniques. It has been demonstrated that these monolayers are not only robust and stable but also emit considerable ECL with benzoyl peroxide coreactant. A key finding from these studies is that the turn-on potential at which ECL is generated depends on whether BPO or H_2O_2 is used as coreactant. The use of two different coreactants which can turn on ECL potential of a single luminophore at different potentials opens potential application in multiplexing assays in which multiple analytes can be detected in one assay by just changing the coreactant.

Chapter three focused on the development of a rapid and affective method of confining a ruthenium ECL luminophore to the electrode. This was achieved by incorporating the ruthenium within a conducting polymer polyanilne via electropolymerization, forming a composite film Ru-PANI. The structural analysis using Raman further provided evidence that Ru-complex was incorporated on the PANI backbone, whereby the vibration absorption bands due to PANI and ruthenium interaction were both observed. The morphology of the PANI-Ru composite film confined to the electrode was investigated with Atomic force microscopy and showed well defined globular like structures of PANI-Ru. The ECL of the electrodeposited

PANI-Ru composite thin film generated by the oxidative coreactant pathway using TPA was investigated. Significantly it was seen that the PANI-Ru composite exhibits high ECL efficiency of 1%, that is the highest reported in literature for a solid state ECL luminophore. This strategy of luminophore confining a ruthenium ECL luminophore to the surface of an electrode has opened up possible applications especially in detection assays

Chapter four reports on DNA binding induced ECL generation at monolayers of a novel $[Ru(dppz)(bpyArCOOH)_2]^{2+}$ dye. Here a switchable ECL surface has been investigated, which can useful in determining DNA binding and hybridization events.

The objectives of the chapter included investigation and quantication DNA binding, to probe if the binding can induce molecular light switch characteristics. Evidence of DNA of binding to $[Ru(dppz)(bpyArCOOH)_2]^{2+}$ monolayer was observed from the voltammetry and the Raman, luminescence and electrochemistry studies. Upon DNA binding to dry $[Ru(dppz)(bpyArCOOH)_2]^{2+}$ monolayers, a significant 50 % increase in luminescence was observed. Similarly ECL investigations also showed that DNA binding enhances the ECL of the $[Ru(dppz)(bpyArCOOH)_2]^{2+}$ monolayer. Strikingly the ECL efficiency of the $[Ru(dppz)(bpyArCOOH)_2]^{2+}$ significantly enhanced from 0.018± 0.02% to 0.20 ± 0.01 %. In the presence of DNA. One of the key findings from the work is that intercalative binding takes place between the DNA and the monolayer, as the ionic strength studies showed increasing the NaCl concentration between 0.2 M to 0.6 M hardly changed the ECL intensity of the $[Ru(dppz)(bpyArCOOH)_2]^{2+}$ -DNA . Moreover the association constant of DNA to the monolayer is 2.56 $x10^4$, which shows that the binding affinity of DNA to $Ru(dppz)(bpyArCOOH)_2]^{2+}$ is essentially low. This result is not surprising as the

packed monolayer of $[Ru(dppz)(bpyArCOOH)_2]^{2+}$ is expected to be less accessible to the DNA.

Chapter 5 reports on the generation of ECL from living cancer cells at positive potentials using $[Ru(bpy)_2Qbpy]^{2+}$. The study focuses on developing reagent less method of monitoring metabolic cell status over time by investigating the ECL from whole cells in DPBS or in cell growth medium (DMEM), lysed or captured cells. The results showed that in the absence of cells or $[Ru (bpy)_2Qbpy]^{2+}$ on the electrode no ECL is observed, suggesting that ECL requires both the presence of the cells and the luminophore. The results are consistent with adenosine 5' triphosphate released from the cancer cells acting as a co-reactant.

The results from ECL detection from cells in DMEM media have shown that ECL can be detected for 5 h compared to 2 h when the cells are in DPBS. Suggesting that in culture medium the cells are metabolically active for a longer period compared to when the cells are in DPBS. There are three key findings from this study, firstly there is a rapid decrease in metabolic activity of cell as time increases, as indicated by ECL experiments of whole cells in DMEM. Secondly a culture medium extends ECL detection from the cells as it offers a DMEM offers a more benign environment to encourage cell health and lastly ECL detected is a measure of metabolic activity from the cells. Inhibition studies using Antimycin have indicated that decreasing the level of ATP in the cells has a direct effect on the ECL. Confirming that the ECL observed is consistent with the detection of ATP from the cells. However, control experiments performed with ADP in solution as coreactant showed that the potential

at which the ECL maximum is observed from ADP is indistinguishable from what is obtained when ATP a coreactant. This suggests that the ECL that is observed from the cells is potentially due to the presence of both adenosine triphosphate and adenosine diphosphate. It should be noted that there is real need to distinguish between living and dead cells in manyenvironmental applications such as testing for *Escherichia coli* in food and water. Significantly since the ECL detected from the live cell is related to the metabolic activity, ECL can be potentially usefull in such environmental tests

6.2. FUTURE RECOMMENDATIONS

It was previously highlighted from Chapter two that the ECL turn-on potential at which ECL with BODIPY is dictated by the identity of the coreactant used *i.e* BPO or H_2O_2 is used as coreactant. Moreover, the photophysics studies of BODIPY showed that this dye exhibits sharp absorbance peaks which are useful in multiplexing assays. It would therefore useful in future experiments to explore multiplexing assays. For example in an antibody sandwich assay, the same luminophore can be used to label the different primary antibodies, and then different correatants can be used to label secondary antibodies. This can potentially allow different targets within the single spot to be quantified.

Chapter 4 double stranded DNA binding to $[Ru(dppz)(bpyArCOOH)_2]^{2+}$ monolayers induces the molecular light switch effect.In the future it would be good to investigate whether the light switch the effect would be observed upon binding single stranded DNA to $[Ru(dppz)(bpyArCOOH)_2]^{2+}$ monolayers.

In Chapter 5 an attempt to capture living cells on the electrode was also carried out using poly-L-lysine as the binding agent. The objective was to evaluate whether analogus metal complex monolayers could be used as cell-capture substrates for label free detection of live cells. Although cells were captured, the ECL obtained from the captured cells was low. Low ECL production was attributed to low electroactivity of the cell modified electrode. Future work will focus on reducing the capture density to improve ion transport through the films. Furthermore poly-Lysine does discriminate between cells which are alive or dead, in the future to capture cells antibodies which are having specific binding to HeLa should be used to increase the number of cells which are captured on the electrode. Another future aspect would be to monitor the ECL of the cells in their cell culture medium, as the ECL results from the cells in contact with the cell growth medium has shown that the metabolic activity of the cells is extended , as reflected by the ECL results. Parrallel to these experiments of monitoring the ECL in cell culture media, it would be good to monitor the morphology of the cells using confocal microscopy simultaneously experimental time the ECL measurement are conducted

APPENDIX 1: ^{1}H NMR SPECTRA OF BODIPY in DMSO-d_6.

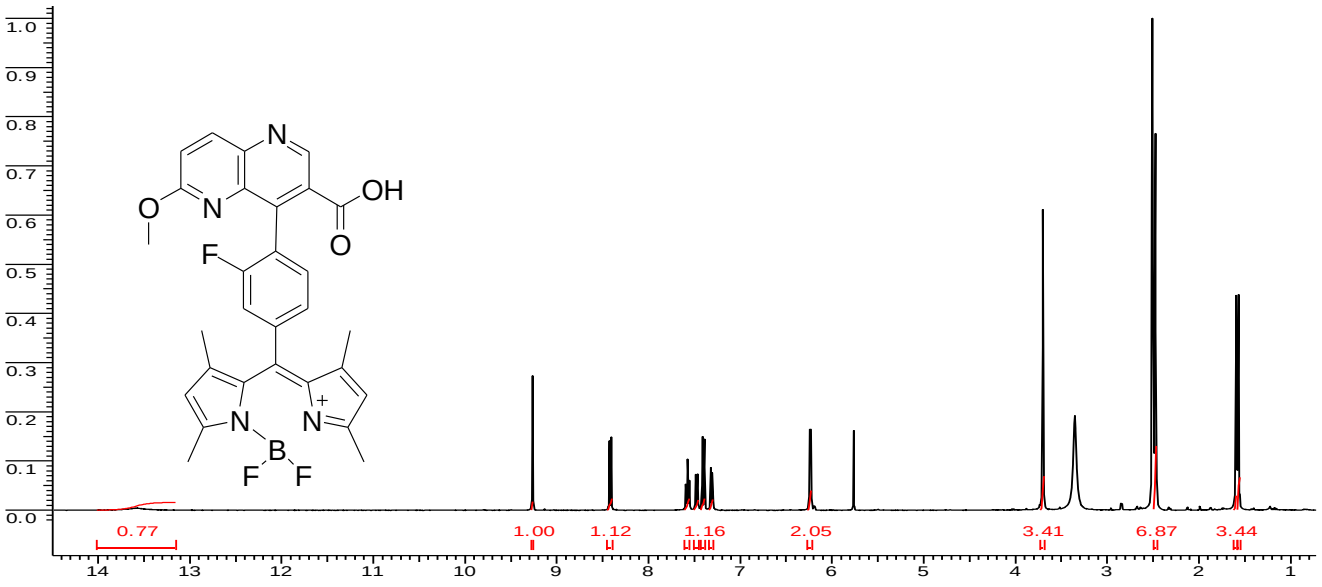

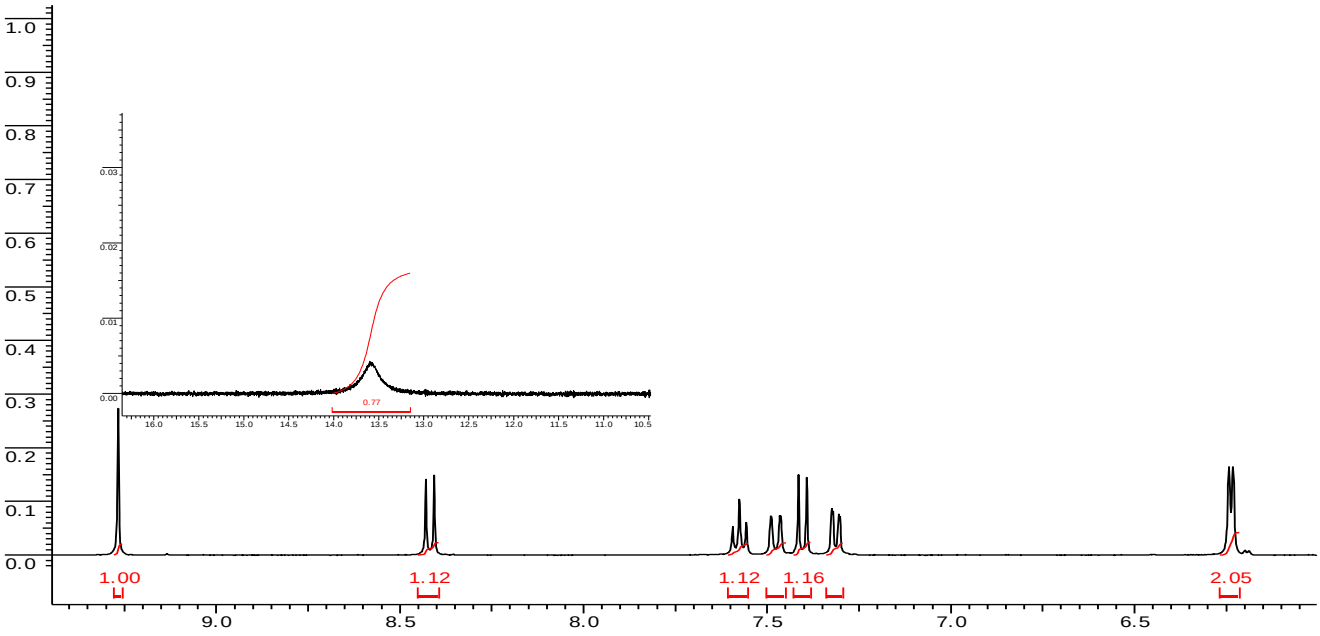

Elemental Composition Report

Single Mass Analysis

Tolerance = 20.0 PPM / DBE: min = -1.5, max = 1000.0

Isotope cluster parameters: Separation = 1.0 Abundance = 1.0%

Monoisotopic Mass, Odd and Even Electron Ions

16 formula(e) evaluated with 1 results within limits (all results (up to 1000) for each mass)

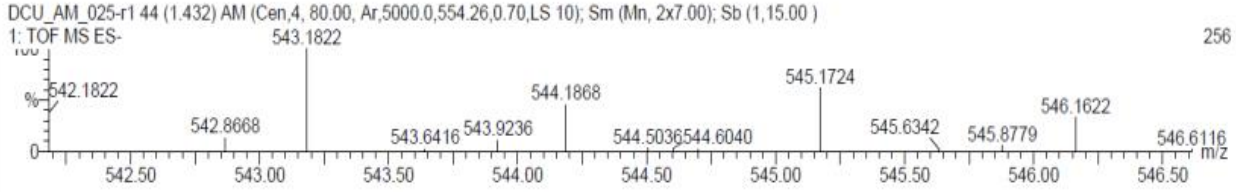

Minimum:				-1.5		
Maximum:		200.0	20.0	1000.0		
Mass	Calc. Mass	mDa	PPM	DBE	Score	Formula
543.1822	543.1815	0.7	1.2	19.5	1	C29 H23 B N4 O3 F3

APPENDIX 2: ^{1}H NMR SPECTRA OF $[Ru(bpy)_2 PICH_2]^{2+}$ IN DMSO-d_6.

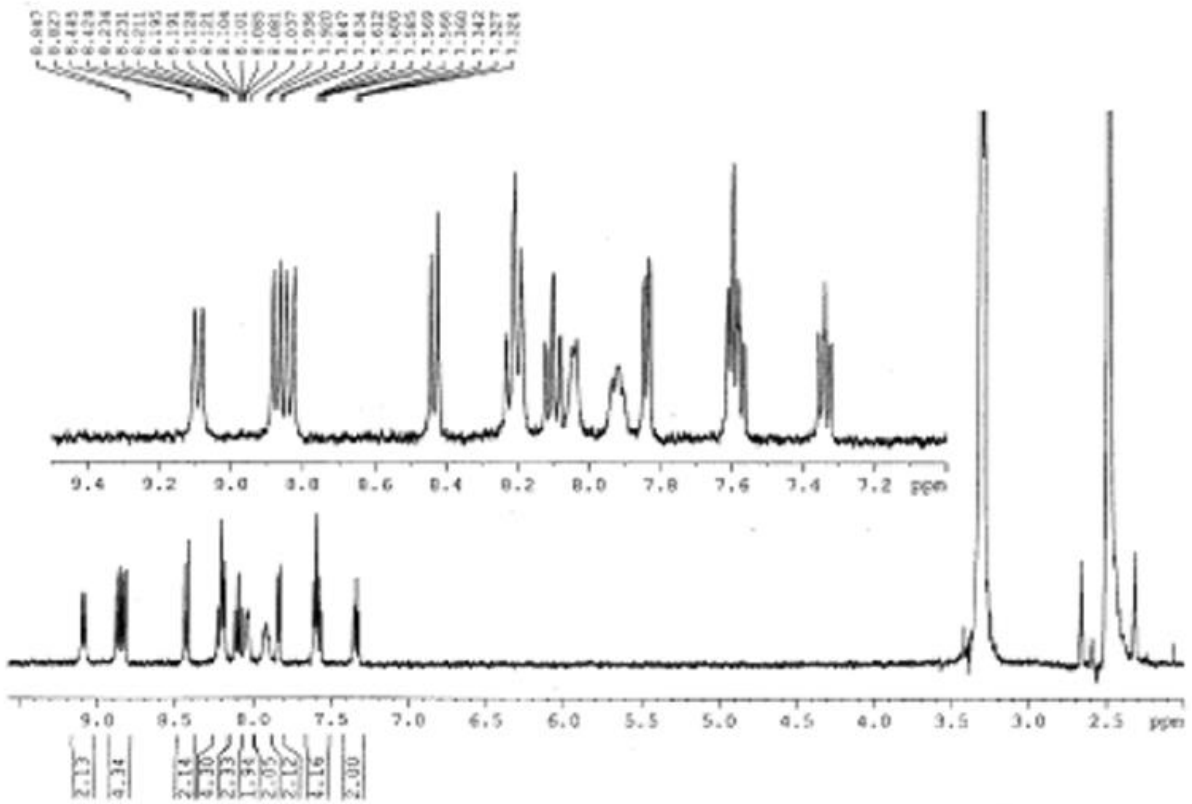

APPENDIX 3 : SYNTHESIS METHOD FOR $[RU(DPPZ)(BPYARCOOH)_2]^{2+}$

$Ru(dppz)(DMSO)_2Cl_2$

$Ru(DMSO)_4Cl_2$ (500 mg, 1.03 mmol) and dppz (290 mg, 1.03 mmol, 1 equiv) were heated at reflux in ethanol (35 mL) for 2 h. The reaction was then cooled to room temperature and concentrated to *ca*. 5 mL *in vacuo*. The precipitate formed was filtered, washed with minimal cold ethanol and copious amounts of a 1/1 mixture of hexane/diethyl ether and dried under nitrogen. Yield: brown solid, 625 mg (1.02 mmol, 99 %). ^{1}H NMR (400 MHz, $CDCl_3$) δ (ppm): 10.22 (d, 1 H); 10.05 (d, 1 H); 9.79 (d, 1 H); 9.69 (d, 1 H); 8.43 (m, 2 H); 8.11 (t, 1 H); 8.05 (m, 2 H); 7.93 (t, 1 H); 3.65 (s, 3 H); 3.60 (s, 3 H); 3.26 (s, 3 H); 2.70 (s, 3 H). ^{13}C NMR (100 MHz, $CDCl_3$) δ (ppm): 157.66, 154.26, 152.02, 150.162, 142.90, 139.58, 139.49, 134.89, 133.91, 132.04, 130.36, 129.88, 129.68, 126.10, 126.03, 47.20, 46.47, 45.49, 44.39. Anal. Calculated (Found) for $C_{22}H_{22}Cl_2N_4O_2S_2Ru$: C 43.28 (43.78); H 3.63 (3.35); N 9.18 (9.26); Cl 11.61 (11.42). HR-MS (ESI-TOF) *m/z*: Calculated for $C_{22}H_{22}Cl_2N_4O_2S_2Ru$: 609.9605; Found: 609.9604.

$[Ru(dppz)(bpyArCOOH)_2]^{2+}$

$[Ru(dppz)(DMSO)_2Cl_2]$ (100 mg, 0.164 mmol) and bpyArCOOH (90 mg, 0.328 mmol, 2 equiv) were added to a 9/1 ethylene glycol/water mixture (10 mL) and the resulting suspension was heated at reflux for 6 h. The resulting deep red mixture was cooled to room temperature and the PF_6^- salt precipitated by the addition of a saturated aqueous solution of ammonium hexafluorophosphate. The crude solid was isolated by filtration and washed well with water. The solid was then dissolved in acetone and filtered through a narrow bed of celite. The filtrate was concentrated *in vacuo* and added dropwise to rapidly stirring diethyl ether to precipitate bright orange solids which were filtered, washed with ether and dried in the vacuum to yield the pure PF_6^- salt as a mixture of geometric isomers. The chloride form of the complex was quantitatively obtained by adding a filtered concentrated acetone solution of the PF_6^- salt to a saturated LiCl solution in acetone. The chloride salt precipitated immediately and was filtered to provide the product as an orange solid. Yield: Isomer mixture, orange solid, 128 mg (0.127 mmol, 77 %). The isomers partially resolve in low yield on silica using 70/26/4/2 $CHCl_3$/MeOH/H_2O/AcOH as eluent which simplifies the ^{1}H NMR analysis but the compound was used in the present work as the bulk mixture of isomers. ^{1}H NMR (600 MHz, DMSO-d_6): *Partially resolved isomer*: 9.65 (d, 2H); 9.22 (m, 4 H); 8.53 (dd, 2 H); 8.39 (m, 2 H); 8.28 (m, 2 H); 8.20 (m, 3 H); 8.11 (q, 3 H); 8.05 (m, 7 H); 7.97 (m, 2 H); 7.88 (d, 1 H); 7.80 (m, 3 H); 7.64 (q, 1 H); 7.43 (q, 1 H). Anal. Calculated. (Found) for $C_{52}H_{34}N_8O_4Cl_2Ru.6H_2O$: C 56.02 (56.01); H 4.16 (3.64); N 10.05 (9.74); Cl 6.36 (6.55). HR-MS (ESI-TOF) *m/z*: Calculated for $C_{52}H_{34}N_8O_4Cl_2Ru$ $[M]^+$: 1006.1135; Found: 1006.1132.

APPENDIX 4: H NMR (600 MHZ, DMSO-D_6) SPECTRUM OF $[RU(DPPZ)(BPYARCOOH)_2]^{2+}$

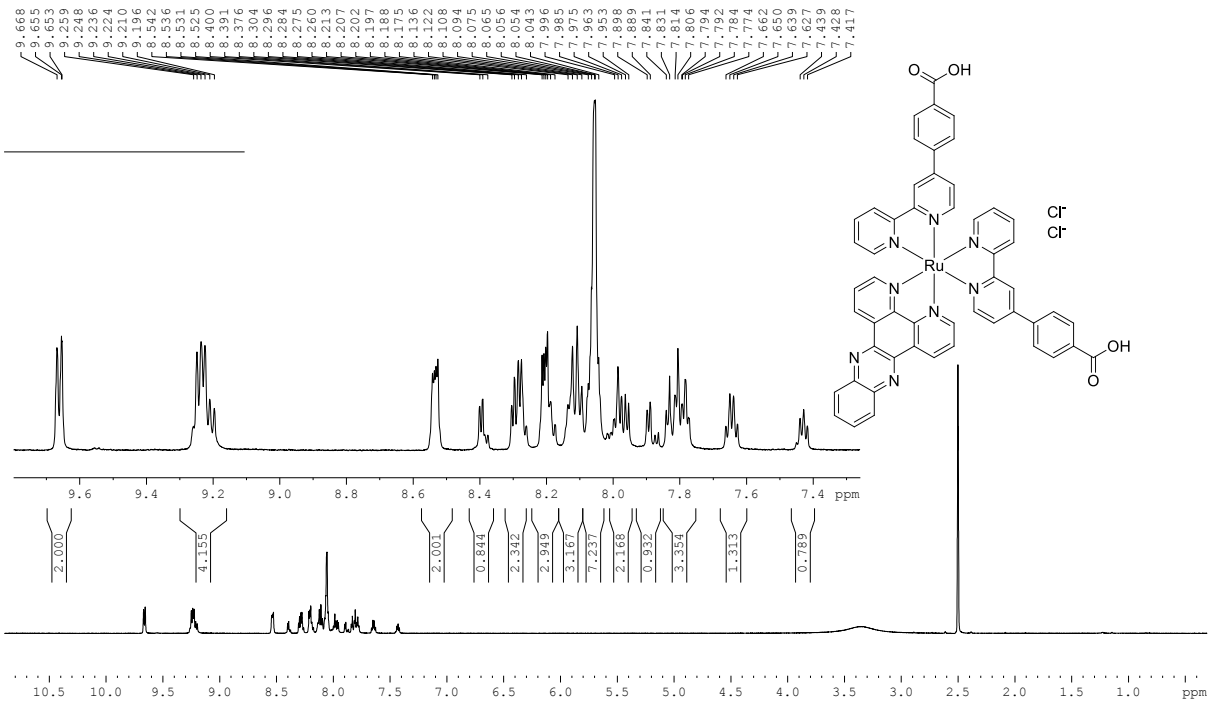

Single Mass Analysis $[M]^+$: Mass Spectrum of $[Ru(dppz)(bpyarcooh)_2]Cl_2$.

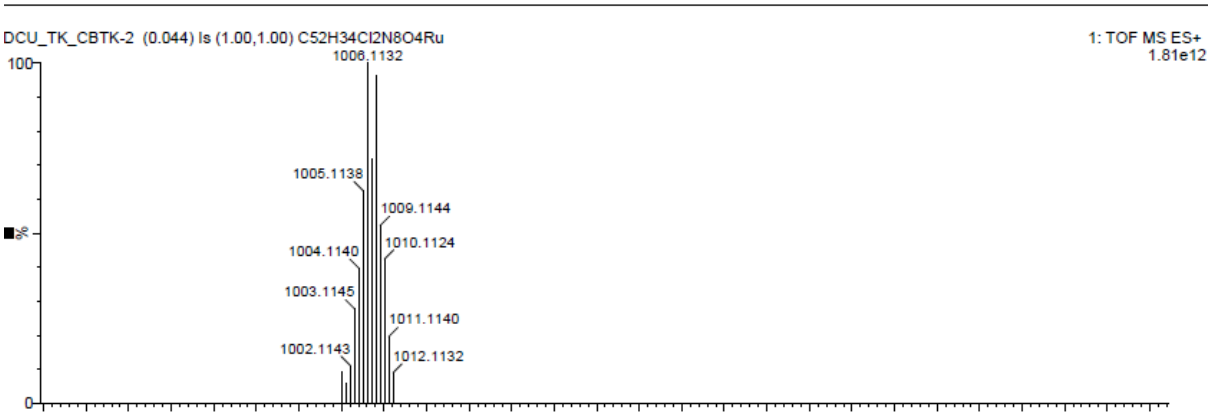

APPENDIX 5: PUBLISHED PAPER 1

Electrochemistry Communications 31 (2013) 116–119

Contents lists available at SciVerse ScienceDirect

Electrochemistry Communications

journal homepage: www.elsevier.com/locate/elecom

Tuning the electrochemiluminescence potential from immobilised BODIPY by co-reactant selection

Anita Venkatanarayanan [a,b], Aaron Martin [b], Kerileng M. Molapo [b,c], Emmanuel I. Iwuoha [c], Tia E. Keyes [a,b], Robert J. Forster [a,b,*]

[a] Biomedical Diagnostics Institute, National Center for Sensor Research, Dublin City University, Dublin 9, Ireland
[b] School of Chemical Sciences, National Center for Sensor Research, Dublin City University, Dublin 9, Ireland
[c] Sensor Lab, Chemistry Department, University of the Western Cape, Cape Town, South Africa

ARTICLE INFO

Article history:
Received 6 March 2013
Received in revised form 18 March 2013
Accepted 18 March 2013
Available online 25 March 2013

Keywords:
Electrochemiluminescence (ECL)
BODIPY
Self assembled monolayer
Optical sensor

ABSTRACT

A thin film of the novel surface active ECL luminophore, 4,4-difluoro-4-bora-3a,4a-diaza-s-indacene, BODIPY, is used to demonstrate that the ECL turn on potential can be controlled through the identity of the co-reactant. The films were very stable when in contact with organic solvents and surface coverages of 1-2 nmol cm^{-2} are observed. Significantly, the potential at which ECL is generated is dictated by the identity of the co-reactant, either benzoyl peroxide or hydrogen peroxide, which opens new avenues for multi-analyte detection by changing the identity of the co-reactant rather than the dye.

1. Introduction

Electrochemiluminescent materials [1–4] where the potential at which emission can be controlled are important for the development of multianalyte, single spot, sensors. BODIPYs, 4,4-difluoro-4-bora-3a,4a-diaza-s-indacenes, are attractive for biosensor development since their spectroscopic and photophysical properties can be fine-tuned by appropriately functionalizing the difluoroboron dipyrromethene core.[5] These dyes exhibit high quantum yields and large extinction coefficients [6,7] and emit substantial ECL in organic solutions in the presence of benzoyl peroxide as a co-reactant.[8] However, practical applications are limited because large amounts of the ECL reagent are required if the assay is carried out in solution and introducing the surface active functionalities needed to immobilise BODIPYs on surfaces can be challenging.

In this contribution, the formation and ECL properties of 2,6-Diethyl-1,3,5,7-tetramethyl-8-[(2-fluorophenyl)-6-methoxy-1,5-naphthyridine-3-N-hydroxysuccinimidyl]-4,4′difluoroboradiazaindacene, BODIPY-NHS, films formed on platinum electrodes via cysteamine coupling is reported. These layers are stable and generate ECL when benzoyl peroxide or hydrogen peroxide is used as the co-reactant. Significantly, the potential for ECL is dictated by the identity of the co-reactant.

* Corresponding author at: School of Chemical Sciences, National Center for Sensor Research, Dublin City University, Dublin 9, Ireland. Tel.: +353 1 7005943; fax: +353 1 7005503.
E-mail address: Robert.Forster@dcu.ie (R.J. Forster).

1388-2481/$ – see front matter © 2013 Published by Elsevier B.V.
http://dx.doi.org/10.1016/j.elecom.2013.03.027

2. Experimental

2.1. Materials and methods

Benzoyl peroxide and H_2O_2 standard solutions were made in anhydrous dimethyl sulfoxide, DMSO, (HPLC Grade) solution with 0.1 M tetrabutylammonium tetrafluoroborate, $TBATFB_4$ (Analar grade), as supporting electrolyte unless otherwise stated. All solutions were degassed for 30 min using nitrogen gas prior to use and all measurements were carried out at 22 ± 2 °C.

Electrochemiluminescence (ECL) and cyclic voltammetry experiments were performed as previously reported [9]. All potentials are quoted against a standard calomel reference electrode.

2.2. Synthesis

2.2.1. 2,6-Diethyl-1,3,5,7-tetramethyl-8-[(2-fluorophenyl)-6-methoxy-1,5-naphthyridine-3-N-hydroxysuccinimidyl]-4,4′-difluoroboradiazaindacene

A carboxy functionalised BODIPY-naphthyridine [9] (100 mg, 0.16 mmol) and *N*-hydroxy succinimide (24 mg, 0.21 mmol) were dissolved in anhydrous MeCN (17 mL) and EDC (40 mg, 0.21 mmol) in anhydrous MeCN (5 mL) added and allowed to react with stirring under N_2 until all the starting material had been consumed. The reaction mixture was then filtered and concentrated to dryness with the crude solid purified on silica gel (50:50 EtOAc:hex) to give the active ester BODIPY (75 mg, yield 65%) as a bright red solid. The structure and purity were confirmed by proton and carbon NMR and high-resolution MS (TOF MS ES^+): $m/z = 720.2596$, calcd for

Electrochemistry Communications 48 (2014) 95–98

Contents lists available at ScienceDirect

Electrochemistry Communications

journal homepage: www.elsevier.com/locate/elecom

Short communication

High efficiency electrochemiluminescence from polyaniline:ruthenium metal complex films

Kerileng M. Molapo [a,c], Anita Venkatanarayanan [a], Ciaran M. Dolan [a], Una Prendergast [b], Priscilla G. Baker [c], Emmanuel I. Iwuoha [c], Tia E. Keyes [a], Robert J. Forster [a,*]

[a] School of Chemical Sciences, Dublin City University, Dublin 9, Ireland
[b] Celtic Alliance for Nanohealth, Dublin City University, Dublin 9, Ireland
[c] Sensor Lab, Chemistry Department, University of the Western Cape, Cape Town, South Africa

ARTICLE INFO

Article history:
Received 17 July 2014
Received in revised form 21 August 2014
Accepted 21 August 2014
Available online 29 August 2014

Keywords:
Electrochemiluminescence
Polyaniline
Ruthenium

ABSTRACT

Electrochemiluminescent films have been formed by electrodepositing polyaniline, PANI, in the presence of $[Ru(bpy)_2PIC]^{2+}$; bpy is 2,2′-bipyridyl and PIC is (2,2′-bipyridyl)-2(4-carboxylphenyl) imidazo [4,5][1,10] phenanthroline. The homogeneous charge transport diffusion coefficient, D_{CT}, for the $Ru^{2+/3+}$ couple within the PANI film is $2.6 \pm 0.9 \times 10^{-10}$ cm^2s^{-1}. The large D_{CT} facilitates a fast regeneration of Ru^{3+} and, coupled to a relatively rigid microenvironment, results in a high ECL intensity in the presence of tripropylamine as a co-reactant compared to $[Ru(bpy)_3]^{2+}$. Significantly, despite the conducting nature of the polymer backbone, the $[Ru(bpy)_2PIC]^{2+}$ loaded PANI has the highest efficiency, 1.00%, yet reported for a surface confined ruthenium complex.

1. Introduction

In electrochemiluminescence, ECL, electrochemically generated intermediates undergo a highly exergonic reaction to produce an electronically excited state that emits light. ECL detection in bioassays [1] offers significant advantages, including inherent sensitivity, since unlike optically driven emission, it does not need a light source. Furthermore, it also offers temporal and spatial control over the chemiluminescent reaction, making it a powerful approach for multiplexed assays especially when the luminophore is confined to an electrode surface [2]. However, identifying the optimum matrix for immobilising the luminophore is challenging since fast regeneration of the luminophore is desirable, but equally quenching by the matrix and the electrode surface needs to be minimised [3].

Conducting polymers with bound redox centres can show high ionic and electronic conductivity [4] that could lead to a brighter ECL since more luminophores would be generated per unit time. However, depending on their optical and redox properties, the electrochemically generated excited state may be quenched, e.g., by electron transfer to or from the excited state or by resonant energy transfer [5].

In this contribution, we report on the ECL properties of $[Ru(bpy)_2PIC]^{2+}$ within polyaniline, PANI, films; bpy is 2,2′-bipyridyl and PIC is (2,2′-bipyridyl)-2(4-carboxylphenyl) imidazo [4,5][1,10] phenanthroline. Incorporation of the charged metal complex has been achieved during potentiostatic electropolymerisation of aniline. The resulting films show well defined redox processes associated with the $Ru^{2+/3+}$ couple and reveal significant electronic interactions between the PANI and ruthenium complex. Strikingly, the ECL generated in the presence of tripropylamine, TPA, as co-reactant is significantly brighter than that found for ruthenium tris-bipyridyl and the overall efficiency of the ECL generation of the composite is amongst the highest yet observed for a confined ECL luminophore.

2. Experimental

2.1. Materials and methods

$[Ru(bpy)_2PIC]^{2+}$ was prepared as described previously [6]. All reagents were purchased from Sigma Aldrich and were of Analar grade. Electrochemiluminescence and electrochemistry experiments were performed as described elsewhere [7]. All solutions were prepared using Milli-Q water (18 MΩ cm) and fully deoxygenated with nitrogen prior to use. Electrochemical measurements were carried out at 22 ± 2 °C.

2.2. Composite film formation

The Ru–PANI complex films were deposited at a fixed potential whilst measuring the charge passed. Briefly, ITO electrodes (1.25 cm^2) were cleaned by sonicating in deionised water for 5 min followed by sonication in acetone for 5 min. The electrodes were then dried under a stream of nitrogen. The ITO electrodes were then placed in an electrochemical cell containing 0.1 M HCl, 0.2 M aniline and 1 mM $[Ru(bpy)_2PIC]^{2+}$ and

* Corresponding author. Tel.: +353 1 7005943; fax: +353 1 7005503.
E-mail address: Robert.Forster@dcu.ie (R.J. Forster).

http://dx.doi.org/10.1016/j.elecom.2014.08.022
1388-2481/